Universidad de Oviedo

Programa de Doctorado de Ingeniería Química, Ambiental y Bioalimentaria

Development of novel bacteriophage-based products for biofilm removal

---

Desarrollo de nuevos productos basados en fagos para la eliminación de biopelículas

Ana Catarina Leal Duarte

Oviedo, 2024

Universidad de Oviedo

Programa de Doctorado de Ingeniería Química, Ambiental y Bioalimentaria

Development of novel bacteriophage-based products for biofilm removal

Desarrollo de nuevos productos basados en fagos para la eliminación de biopelículas

Oviedo 2024

Doctoral thesis

Ph.D in Chemical Engineering, Environmental and Bioalimentary

Ana Catarina Leal Duarte

Work performed under supervision of

Doctor Pilar García Suaréz

and

Doctor Lucía Fernández Llamas

IPLA CSIC

Consejo Superior de Investigaciones Científicas

This work was performed at the Instituto

de Productos Lácteos de Asturias (IPLA, CSIC)

Universidad de Oviedo

RESUMEN DEL CONTENIDO DE TESIS DOCTORAL

1.- Título de la Tesis	
Español/Otro Idioma: Desarrollo de nuevos productos basados en fagos para la eliminación de biofilms	Inglés: Development of novel bacteriophage-based products for biofilm removal

2.- Autor	
Nombre: Ana Catarina Leal Duarte	
Programa de Doctorado: Doctorado en Ingeniería Química, Ambiental y Bioalimentaria	
Órgano responsable: Centro Internacional de Postgrado	

RESUMEN (en español)

El aumento gradual de la resistencia a los antibióticos en bacterias patógenas es una de las mayores amenazas a día de hoy, no solo afectando a la salud humana, sino también a la economía mundial, estimándose que el tratamiento de la resistencia a los antibióticos podría costar billones a la economía mundial en el año 2050. *Staphylococcus aureus* y *Staphylococcus epidermidis* son dos agentes causantes habituales de infecciones nosocomiales, frecuentemente asociadas con la formación de biopelículas. Además, *S. aureus* está implicado en intoxicaciones alimentarias debido a su capacidad para producir enterotoxinas. En este contexto, la terapia fágica se propone como una estrategia segura frente a los antimicrobianos convencionales que podría ayudar a controlar la propagación de la resistencia a los antibióticos. En esta Tesis, se han estudiado varias estrategias encaminadas a optimizar la utilización de los bacteriófagos para combatir estos dos patógenos en entornos clínicos e industrias alimentarias. En primer lugar, se evaluó el impacto de la temperatura en la infección por el fago *Kayvirus rodi* (phiIPLA-RODI). Los datos obtenidos mostraron que este fago es más eficaz a temperatura ambiente (25 ºC) que a temperatura corporal (37 ºC) para la eliminación de cultivos planctónicos y biofilms de varias cepas de *S. aureus* con distintos grados de susceptibilidad. Por ello, *K. rodi* es un buen candidato para la descontaminación de superficies a temperatura ambiente, pero su eficacia en el contexto clínico estaría restringida a las cepas más susceptibles. Estos resultados llevaron a la exploración de diferentes estrategias para la eliminación más eficaz de biopelículas de *S. aureus* por *K. rodi* a temperatura corporal, entre ellas, la combinación de fagos y sus proteínas derivadas (endolisinas y polisacárido despolimerasas). La primera combinación consistió en una mezcla de este fago virulento y la proteína quimérica CHAPSH3b. Los resultados revelaron la existencia de sinergia entre ambos antimicrobianos frente a biofilms de 24 h, observándose una mayor reducción en los recuentos de células viables cuando se aplicaron el fago y la proteína quimérica juntos, en comparación con los tratamientos individuales. Por un lado, la proteína lítica reduce la población bacteriana inicial y ayuda a limitar el desarrollo de resistencia al fago durante el tratamiento. Por su parte, el fago previene el recrecimiento de la población bacteriana una vez q la proteína deja de ser activa. La segunda combinación ensayada en este trabajo fue una mezcla del fago *K. rodi* y una polisacárido despolimerasa (Dpo7), los cuales también actuaron de modo sinérgico.

Los resultados obtenidos sugieren que el tratamiento con Dpo7 reduce, pero no elimina, los polisacáridos de la matriz extracelular. Además, ensayos de actividad realizados en cepas mutantes no identificaron los ácidos teicoicos o el PNAG/PIA como el receptor exclusivo de Dpo7, por lo que proponemos que ambos pueden ser degradados por este enzima, o que hay otro polisacárido aún por caracterizar en la superficie bacteriana. Por último, se aisló y caracterizó un nuevo fago virulento, IPLA-AICAT (AICAT), frente a *S. epidermidis*, y se obtuvieron datos acerca de su morfología, estabilidad y genoma. Los resultados mostraron que este fago pertenece a la familia *Herelleviridae* y tiene un amplio rango de huésped frente a cepas clínicas de *S. epidermidis*, teniendo además potencial para la eliminación de biopelículas en combinación con la proteína lítica CHAPSH3b y la vancomicina. En su conjunto, los resultados obtenidos en este trabajo destacan el impacto de las respuestas bacterianas a factores ambientales en las interacciones fago-huésped e indican que la combinación de diferentes antimicrobianos con los bacteriófagos, como proteínas derivadas de fagos y antibióticos, puede ser una alternativa viable para eliminar biofilms de estafilococos de forma eficaz.

RESUMEN (en Inglés)

The gradual increase in antibiotic resistance in bacteria is one of the biggest threats nowadays, not only affecting human health, but also the global economy, since antimicrobial resistance (AMR) treatment could cost the world's economy billions by 2050. *Staphylococcus aureus* and *Staphylococcus epidermidis* are significant causative agents of nosocomial infections, often associated with biofilm formation. *S. aureus* is also involved in food poisoning due to its ability to produce enterotoxins. In this context, phage therapy is being proposed as a safe alternative strategy to conventional antimicrobials that could help to control the spread of antibiotic resistance. However, phage-based regimes need to be optimised to successfully achieve biofilm removal. This work reports several strategies aimed at maximizing antibiofilm efficacy of phages against these two pathogens in clinical settings and food industries. First, the impact of temperature on infection by the *S. aureus* phage *Kayvirus rodi* (phiIPLA-RODI) was explored. Our data show that this phage was more effective against both planktonic and biofilm *S. aureus* cultures at room temperature (25 ºC) compared to body temperature (37 ºC) for several strains with varying degrees of phage susceptibility. Therefore, *K. rodi* phage would be a very good candidate for surface decontamination at room temperature, but its therapeutic potential in the clinic would not be so consistent, depending on the susceptibility of the individual strains. These results led to exploration of different strategies that allow more efficacious elimination of *S. aureus* biofilms by *K. rodi* at human body temperature, studying the combination of phages with their derived proteins (lysins and polysaccharide depolymerases). The first combination was made with this virulent phage and the chimeric protein CHAPSH3b. The results revealed the existence of synergy between both antimicrobials in 24-h-old biofilms, with greater reduction in viable cell counts observed when phage and lysin were applied together compared to the individual treatments. CHAPSH3b helps deplete the starting bacterial population and curtail the development of phage resistance during treatment. In turn, the phage keeps bacterial regrowth under control after the lytic protein ceases to be active. The second combination tested in this work

consisted of *K. rodi* and a polysaccharide depolymerase (Dpo7), which also exhibited a synergistic interaction. The results suggested that Dpo7 treatment reduced but not eliminated extracellular matrix polysaccharides. Activity assays on mutant strains did not identify teichoic acids or PNAG/PIA as the exclusive target of Dpo7, proposing that may be both are degraded by this enzyme or that there is another unexplored target polysaccharide on the bacterial surface. Lastly, a new virulent phage infecting *S. epidermidis*, *Staphylococcus* phage IPLA-AICAT (AICAT), was isolated and characterised in terms of morphology, stability and genome sequence. This phage belongs to the *Herelleviridae* family having a wide-host range against clinically-relevant *S. epidermidis* strains. Besides, it showed a good potential for biofilm removal in combination with the lytic protein CHAPSH3b and vancomycin. Overall, this information highlights the impact of bacterial responses to environmental factors on phage-host interactions and demonstrates that the combination of different antimicrobials, such as phage derived proteins or antibiotics, with bacteriophages can be a viable strategy to combat staphylococcal biofilms.

SR. PRESIDENTE DE LA COMISIÓN ACADÉMICA DEL PROGRAMA DE DOCTORADO EN _____

TABLE OF CONTENTS

LIST OF FIGURES

1. Introduction

3. Experimental work

Chapter 1

Chapter 2

Chapter 3

7. Suplementary Material

LIST OF TABLES

3. Experimental work

Chapter 1

Chapter 2

Chapter 3

7. Suplementary Material

LIST OF ABBREVIATIONS

Abi – Abortive infection

agr – Accessory gene regulator

AIP – Autoinducing peptide

AMPs – Antimicrobial peptides

attB – Bacterial attachment site

attP – Phage attachment site

Bap – Biofilm-associated protein

CA-MRSA – Community-associated MRSA

Cas – CRISPR Associated (proteins)

ClfA – Clumping factor A

ClfB – Clumping factor B

CoNS – coagulase-negative staphylococci

CoPS – Coagulase-positive staphylococci

CP – Capsular polysacchride

CRISPR – Clustered Regularly Interspaced Short Palindromic Repeats

dsDNA – Double-stranded DNA

dsRNA – Double-stranded RNA

Eap – Extracellular adherence protein

eDNA – Extracellular DNA

EFSA – European Food and safety Authority

EMA – European Medicines Agency

EPS – Extracellular polymeric substance

ESBL – Extended spectrum β-lactamase

FBOs – Foodborne outbreaks

Fnbp – Fibronectin-binding proteins

Gro-P – Glycerol phosphate

HA-MRSA – Hospital-acquired MRSA

Hlb – Beta toxin

ICTV – International Committee on Taxonomy of Viruses

LA-MRSA – Livestock-associated MRSA

LPS – Surface lipopolysaccharides

LTA – Lipoteichoic acid

MDR – Multidrug resistance

mecA – Methicillin-resistance gene

MRSA – Methicillin-resistant *Staphylococcus aureus*

MRSE – Methicillin-resistant *Staphylococcus epidermidis*

MSCRAMMs – Microbial surface components recognizing adhesive matrix molecules

PAS – Phage antibiotic synergy

PBP2a – Penicillin-binding protein 2a

PBPs – Penicillin-binding proteins

PGA – Poly-γ-DL-glutamic acid

PIA – Polysaccharide intercellular adhesion

PJI – Periprosthetic Joint Infection

PNAG – Poly-β-1-6-N-acetylglucosamine

PSMs – Phenol-soluble modulins

QS – Quorum-sensing

Rbo-P – Ribitol phosphate

RBPs – Receptor binding proteins

R-M – Restriction-Modification

SaPIs – *S. aureus* pathogenicity islands

SCC*mec* – Staphylococcal chromosome cassette *mec*

SE*l* – Staphylococcal enterotoxin-like

SEs – Staphylococcal enterotoxins

SrrAB – Staphylococcal respiratory response regulator

ssDNA – Single-stranded DNA

ssRNA – Single-stranded RNA

STEC – Shiga toxin-producing *E. coli*

TSST – Toxic shock syndrome toxin

USDA – US Department of Agriculture

VAPGHs – Virion-associated peptidoglycan hydrolases

VRE – Vancomycin-resistant enterococci

VRSA – Vancomycin-resistant *Staphylococcus aureus*

VRSE – Vancomycin-resistant *Staphylococcus epidermidis*

WHO – World Health Organization

WTA – Wall teichoic acid

ABSTRACT
RESUMEN

ABSTRACT

The gradual increase in antibiotic resistance in bacteria is one of the biggest threats nowadays, not only affecting human health, but also the global economy, since antimicrobial resistance (AMR) treatment could cost the world's economy billions by 2050. *Staphylococcus aureus* and *Staphylococcus epidermidis* are significant causative agents of nosocomial infections, often associated with biofilm formation. *S. aureus* is also involved in food poisoning due to its ability to produce enterotoxins. In this context, phage therapy is being proposed as a safe alternative strategy to conventional antimicrobials that could help to control the spread of antibiotic resistance. However, phage-based regimes need to be optimised to successfully achieve biofilm removal. This work reports several strategies aimed at maximizing antibiofilm efficacy of phages against these two pathogens in clinical settings and food industries. First, the impact of temperature on infection by the *S. aureus* phage *Kayvirus rodi* (phiIPLA-RODI) was explored. Our data show that this phage was more effective against both planktonic and biofilm *S. aureus* cultures at room temperature (25 ºC) compared to body temperature (37 ºC) for several strains with varying degrees of phage susceptibility. Therefore, *K. rodi* phage would be a very good candidate for surface decontamination at room temperature, but its therapeutic potential in the clinic would not be so consistent, depending on the susceptibility of the individual strains. These results led to exploration of different strategies that allow more efficacious elimination of *S. aureus* biofilms by *K. rodi* at human body temperature, studying the combination of phages with their derived proteins (lysins and polysaccharide depolymerases). The first combination was made with this virulent phage and the chimeric protein CHAPSH3b. The results revealed the existence of synergy between both antimicrobials in 24-h-old biofilms, with greater reduction in viable cell counts observed when phage and lysin were applied together compared to the individual treatments. CHAPSH3b helps deplete the starting bacterial population and curtail the development of phage resistance during treatment. In turn, the phage keeps bacterial regrowth under control after the lytic protein ceases to be active. The second combination tested in this work consisted of *K. rodi* and a polysaccharide depolymerase (Dpo7), which also exhibited a synergistic interaction. The results suggested that Dpo7 treatment reduced but not eliminated extracellular matrix polysaccharides. Activity assays on mutant strains did not identify teichoic acids or PNAG/PIA as the exclusive target of Dpo7, proposing that may be both are degraded by this enzyme or that there is

another unexplored target polysaccharide on the bacterial surface. Lastly, a new virulent phage infecting *S. epidermidis*, *Staphylococcus* phage IPLA-AICAT (AICAT), was isolated and characterised in terms of morphology, stability and genome sequence. This phage belongs to the *Herelleviridae* family having a wide-host range against clinically-relevant *S. epidermidis* strains. Besides, it showed a good potential for biofilm removal in combination with the lytic protein CHAPSH3b and vancomycin. Overall, this information highlights the impact of bacterial responses to environmental factors on phage-host interactions and demonstrates that the combination of different antimicrobials, such as phage derived proteins or antibiotics, with bacteriophages can be a viable strategy to combat staphylococcal biofilms.

RESUMEN

El aumento gradual de la resistencia a los antibióticos en bacterias patógenas es una de las mayores amenazas a día de hoy, no solo afectando a la salud humana, sino también a la economía mundial, estimándose que el tratamiento de la resistencia a los antibióticos podría costar billones a la economía mundial en el año 2050. *Staphylococcus aureus* y *Staphylococcus epidermidis* son dos agentes causantes habituales de infecciones nosocomiales, frecuentemente asociadas con la formación de biopelículas. Además, *S. aureus* está implicado en intoxicaciones alimentarias debido a su capacidad para producir enterotoxinas. En este contexto, la terapia fágica se propone como una estrategia segura frente a los antimicrobianos convencionales que podría ayudar a controlar la propagación de la resistencia a los antibióticos. En esta Tesis, se han estudiado varias estrategias encaminadas a optimizar la utilización de los bacteriófagos para combatir estos dos patógenos en entornos clínicos e industrias alimentarias. En primer lugar, se evaluó el impacto de la temperatura en la infección por el fago *Kayvirus rodi* (phiIPLA-RODI). Los datos obtenidos mostraron que este fago es más eficaz a temperatura ambiente (25 ºC) que a temperatura corporal (37 ºC) para la eliminación de cultivos planctónicos y biofilms de varias cepas de *S. aureus* con distintos grados de susceptibilidad. Por ello, *K. rodi* es un buen candidato para la descontaminación de superficies a temperatura ambiente, pero su eficacia en el contexto clínico estaría restringida a las cepas más susceptibles. Estos resultados llevaron a la exploración de diferentes estrategias para la eliminación más eficaz de biopelículas de *S. aureus* por *K. rodi* a temperatura corporal, entre ellas, la combinación de fagos y sus proteínas derivadas (endolisinas y polisacárido despolimerasas). La primera combinación consistió en una mezcla de este fago virulento y la proteína quimérica CHAPSH3b. Los resultados revelaron la existencia de sinergia entre ambos antimicrobianos frente a biofilms de 24 h, observándose una mayor reducción en los recuentos de células viables cuando se aplicaron el fago y la proteína quimérica juntos, en comparación con los tratamientos individuales. Por un lado, la proteína lítica reduce la población bacteriana inicial y ayuda a limitar el desarrollo de resistencia al fago durante el tratamiento. Por su parte, el fago previene el recrecimiento de la población bacteriana una vez q la proteína deja de ser activa. La segunda combinación ensayada en este trabajo fue una mezcla del fago *K. rodi* y una polisacárido despolimerasa (Dpo7), los cuales también actuaron de modo sinérgico. Los resultados

obtenidos sugieren que el tratamiento con Dpo7 reduce, pero no elimina, los polisacáridos de la matriz extracelular. Además, ensayos de actividad realizados en cepas mutantes no identificaron los ácidos teicoicos o el PNAG/PIA como el receptor exclusivo de Dpo7, por lo que proponemos que ambos pueden ser degradados por este enzima, o que hay otro polisacárido aún por caracterizar en la superficie bacteriana. Por último, se aisló y caracterizó un nuevo fago virulento, IPLA-AICAT (AICAT), frente a *S. epidermidis*, y se obtuvieron datos acerca de su morfología, estabilidad y genoma. Los resultados mostraron que este fago pertenece a la familia *Herelleviridae* y tiene un amplio rango de huésped frente a cepas clínicas de *S. epidermidis*, teniendo además potencial para la eliminación de biopelículas en combinación con la proteína lítica CHAPSH3b y la vancomicina. En su conjunto, los resultados obtenidos en este trabajo destacan el impacto de las respuestas bacterianas a factores ambientales en las interacciones fago-huésped e indican que la combinación de diferentes antimicrobianos con los bacteriófagos, como proteínas derivadas de fagos y antibióticos, puede ser una alternativa viable para eliminar biofilms de estafilococos de forma eficaz.

INTRODUCTION

1. INTRODUCTION

1.1. Antibiotic resistance: A worldwide public health concern

Antibiotic resistance is a pressing global issue that has been intensified by the widespread use of antibiotics in various fields. Indeed, isolation of microorganisms carrying resistance determinants has been observed in remarkably diverse settings, including hospitals, communities, foods and the environment. Recognizing the importance of the situation, various international agencies and countries have acknowledged the necessity of implementing a One Health approach to address antimicrobial resistance (Collignon and McEwen, 2019). The concept of One Health is defined by the World Health Organization (WHO) and the One Health High Level Expert Panel as an integrated unifying approach that aims to sustainably balance and optimize the health of people, animals and ecosystems, tackling the design and implement programs, policies, legislation and research involving the coordination of multiple sectors. The areas of work in which this One Health approach proves to be especially relevant include ensuring food and water safety, the control of zoonoses (diseases that can spread between animals and humans, such as the flu, rabies and the Rift Valley fever), pollution management and combating antibiotic resistance (World Health Organization, 2017; Adisasmito *et al.*, 2022). Some of the most infamous antibiotic-resistant bacteria belong to the so-called ESKAPE group: *Enterococcus faecium, Staphylococcus aureus, Klebsiella pneumoniae, Acinetobacter baumanii, Pseudomonas aeruginosa,* and *Enterobacter* sp., which are major nosocomial pathogens, known for their ability to quickly acquire resistance to multiple drugs. However, antibiotic resistance affects pretty much all species of clinical importance.

The food chain has also been identified as a major point of transmission of antibiotic resistance determinants amongst bacteria, both pathogenic and non-pathogenic, that can subsequently reach the clinical environment (Bengtsson-Palme, 2017; Flórez *et al.*, 2021). To solve this problem, on 28 January 2022, new rules restricting the use of veterinary antimicrobials started to be applied across the EU, banning the routine use of antibiotics and restricting preventive use to exceptional treatments of individual animals. Similarly, the USDA (US Department of Agriculture) has released a new rule, effective from June 2023, which requires animal owners to obtain a veterinary prescription in order to purchase antibiotics (EMA, 2020; Schmerold *et al.*, 2023). This highlights the importance of controlling the presence of antibiotic-resistant microorganisms during food

production, when used as therapeutics or as growth promoters. Indeed, antimicrobial resistance data on zoonotic bacteria from humans, animals and food are collected in some countries, e.g., data on *Salmonella* spp., *Campylobacter jejuni* and *Campylobacter coli* in humans and food-producing animals (broilers, laying hens and turkeys, fattening pigs and bovines) and meat. Also, extended spectrum β-lactamase (ESBL)-/AmpC β-lactamases (AmpC)-/carbapenemases (CP)-producing *Escherichia coli* and methicillin-resistant *S. aureus* (MRSA) strains are monitored in animals and meat (EFSA and ECDC, 2023b).

One way of controlling the spread of antibiotic resistance in the food sector is by raising food safety standards. Indeed, foodborne outbreaks (FBOs) still occur despite the dramatic improvements made in this field over the past decades. Indeed, the burden of foodborne diseases remains a significant public health concern worldwide, with the latest data showing an upward trend in the number of outbreaks caused by certain pathogens (EFSA and ECDC, 2023a). A particular threat is posed by the emergence of evolving foodborne pathogens, a dynamic process linked to the potential of microorganisms to acquire new virulence factors and antibiotic resistance genes (Banerji *et al.*, 2021). Additionally, emerging foodborne pathogens are gaining significance such as non-O157 Shiga toxin-producing *E. coli* (STEC), *Arcobacter butzleri*, and *Helicobacter pullorum* (Akhlaghi *et al.*, 2024). Foodborne illnesses result from the ingestion of food or water contaminated with bacteria and/or their toxins, parasites, viruses, chemicals, or other agents. The last report published by the European Food and safety Authority (EFSA) indicated that 5,763 FBOs, 48,605 cases of illness, 2,783 hospitalisations and 64 deaths were reported in 2022 (EFSA and ECDC, 2023a). In many cases, serious outbreaks are caused by products manufactured from food-producing animals, which are the major reservoirs for many foodborne pathogens. Amongst bacteria, the most relevant pathogens include *E. coli* O157:H7, *Salmonella, Listeria monocytogenes, Campylobacter, S. aureus* and *Clostridium*. These microorganisms are the most recurrent causes of food-related disease and mortality worldwide and present an evident challenge for the food industry and health authorities (Lee and Yoon, 2021). Indeed, according to "The European Union One Health 2022 Zoonoses Report", campylobacteriosis was confirmed as the most commonly reported zoonosis (61.3%), followed by salmonellosis, yersiniosis, STEC infections and listeriosis (EFSA and ECDC, 2023a; CDC, 2024). However, FBOs are not always due to ingestion of live bacteria. Bacterial toxins are also drawn in this problem, with illnesses due to their consumption rating 0.25 per 100,000 inhabitants. In 2022, *S.*

aureus enterotoxins were the second most frequently reported bacterial toxin in the EU, and first for the number of hospitalisations and deaths, being dairy products the main food category associated with these toxins (EFSA and ECDC, 2023a).

1.2. *S. aureus* and *Staphylococcus epidermidis*

1.2.1. Description and taxonomy

The genus *Staphylococcus* belongs to the family *Staphylococcaceae*, order Bacillales, class Bacilli, phylum Bacillota (formerly known as Firmicutes), and comprises more than 40 species of facultative anaerobic Gram-positive bacteria. The cells are spherical, and can appear as single cells, paired cocci, short chains or forming grape-like clusters. Staphylococci are catalase-positive, non-motile and non-sporulating. Members of this genus are ubiquitous in the environment and can be found in air, dust, humans (nose and skin), animals and diverse environmental surfaces (Argudín *et al.*, 2010). Even though most species are harmless to humans and animals, some can behave as pathogens, giving rise to diverse infections of veterinary or clinical importance (Nocera *et al.*, 2023). The most relevant species in the context of human medicine are *S. aureus* and *S. epidermidis*, *S. aureus* being the best characterized due to its virulence and antimicrobial resistance (Lindsay, 2019). One of *S. aureus* virulence factors is the production of coagulases, polypeptides that bind to and activate prothrombin, which, in turn, converts fibrinogen to fibrin and promotes the clotting of plasma or blood. The ability of coagulases to mediate adhesion and contribute to the lethality of bacteremia underscore their importance in staphylococcal infections (McAdow *et al.*, 2012). Based on the production of these peptides, staphylococci can be divided into two different categories: coagulase-positive staphylococci (CoPS) and coagulase-negative staphylococci (CoNS).

S. aureus is both a human commensal microorganism and a pathogen, belonging to the CoPS. This bacterium has been associated with multiple diseases including moderate to severe infections, such as sepsis, osteomyelitis and pneumonia, as well as foodborne illness resulting from the ingestion of enterotoxins produced by some strains (Kadariya *et al.*, 2014). In this context, *S. aureus* is one of the most frequent pathogens isolated from foods of animal origin. Many strains have zoonotic potential, moving between humans and animals, including livestock, pets, and wildlife (Kadariya *et al.*, 2014; Ghabbour *et al.*, 2022). The versatility of this microorganism is related to its possession of diverse virulence factors, such as the production of enterotoxins, DNAses or coagulases, and its

antibiotic resistance (Ortega *et al.*, 2010). In this sense, the WHO has recently included *S. aureus* on the list of bacteria for which new antibiotics are urgently needed, specifically methicillin- and vancomycin-resistant strains (MRSA and VRSA, respectively) (WHO, 2017).

In contrast to *S. aureus*, *S. epidermidis* is included in the CoNS. This commensal bacterium is part of the human microbiota, being one of the most abundant inhabitants of skin and mucosae. Indeed, colonization by this microorganism promotes skin barrier development, maintains homeostasis, actively coordinates the skin response to injury and controls invasion by opportunistic pathogens through the secretion of phenol soluble modulins (PSMs), which have protective functions on the skin and promote the production of host antimicrobial peptides (AMPs) (Severn and Horswill, 2023). Even though it may seem harmless, this bacterium is an opportunistic pathogen responsible for a variety of device-related infections in humans, particularly orthopedic-device-associated infections (Brescó *et al.*, 2017). Antibiotic resistance is also a problem in this species, especially methicillin resistant strains (MRSE).

1.2.2. Main virulence factors

S. aureus produces a plethora of virulence factors that contribute to its pathogenicity and ability to cause infections. Some of these virulence factors are shared by *S. epidermidis*, although the virulence arsenal of this species is fairly small in comparison with its infamous relative (Figure 1.1). Both strains have the capacity to adhere to biotic and abiotic surfaces. The interaction with biotic surfaces, like human tissues, is facilitated by a diverse set of connections between the receptor and microbial surface components recognizing adhesive matrix molecules (MSCRAMMs). In *S. aureus* these surface proteins are used by bacteria to interact with host molecules, such as collagen (mostly via Cna), fibronectin (via FnbAB), and fibrinogen (with ClfAB and Fib), thereby mediating adherence to components of the host extracellular matrix (Vazquez *et al.*, 2011). Another type of cell wall-anchored proteins implicated in adhesion and immune evasion includes clumping factor A (ClfA) and clumping factor B (ClfB), as well as the fibronectin-binding proteins (FnbpA and FnbpB), which are associated to tissue invasion, and contribute to the development of arthritis, endocarditis and invasion of the endothelium (Foster *et al.*, 2014). *S. aureus* also produces a multifunctional cell wall-anchored protein, named protein A, that interacts with human IgG, contributing to immune evasion (Palmqvist *et*

al., 2002). In the case of *S. epidermidis*, SdrG stands out as one of the best-known and most extensively studied adhesins; however, other proteins such as SdrF, SesC and Embp are involved in the adhesion of this bacterium due to their affinity to collagen and keratin, fibrinogen and fibronectin, respectively (França *et al.*, 2021).

The different components of the cell wall also participate in virulence. For example, the capsular polysaccharide (CP) is an extracellular component that serves as an essential virulence factor due its anti-phagocytic properties, which are important for immune evasion by masking surface proteins (Keinhörster *et al.*, 2019). To date, there are eleven types of CP known in *S. aureus*, although only two serotypes, type 5 and type 8, are clinically relevant since they are predominant among clinical infection isolates from various geographic origins. Strains with these serotypes produce nonmucoid colonies and their morphology is indistinguishable from that of strains lacking a capsule. Indeed, most staphylococcal strains are considered microencapsulated, with the exception of serotypes 1 and 2, which are heavily encapsulated (Watts *et al.*, 2005). In the case of *S. epidermidis*, some strains produce an extracellular polymer called poly-γ-DL-glutamic acid (PGA), an anionic macromolecule located on the surface and covalently linked to peptidoglycan. This capsule facilitates bacterial growth and survival in high osmolarity environments, such as the human host, and prevents phagocytosis by neutrophils (Kocianova *et al.*, 2005). The polysaccharide intercellular adhesin (PIA) also represents a particularly important constituent of the immune evasion strategies in *S. epidermidis* strains, forming a positively-charged capsule around the cells, which is a general mechanism to shield bacteria from immune recognition (Le *et al.*, 2018).

Teichoic acids are anionic polymers that play a crucial role in maintaining the structural integrity of the cell wall and are involved in various cellular processes. They can be classified into wall teichoic acids (WTAs) and lipoteichoic acids (LTAs), based on their linkage to either peptidoglycan or the cytoplasmic membrane, respectively (Ultee *et al.*, 2020). The composition of peptidoglycan-bound WTAs varies among organisms and species, but the most common structures contain either glycerol phosphate (Gro-P) or ribitol phosphate (Rbo-P) repeating units. In *S. epidermidis*, WTAs are composed of Gro-P repeating units, substituted with glucose, galactose and N-acetylated aminosugars, as well as D-alanyl, L-lysyl or acetyl residues, whereas *S. aureus* WTAs consist of Rbo-P repeating units in which the ribitol residue may be substituted with D-alanine (D-Ala) or N-acetyl-D-glucosamine (GlcNAc) (Holland *et al.*, 2011; Brown *et al.*, 2013). WTAs are

involved in the interaction of Gram-positive bacteria with their host cells, and mediate other biological roles. Glycosyl modifications on WTAs are critical for pathogenesis, immunological recognition, antibiotic resistance, phage infection and attachment of cell wall hydrolases (Brown et al., 2012, 2013). In *S. aureus*, the enzymes responsible for WTA GlcNAcylation are the α-glycosyltransferase *tarM* and the β-glycosyltransferase *tarS*. Both these enzymes reside in the cytoplasm and decorate nascent WTA chains before transport and attachment to the peptidoglycan sacculus (Sobhanifar *et al.*, 2016).

Apart from virulence-related structural components, these bacteria also have the ability to synthetize toxins. *S. aureus* produces a wide range of enterotoxins, during the logarithmic phase of growth or through the transition from the exponential phase to the stationary phase (Derzelle *et al.*, 2009). Staphylococcal enterotoxins (SEs), one of the most important virulence factors in *S. aureus*, are members of a family of nine major serological types of heat stable enterotoxins (SEA, SEB, SEC, SED, SEE, SEG, SEH, SEI, and SEF) (Kadariya *et al.*, 2014). They are active in low and high quantities (an estimated 0.1 μg of SEs can cause staphylococcal food poisoning in humans) and are resistant to environmental conditions like temperature and low pH. They are also resistant to proteolytic enzymes such as pepsin or trypsin, enabling them to be fully functional in the gastrointestinal tract after ingestion. SEA is the most common toxin implicated in *S. aureus* food poisoning outbreaks. The high incidence of food poisoning is attributed to inadequate pasteurization or decontamination of the original product source, as well as contamination during food preparation and handling by carriers of the organism. The disease has a short incubation period and is characterized by symptoms such as nausea, vomiting, abdominal pain, cramps, and diarrhea (Argudín *et al.*, 2010). Staphylococcal enterotoxin-like (SE*l*s) toxins are another group of exotoxins closely related to SEs, associated with shock-like syndromes (Benkerroum, 2018). The best known *S. aureus* superantigen is the toxic shock syndrome toxin (TSST), an acute systemic illness characterized by hypotension, fever and rash (Otto, 2014). Moreover, *S. aureus* produces a collection of pore-forming toxins capable of targeted killing of select host cells by creating channels in the plasma membrane, called leukotoxins (Yoong and Torres, 2013). Unlike *S. aureus*, *S. epidermidis* does not usually cause infections in healthy individuals. Of note, the only toxin produced by *S. epidermidis* is the N-formylated alpha-helical peptide δ-toxin (McKevitt *et al.*, 1990), which has been implicated in subacute or chronic infections (Vuong and Otto, 2002).

Both *S. aureus* and *S. epidermidis* secrete other enzymes that also contribute to pathogenicity. For instance, *S. aureus* secretes a variety of enzymes, including hemolysins, serine proteases, hyaluronidase, lipases, and cysteine proteases that are involved in processes such as tissue penetration, induction of vascular leakage, and evasion of host immune responses. In comparison, *S. epidermidis* produces fewer tissue-destructive enzymes, although the production of hemolysin and proteases has also been described in this species (Oleksy *et al.*, 2004). The expression of these enzymes is tightly coordinated in a highly complex process involving various regulatory networks. Some of the regulators involved include the staphylococcal accessory gene regulator (*agr*), SaeRS, SrrAB and ArlSR, among others (Cheung *et al.*, 2021). The most extensively studied is *agr*, which is a quorum-sensing (QS) system that controls the transition from exponential to stationary growth phases (Yarwood and Schlievert, 2003; Olson *et al.*, 2014). In this sense, the products of the *agrD* and *agrB* genes allow the synthesis, modification and secretion of an autoinducing peptide (AIP) that accumulates throughout bacterial growth. When bacterial density increases, the AIP activates the transmembrane protein AgrC that further activates AgrA and finally promotes the expression of target genes (Peng *et al.*, 2023).

Regarding the spread of pathogenicity determinants, it is worth mentioning the *S. aureus* pathogenicity islands (SaPIs), genetic elements (14–27 kb) that contain phage-like elements, as well as genes encoding superantigen toxins and other virulence and antibiotic resistance factors. SaPIs are mobilized by specific bacteriophages (phages). When a so-called helper phage infects a host cell, a phage proteins bind to the SaPi, which gets excised and starts to replicate, ultimately being packaged into phage-like particles that can infect new host bacteria (Tormo-Más *et al.*, 2010; Chee *et al.*, 2023).

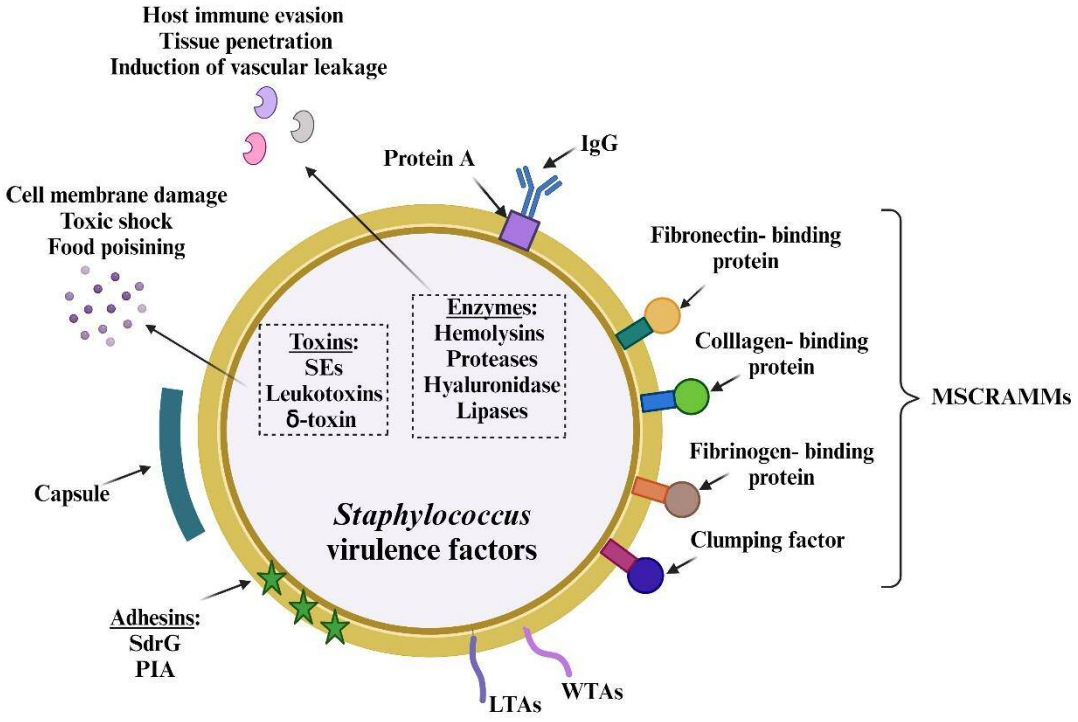

Figure 1.1 – Main virulence factors of *S. aureus* and *S. epidermidis.* (Created with BioRender.com)

1.2.3. Resistance to antibiotics

Infections caused by staphylococci used to be commonly treated with β-lactams, an antibiotic class that comprises penicillins, cephalosporins, monobactams, and carbapenems. These antibiotics are bactericidal agents that interrupt bacterial cell-wall formation as a result of covalent binding to essential penicillin-binding proteins (PBPs), enzymes that are involved in the terminal steps of peptidoglycan cross-linking (Lobritz *et al.*, 2022). However, their efficacy against staphylococcal infections has been dwindling due to the gradual acquisition of resistance by these bacteria. For example, penicillin resistance was observed only 10 years after introduction of this antibiotic in the clinic due to transfer of a plasmid harbouring the penicillinase-coding gene *penZ* (now *blaZ*), affecting 80% of all isolates just two decades later (Novick and Bouanchaudt, 1971; Chambers, 2001). This prompted the development of penicillinase-resistant β-lactams, which include methicillin. Once again, resistance arose soon after this new compound became available, leading to the selection and spread of MRSA and MRSE strains. There are three potential mechanisms that explain resistance to methicillin: the production of β-

lactamases, modification of transpeptidases and intrinsic resistance to methicillin. Intrinsic resistance is mediated by the *mecA* gene (methicillin-resistance gene) located in the staphylococcal chromosome cassette *mec* (SCC*mec*), which encodes the low-affinity penicillin-binding protein 2a (PBP2a). This protein is a monofunctional DD-transpeptidase that participates in an essential step in cell wall synthesis, but is refractory to inhibition by β-lactam antibiotics (Archer *et al.*, 1994; Otero *et al.*, 2013). SCC*mec* types in CoNS are more heterogeneous than those in MRSA, suggesting the possibility of gene transfer amongst organisms other than staphylococci (Hanssen and Ericson Sollid, 2006; Zhang *et al.*, 2009). In this sense, CoNS have been recognised as reservoirs of SCC*mec* based on evidence of horizontal gene transfer of the SCC*mec* elements from CoNS to *S. aureus* together with the diversity of these elements in CoNS species (Martínez-Meléndez *et al.*, 2015; Liu *et al.*, 2016). Indeed, genes conferring resistance to numerous antibiotics are usually located on mobile genetic elements, circulating in different environments (hospitals, veterinary, and effluents) and geographical locations (Silva *et al.*, 2022). At first, methicillin resistant strains were isolated from hospitalized patients, the so-called hospital-acquired MRSA (HA-MRSA). Later on, MRSA infections began to appear in the community, in people with no contact with the hospital environment, and were therefore called community-associated MRSA (CA-MRSA). HA-MRSA are usually more resistant to drugs than CA-MRSA (Marcotte and Trzeciak, 2003). More recently, MRSA strains have been isolated from different animal species, and are called livestock-associated MRSA (LA-MRSA). Most LA-MRSA have been found in people who have direct contact with animals (Crespo-Piazuelo and Lawlor, 2021). Despite the seriousness of the situation, during the period 2017-2021, there was a significant decrease in the EU/EEA population-weighted percentage of MRSA isolates from 18.4% to 15.8%. Nevertheless, MRSA is still an important pathogen in the EU/EEA, with percentages remaining high in several countries (ECDC and WHO, 2023). Resistant strains are frequently isolated in foods from animal origin, especially milk and meat. In the case of *S. aureus*, it can enter the food chain at different points, e.g. from livestock, which constitutes a health problem at the level of primary production (EFSA and ECDC, 2023a). Thus, this microbe causes important infections such as mastitis in dairy cattle or dermatitis in pigs (Park *et al.*, 2013; Silva *et al.*, 2014). These infections generally require the use of antibiotics, which in turn contributes to the selection of resistant strains.

Due to the increase in infections caused by MRSA and MRSE, new antibiotics against staphylococcal infections have been introduced in medical practice: the glycopeptides vancomycin and teicoplanin, linezolid and daptomycin. Vancomycin is the last resort drug of choice to treat MRSA infections. This antibiotic inhibits the late stages of peptidoglycan synthesis by binding to D-Ala-D-Ala termini of the pentapeptide-ending precursors localized at the outer surface of the cytoplasmic membrane (van Bambeke *et al.*, 2017). However, acquisition of the *vanA* cluster from vancomycin-resistant enterococci (VRE) led to the appearance of VRSA and vancomycin-resistant *S. epidermidis* (VRSE). Genes in this cluster encode proteins that reprogram cell wall biosynthesis, thus evading the action of the antibiotic (Binda *et al.*, 2014). Resistance to linezolid and daptomycin in *S. aureus* isolates has also been identified, although it is less common (Mendes *et al.*, 2014; Sader *et al.*, 2014).

1.3. Biofilms

1.3.1. Main characteristics

In nature, bacteria tend to adopt a sessile lifestyle to prolong survival on surfaces, both as a single or a mixed species community. Biofilms can be defined as an aggregation of microorganisms embedded within a self-produced matrix of extracellular polymeric substance (Lister and Horswill, 2014; Karygianni *et al.*, 2020). These communities are known to harbour multiple cell types, leading to the development of heterogeneous populations within the extracellular matrix that, in combination with physicochemical gradients, significantly influences their structure and behaviour. Oxygen, pH, chemical gradients, substrate availability and stress have been demonstrated to create microenvironments inside the biofilms where local conditions differ substantially from those in the surrounding solution (Vlamakis *et al.*, 2008; Hidalgo *et al.*, 2009).

The formation of these multicellular structures is a complex process involving the initial adherence of bacterial cells to a biotic or abiotic surface, followed by the production of an extracellular polymeric substance (EPS). This so-called extracellular matrix consists mainly of polysaccharides, proteins and extracellular DNA (eDNA) (Karygianni *et al.*, 2020). In terms of architecture, biofilms can exhibit different 3D shapes, such as mushroom-like, pillar-like, hilly, or flat multicellular structures (Pamp *et al.*, 2009). The EPS of biofilms is one of the major reasons why infections caused by bacterial biofilms are particularly problematic. Indeed, EPS normally offers both protection and stability

from harsh environmental conditions, making it difficult to fully eliminate biofilms by conventional chemical or physical means, and increasing tolerance to antibiotics when compared to their planktonic (free swimming) counterparts (Flemming and Wingender, 2010). Additionally, the biofilm extracellular matrix can be considered a hotspot for the diffusion of antibiotic resistance genes due to the greater frequency and speed of horizontal gene transfer, thus acting as a reservoir of multidrug-resistant cells (Michaelis and Grohmann, 2023). Bacteria can also acquire or develop antibiotic resistance via spontaneous mutations in their chromosomal genes. Some studies have identified an increase in the mutation rate associated with the sessile lifestyle (Driffield *et al.*, 2008). However, most of the apparent resistance or regrowth of bacteria within the biofilm arises from the greater presence of metabolically inactive persister cells compared to planktonic populations (Lewis, 2008; Qu *et al.*, 2010). The slow growth and severely limited metabolic activity of these cells may prevent the action of many antibiotics. Moreover, the presence of different conditions such as oxygen and nutrient limitation, leads to different metabolic cell states and, consequently, to the existence of distinct zones within the biofilm exhibiting varying degrees of resistance or tolerance to antimicrobials (De la Fuente-Núñez *et al.*, 2013).

1.3.2. Biofilm development

Biofilm formation can be divided into three main stages: attachment to a surface, proliferation and formation of the mature biofilm structure, and finally dispersion (Figure 1.2). This process involves an army of regulatory factors and molecular mechanisms. In the first stage, individual cells adhere to a surface in a reversible manner. Then, cells start to produce EPS, which provides structural support to the adhered cells. At this stage, the biofilm cells acquire characteristics distinct from their planktonic forms and start to interact with each other. Indeed, EPS plays a key role in signalling, participating in the regulation of gene expression and coordinating the behaviour of cells within the biofilm. Another important function of the EPS is in genetic exchange. The EPS matrix can facilitate the transfer of genetic material between cells within the biofilm, promoting genetic diversity and enhancing the adaptability of the biofilm community including cohesion, scaffolding, stability and protection against antibiotics (Karygianni *et al.*, 2020). Then adherence becomes irreversible, indicating the beginning of biofilm maturation. Biofilm cells continue to produce EPS until the structure reaches a maximum

thickness. Maturation is associated with the upregulation of microbial metabolic genes. This is exemplified by a switch from aerobic energy production to fermentative processes, and a general downregulation of active cell processes, such as protein, DNA, and cell wall biosynthesis (Vlaeminck *et al.*, 2022). Furthermore, the involvement of cell-to-cell signals and the release of eDNA have been identified as critical factors, highlighting the importance of intercellular communication and matrix components during this stage (DeFrancesco *et al.*, 2017). In the final stage, detachment and dispersion, single cells are allowed to escape from the biofilm structure and resume a planktonic lifestyle. This process is essential for bacteria to colonize new habitats and is implicated in the transmission of bacteria from environmental reservoirs to human hosts, as well as in the exacerbation and spread of infections within a host (Ibáñez de Aldecoa *et al.*, 2017; Rumbaugh and Sauer, 2020). This mechanism is cyclic and the microbial cells released from a mature biofilm can attach to new surfaces to form a new biofilm (Costerton *et al.*, 1978).

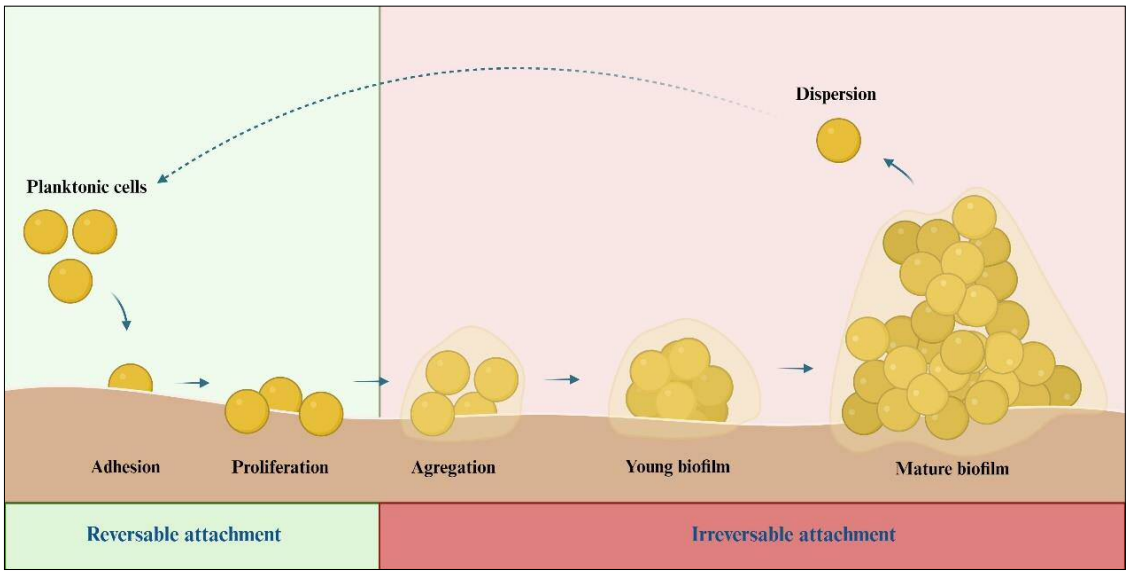

Figure 1.2 – Stages of biofilm formation and development. (Created with BioRender.com)

1.3.3. Biofilms formed by *Staphylococcus*

The primary adherence of *Staphylococcus* is arbitrated by the hydrophobic interactions between bacteria and surfaces. This adherence is mediated by the expression of surface proteins, such as MSCRAMMs, which have hydrophobic regions that facilitate binding to hydrophobic surfaces. There are two families of MSCRAMMs in *S. aureus*: those that are related to ClfA and those that are similar to the collagen-binding protein (the Cna family). These proteins bind ligands by mechanisms that involve large conformational changes exemplified by the ability of ClfA and SdrG to bind to fibrinogen and the collagen-binding capability of Cna (Foster, 2019). Another molecule involved in initial adhesion is the autolysin AtlA, a major peptidoglycan hydrolase that has been shown to aid in cell attachment to surfaces, influencing biofilm formation, contributing to cell separation during division and cell lysis induced by β-lactam antibiotics (Biswas *et al.*, 2006). In *S. epidermidis,* specific adhesion is mediated by bacterial cell wall receptors such as Fbe, SdrG, autolysins (AtlE and Aae), and Embp, which respectively bind to fibrinogen, collagen, vitronectin and fibronectin (Linnes *et al.*, 2012).

In staphylococcal biofilms, the major components of the biofilm matrix include PIA, also known as poly-β-1-6-N-acetylglucosamine (PNAG), eDNA and proteins. The synthesis of PIA/PNAG is carried out by the products of the *ica* operon (*icaADBC*) and is controlled by the regulatory gene *ica*R (Otto, 2009; Nguyen *et al.*, 2020). Bacteria that do not produce this exopolymer are, in general, less adherent than those that do produce it and, therefore, less pathogenic, while strains that produce PNAG are more virulent (Kropec *et al.*, 2005). Surface proteins, such as the biofilm-associated protein (Bap) and SasG, play a crucial role in assembling as scaffold components of the biofilm matrix of *S. aureus*, while eDNA is also an important structural component (Cucarella *et al.*, 2001; Valle *et al.*, 2020). Moreover, *S. aureus* uses cytoplasmic proteins that associate with the cell surface in response to decreasing pH. This matrix facilitates the subsequent binding of eDNA through electrostatic interactions (Foulston *et al.*, 2014; Dengler *et al.*, 2015). However, the importance of individual proteins varies largely between strains. Indeed, Bap-dependent biofilms have not been identified in any human isolates; as such, it is more likely that Bap plays a role in bovine mastitis than in human diseases (Lasa and Penadés, 2006). eDNA is produced through the autolysis of a sub-population of the biofilm cells, mediated through the activity of primary murein hydrolases, encoded by the *atl* and *lytM* genes (Thomas and Hancock, 2009). These hydrolases degrade peptidoglycan during cell

wall rearrangements and cell division. Increased expression of these enzymes allows for autolysis in *S. aureus*, which is regulated through the activity of the *cidABC* and *lrgAB* operons, catalysing the decision of the cell to commit suicide (Lister and Horswill, 2014). Biofilm maturation is associated with the secretion of the extracellular adherence protein (Eap) and beta toxin (Hlb), a neutral sphingomyelinase, found to have a structural role in the *S. aureus* biofilm matrix, in cooperation with eDNA from lysed cells (Sugimoto *et al.*, 2013; Lister and Horswill, 2014). To promote maturation, small amphipathic α-helical peptides with surfactant properties are also secreted, the phenol-soluble modulins (PSMs), which contribute to the biofilm-structuring process. PSMs are also involved in the last stage of the biofilm life cycle, dispersion. Due to their amphipathic properties, PSMs act as a surfactant to disrupt the extracellular polymeric matrix enabling nutrients to be delivered to deeper biofilm layers as well as leading to cell detachment, a prerequisite for the systemic dissemination of a biofilm infection (Le *et al.*, 2019). *S. aureus* also secretes a potent DNAse, known as micrococcal nuclease, that degrades eDNA, and proteinases, involved in the degradation of proteinaceous matrix components. These enzymes also take part in biofilm detachment (Lauderdale *et al.*, 2009; Kiedrowski and Horswill, 2011).

In general, *S. aureus* biofilm development is a multifaceted process influenced by multiple regulatory systems or regulators. One of them is QS signalling via the *agr* and the LuxS/AI-2 systems, which control biofilm formation in different ways. The *agr* system contributes to dispersion of the bacterial biofilm by upregulating the transcription of RNAIII, an effector molecule that induces the expression of secreted virulence factors, such as proteases and toxins, while inhibiting the expression of surface adhesion proteins (Lu *et al.*, 2019). The LuxS/AI-2 system enables bacteria to make collective decisions about the expression of a specific set of genes. In the case of *S. aureus* this system reduces PIA/PNAG production (Boles and Horswill, 2008; Peng *et al.*, 2023), resulting in lesser biofilm formation. Another example is the two-component regulatory system SrrAB (staphylococcal respiratory response regulator). This is a major regulator of respiratory growth and virulence in *S. aureus*, which is critical for survival under environmental conditions such as hypoxia and oxidative stress. In turn, the SaeRS system is a key regulator of toxin and exoprotein production, which is also important in evasion of innate immunity and pathogenesis (Peng *et al.*, 2023). One of the main global regulators of virulence and biofilm formation is the staphylococcal accessory regulator, a DNA-

binding protein encoded by the *sar*A locus (Balamurugan *et al.*, 2017). SarA is necessary for *ica* operon transcription and, as a result, PIA/PNAG production. Another role of *sar*A in biofilm formation is the inhibition of extracellular proteases production (Chan and Foster, 1998; Tormo *et al.*, 2005).

The presence of *S. aureus* and *S. epidermidis* in the form of a biofilm represents a considerable challenge for the food industry and the medical community. Thus, the ability of these bacteria to adhere and form biofilms on various surfaces within hospitals, including medical devices, enhances their persistence in the hospital environment, leading to increased risk of nosocomial infections and antibiotic resistance. Moreover, it has been estimated that between 65 and 80% of all bacterial infections (especially chronic conditions) arise from biofilms, including both device- and non-device-associated infections. Globally, the prevalence of multidrug resistance in biofilms from hospital-acquired infections ranges from 17.9 to 100%. *S. aureus* and *S. epidermidis* are common causative organisms of multidrug-resistant infections, together with *Streptococcus* spp., Gram-negative bacilli, *Enterococcus* and *Candida* spp. These figures are likely to increase due to the frequent use of indwelling medical devices, mechanical heart valves and other implants (Maillard and Centeleghe, 2023). Data regarding device-related infections indicate a prevalence of 2% for breast implants, 2% for joint prostheses, 4% for mechanical heart valves, 10% for ventricular shunts, 4% for pacemakers and defibrillators, and about 40% for ventricular-assisted devices (Jamal *et al.*, 2018).

In the food industry, it is very common to detect the presence of biofilms in various locations, such as pipelines, equipment and various materials, since they can form on practically any type of surface, including plastic, glass, wood, stainless steel and even on the food itself, making them difficult to eradicate through routine cleaning and disinfection practices (Gutiérrez *et al.*, 2016). These biofilms can persist for extended periods, cross-contaminating different surfaces in food processing plants and potentially leading to decreased food quality and safety. Moreover, inadequate disinfection and handling measures in animal husbandry can also eventually result in food poisoning, since bacteria can contaminate milk or meat (Paterson *et al.*, 2012), These cases of contamination are mostly associated with the use of antibiotics, which are extensively used in food animal production. This, in turn contributes to the selection of resistant bacterial strains including foodborne pathogens, which can potentially lead to antibiotic-resistant infections in humans.

1.4. Bacteriophages

1.4.1. Main characteristics

Frederick Twort discovered phages back in 1915 (Twort, 1915); however, it was in 1917 at the Pasteur Institute in Paris that Franco-Canadian microbiologist Félix d'Herelle proposed phages as antimicrobial agents (Fruciano and Bourne, 2007). Phages are viruses that specifically infect bacteria and, therefore, can be considered as natural antimicrobials. With this in mind, d'Herelle explored their use for the treatment of bacterial diseases, a strategy known as phage therapy. About 20 years after the discovery of phages, Alexander Fleming identified the first antibiotic – penicillin. The success of antibiotics along with issues associated with phage therapy, including some early clinical failures, scientific controversies and ethical concerns, dictated the end of phage therapy in the USA and in most Western European countries. Yet, the continuous use of antibiotics in the last century led to a huge rise in antibiotic resistance and, consequently, an increasing number of deaths caused by bacterial infections. This sparked renewed interest in phages for therapeutic applications.

Phages are parasites that invade the bacterial cell and multiply by using the bacterial machinery (Wu *et al.*, 2017). After the infection, they either form a stable association with the host or kill the infected cell. Moreover, phages are highly specialized regarding their target bacterium, and infect the cell through the interaction between phage proteins (receptor binding proteins or RBPs) and specific receptors on the bacterial surface. This specificity gives phages a big advantage over antibiotics; otherwise they would infect commensal bacteria and potentially alter the normal microbiota composition, leading to dysbiosis. Additionally, the mechanism of action of phages is very different from that of antibiotics, which drastically limits the development of cross-resistance. As a result, bacterial viruses are generally able to tackle antibiotic resistant bacteria. Another positive aspect of bacteriophages as antimicrobial agents is their ubiquity. As the most abundant living entities on the planet, phages can be easily found and isolated from bacteria-containing samples (e.g. environmental samples like pond water or soil, sewage water, wastewater from hospitals, or even patients who are recovering from an infection). Another advantage is their self-replicating ability, which, coupled with their specificity and safety profile, is crucial for their effectiveness as therapeutic agents. This property allows phages to remain available for longer periods of time, compared with other types

of antimicrobials, whose concentrations invariably decrease after their application. Furthermore, the existence of a vast pool of phages in nature makes their use more versatile in terms of formulation development and application (Fernández *et al.*, 2019). However, this also poses a challenge in terms of regulatory requirements because of the evolving and/or diverse composition of therapeutic phage preparations.

1.4.2. Morphology and Taxonomy

There are various types of phages, with different sizes and shapes: they can be tailed, polyhedral, filamentous or pleomorphic, and some have lipid or lipoprotein envelopes (Figure 1.3). Generally, the virion has no envelope and consists of two parts, the head and the tail. The head is a protein shell and contains a single DNA or RNA molecule, and the tail is a protein tube whose distal end binds to the surface receptors on susceptible bacterial cells (Anthony and Comps, 2005). The International Committee on Taxonomy of Viruses (ICTV) developed a universal taxonomic system for all viruses infecting animals, plants, fungi, bacteria and archaea. The classification of viruses used to be based on their morphology and genome type: double-stranded DNA (dsDNA), single-stranded DNA (ssDNA), double-stranded RNA (dsRNA) or single-stranded RNA (ssRNA) (Lefkowitz *et al.*, 2018). However, the ICTV has recently changed the taxonomy of bacterial viruses. This shift was due to the increase in available genomic sequences, and aims to contribute to a better understanding of viral diversity and evolution. The most drastic change in phage classification has been the abolishment of the morphology-based families *Myoviridae*, *Podoviridae*, and *Siphoviridae,* nonless morphological (non-taxonomic) identifiers such as "podovirus", "myovirus", or "siphovirus" can still be used (Turner *et al.*, 2023). The removal of the order *Caudovirales*, which has been replaced by the class *Caudoviricetes* to group all tailed bacterial and archaeal viruses with icosahedral capsids and a dsDNA genome was another big change. This class now contains 14 families assigned to four orders. Moreover, twenty-two new families have been delineated, 21 of which were newly established and one was promoted from the level of subfamily (Turner *et al.*, 2023). Among them, the *Autographiviridae* family contains the largest number of sequences; however, with the evolution of genetic tools, it will be possible to understand the relationships amongst viruses and, with that, delineation of higher taxa will emerge.

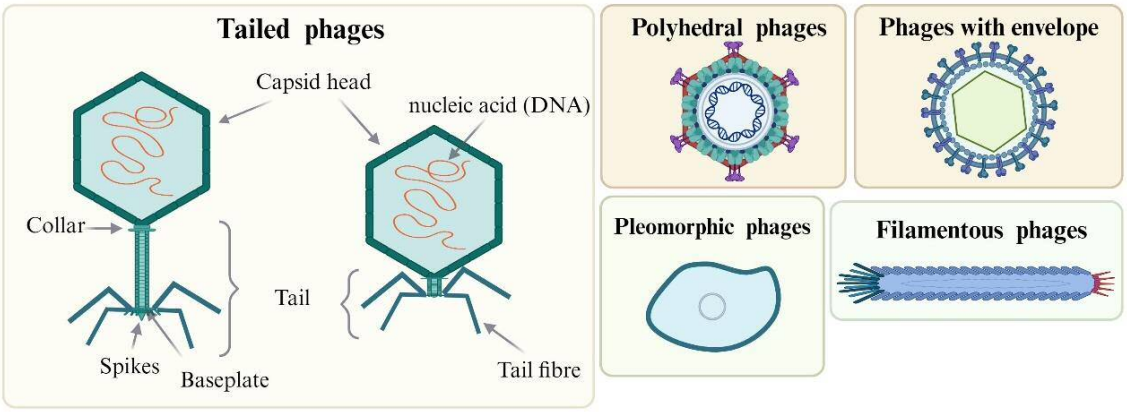

Figure 1.3 – Schematic representation of the main types of prokaryotic viruses with dsDNA. (Created with BioRender.com)

1.4.3. Phage life cycle

As mandatory intracellular parasites of bacteria, phages need to use the machinery of a host cell in order to replicate. In this sense, phages can use different strategies to multiply within the infected cell, generally adopting one of two distinct life cycles: the lytic life cycle or the lysogenic life cycle (Figure 1.4). Phages that only undergo the lytic life cycle are known as virulent, whereas phages that may also follow the lysogenic life cycle are known as temperate phages.

The lytic life cycle is characterized by rapid viral replication and lysis of the infected cell. The infection process starts with the recognition and binding of a phage to the host using specific receptors. The primary phage receptors vary depending on the type of bacteria being targeted. These receptors can be proteins, capsular polysaccharides, lipopolysaccharide or teichoic acids (Rakhuba *et al.*, 2010). For phages that infect Gram-positive bacteria, peptidoglycan is a crucial phage receptor, as it is a major polymer on the bacterial surface, along with WTA that are covalently attached to the peptidoglycan layer, and surface-exposed polysaccharides (Dowah and Clokie, 2018). These components serve as attachment sites for phages, facilitating the initial interaction between the virus and the bacterial host. Phage adsorption typically occurs in a three-step process involving initial contact, reversible attachment, and irreversible binding. Successful binding of the phage to its host leads to the injection of the phage genetic material into the bacterial cell. Once inside the cell, phages begin to replicate very quickly using the metabolism of the host, starting with the transcription of the early genes. This results in the synthesis of proteins that, in general, are involved in the control of the cell

metabolic machinery, inhibiting, activating or directing the expression of host proteins in order to protect the viral genome against bacterial defence mechanisms and adapt the cellular metabolism towards an efficient infection cycle (Roucourt and Lavigne, 2009). Intermediate genes are then expressed and replication of the phage genome takes place. Finally, late genes are expressed, leading to the synthesis of structural proteins necessary for the formation of new phage particles. The next step is assembly, a complex process that involves the coordinated interaction of various phage proteins and genetic elements, generally involving the association of capsid proteins with internal scaffolding proteins, forming the structural basis for the phage particle (Aksyuk and Rossmann, 2011). Typically, lysis of the host bacterium ends the process, allowing the release of newly formed virions that will be able to infect other cells. In this step, some lytic phages use single proteins, amurins, to inhibit the synthesis of bacterial peptidoglycan (Bernhardt *et al.*, 2000). However, most of them utilize two groups of proteins that cooperate to cause bacterial cell lysis, namely holins and endolysins. The role of holins is to perforate the host cytoplasmic membrane and thus give endolysins access to their enzymatic target, bacterial peptidoglycan (Young *et al.*, 2000). Peptidoglycan cleavage by these proteins ultimately makes the host cell burst by hypotonic lysis, thereby releasing the phage progeny.

In contrast, the lysogenic life cycle is characterized by the integration of the phage DNA into the bacterial chromosome. The integrated phage DNA, known as a prophage, can then replicate along with the host DNA and is passed on to daughter cells during cell division. This integration allows the phage to persist in the host population without actively producing new phage particles (Campbell, 2003). This process occurs through the attachment sites of viral DNA, phage attachment site (*attP*), and the host cell, bacterial attachment site (*attB*). These specific sequences facilitate the recombination process, catalysed by phage integrase enzymes that bind to the attachment sites. Recombination between *attP* and *attB* results in the formation of hybrid attachment sites (*attL* and a*ttR*), marking the integration of the phage genome into the bacterial chromosome (Bland *et al.*, 2017). The transition from lysogeny to the lytic cycle involves a switch from the dormant state to an active state where new phage particles that lyse the host cell are released to infect new host cells. This changeover can be triggered by various factors, such as environmental stress (e.g., exposure to UV light, mitomycin C, etc.). One of the fundamental cellular mechanisms that contributes to DNA repair and maintenance of

genomic stability is the host SOS system. After activation of this system, the host protein RecA is expressed and specifically degrades the CI repressor (responsible for maintaining the lysogeny state), inducing the expression of all the genes involved in the lytic cycle (Kaushik *et al.*, 2022). In some cases, lysogeny can confer new functions to the host bacterium through a process known as lysogenic conversion, where genes carried by the phage genome alter the phenotype of the host cell. This can include the acquisition of new traits, such as antibiotic resistance, toxin production or biofilm formation, which can impact the survival and behaviour of the host bacterium (Gummalla *et al.*, 2023).

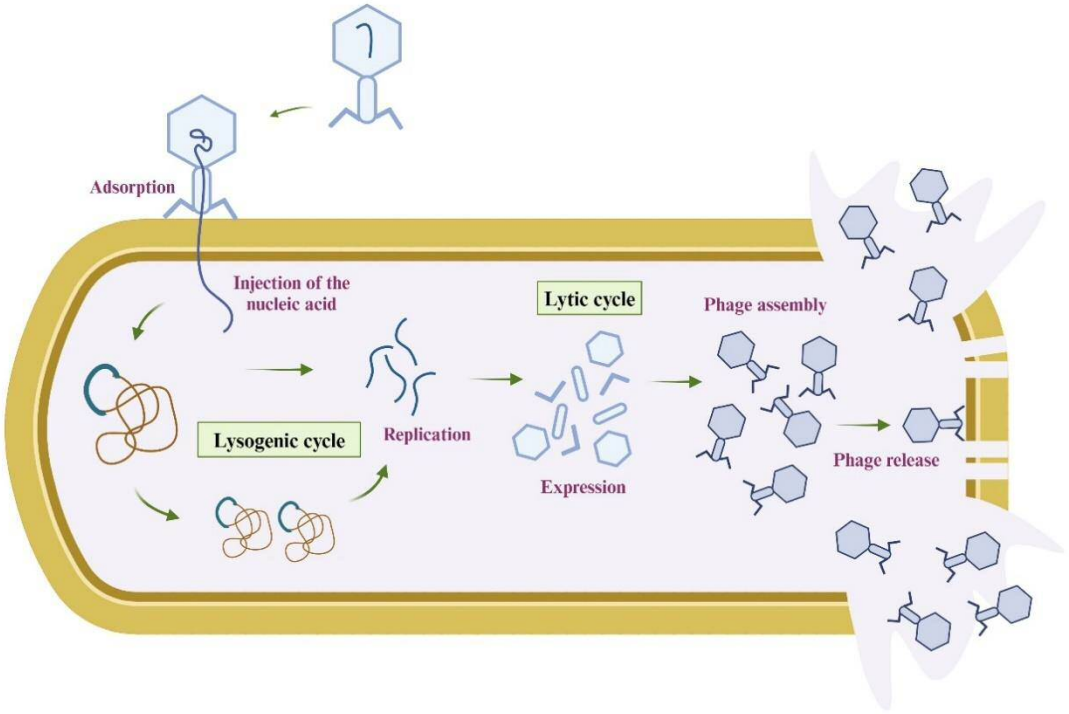

Figure 1.4 - Lytic and lysogenic life cycles of phages. In both cases the infection starts with the adsorption of a free virus particle to a susceptible bacterium. In virulent phages (lytic life cycle), the infection leads to rapid bacterial lysis followed by the release of free viral particles. In temperate phages (lysogenic life cycle), the infection can either lead to the integration of the prophage into the bacterial chromosome or to cell lysis. The prophage can either be transmitted vertically with the replication of lysogenic bacteria or reactivate the lytic cycle and release free viral particles. Adapted from (Fernández *et al.*, 2023).

1.4.4. Phage resistance

The evolution of resistance mechanisms in bacteria is a complex process influenced by various factors. These mechanisms are essential to the dynamics between bacteria and phages and, therefore, play a key role in regulating bacterial populations in all habitats. The development of phage resistance is also very important in the context of phage therapy, which has been proposed as an alternative approach to combat antibiotic resistance. Bacteria can avoid being infected by phages in several ways. First, by superinfection immunity typically associated with lysogeny, which serves to prevent bacteria from being infected by two or more related phages, or to protect the lysogen from being lysed (Rostøl *et al.*, 2024). Moreover, bacteria employ a range of mechanisms to inhibit phage adsorption that includes altering cell surface structures, production of specific polysaccharides, and mutating host genes (Xia et al., 2011). Also, the so-called Restriction-Modification (R-M) systems, identified in 90% of prokaryotes, are a crucial component of bacterial defence mechanisms against foreign DNA. These systems consist of two main enzymes: restriction endonucleases (restriction enzymes), which recognize specific DNA sequences and cleave them, and DNA methyltransferases (modification enzymes) that methylate the same DNA sequence to protect the bacterial genome from self-digestion by the restriction enzymes (Shaw *et al.*, 2023). Besides R-M systems, bacteria possess a sophisticated mechanism to defend against foreign genetic material, in this case sequences directly derived from the virus. These adaptive immune systems, named Clustered Regularly Interspaced Short Palindromic Repeats (CRISPRs), are DNA sequences composed of a succession of repeats separated by unique sequences called spacers. The CRISPR-Cas systems consist of two main components: the CRISPR-associated (Cas) proteins, working as the catalytic core of the system and responsible for cleaving DNA, and the CRISPR locus, functioning as the genetic memory that guides the catalytic activity against foreign DNA. In staphylococci, CRISPR-Cas systems are rare, but when present, they are located within the SCC*mec* element and can be mobilized by SCC*mec*-encoded recombinases (Mikkelsen et al., 2023). Bacteria may also harbour diverse heterologous proteins that confer resistance through the abortion of phage infection. Unlike the aforementioned antiphage systems, these abortive infection (Abi) systems result in the death of the infected cell. Abi systems are generally activated by the presence of certain phage proteins or peptides and prevent the release of new infective particles (Lopatina *et al.*, 2020). Even though there is an increasingly large list of

identified defence systems implicated in bacterial resistance to phages, these are the best known examples.

Phages, in turn, are capable of countering these resistance mechanisms. This adaptability manifests itself in several forms, such as receptor adaptations by random mutations that result in decreased phage adsorption, the evasion of bacterial CRISPR-Cas immunity using anti-CRISPR proteins, and the hijacking of host antitoxins to prevent abortive infection. Phage diversity is generated by point mutations, genome rearrangements, and the exchange of genetic material with other phage particles or bacteria (Samson *et al.*, 2013). From the perspective of phage therapy applications, the ability to engineer, mutagenize, and screen for new phages in a high-throughput manner may further enable the rapid creation of functionalized phages that can overcome bacterial resistance mechanisms. For now, the most common strategy to curtail the development of phage resistance is the administration of multiple phages targeting different receptors in the bacterial cell and combined in a single phage preparation, known as phage cocktail. The chances of bacteria evolving resistance to multiple phages are lower compared to a single phage preparation, although not impossible. In any case, even if phage resistance arises, this does not impede a positive therapeutic outcome. In some cases, the cellular modifications that promote phage resistance of the bacterial population reduce their fitness and/or increase its susceptibility to antibiotics, and thus work synergistically with the antibiotics to promote their efficacy (Fernández *et al.*, 2020). This phenomenon is known as phage antibiotic synergy (PAS). On the other hand, the patient's immune system, given an adequate response, can eradicate emerged resistant bacterial mutants (Roach *et al.*, 2017). In many cases, phage resistance is associated with the loss of a major virulent factor, and facilitates clearing of the infection (De Angelis et al., 2021).

1.4.5. Phage-host interactions

Phages display significant diversity in natural environments, impacting microbial communities and ecosystem dynamics. Their genetic diversity contributes to the capacity to infect a wide range of bacterial hosts. Indeed, recombination has been identified as a significant factor in phage diversity, enabling the coexistence of multiple phage populations with diverse host recognition receptors (Bellas *et al.*, 2020). The relationship between phages and bacteria is complex, although the evolutionary dynamics of these two players is generally described as an arms-race. In this hypothesis, continuous

bacterial exposure to phage predation leads to bacterial evolution toward avoiding phage infection. In turn, phages are intracellular parasites and are constantly pressured to assault bacterial cells and surpass cell defence mechanisms to successfully takeover the bacterial metabolism, a necessary step in order to replicate itself and generate new virions that are released upon cell lysis. This model appears to be straightforward since phages have an important role in microbial communities by controlling their density, and, in the case of prophages, also in bacterial communication (Maxwell, 2019), bacterial resistance (Chen *et al.*, 2022), bacterial escape from host immune system (Sweere *et al.*, 2019), virulence (Gummalla *et al.*, 2023), evolution, genetic material exchange (Mazaheri Nezhad Fard *et al.*, 2011), biofilm formation (Secor *et al.*, 2015) and superinfection exclusion (Kuntová *et al.*, 2023). Indeed, bacteriophages play a main role in transmission of antibiotic resistance in different enviroments, including foods. Phage particles carrying antibiotic resistance genes were identified in several foods such as chicken, fish, and mussels (Blanco-Picazo *et al.*, 2023) and dairy products (Blanco-Picazo *et al.*, 2022). Moreover, a recent work has shown the mutualistic relationship between phages and bacteria. Phages able to carry out generalized transduction are beneficial for hosts, e.g. antibiotic susceptible cells become resistant to both antibiotics and phage by integrating the generalized transducing temperate phages. This allows bacterial survival and therefore provide phage abundant cells for propagation (Fillol-Salom *et al.*, 2019).

In addition, environmental conditions such as temperature (Shan *et al.*, 2014), pH (Fernández *et al.*, 2021), nutrient availability, presence of host cells, and presence of polymicrobial communities can influence prey-predator interactions. More recently, Erez et al. (2017) described a system that represents a form of virus-virus communication based on the production of a small signalling peptide (arbitrium) whose accumulation allows phages to measure their population density and control the lysogeny process, thus preventing extinction of the bacterial population (Erez *et al.*, 2017).

As such, phages can be parasites or predators depending on their life cycle. This is the reason why only strictly lytic phages can be used for phage therapy. Still, the interactions of lytic phages with their bacterial hosts remain poorly understood and primarily limited to laboratory conditions. Moreover, the obtained results are usually dependent on the phage-bacteria pair and the specific environmental conditions, making it difficult to draw more general conclusions. Nonetheless, new insights into phage biology have been acquired through the application of genomics, proteomics, transcriptomics, and

metabolomics, which have provided useful information about the molecular mechanisms involved in phage-bacteria interactions (Fernández *et al.*, 2018).

1.4.6. *Staphylococcus* phages

Staphylococcus phages represent a valuable resource in the fight against staphylococcal infections, particularly in the context of antibiotic resistance and biofilm formation. Their diverse host range, virulence-targeting capabilities, and biocontrol potential emphasize their significance in developing novel therapeutic approaches for combating infections. In this context, phages infecting *Staphylococcus* are tailed and belong to the order *Caudoviricetes*. From a therapeutic point of view, to ensure the death of the infected bacteria, virulent phages are the best option to use, since they only carry out the lytic cycle. A major determinant of phage-host specificity is the bacterial surface structures that serve as phage receptors. In the case of staphylococci, the primary receptor is often WTA. Phages bind to these surface structures using a variety of fibers or RBPs present on the virions (Hawkins *et al.*, 2022). However, one of the most common resistance mechanisms in *S. aureus* is the acquisition of mutations affecting WTAs biosynthesis. The recognition of this receptor varies depending on the phage family; yet, deletions or point mutations in the undecaprenyl-phosphate N-acetylglucosaminyl 1-phosphate transferase *tagO* gene confer resistance to almost all types of phages (both virulent and temperate phages) (Xia *et al.*, 2011; Fernández *et al.,* 2021). Most strains express polyribitol phosphate WTA substituted with D-Ala and GlcNAc. WTA sugar modifications are highly variable and have been implicated in bacteriophage susceptibility. Thus, the product of gene *tar*M is capable of glycosylating WTA, which seems to be essential for infection by some phages (Xia *et al.*, 2010). In some cases, resistance may occur as a result of the deletion or inactivation of the *tar*S gene or the simultaneous activity of the *tar*S and *tar*M genes (Li *et al.*, 2015). Apart from that, high production of protein A can mask the phage receptor and reduce adsorption (Nordström and Forsgren, 1974). The production of capsule can also influence adsorption; nevertheless, these modifications are typically temporary and are influenced by fluctuations in environmental factors (Wilkinson and Holmes, 1979).

1.5. Phage proteins with therapeutic potential

Phage proteins play vital structural and functional roles, participating in viral replication, transcription and polyprotein processing, or contributing to the infectivity and biological functions of the virus. The latter group, the so-called virion proteins, are crucial components of mature phage particles, facilitating bacterial infection through local cell wall degradation (Zhang *et al.*, 2015). Proteins involved in degrading cell wall components, be it peptidoglycan (lytic proteins) or other polysaccharides (capsule, extracellular polysaccharides, lipopolysaccharide, etc.) have potential as therapeutic agents in their own right.

1.5.1. Lytic proteins

Enzymes with peptidoglycan-degrading activity are called peptidoglycan cell wall hydrolases, and can be divided into two groups: virion-associated peptidoglycan hydrolases (VAPGHs) or exolysins, which participate in the initial phage infection steps facilitating entry of the viral DNA into the cytoplasm, and endolysins, proteins that mediate bacterial lysis at the end of the lytic infection cycle by degrading peptidoglycan. Both types of lytic proteins are useful as antimicrobials resulting in cell lysis when added exogenously (Gutiérrez *et al.*, 2019). This is particularly true for Gram-positive bacteria, which lack an outer membrane. In contrast, the outer membrane present in the cell wall of Gram-negative bacteria forms a barrier that prevents lysins from accessing and degrading the peptidoglycan layer underneath, thereby protecting bacteria from lysin attack (Lai *et al.*, 2020). Both endolysins and VAPGHs encoded by *S. aureus* phages have a modular structure, containing distinct functional domains. This modular organization provides lytic proteins with substrate specificity and facilitates the performance of protein engineering in order to design new proteins with enhanced antimicrobial activities. Typically, lysins have two distinct functional domains consisting of an N-terminal catalytic domain for peptidoglycan hydrolysis, which is conserved among lysins, and a C-terminal binding domain for the recognition of surface moieties on the bacterial cell walls. The catalytic domains of phage lytic proteins are classified into three basic types based on peptidoglycan bond specificity: amidases that hydrolyse the amide bond connecting the glycan strand and stem peptide; endopeptidases that cleave the bond within the interpeptide bridge, and glycosidases that hydrolyse linkages within the amino

sugar moieties (Gutiérrez *et al.*, 2018). Lysins from phages infecting Gram-negative bacteria have a globular structure with a cationic or amphipathic region at the C-terminal that interacts with the negatively-charged surface lipopolysaccharides (LPS) and facilitate their permeation across the outer membrane (Lai *et al.*, 2020). The lytic activity of Gram-negative endolysins from the outside generally requires a disrupting agent, such as EDTA or a cationic peptide. In this regard, genetically modified endolysins, named Artilysins, have been designed by fusing a cationic peptide to an endolysin (Briers and Lavigne, 2015). Another interesting strategy to enhance endolysins activity in Gram-negative bacteria involves the use of colicin-like bacteriocins fused to endolysins (Lysocins), which are able of periplasmic import (Heselpoth *et al.*, 2019), or by combining the specificity of phage RBPs with the antimicrobial activity of endolysins into endolysin hybrids (Innolysins), to target outer membrane proteins (Zampara et al., 2020). A similar approach, involving fusion of lytic proteins to the cell-penetrating peptide TAT, allowed the eradication of intracellular *S. aureus* in bovine mammary alveolar cells by enabling the protein to go through eukaryotic membranes (Keller *et al.*, 2022). No resistance issue has yet been reported linked to the exogenous use of lysins; however, unlike phages, endolysins do not exhibit an increase in concentration over the course of treatment or remain active for a long time, as their stability is highly affected by environmental factors (Gerstmans *et al.*, 2018).

Based on their properties, endolysins have been suggested as alternative biocontrol agents. Furthermore, endolysins have already been used to avoid pathogen contamination in food systems. For example, endolysin PlyV12 has demonstrated a very high lytic activity against both antibiotic-resistant *E. faecalis and E. faecium* (Yoong *et al.*, 2004). As lytic proteins have potential as antimicrobials, the strategy relies on the combination with other antimicrobial agents such as disinfectants or even other phage-encoded proteins (Daniel *et al.*, 2010). Additionally, synergy was reported for the combination of a holin (HolA) and a lysin (CwlQ) encoded by a *Vibrio alginolyticus* phage (Luo *et al.*, 2018). The combination of lytic proteins with antibiotics has also yielded positive results. Thummeepak *et al*. (2016) evaluated the synergism between LysABP-01 lysin and seven commonly used antibiotics against one multidrug resistant (MDR) and four extremely drug resistant strains of *A. baumannii* . The results revealed elevated antibacterial activity in a combination of LysABP-01 and colistin that allowed reducing their minimum inhibitory concentrations (MICs) up to 32-fold and 8-fold, respectively.

1.5.2. Polysaccharide depolymerases

In addition to phage lytic proteins, phages produce other enzymes that help the virus penetrate the carbohydrate barrier posed by the host cell envelope in order to access its receptor and/or inject phage DNA into the bacterial cells, called bacteriophage-encoded depolymerases. Not all phages encode depolymerases with exopolysaccharide-degrading activity, but phages that infect encapsulated bacteria tend to produce such enzymes. These proteins are very diverse and can be divided into two classes according to their mechanism of action, hydrolases and lyases (Latka *et al.*, 2017). The potential substrates include CP, LPS, extracellular polysaccharides and WTA. Most phage exopolysaccharide depolymerases are structural tail proteins. Different activities have been found within them that can be summarized in three types: alginate lyase, responsible for breaking the glycosidic bond of the alginate polymers that form the capsule of some bacteria; endosialidase, which catalyzes the cleavage of the α-2,8 bond between the N-acetylmuramic acid of the peptidoglycan and the carbohydrate polymer that makes up the capsule; and hyaluronidase, degrading hyaluronic acid, which is the major component of the capsule that surrounds streptococci (Guo *et al.*, 2023).

Exopolysaccharide depolymerases have an interesting biotechnological application, since they can eliminate the physical barrier that protects bacteria, or the matrix of biofilms, which favours the diffusion and action of antibiotics, disinfectants or phages (Oliveira *et al.*, 2022; Guo *et al.*, 2023). Like endolysins, phage depolymerases display a synergistic effect with some antibiotics against biofilm-forming pathogens. For instance, (Chen *et al.*, 2022) evaluated the combinational effects of Dpo71, encoded by a lytic phage, with serum or colistin to target MDR *A. baumannii* , observing enhanced antibiofilm activity compared with the monotherapies. Also, this depolymerase was able to promote the *in vivo* antibacterial activity of colistin, markedly improving the survival rate of infected *G. mellonella*.

1.6. Applications of phages and phage proteins

The first application of phages was for the treatment of human infections. Phage therapy includes various approaches beyond single phage therapy, such as phage cocktail therapy or the combination of phages with other antimicrobials. Phage preparations can be applied

topically for the treatment of infected wounds in the form of gels or ointments. This is the case of the commercial preparation named PhageBioderm (Phage Therapy Center). The therapeutic efficacy of this product has been tested on 107 patients with ulcers caused by different pathogens such as *P. aeruginosa*, *S. aureus* and various species of the genus *Streptococcus*. In these patients, conventional therapy was not successful, but after the use of PhageBioderm, the wounds or ulcers healed completely in 70% of the cases (Markoishvili *et al.*, 2002). Phages have also been used to treat otitis, the most frequent infection in humans and animals. Indeed, tests carried out with phages in pets with otitis caused by *P. aeruginosa* showed encouraging results (Wright *et al.*, 2009). Moreover, recent investigations using animal models have explored phage treatment against a range of clinically significant pathogens. When challenged with gut-derived sepsis due to *P. aeruginosa*, oral administration of phages saved 66.7% of mice from mortality compared to 0% in the control group (Watanabe *et al.*, 2007). Additional animal studies show similarly promising results for multidrug-resistant *S. aureus*. For instance, (Wills *et al.*, 2005) showed that phages prevented abscess formation in rabbits when injected simultaneously with the bacteria. The first controlled trials in humans were carried out in the United States, and demonstrated the safety of a phage cocktail against *E. coli*, *S. aureus*, and *P. aeruginosa* in 42 patients with leg ulcers (Rhoads *et al.*, 2009). Recently, implant-associated infections caused by antibiotic-resistant bacterial strains were treated with combined phage/antibiotic therapy. The rate of periprosthetic joint infection (PJI) relapses in 45 adult patients treated with this combination was eight times lower than that in the antibiotic treatment (Fedorov *et al.*, 2023). At the same time, animal models have been used to evaluate the elimination of biofilms by phages. For example, plastic catheters with preformed biofilms of MRSA or *P. aeruginosa* were implanted in mice, which were then treated by intraperitoneal injection with a mixture of phages and/or antibiotics. The findings revealed a synergistic effect between phage and antibiotic, completely eradicating the biofilm formed by MRSA, and considerably reducing the biofilm formed by *P. aeruginosa* (Yilmaz *et al.*, 2013). In addition, studies using a rat model of *S. aureus* biofilm-associated PJI revealed that the combined effect of phages and vancomycin provided a considerably greater therapeutic value than individual therapies. It must be noted that phage therapy alone decreased the bacterial load within joint tissue and on the titanium implant of the infected knee in the first week of therapy and no detrimental

systemic or local damage was detected after multiple doses containing high quantities of lytic phages (Morris *et al.*, 2019).

The use of phage-encoded lytic enzymes as therapeutics is also very promising. Yang *et al*. (2014) produced a novel chimeric lysin, by combining the active site of a lysin with a cell wall binding domain (ClyH) that was capable of saving mice challenged with MRSA bacteremia (Yang *et al.*, 2014). On the other hand, Gutiérrez *et al*, 2020 characterized an endolysin encoded by staphylophage *Kayvirus rodi* (LysRODI) and demonstrated its efficacy to prevent mammary infections by *S. aureus* and *S. epidermidis* (Gutiérrez *et al.*, 2020). Furthermore, the treatment of systemic as well as localized burn wound infections in mice using endolysins combined with antibiotics was also studied. The results demonstrated that a combination therapy using endolysin MR-10 and minocycline was found to be more effective in controlling the entire process of burn wound infection (MRSA) in mice compared to antibiotic or endolysin given alone (Chopra *et al.*, 2016).

Phages can also be implemented as a biocontrol tool in the food industry to reduce bacterial contamination, which has serious implications for the health of consumers and the Public Health system (EFSA and ECDC, 2023a). The main advantage of this strategy is its feasibility to be used in the different stages of the chain, including primary production (crops and livestock), factories and in the final products. Traditional food preservation methods are fundamentally based on heat treatments, which, although effective, have some negative effects on the product, such as the loss or reduction of nutrients and alteration of its organoleptic properties. Phage-derived products can offer an alternative to inhibit pathogenic or spoilage bacteria along the food chain, providing a longer product shelf life. In primary production, there are already some phage-based products available to fight pathogens affecting crops or farm animals. This is the case of companies such as PhageLab (https://phage-lab.com/es/), which manufactures phage-based products for the control of bacterial growth in breeding facilities belonging to the poultry, cattle and aquaculture industries, with the aim of reducing the use of antibiotics in the primary sector. Additionally, ListShield™ (Intralytix, Inc., https://www.intralytix.com/) or PhageGuard Listex (Phageguard, https://phageguard.com/solutions/listeria) have been proposed as disinfectants that prevent *Listeria* contamination in processing plants and on ripened cheese surfaces, while leaving the necessary bacterial starter cultures unharmed. In food safety, phages and/or

their lytic proteins can also be used to prevent and/or detect contamination at different points in the food chain (García *et al.*, 2008).

With this in mind, phages offer a promising alternative to treat infectious diseases or eliminate pathogens associated with different human activities such as agriculture, veterinary and human medicine, food processing and wastewater treatment. There are some examples of the use of phages in agriculture, i. e., the product Agriphage (Omnilytics, https://www.agriphage.com/) was developed for the treatment of tomatoes, peppers, apples, pears, citrus, peaches, cherries, almonds, walnuts, and hazelnuts. One example of veterinary applications of phages is Phagein (PhageLab, https://phage-lab.com/technology/) for diarrhea in calves. To date no commercial products have been developed for waste treatment but several studies are ongoing.

BACKGROUND AND OBJECTIVES

2. BACKGROUND AND OBJECTIVES

Multidrug resistance in pathogenic bacteria is one of the major public health problems worldwide, affecting not only human health and the food production chain, but also the global economy. As a result, the development and application of new technologies to eliminate these pathogenic microorganisms has become a priority. In clinical settings, the emergence of antibiotic resistance in bacteria makes the treatment of numerous infectious diseases more difficult, driving the urgent search for new antimicrobials that are harmless to humans and do not generate bacterial resistance. In the food sector, consumers demand healthy products, of high quality and guaranteed safety, but with minimal processing. In this context, bacteriophages, through phage therapy and biocontrol, acquire special importance as possible alternatives for the elimination of pathogenic bacteria.

Our research group (DairySafe) began over a decade ago studying the application of phages and their lytic proteins as antimicrobial agents for improving the quality and safety of dairy products. Throughout this period, phages that specifically infect *S. aureus* strains of food origin have been isolated and characterized (García *et al.*, 2009). Later on, and due to the importance of addressing the problem of antibiotic resistance from a One Health perspective, *S. epidermidis* phages were also included in our studies (Gutiérrez *et al.*, 2015). Evaluation of two wide host range myophages, *Kayvirus rodi* (phiIPLA-RODI) and *Sepunavirus* IPLA-C1C (phiIPLA-C1C), confirmed their lytic activity against several staphylococcal strains from clinical, veterinary and food origin. For instance, 70.2% of the MRSA strains belonging to a collection of clinical isolates from Northern Spain displayed susceptibility to *K. rodi* and resistance to phiIPLA-C1C (Salas *et al.*, 2020). Furthermore, both exhibited the ability to remove preformed biofilms and/or inhibit biofilm formation, which is considered an essential property of phages aimed at fighting pathogenic bacteria (Gutiérrez *et al.*, 2015). Interesting studies carried out in our group also shed light regarding the interaction between phage *K. rodi* with its host, demonstrating that low-level predation by this virus resulted in increased adhered biomass in late stages of *S. aureus* biofilm development (Fernández *et al.*, 2017b). These results led us to dig deeper into this phenomenon and study the mechanisms behind the changes in biofilm architecture and transcriptional profile associated with phage pressure. Our research revealed that environmental pH can modulate the ability of the bacterial

population to thrive under viral pressure by fine-tuning the effects of phage attack in a way that benefits both phage and host (Fernández *et al.*, 2021).

Apart from the use of phages themselves, our team has also worked on characterizing and improving phage lytic proteins (endolysins and virion-associated peptidoglycan hydrolases) with antimicrobial properties against *S. aureus* strains. For instance, the lytic activity of virion-associated protein HydH5 was enhanced by fusion of its CHAP catalytic domain with the cell-wall binding domain (SH3b) from lysostaphin, resulting in a new chimeric protein, CHAPSH3b (Rodríguez-Rubio *et al.*, 2012). This protein displayed a high lytic activity as well as biofilm-removal properties against *S. aureus* and *S. epidermidis* strains (Gutiérrez *et al.*, 2017). Fernández *et al.* (2017) also revealed that subinhibitory doses of CHAPSH3b can hamper biofilm formation by some *S. aureus* strains by triggering downregulation of several genes coding for bacterial autolysins (Fernández *et al.*, 2017a). On the other hand, a protein with exopolysaccharide depolymerase activity (Dpo7) was identified in phage vB_SepiS-phiIPLA7, which exhibits plaques surrounded by an increasing halo zone. This protein (98.5 kDa) contains two catalytic domains, a putative pectin lyase domain at the amino-terminal region, and a putative peptidase domain at the C-terminus. Preliminary studies demonstrated the antibiofilm activity of Dpo7 against *S. aureus* and *S. epidermidis* (Gutiérrez *et al.*, 2015). The extensive knowledge about *S. aureus* and *S. epidermidis* phages and their proteins as antimicrobial agents has allowed our group to further the study of their effectiveness in eliminating biofilms, with a view to their future application as disinfectants in different sectors.

In this context, the main goal of this Doctoral Thesis was to develop a novel set of phage-based antimicrobial products to be used as disinfectants against *S. aureus* and *S. epidermidis* in clinical settings and food industries, in order to understand the dynamics between a virulent phage and its host using different combinations with novel antimicrobials for biofilm removal. To do that, three specific objectives were established:

Objective 1. Determine the impact of temperature on the host infection by phage *Kayvirus rodi* during staphylococcal biofilm formation (addressed in chapter 1)

Objective 2. Study the putative interactions (synergy or antagonism) between phages and phage-derived proteins against *S. aureus* biofilms (addressed in chapter 2)

Objective 3. Isolate and characterise new bacteriophages infecting *S. epidermidis* strains and study their antimicrobial/antibiofilm activity in combination with other compounds (addressed in chapter 3)

EXPERIMENTAL WORK

CHAPTER 1

3.1. Temperature is a key environmental factor modulating phage infection of bacterial biofilms

Microorganisms are greatly influenced by their surrounding conditions (e.g., temperature, pH, salinity and nutrients availability), which are known to affect their capacity to multiply and survive. This phenomenon is even more complex in sessile microbial communities, where cells are in different metabolic states. Environmental cues sometimes have a direct impact on phage particle stability (i.e. extreme pH), but may also modulate host susceptibility to phages. Our previous work on the influence of pH in the composition and behaviour of biofilms under phage pressure led us to study the impact of other environmental factors that may vary in biofilm treatment scenarios. In this chapter, we explore the impact of temperature on the phage-host system. We found that *Kayvirus rodi* is a more effective predator at room temperature (25 ºC) compared to body temperature (37 ºC), against both planktonic cultures and biofilms formed by several strains with varying degrees of phage susceptibility. This impact was shown to involve multiple underlying mechanisms, including temperature effect on the mutation rate, phage adsorption and/or burst size depending on the strain.

Overall, we reveal the complexity of phage-host interactions, which is further complicated by the conditions under which this interaction takes place. All of this must be taken into account when trying to use bacteriophages for therapeutic purposes; for instance, in order to determine the most appropriate dose or select the best virus for each specific application.

All of the results obtain are described in the following section:

3.1.1. Multipronged impact of environmental temperature on *Staphylococcus aureus* infection by phage *Kayvirus rodi*

3.1.1. Multipronged impact of environmental temperature on *Staphylococcus aureus* infection by phage *Kayvirus rodi*

ABSTRACT

Environmental cues sometimes have a direct impact on phage particle stability, as well as bacterial physiology and metabolism, having a profound effect on phage infection outcome. Here, we explore the impact of temperature on the interplay between phage *Kayvirus rodi* (phiIPLA-RODI) and its host, *Staphylococcus aureus*. Our results show that *K. rodi* is a more effective predator at room (25 ºC) compared to body temperature (37 ºC) against planktonic cultures of several strains with varying degrees of phage susceptibility. Further characterization of this phenomenon was carried out with strains IPLA15 and IPLA16, which exhibited a 7-log units and a 1-log unit decrease in susceptibility at 37 ºC, respectively. Our results demonstrated that the phage also had a greater impact at room temperature during biofilm development and for the treatment of preformed biofilms. There was no difference in phage adsorption between the two temperatures for strain IPLA16, while adsorption of *K. rodi* to IPLA15 was reduced at 37 ºC compared to 25 ºC. Regarding infection parameters, we observed longer duration of the lytic cycle at 25 ºC for both strains, and infection of IPLA15 by *K. rodi* resulted in a smaller burst size at 37 ºC than at 25 ºC. Finally, we also found that the rate of phage resistant mutant selection was higher at 37 ºC for both strains, being 1 log unit higher for IPLA15. Altogether, this information highlights the impact that bacterial responses to environmental factors have on phage-host interactions.

INTRODUCTION

In order to survive, bacteria have to constantly adapt to their surrounding environment by undergoing physiological and metabolic changes. Such adaptations may also affect their susceptibility to antibiotics or disinfectants, and have an impact on the success of antimicrobial therapies (Fernández and Hancock, 2012; Ramamurthy *et al.*, 2022). For this reason, it is very important to study the efficacy of different strategies under environmental conditions that mimic potential therapeutic settings. Bacteriophages, viruses that infect and kill bacteria, are no exception. In fact, their own stability and infectivity might be directly affected by variations in certain environmental cues (Denes and Wiedmann, 2014; Wdowiak *et al.*, 2022). Moreover, given their key role as modulators of microbial communities, it is also necessary to understand the nature of phage-host interactions in different environments. This might provide new clues regarding differences in the composition of microbial communities observed in distinct niches. Additionally, it will be valuable to predict the potential impact on natural bacterial populations of widespread phage application in human or animal therapy and as decontamination agents.

Temperature is known to play a major part in regulating microbial physiology. For instance, numerous virulence factors of pathogenic bacteria exhibit temperature-dependent expression (Konkel and Tilly, 2000; Guijarro *et al.*, 2015). Indeed, researchers have generally found a tight connection between the production of virulence determinants and infection temperature. In turn, transcription of virulence-related genes was turned off under optimal *in vitro* growth conditions. This phenomenon has not been so well studied regarding antibiotic resistance, although there are some examples in literature reporting temperature modulation of antimicrobial susceptibility (de Silva *et al.*, 2017; Jetter *et al.*, 2010). In the case of phages, temperature can influence infection dynamics in multiple ways. On the one hand, stability of the phage particle varies greatly depending on temperature, with higher values generally being more detrimental to phage structure integrity (Jończyk-Matysiak *et al.*, 2019). On the other hand, temperature may affect important infection and multiplication parameters, such as receptor abundance on the cell surface, expression of antiphage defense systems or bacterial growth rate (Kim *et al.*, 2012; Leon-Velarde *et al.*, 2016; Zaburlin *et al.*, 2017). Therefore, the choice of a given phage for a specific antimicrobial application should take into account the temperature at

which it is more effective. Some phages will then be mainly used in human therapy, while others might be more suitable for biofilm elimination from industrial or clinical surfaces.

Most bacteria in natural and man-made environments are part of complex communities called biofilms, in which a self-produced extracellular matrix protects the individual cells from external challenges. These structures are notoriously resistant to antimicrobials (de la Fuente-Núñez *et al.*, 2013). Furthermore, as the most common lifestyle of bacterial cells, biofilms are frequently involved in bacterial infections, especially chronic infectious diseases (Penesyan *et al.*, 2021). Therefore, it is likely that the majority of phage-bacteria encounters, including those that take place during phage therapy applications, occur in the context of a biofilm. Nonetheless, bacteriophages can penetrate biofilms and infect their target cells, being interesting as potential antibiofilm agents (González *et al.*, 2018). With this in mind, it is particularly important to assess how changes in environmental factors, like temperature, affect phage infection of biofilm cells. However, the studies available so far had mainly focused on temperature-dependent infection of planktonic cultures.

Kayvirus rodi (phiIPLA-RODI) is a myophage belonging to the *Herelleviridae* family, and has the ability to infect staphylococcal biofilms, especially those formed by the human and bovine pathogen *Staphylococcus aureus* (Gutiérrez *et al.*, 2015). Recent data indicate that biofilm treatment by *K. rodi* is dependent on the environmental pH (Fernández *et al.*, 2021), being more effective at pH values greater than 5.5. In contrast, more acidic environments lead to phage inactivation and promote formation of eDNA-rich biofilms. Until now, all experiments assessing the interaction between this phage and its host had been carried out at 37 ºC, a temperature mimicking that found in the human body. However, *S. aureus* biofilms can also grow at room temperature, establishing a reservoir on hospital or industrial surfaces from where it can then start an infection or contaminate foods. Under these conditions, bacterial cells may exhibit different phage susceptibility to that observed at body temperature. With this in mind, the aim of this study was to understand the impact of temperature on the infection of *S. aureus* by *K. rodi*, especially during biofilm formation. This information will help us better define the interactions between this virus and its host in different settings, and will be useful to determine if *K. rodi* is a good candidate for eliminating staphylococcal contamination from surfaces at room temperature.

MATERIALS AND METHODS

Bacterial strains, bacteriophage and culture conditions

The *S. aureus* strains used in this study are listed in Table 3.1 and were routinely grown in TSB (Tryptic Soy Broth, Scharlau, Barcelona, Spain) at 37 ºC or 25 ºC with shaking, or on TSA (TSB supplemented with 2% agar) plates (AppliChem, Germany). Bacteriophage *Kaivirus rodi* was propagated on strain IPLA16 as previously described (Gutiérrez *et al.*, 2015).

Table 3.1 - Origin and phage susceptibility of *S. aureus* strains used in this study.

Strain	Description	MIC 25 ºC	MIC 37 ºC	Reference
IPLA15	Meat industry surface	10 PFU/ml	10^8 PFU/ml	Gutiérrez *et al.*, 2012
IPLA16	Meat industry surface	10 PFU/ml	10^2 PFU/ml	Gutiérrez *et al.*, 2012
SA113	Derivative of strain NCTC8325	10^3 PFU/ml	$>10^8$ PFU/ml	Iordanescu and Surdeanu, 1976
ISP479r	Derivative of strain NCTC8325	10^3 PFU/ml	10^4 PFU/ml	Toledo-Arana *et al.*, 2005
Newman	Wild type	10 PFU/ml	10^6 PFU/ml	Duthie *et al.*, 1952
Sa9	Cow mastitis	10 PFU/ml	10^3 PFU/ml	García *et al.*, 2007
132	Clinical strain	10^4 PFU/ml	10^8 PFU/ml	Vergara-Irigaray *et al.*, 2009
15981	Clinical strain	10 PFU/ml	$>10^8$ PFU/ml	Valle *et al.*, 2003
V329	Cow mastitis	10^4 PFU/ml	10^8 PFU/ml	Cucarella *et al.*, 2001

Phage susceptibility of planktonic cultures

Phage susceptibility of the different strains was determined as previously described by using a modification of the broth microdilution assay (Fernández *et al.*, 2017). The minimum inhibitory concentration (MIC) was determined as the lowest starting phage titer that visibly inhibited bacterial growth after 24 h of incubation at 25 ºC or 37 ºC. The final MIC values for each strain and temperature were determined as the mode of at least three independent experiments.

In order to monitor the evolution of the bacterial population in the presence of increasing phage concentrations, growth of strains IPLA15 and IPLA16 was monitored for 20 h at 25 or 37 ºC by measuring the OD_{600} every 15 minutes using a multiwell plate reader Tecan Infinite M Nano (Tecan Trading AG).

Isolation of phage resistant mutants

In order to estimate the frequency of selection of phage resistance, overnight cultures of strains IPLA15 and IPLA16 were grown in TSB at 37 ºC with shaking. 100 µl from these cultures were mixed with an equal volume taken from a phage stock containing 10^9 PFU/ml and incubated for 10 minutes at 25 ºC or 37 ºC. The phage-bacteria mixtures were then added to 5 ml of soft agar (TSB supplemented with agar at 0.7 %) and poured onto TSA plates. Once dry, the plates were incubated at 25 ºC or 37 ºC for 24 hours and, subsequently, the colonies that grew on the agar were counted and used to calculate the frequency of phage resistant mutants by dividing the number of survivors by the inoculum (10^8 CFUs).

Some of the surviving colonies were then picked and analysed for their growth at 37 ºC in the presence of increasing phage concentrations as described above. Additionally, phage susceptibility of the same cultures was determined by using the spot assay. Briefly, a 1:10 dilution from an overnight culture of each mutant was prepared in PBS. From this cell suspension, 100 µl were added to 5 ml of soft agar and poured onto a TSA plate. The plates were allowed to air dry for 10 minutes and then 10 µl of phage stock (10^9 PFU/ml) were spotted on the center of each plate. Following overnight growth at 37 ºC, the plates were assessed for the presence of a lytic halo due to the phage. Mutants that did not exhibit halo formation were considered bacteriophage insensitive mutants (BIMs).

One-step growth curves

To determine the infection parameters of phage *K. rodi* at each temperature, 10-ml cultures of *S. aureus* IPLA16 and IPLA15 were grown in TSB at 25 ºC or 37 ºC to an OD_{600} of 0.1 and then pelleted at 4,000 × g. Each culture was then resuspended in 1 ml of PBS and phage was added at an MOI of 0.1 (10^7 PFU/ml). Adsorption was allowed for 10 minutes at 25 ºC or 37 ºC and then the cells in the different samples were pelleted at 12,000 × g in a benchtop centrifuge to eliminate the free phages and resuspended in 10 ml of PBS. The samples were titrated (time point 0) and then incubated at the same temperature used for the adsorption step. Aliquots were taken every 15 minutes for titration for a total of 60 or 90 minutes for experiments carried out at 37 ºC or 25 ºC, respectively.

Biofilm treatment assays

S. aureus biofilms were grown as previously described (Fernández *et al.*, 2017). Briefly, overnight cultures of strains IPLA15 and IPLA16 were diluted in fresh TSBg medium (TSB with 0.25% glucose) to obtain 10^6 CFU/ml. Two ml from these cell suspensions were used to inoculate each well of a 12-well microtiter plate (Thermo Scientific, NUNC, Madrid, Spain). Biofilms were allowed to develop for 24 h at 25 ºC or 37 ºC. Next, the planktonic phase was removed and treatment was added to each well (1 ml of TSB alone or containing 10^9 PFU/ml of phage *K. rodi*). The microtiter plates were incubated again for 24 hours at the same temperature used for biofilm formation. After incubation, the planktonic phase was removed and the number of viable in the adhered phase was determined by serially diluting the samples. In order to harvest the attached phase, the biofilm was washed twice with PBS and subsequently scraped with a sterile pipette tip.

Efficiency of plating (EOP) and phage adsorption assays

To determine the EOP, a suspension of phage *K. rodi* was titrated on strains IPLA15 and IPLA16 by the overlay agar method. The resulting plates were then incubated at 25 ºC or 37 ºC for 24 hours, after which the number of lytic plaques on each plate was counted. The EOPs were determined by dividing the phage titer obtained under the test conditions by the phage titer estimated under reference conditions (*S. aureus* IPLA16 at 37 ºC).

The phage adsorption rate was determined as previously described, with some modifications (Agún et al., 2018). First, overnight cultures of *S. aureus* IPLA16 and IPLA15 were diluted 1:100 into fresh TSBg and used to inoculate the wells of a 12-well microtiter plate (2 ml per well). These plates were then incubated at 25 ºC or 37 ºC for 20-24 hours. Afterwards, the planktonic phase was removed and biofilm cells were washed with PBS and scraped and resuspended in 1 ml of PBS and then diluted to an OD_{600} of 1. From these suspensions, 900 µl aliquots (~10^8 CFU/ml) were then and mixed with 100 µl of a phage suspension to obtain a final MOI of 0.1. A sample containing only PBS and phage with no bacterial cells was used as a control. Next, phage adsorption was allowed to occur for 5 minutes at room temperature. Non-adsorbed phage particles were then isolated by centrifuging the samples for 3 minutes at 10,000 × g, and the adsorption rate was calculated as follows:

adsorption rate = [(phage titer in supernatant of control – phage titer in supernatant sample) / (phage titer in supernatant of control)] x 100

Transcriptional analysis

In order to carry out the transcriptomic analysis, total RNA was isolated from *S. aureus* IPLA 16 biofilms grown for 24 h at 25 ºC or 37 ºC. To harvest the adhered cells, biofilms were washed with PBS upon removal of the planktonic phase, and scraped with a pipette tip in a solution containing 0.5 ml of PBS and 1 ml of RNA protect (Qiagen). Following 5 min of incubation at room temperature, bacterial cells were pelleted at 5,000 × g for 10 min and stored at -80ºC until further processing. After thawing the samples, cells were lysed by mechanical disruption in a solution of phenol-chloroform 1:1, glass beads (Sigma) and 80 mM DTT by using a FastPrep®-24. RNA isolation was performed with the Illustra RNA spin Mini kit (GE Healthcare) and the resulting samples were treated with Turbo DNAse (Ambion) to remove traces of genomic DNA. For storage, 1 µl of Superase inhibitor (Ambion) was added to each 50-µl sample. RNA concentration and quality were determined by using a microplate spectrophotometer Epoch (Biotek) and agarose gel electrophoresis, respectively.

A total of 10 µg of RNA from each sample were sent to Macrogen Inc. (South Korea) for sequencing using the Illumina HiSeq2000 platform (Illumina, San Diego, CA, USA). FASTQC v. 0.11.3 (Andrews, 2010) was used to perform quality control of the reads, and the RNA-seq reads were then mapped to the *S. aureus* IPLA16 genome (GenBank accession number: CP134617.1) with BowTie2 (Langmead and Salzberg, 2012). From the output of this program, only the uniquely mapped reads were kept for the subsequent step. Differential gene expression analysis was carried out using EDGE-pro (Magoc *et al.*, 2013) and the R package DEseq2 (Love *et al.*, 2014).

Transcriptional changes in selected genes of strain IPLA15 were analyzed by quantitative reverse transcription-PCR (RT-qPCR). To do that, 0.5 µg of purified RNA were converted into cDNA with the iScript™ Reverse Transcription Supermix for RT-qPCR (BioRad) according to the manufacter's instructions. The resulting cDNA was then diluted 1:25 and 2.5 µl were added to each reaction together with Power SYBR Green PCR Master Mix (Applied BioSystems) for qPCR analysis.

RNA-Seq data have been deposited in NCBI's Gene Expression Omnibus (GEO) under the GEO series accession number GSE255751.

Biofilm development under phage predation

Overnight cultures of *S. aureus* IPLA16 and IPLA15 were diluted in TSBg to obtain a cell suspension containing 10^6 CFU/ml that was used to inoculate 12-well microtiter plates with 1 ml per well. Afterwards, each well was treated with 1 ml from suspensions containing different phage titers, ranging from 0 (control well) to 10^3 PFU/ml. Biofilms were then allowed to grow for 3, 5, 7, 9 or 24 hours at 25 ºC. At these time points, the number of viable cells and phage particles was determined for both the planktonic phase and the biofilm. The adhered cells were recovered after washing twice with PBS and scraping with a pipette tip in 1 ml of PBS per well. The resulting suspension was serially diluted, plated on TSA and incubated at 37 ºC for 24 hours. The next morning, the colonies grown in the different dilutions were counted and used to determine the number of viable cells. The number of active phage particles was determined by titration using the double layer agar technique, using strain IPLA16 as a host and incubation at 37 ºC. The pH of the planktonic phase was also monitored with a calibrated pH meter.

The effect of pH on phage-bacteria interaction was further studied by using a modification of the model developed by Fernández *et al.* (2021). The steps taken to adapt the model parameters for 25 ºC are described in Supplementary material 7.1.

Statistical analysis

Data corresponding to at least three biological replicates was analyzed with Student's t-test. P-values < 0.05 were considered significant.

RESULTS

Planktonic cells from different *S. aureus* strains are more susceptible to *Kayvirus rodi* at 25 ºC than at 37 ºC

In order to compare phage susceptibility at ambient and body temperature, we first carried out MIC determination assays with several *S. aureus* strains. The general trend observed for all strains was that *K. rodi* was more successful at inhibiting the bacterial population at 25 ºC compared to 37 ºC. In some cases, the starting phage concentration required for growth inhibition increased by at least 7 log orders (*S. aureus* IPLA15 and *S. aureus* 15981) at body temperature (Table 3.1). In contrast, the difference between the two incubation conditions was much smaller in other strains (IPLA16, ISP479r and Sa9) that happened to be the most susceptible at 37 ºC (Table 3.1). We selected IPLA15 and IPLA16 for subsequent experiments as representative of these two groups of strains, (i.e. *S. aureus* IPLA15 with a high difference in phage susceptibility between both temperatures, and *S. aureus* IPLA16 with only one log unit difference between 25 ºC and 37 ºC).

To observe the dynamics of phage inhibition more closely, we monitored growth of strains IPLA15 and IPLA16 under different degrees of phage predation at the two temperatures. These experiments confirmed the trends described above and showed that, at 37 ºC, strain IPLA15 only started to show some effect of phage infection when the starting concentration of *K. rodi* was 10^3 PFU/ml, with no noticeable impact at lower phage concentrations (Figure 3.1A). Also, at higher phage titers (> 10^4 PFU/ml) we observed delayed growth of the bacterial population, potentially due to the selection of bacteriophage resistant mutants (Figure 3.1A). In contrast, growth of IPLA16 at the same temperature was already diminished at 1 and 10 PFU/ml and completely inhibited at higher phage concentrations (Figure 3.1B). The results were very different at 25 ºC, since growth of both strains was completely inhibited when the starting phage titer was low, specifically 10 PFU/ml and 100 PFU/ml for strains IPLA16 and IPLA15, respectively (Figure 3.1C and 3.1D).

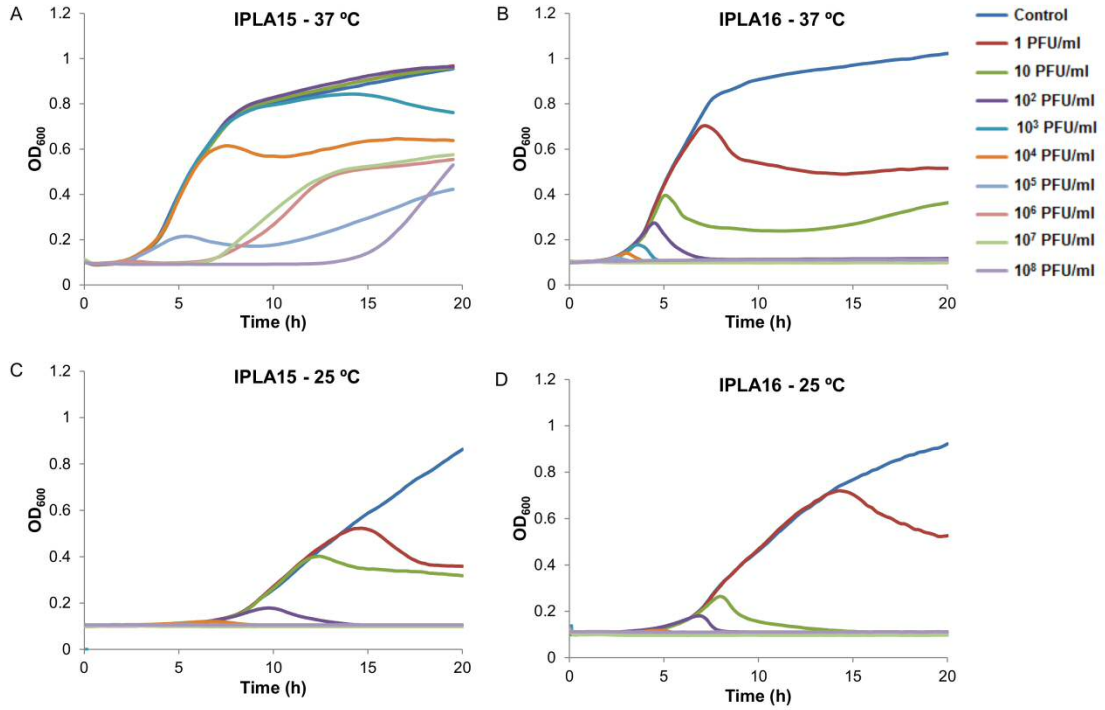

Figure 3.1 - Growth curves of *S. aureus* strains IPLA15 (A and C) and IPLA16 (B and D) at 37 ºC (A and B) and 25 ºC (C and D) in the presence of increasing concentrations of phage *K. rodi* ranging from 0 (control) to 10^8 PFU/ml. OD_{600} was monitored for 20 hours. Data correspond to one representative experiment out of three independent repeats showing the same trend.

Next, we compared the efficiency of plating of phage *K. rodi* of these two strains at 25 ºC and 37 ºC. The phage titer obtained on IPLA16 grown at 37 ºC was used as a reference; as a result, the EOP for this combination was 1. In comparison, titration of IPLA15 at body temperature was significantly lower, with an average EOP value of 0.51±0.24 (p-value = 0.0097). In contrast, the EOPs at room temperature were significant higher for both strains compared to the values obtained at 37 ºC, with average values of 1.88±0.52 (p-value = 0.0022) and 1.87±0.37 (p-value = 0.0061) for IPLA15 and IPLA16, respectively.

Infection by phage *Kayvirus rodi* during biofilm development at 25 ºC

In our previous studies, we had characterized biofilm establishment by *S. aureus* IPLA16 in the presence of different starting phage concentrations at 37 ºC. Here, we aimed to monitor the dynamics between bacterial growth and phage multiplication at 25 ºC and assess the impact of environmental temperature on phage-host interaction. To do that, the number of cells and active phage particles were determined at different time points during growth at 25 ºC in the presence of different starting MOIs both in the biofilm and the planktonic phase. These experiments confirmed that bacterial growth was slower at room compared to body temperature (Figure 3.2A and 3.2B), as previously observed in well-mixed cultures (Figure 3.1). The growth rate of the attached phase during mid exponential and late exponential phase were 2.78 and 2.48 h^{-1}, while the equivalent rates in the planktonic phase were 2.64 and 2.20 h^{-1} (supplementary material Figure 7.1A and 7.1B). At 37 ºC, according to the data obtained by Fernández *et al.* (2021), the growth rates of the biofilm were 3.70 and 2.48 h^{-1}, whereas the values estimated for the planktonic phase were 3.70 and 2.38 h^{-1} (supplementary material Figure 7.1A and 7.1B).

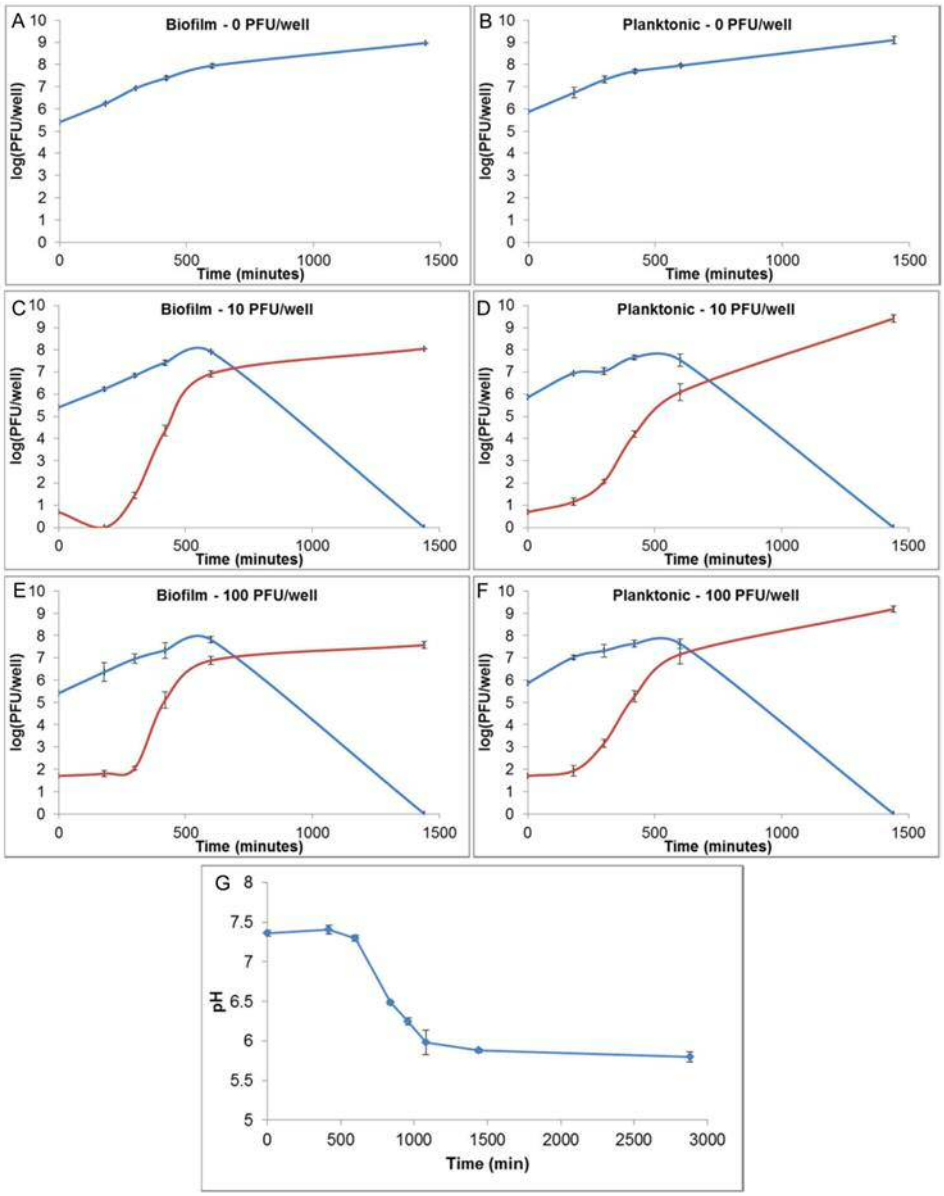

Figura 3.2 - Development of *S. aureus* IPLA16 biofilms under predation by phage *K. rodi* in TSBg for 24 hours at 25 ºC. The starting phage titer was 0 PFU/well (A and B), 10 PFU/well (C and D) or 100 PFU/well (E and F). In each time point, the number of viable cells (blue line) and phage titer (red line) were determined for the biofilm (A, C and E) and the planktonic phase (B, D and F). The pH of the growth medium was also monitored throughout the incubation (G). Data correspond to the average and standard deviation of three independent repeats.

On the other hand, similarly to the data obtained for well-mixed cultures, the phage was more effective at 25 ºC than at 37 ºC. Indeed, a starting phage number of 10 PFU/well (MOI = 0.0001) was sufficient to reduce the number of bacteria below the level of detection at 25 ºC in both the adhered and the planktonic phases (Figure 3.2C and 3.2D, respectively), and the same result was observed for a starting phage number of 100 PFU/well (MOI = 0.001) (Figure 3.2E and 3.2F, respectively). In contrast, 10^3 PFU/well (MOI = 0.01) were required for the same effect on the biofilm population at 37 ºC and 10^2 PFU/well (MOI = 0.001) to deplete the planktonic population below detection levels (Fernández *et al.*, 2017). However, when comparing the phage propagation rates between the two temperatures, values were generally lower at 25 ºC (supplementary material Figure 7.1C and 7.1D). The only exception to this was phage multiplication in the biofilm during mid logarithmic phase, which occurred at a very similar rate in both cases (11.58 h^{-1} and 12.02 h^{-1} at 25 ºC and 37 ºC, respectively).

Given the importance of pH for phage-bacteria interactions in the context of biofilm formation at 37 ºC, we also monitored pH evolution at 25 ºC (Figure 3.2G). After 24 h, the pH value was 5.88, which remained stable even if incubation was prolonged for another 24 h, with an average of 5.80 after 48 h. This value is significantly higher than that obtained in TSBg at 37 ºC, which was approximately 4.75 (Fernández *et al.*, 2017), and is above the estimated pH at which phage inactivation starts (about 5.5). Therefore, the lack of phage inactivation may have an impact on the overall outcome of the infection and contribute to the efficacy of the virus.

To study the potential role of pH more in depth, we entered all the above-mentioned parameters into a previously developed simulation model (Supplementary material 7.1). First, we ran this revised model considering the pH change rate estimated at 37 ºC by Fernández *et al.* (2021) and allowed the pH to decrease down to 4.75. We observed that the decline in pH during growth was considerably slower at 25 ºC compared to 37 ºC, which correlates well with the lower growth rates observed at this temperature (Figure 3.3). However, the pH would be expected to reach 4.75 after approximately 14 hours of growth. This does not reflect the experimental data, indicating that the pH descent rate might also be different even for an equal increase in cell number. Next, we estimated the pH change rate from the experimental data obtained at 25 ºC and entered the resulting values in the model. At 37 ºC, the decrease in pH in a 30-minute interval took place at a rate of 0.99 or 0.96 depending on the growth state of the bacterial population (Fernández

et al., 2021). The equivalent values obtained at 25 ºC were 1 or 0.99, which led to a much slower increase in the acidity of the medium (Supplementary data 7.1). When running the model with these new rates, the predicted pH evolution throughout growth was much more similar to the experimental values, with a minimum pH of 5.78 reached 20 hours after inoculation (Figure 3.3A). This suggests that, in addition to a slower growth, the metabolic pathways active at room temperature might also result in a lesser acidification of the medium compared to those that predominate at 37 ºC.

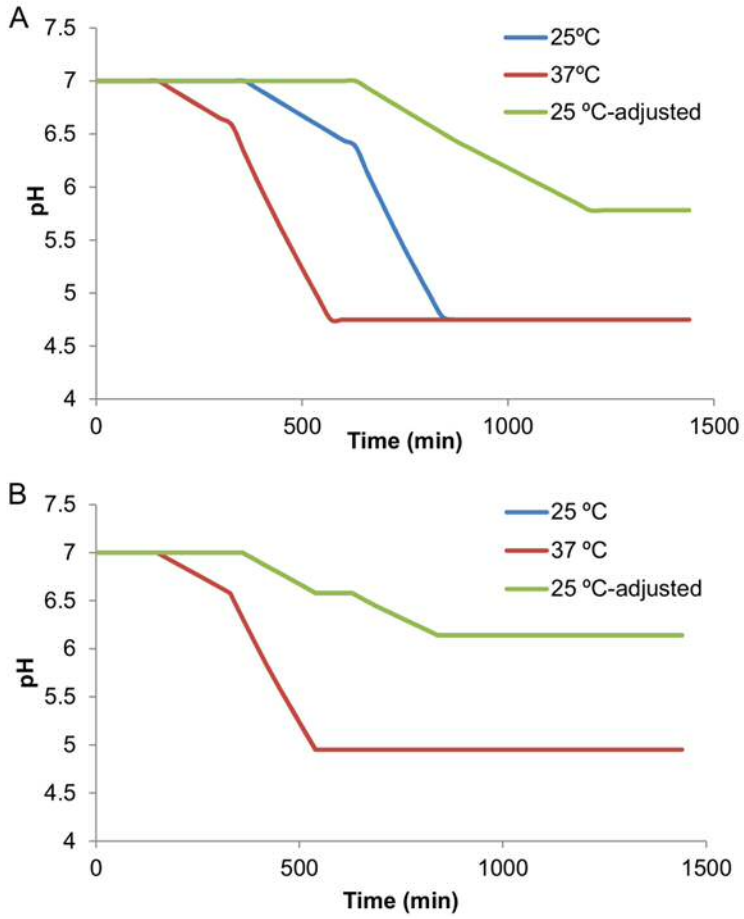

Figure 3.3 - Changes in the pH of the growth medium during biofilm development of *S. aureus* IPLA16 without phage (A) or with a starting phage titer of 10 PFU/well (B) as estimated with a phage-infection model. This model considers the bacterial growth and phage propagation parameters estimated experimentally at 25 ºC (blue line) and 37 ºC (red line). The green line corresponds to the 25 ºC model adjusted with new pH change rates determined from the data obtained during biofilm development at this temperature. It must be noted that the green and blue lines overlap in the second graph.

Despite the difference in the final pH obtained for these two versions of the model, it must be noted that the predictions regarding the impact of the phage on the bacterial population were exactly the same (supplementary material Figure 7.2). Indeed, even when a low starting MOI of 10 was used, the population was controlled by the phage before the pH went below 6.14, so no phage inactivation was observed (Figure 3.3B). Therefore, it appears that the fact that the pH was not acidic enough for phage inactivation at 25 ºC under the conditions of the experiment did not affect the outcome of phage-bacteria competition.

Infection of preformed biofilms by phage *Kayvirus rodi* is also more effective at 25 ºC than at 37 ºC

Biofilm cells often exhibit greater resistance against antimicrobial agents than planktonic cells thanks to their complex structure, diversity and specific adaptations. For this reason, the impact of temperature on phage infection might differ between sessile and free-living cells. With this in mind, we assessed the influence of temperature during phage treatment of preformed biofilms. Even though biofilms were grown in TSBg as usual, the phage was added in TSB in order to avoid the impact of pH on phage inactivation and biofilm formation previously described by Fernández *et al.* (2021). Again, *K. rodi* displayed improved antibacterial activity at 25 ºC, resulting in an average 1-log reduction in attached viable cells compared to the untreated control for both strains (Figure 3.4A). At 37 ºC, however, phage treatment did not result in any difference in cell counts for either strain (Figure 3.4A).

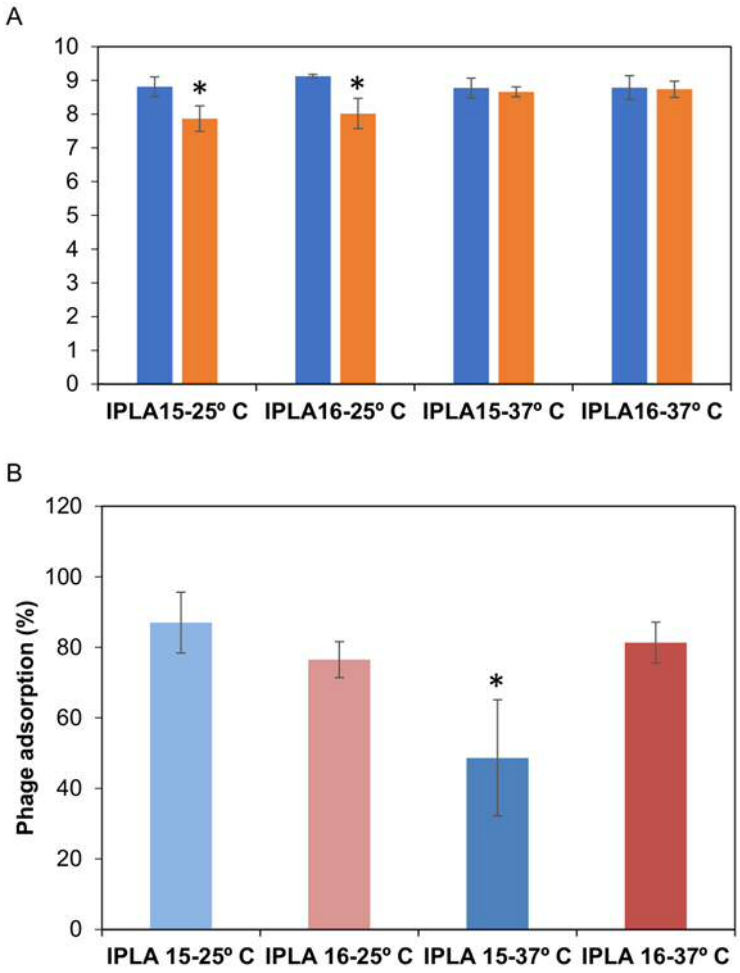

Figure 3.4 - Biofilm treatment with phage *K. rodi* and phage adsorption to biofilm cells at 25 ºC and 37 ºC. A) 24-hour old biofilms of strains IPLA15 and IPLA16 grown at 25 ºC or 37 ºC and then treated with 10^9 PFU/ml of phage *K. rodi* suspended in TSB (orange bars) or with medium alone (blue bars) at the same temperature. The next day, the number of viable cells in the biofilms was determined by serial dilutions and plating on TSA plates. Values correspond to the mean and standard deviation of three independent repeats. Statistical analysis was performed by comparing cell counts corresponding to each treatment to its control. B) Sessile cells were harvested from biofilms grown at 25 ºC or 37 ºC and then incubated with phage *K. rodi* at an MOI of 0.1 for 10 minutes at room temperature. The number of free, non-adsorbed phages was then determined. Values represent the mean and standard deviation of three independent repeats. Statistical analysis was performed by comparing adsorption rates for each strain at 37 ºC to the values estimated at 25 ºC. *, p-value < 0.05

Biofilm cells of *S. aureus* IPLA16 show increased expression of wall teichoic acids (WTA) biosynthesis genes at 25 ºC

Next, we examined the transcriptome of *S. aureus* IPLA16 biofilms grown at 25 ºC and 37 ºC to explore the possible explanation for the difference in phage susceptibility observed between these two temperatures. In total, there were 1381 genes that displayed differential expression between the two assayed conditions (supplementary material Table 7.1).

Out of these genes, 40 were involved in processes related to cell wall biosynthesis and turnover and, consequently, their level of expression may have an impact on phage adsorption and infection (Table 3.1). For instance, multiple genes involved in wall teichoic acids synthesis (*tarI'*, *tagO*, *tarJ'*, *tagG*, *tarK*, *tarA*, *tarB*, *tarI*, *tagH_1*, *tarJ*, *tarF*, *tarD*, and *tagX*) displayed lower expression at 37 ºC. Given that WTAs are the receptor of *S. aureus* phages, it is possible that this lesser transcription results in a lower level of adsorption at this temperature compared to 25 ºC. It must be noted that the genes related to glycosylation of the WTAs (*tarM* and *tarS*) did not display any significant difference in expression between the two temperatures. In the case of *tarM*, this would not have any impact in this strain anyway, since it has a mutation that prevents synthesis of a functional TarM protein. Genes involved in the D-alanylation of WTAs (*ddl* and *dltD*) also exhibited higher expression at 25 ºC although their potential role in affecting phage infection is not clear.

We also found differential expression in four genes involved in phage defense mechanisms, namely RL451_07865, RL451_09500, RL451_09505 and RL451_09525, which were transcribed more at 25 ºC (supplementary material Table 7.1). However, this would result in lesser and not increased susceptibility at this temperature.

Although not directly related to phage infection, we also observed dysregulation of genes involved in biofilm formation. For example, *icaA* and *icaD* (involved in exopolysaccharide biosynthesis), *spa* (coding for protein A), adhesin-encoding gene *fnbA* and serine protease *splB* were all overexpressed at 37 ºC (supplementary material Table 7.1). In contrast, proteases *aur*, *sspA*, *sspB* and *sspC*, autolysins *atl* and *sle1*, the nuclease *nuc*, as well as the negative regulator of the *ica* operon *icaR* were all expressed more at 25 ºC (supplementary material Table 7.1). As can be expected, genes involved in the heat shock response, such as intracellular proteases and chaperonins (*clpX*, *clpL*, *clpP_1*, *groS*,

clpC, *dnaJ*, *groL*, *dnaK* and *clpB*), were overexpressed at 37 ºC (supplementary material Table 7.1). Genes involved in metabolism were also differentially expressed between the two conditions. For instance, genes involved in acetate and ethanol fermentation (*pflA* and *pflB*), the pyruvate dehydrogenase complex (*pdhA*, *pdhB*, *pdhC* and *pdhD*) and the TCA cycle (*gltA*, *acnA*, *sucD*, *sucC*, *sdhA*, *sdhC* and *mqo1*) displayed higher levels of transcription at 37 ºC (supplementary material Table 7.1). By contrast, other genes were expressed at a higher rate at 25 ºC, such as L-lactate dehydrogenase (*ldh*) and genes involved in nitrate respiration (*narH*, *narG*, *narT* and *narX*) (supplementary material Table 7.1).

Phage *Kayvirus rodi* displays increased adsorption to biofilm cells of strain IPLA15 at 25 ºC compared to 37 ºC

In view of the results obtained with RNA-seq analysis, we tested the adsorption of phage *K. rodi* to biofilm cells of *S. aureus* IPLA16 grown at the two temperatures. However, no significant differences were found between the two conditions (Figure 3.4B). In contrast, the phage displayed decreased adsorption to biofilm cells of strain IPLA15 grown at 37º C compared to the values obtained at 25º C, with average adsorption rates of 49% and 87%, respectively (Figure 3.4B).

Next, we examined the expression of genes involved in cell wall biosynthesis in strain IPLA15 at the two temperatures by RT-qPCR (supplementary material Table 7.2). Unlike IPLA16, strain IPLA15 did not exhibited differential expression of genes involved in the synthesis of the WTA backbone (*tagO*) or the capsule (*capA*), which were upregulated at 25 ºC in IPLA16 (Table 3.2). However, we did observe a 3-fold higher transcription of *tarM* at 37 ºC, a gene involved in α-glycosylation of WTA. According to Yang *et al.* (2023), this modification hinders access of the phage to the WTA backbone and would, therefore, explain the lower adsorption rate of the phage to IPLA15 at 37 ºC. Some genes, *oatA* and *tarS*, did not exhibit any changes in either strain.

Table 3.2 - List of genes related to the cell wall that are dysregulated in biofilms of strain IPLA16 grown at 37 ºC compared to those developed at 25 ºC according to RNA-seq

Gene ID	Gene name	Gene product	FC
RL451_08590	*tarI'*	Ribitol-5-phosphate cytidylyltransferase 2	-6.31
RL451_11505	*femA_3*	Aminoacyltransferase FemA	-5.94
RL451_06310	*mgrA*	HTH-type transcriptional regulator MgrA	-5.35
RL451_05990	*tagO*	putative undecaprenyl-phosphate N-acetylglucosaminyl 1-phosphate transferase	-4.89
RL451_08585	*tarJ'*	Ribulose-5-phosphate reductase 2	-4.83
RL451_06555	*tagG*	Teichoic acid translocation permease protein TagG	-4.54
RL451_02975	*murG*	UDP-N-acetylglucosamine--N-acetylmuramyl-(pentapeptide) pyrophosphoryl-undecaprenol N-acetylglucosamine transferase	-4.27
RL451_05525	*dltA_1*	D-alanine--D-alanyl carrier protein ligase	-4.13
RL451_05515	*dltC*	D-alanyl carrier protein	-4.12
RL451_08580	*tarK*	Teichoic acid ribitol-phosphate polymerase TarK	-4.12
RL451_06565	*tarA*	N-acetylglucosaminyldiphosphoundecaprenol N-acetyl-beta-D-mannosaminyltransferase	-3.77
RL451_06550	*tarB*	Teichoic acid glycerol-phosphate primase	-3.74
RL451_07585	*sle1_2*	N-acetylmuramoyl-L-alanine amidase sle1	-3.50
RL451_01200	*atl_1*	Bifunctional autolysin	-3.46
RL451_08570	*tarI*	Ribitol-5-phosphate cytidylyltransferase 1	-3.21
RL451_13175	*ddl*	D-alanine--D-alanine ligase	-3.15
RL451_09095	*cap8A_1*	Capsular polysaccharide type 8 biosynthesis protein cap8A	-2.97
RL451_02300	*pbpH*	Penicillin-binding protein H	-2.94
RL451_04600	*ftsW*	putative peptidoglycan glycosyltransferase FtsW	-2.79
RL451_03200	*femA_1*	Aminoacyltransferase FemA	-2.78
RL451_06420	*sle1_1*	N-acetylmuramoyl-L-alanine amidase sle1	-2.72
RL451_05510	*dltD*	Protein DltD	-2.67
RL451_00535	*tagH_1*	Teichoic acids export ATP-binding protein TagH	-2.63
RL451_08565	*tarJ*	Ribulose-5-phosphate reductase 1	-2.53
RL451_01300	*murJ*	Lipid II flippase MurJ	-2.33
RL451_08575	*tarF*	Teichoic acid glycerol-phosphate transferase	-2.31
RL451_06540	*tarD*	Glycerol-3-phosphate cytidylyltransferase	-2.19
RL451_06545	*tagX*	Putative glycosyltransferase TagX	-2.07
RL451_03910	*femA_2*	Aminoacyltransferase FemA	2.10
RL451_08885	*murQ*	N-acetylmuramic acid 6-phosphate etherase	2.22
RL451_06445	*graS_1*	Sensor histidine kinase GraS	2.47
RL451_12970	*murA2*	UDP-N-acetylglucosamine 1-carboxyvinyltransferase 2	2.49
RL451_13445	*agrA*	Accessory gene regulator A	2.67
RL451_03915	*lytN*	putative cell wall hydrolase LytN	3.20
RL451_09195	*wbnH*	O-antigen biosynthesis glycosyltransferase WbnH	3.28
RL451_09020	*mnaA_1*	UDP-N-acetylglucosamine 2-epimerase	3.33
RL451_08950	*dltA_2*	D-alanine--poly(phosphoribitol) ligase subunit 1	3.34
RL451_12035	*atl_3*	Bifunctional autolysin	3.36
RL451_02815	*ponA*	Penicillin-binding protein 1A/1B	3.71
RL451_08455	*lytM*	Glycyl-glycine endopeptidase LytM	5.48

One-step growth curve at 25 ºC vs 37 ºC

Temperature-dependent differences in infection parameters might also be contributing to the greater susceptibility observed at room temperature in both planktonic cultures and biofilms. This possibility was explored by performing one-step growth curve experiments (Figure 3.5). We observed that burst size was significantly lower in strain IPLA15 at 37 ºC (9.19±1.67) compared to the same strain at 25 ºC (62.64±9.09) (p-value=0.008) and to strain IPLA16 at 37 ºC (57.52±12.97) and 25 ºC (64.56±18.36) (p-values=0.02 and 0.03, respectively). By contrast, there was no significant difference between the burst size values obtained in strain IPLA16 at the two temperatures (p-value=0.62). The duration of the burst time (latent plus rise period) was longer at 25 ºC (75 minutes) compared to 37 ºC (45 minutes) for both strains. This is to be expected given the slower growth of the bacterial culture at the lower temperature, but, if anything, it would indicate a delay in phage propagation.

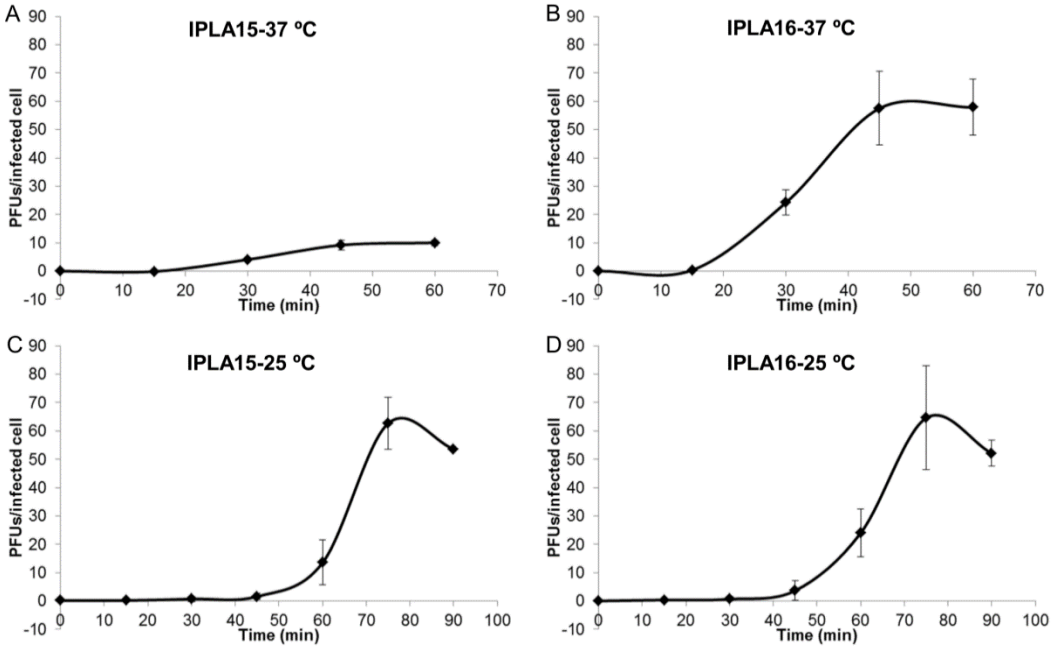

Figure 3.5 - One-step growth curves of phage *K. rodi* on strains IPLA15 (A and C) and IPLA16 (B and D) at 37 ºC (A and B) and 25 ºC (C and D). Each data point represents the numbers of PFU per infected cell, and corresponds to the mean and the standard deviation of three independent experiments.

Phage resistant mutants

In strain IPLA15, growth curve experiments indicated that its greater ability to withstand phage predation at 37 ºC compared to 25 ºC might be related to the development of a resistant population (Figure 3.1A). For this reason, we explored the frequency of phage resistant colony selection at both temperatures and found that, for strains IPLA16 and IPLA15 at 37 ºC the values were $2.70 \times 10^{-7} \pm 2.35 \times 10^{-7}$ and $2.93 \times 10^{-6} \pm 6.42 \times 10^{-7}$, respectively, indicating a 1-log increase in the number of bacterial colonies grown in the presence of the phage for the latter isolate (Figure 3.6A). By contrast, the frequency of phage resistance selection at 25 ºC was $< 10^{-8}$ for both strains.

Regarding the resistant colonies grown at 37 ºC, we sought to confirm whether they were bacteriophage insensitive mutants (BIMs). This was the case for all colonies analysed for strain IPLA16, but IPLA15 resistant colonies were not all BIMs and displayed at least some degree of phage susceptibility in the spot assay (approximately only 20% of the colonies were BIMs). This prompted us to monitor their growth in a liquid culture in the presence of a high starting titer of phage *K. rodi* (10^8 PFU/ml) compared to the parental strain. The results of this experiment showed that the mutant strains exhibited an advantage compared to wild type IPLA15 in the presence of the phage, even though they displayed susceptibility in the spot assay (Figure 3.6B). The mechanism behind resistance in these mutants derived from strain IPLA15 will be explored in a subsequent study.

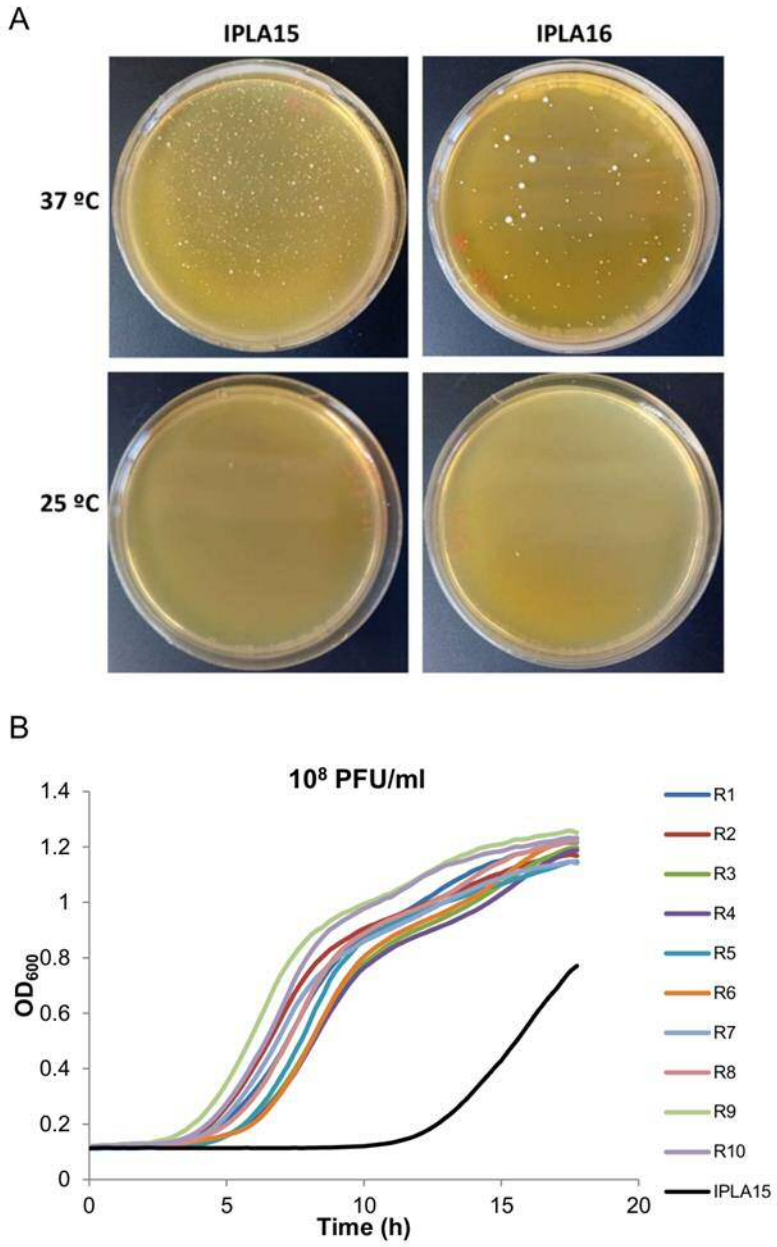

Figure 3.6 - Phage resistance development at 25 ºC and 37 ºC in strains IPLA15 and IPLA16. A) Selection of phage resistant mutants of strains IPLA15 and IPLA16 at 25 ºC or 37 ºC. Each plate was inoculated with 100 µl from an overnight bacterial culture (approximately 10^8 CFUs) and 100 µl from a phage suspension containing 10^8 PFU/ml (10^7 PFUs) mixed with soft agar. These plates were then grown for 24 h at 25 ºC or 37 ºC. B) Growth curves of parental strain *S. aureus* IPLA15 and 10 phage resistant mutants at 37 ºC in the presence of 10^8 PFU/ml of phage *K. rodi*. OD_{600} was monitored for 20 hours. Data represent correspond to one representative experiment out of three independent repeats showing the same trend.

DISCUSSION

Understanding the interplay between bacteria and their viruses will provide us with some answers regarding the differences in composition of microbial communities. Adaptation to an environmental niche will not only have an impact on the ability of a microbe to survive, even thrive, in a given set of conditions, but might also affect their susceptibility to some bacteriophages. This would have dramatic consequences regarding bacterial population structure. Moreover, phages are increasingly considered as promising therapeutics against multidrug resistant bacteria and the notoriously persistent biofilms. In this context, it is crucial to know the potential effects that parameters like temperature, pH or nutrient availability may have on the outcome of phage application. This work examined in depth how the dynamics between a virulent phage and its host change depending on temperature.

The staphylococcal phage *K. rodi* is overall a very effective predator, with a broad host range within the *Staphylococcus* genus, being particularly successful against *S. aureus* strains, including clinical MRSA isolates (Gutiérrez *et al.*, 2015; Salas *et al.*, 2020). This phage is also a promising biofilm removal agent, although its capabilities are somewhat curtailed in acidic environments (Fernández *et al.*, 2021). Besides pH, ambient temperature is another key parameter concerning the use of *K. rodi* as an antibiofilm agent. Specifically, we aimed to compare phage infection at body temperature, which would be representative of infection treatment, to predation at room temperature, which would be relevant for surface disinfection in hospitals or the food industry.

Our results show that this phage has better chances of eliminating *S. aureus* contamination at 25 ºC than at 37 ºC. This same trend was observed for several strains from different origins (clinical, veterinary or food industry) and varying degrees of phage susceptibility. The impact of temperature was particularly noticeable in strains displaying low susceptibility at 37 ºC, because they were highly sensitive to the phage at room temperature. Previous studies have described temperature-dependent infection for other bacteriophages infecting *Yersinia enterocolitica*, *Listeria monocytogenes*, *Pseudomonas fluorescens* or lactic acid bacteria (Leon-Velarde *et al.*, 2016; Tokman *et al.*, 2016; Kim *et al.*, 2012; Sillankorva *et al.*, 2004; Zaburlin *et al.*, 2017). In *S. aureus*, the plaques formed by phage K at 37 ºC are smaller than those observed at 30 ºC, although the influence of temperature was limited to USA300 strains (Lehman *et al.*, 2023). Contrary

to *K. rodi*, most of these phages thrive under conditions that favor growth of the host, such as the *P. fluorescens* phage ϕS1, which was most effective within a temperature range between 22º C and 30 ºC (Sillankorva *et al.*, 2004). Infection at lower temperatures was not as successful and there was no impact on bacterial growth at 37 ºC.

A closer look at bacterial growth dynamics in the presence of a high starting MOI revealed that, at least for some strains, development of a phage resistant population was more likely at 37 ºC than at 25 ºC. This phenomenon would have an effect on bacterial survival under phage predation and contribute to the ability of staphylococcal strains to withstand viral infection at body temperature. This might be due to some extent to the influence of temperature on the mutation rate, established a century ago by Muller (1928), and more recently linked to differences in the metabolic rate (Chu *et al.*, 2018). Nonetheless, further experiments would be necessary to confirm if other factors are also participating such as different responses of these phage resistant mutants to temperature changes. These assays also revealed the selection of a high proportion of mutants exhibiting lesser susceptibility but not full resistance to the phage for strain IPLA15 at 37 ºC. These cells appear to be partly responsible for the greater ability of this strain to survive when *K. rodi* was added at medium to high MOIs. Characterization of these mutants in a subsequent study would help understand the nature of this intermediate resistance phenotype.

Phage infection parameters also varied depending on temperature. For instance, the lytic cycle was longer for the two strains tested at 25 ºC compared to 37 ºC. This is not surprising as phage multiplication requires the bacterial machinery and is, therefore, dependent on the bacterial physiological state (You *et al.*, 2002). Conversely, burst size only decreased at 37 ºC for strain IPLA15, but did not change for *S. aureus* IPLA16. A study on dairy phages by Zaburlin *et al.* (2017) had already reported longer burst times and a varying impact on burst size at suboptimal growth temperatures. Middelboe (2000) also reported an inverse correlation between growth rate and the latent period, but observed a positive correlation with burst size for a marine virus-host system.

Some authors found that temperature sometimes affects phage infection by altering the expression of genes involved in adsorption or phage defense mechanisms. For example, in *Y. enterocolitica*, the *ompF* gene, encoding the receptor of phage ϕR1-RT, displays enhanced transcription at 25 ºC compared to 37 ºC (Leon-Velarde *et al.*, 2016). In turn, *Listeria* exhibited resistance at 25 ºC due to higher expression of a restriction-

modification system, while being susceptible at 37 ºC (Kim *et al.*, 2012). In *S. aureus* IPLA16, we observed increased transcription of genes related to WTA biosynthesis and phage defense mechanisms at 25 ºC. Evidently, the latter would not explain the better phage efficacy at room temperature. On the other hand, greater production of WTA, the main receptor of bacteriophages in staphylococci, might have explained this phenomenon. However, adsorption of *K. rodi* to strain IPLA16 was similar at the two temperatures, suggesting that the amount of WTA available at 37 ºC suffice to obtain maximum adsorption. This might be related to the lack of a functional TarM enzyme, whose modification of WTA hinders infection by various staphylococcal phages (Yang *et al.*, 2023). Unsurprisingly, this strain is amongst the most susceptible at both 37 ºC and 25 ºC. By contrast, phage adsorption was significantly curtailed at 37 ºC in *S. aureus* IPLA15. Transcriptional analysis revealed that this strain did not exhibit differential expression of genes involved in the synthesis of the WTA backbone, but gene *tarM*, involved in WTA glycosylation was expressed more at 37 ºC. It is possible that this modification limits access of the phage receptor binding protein (RBP) to the WTA backbone, thereby hindering adsorption to the cell surface.

Temperature also had an impact on biofilm removal and inhibition by phage *K. rodi*. The better efficacy observed at room temperature is a good sign towards the prospective use of this phage in the development of a surface decontamination product. We found that the phage was especially effective at preventing biofilm formation even with a low starting phage titer. As would be expected, bacterial growth rates were lower at 25 ºC than those estimated by Fernández *et al.* (2021) at 37 ºC. Accordingly, phage propagation rates were also lower in general, with the exception of the biofilm during mid exponential phase. This results in a slower elimination of the bacterial population. However, the phage can actively propagate and kill cells for a longer period at 25 ºC due to the delay in the outset of the stationary phase at this temperature. This might be perhaps the determining factor behind the slight increase in susceptibility of IPLA16 under these conditions compared to a higher temperature.

Given that pH is a very important parameter in the interplay between phage *K. rodi* and *S. aureus* biofilms, we also studied its potential role at different temperatures. We confirmed that the minimum pH reached at 25 ºC during biofilm formation was above that required for phage inactivation. However, further analysis demonstrated that this would not result in improved phage efficacy in our experiments because the phage could

eliminate the bacterial population before the time expected for the pH to reach a value of 5.5. This fact does not exclude the potential influence of a slower decrease in environmental pH at 25 ºC if the experimental setting was different. For example, if the growth medium had a lower starting pH. It must be noted that our exploration of pH change at the two temperatures suggests that it cannot be explained solely by the slower growth rate, but rather to differences in the prevalent metabolic pathways. Transcriptomic analysis did show differences in the expression of multiple metabolism-related genes, although their overall contribution to medium acidification would require a more in depth study.

In conclusion, infection by phage *Kaivirus rodi* of *S. aureus* biofilms and planktonic populations is greatly affected by ambient temperature, with improved efficacy at room compared to body temperature. The mechanisms behind this phenomenon vary in a strain-dependent manner and include differences in phage resistance development, phage adsorption, infection parameters, prolonged phage action and metabolic changes leading to a lesser acidification of the surrounding environment. This study builds upon data obtained for other phage-host pairs demonstrating the importance of understanding how phage modulation of bacterial communities varies depending on the specific niche conditions. Moreover, this information has vital repercussions concerning the development of phage-based antimicrobial strategies.

REFERENCES

Agún S, Fernández L, González-Menéndez E, Martínez B, Rodríguez A, García P. (2018) Study of the Interactions Between Bacteriophage phiIPLA-RODI and Four Chemical Disinfectants for the Elimination of *Staphylococcus aureus Contamination. Viruses*. **10**:103.

Andrews S. (2010). FastQC: a quality control tool for high throughput sequence data. https://www.bioinformatics.babraham.ac.uk/projects/fastqc/ [Accessed November 22, 2023]

Chu XL, Zhang BW, Zhang QG, Zhu BR, Lin K, Zhang DY. (2018) Temperature responses of mutation rate and mutational spectrum in an *Escherichia coli* strain and the correlation with metabolic rate. *BMC Evol Biol.* **18**: 126.

Cucarella C, Solano C, Valle J, Amorena B, Lasa I, Penadés JR. (2001) Bap, a *Staphylococcus aureus* surface protein involved in biofilm formation. *J Bacteriol* **183**: 2888–2896.

de la Fuente-Núñez C, Reffuveille F, Fernández L, Hancock REW. (2013) Bacterial biofilm development as a multicellular adaptation: antibiotic resistance and new therapeutic strategies. *Curr Opin Microbiol*. 2013 **16**: 580-9.

de Silva PM, Chong P, Fernando DM, Westmacott G, Kumar A. (2017) Effect of Incubation Temperature on Antibiotic Resistance and Virulence Factors of *Acinetobacter baumannii* ATCC 17978. *Antimicrob Agents Chemother*. **62**: e01514-17.

Denes T, Wiedmann M. (2014) Environmental responses and phage susceptibility in foodborne pathogens: implications for improving applications in food safety. *Curr Opin Biotechnol*. **26**: 45-9.

Duthie E S, Lorenz LL. (1952) Staphylococcal coagulase: mode of action and antigenicity. *J Gen Microbiol* **6**: 95-107.

Fernández L, González S, Campelo AB, Martínez B, Rodríguez A, García P. (2017) Low-level predation by lytic phage phiIPLA-RODI promotes biofilm formation and triggers the stringent response in *Staphylococcus aureus. Sci Rep*. **7**:40965.

Fernández L, Hancock REW. (2012) Adaptive and mutational resistance: role of porins and efflux pumps in drug resistance. *Clin Microbiol Rev*. **25**: 661-81.

Fernández L, Gutiérrez D, García P, Rodríguez A. (2021) Environmental pH is a key modulator of *Staphylococcus aureus* biofilm development under predation by the virulent phage phiIPLA-RODI. *ISME* J. **15**: 245-259.

García, P., Madera, C., Martínez, B., Rodríguez, A. (2007) Biocontrol of *Staphylococcus aureus* in curd manufacturing processes using bacteriophages. *Int. Dairy* J. **17**: 1232-1239.

Guijarro JA, Cascales D, García-Torrico AI, García-Domínguez M, Méndez J. (2015) Temperature-dependent expression of virulence genes in fish-pathogenic bacteria. *Front Microbiol*. **6**: 700.

Gutiérrez D, Vandenheuvel D, Martínez B, Rodríguez A, Lavigne R, García P. (2015) Two Phages, phiIPLA-RODI and phiIPLA-C1C, Lyse Mono- and Dual-Species Staphylococcal Biofilms. *Appl Environ Microbiol*. **81**: 3336-48.

Iordanescu S, Surdeanu M. (1976) Two restriction and modification systems in *Staphylococcus aureus* NCTC8325. *J Gen Microbiol*. **96**: 277-81.

Jetter M, Spaniol V, Troller R, Aebi C. (2010) Down-regulation of porin M35 in Moraxella catarrhalis by aminopenicillins and environmental factors and its potential contribution to the mechanism of resistance to aminopenicillins. *J Antimicrob Chemother*. **65**: 2089-96.

Jończyk-Matysiak E, Łodej N, Kula D, Owczarek B, Orwat F, Międzybrodzki R, Neuberg J, Bagińska N, Weber-Dąbrowska B, Górski A. (2019) Factors determining phage stability/activity: challenges in practical phage application. *Expert Rev Anti Infect Ther.* **17**: 583-606.

Kim JW, Dutta V, Elhanafi D, Lee S, Osborne JA, Kathariou S. (2012) A novel restriction-modification system is responsible for temperature-dependent phage resistance in *Listeria monocytogenes* ECII. *Appl Environ Microbiol*. **78**: 1995-2004.

Konkel ME, Tilly K. (2000) Temperature-regulated expression of bacterial virulence genes. *Microbes Infect*. **2**: 157-66.

Langmead, B. and Salzberg, S.L. (2012) Fast gapped-read alignment with Bowtie 2. *Nature Methods* **9**: 357-359.

Lehman SM, Kongari R, Glass AM, Koert M, Ray MD, Plaut RD, Stibitz S. (2022) Phage K gp102 Drives Temperature-Sensitive Antibacterial Activity on USA300 MRSA. *Viruses*. **15**: 17.

Leon-Velarde CG, Happonen L, Pajunen M, Leskinen K, Kropinski AM, Mattinen L, Rajtor M, Zur J, Smith D, Chen S, Nawaz A, Johnson RP, Odumeru JA, Griffiths MW, Skurnik M. (2016) *Yersinia enterocolitica*-Specific Infection by Bacteriophages TG1 and ϕR1-RT Is Dependent on Temperature-Regulated Expression of the Phage Host Receptor OmpF. *Appl Environ Microbiol*. **82**: 5340-53.

Love, M.I., Huber, W. and Anders, S. (2014) Moderated estimation of fold change and dispersion for RNA-seq data with DESeq2. *Genome Biology* **15**: 550.

Magoc, T., Wood, D. and Salzberg, S.L. (2013) EDGE-pro: Estimated degree of gene expression in prokaryotic genomes. *Evolutionary Bioinformatics* **9**: 127-136.

Middelboe M. (2000) Bacterial Growth Rate and Marine Virus-Host Dynamics. *Microb Ecol*. **40**: 114-124.

Muller HJ. (1928) The measurement of gene mutation rate in Drosophila, its high variability, and its dependence upon temperature. *Genetics*. **13**: 279–357.

Penesyan A, Paulsen IT, Kjelleberg S, Gillings MR. (2021) Three faces of biofilms: a microbial lifestyle, a nascent multicellular organism, and an incubator for diversity. *NPJ Biofilms Microbiomes*. **7**: 80.

Ramamurthy T, Ghosh A, Chowdhury G, Mukhopadhyay AK, Dutta S, Miyoshi SI. (2022) Deciphering the genetic network and programmed regulation of antimicrobial resistance in bacterial pathogens. *Front Cell Infect Microbiol*. **12**: 952491.

Salas M, Wernecki M, Fernández L, Iglesias B, Gutiérrez D, Álvarez A, García L, Prieto E, García P, Rodríguez A. (2020) Characterization of Clinical MRSA Isolates from Northern Spain and Assessment of Their Susceptibility to Phage-Derived Antimicrobials. *Antibiotics*. **9**: 447.

Tokman JI, Kent DJ, Wiedmann M, Denes T. (2016) Temperature Significantly Affects the Plaquing and Adsorption Efficiencies of *Listeria* Phages. *Front Microbiol*. **7**: 631.

Toledo-Arana A, Merino N, Vergara-Irigaray M, Debarbouille M, Penades JR, Lasa I. (2005*) Staphylococcus aureus* develops an alternative, ica-independent biofilm in the absence of the arlRS two-component system. *J Bacteriol* **187**: 5318-5329.

Valle J, Toledo-Arana A, Berasain C, Ghigo JM, Amorena B, Penadés JR, Lasa I. (2003) SarA and not sigmaB is essential for biofilm development by *Staphylococcus aureus*. *Mol Microbiol*. **48**: 1075-87.

Vergara-Irigaray M, Valle J, Merino N, Latasa C, García B, Ruiz de Los Mozos I, Solano C, Toledo-Arana A, Penadés JR, Lasa I. (2009) Relevant role of fibronectin-binding proteins in *Staphylococcus aureus* biofilm-associated foreign-body infections. *Infect Immun.* **77**: 3978-91.

Wdowiak M, Paczesny J, Raza S. (2022) Enhancing the Stability of Bacteriophages Using Physical, Chemical, and Nano-Based Approaches: A Review. *Pharmaceutics*. **14**: 1936.

Yang J, Bowring JZ, Krusche J, Lehmann E, Bejder BS, Silva SF, Bojer MS, Grunert T, Peschel A, Ingmer H. (2023) Cross-species communication via agr controls phage susceptibility in *Staphylococcus aureus*. *Cell Rep*. **42**: 113154.

You L, Suthers PF, Yin J. (2002) Effects of *Escherichia coli* physiology on growth of phage T7 in vivo and in silico. *J Bacteriol*. **184**: 1888-94.

Zaburlin D, Quiberoni A, Mercanti D. (2017) Changes in Environmental Conditions Modify Infection Kinetics of Dairy Phages. *Food Environ Virol*. **9**: 270-276.

CHAPTER 2

3.2. Positive interactions between bacteriophages and phage-derived proteins can be exploited for the development of improved *Staphylococcus aureus* biofilm eradication strategies

Recalcitrant biofilms formed on biotic and inert surfaces are an important reservoir for staphylococci in different environments. In this context, the combination of bacteriophages with their derived proteins may be a viable, largely unexplored strategy for the treatment of these structures. In the work described in this chapter, we have investigated the effectiveness of two combinations with the aim of boosting the efficacy of phage *Kayvirus rodi* against *S. aureus* biofilms. In the first one, we combined this virulent bacteriophage with the chimeric protein CHAPSH3b. An important advantage of mixing these antimicrobials is the removal of putative bacteriophage insensitive mutants (BIMs) that could be selected in the population, given that they are susceptible to the lytic protein. The second mixture used in our work was intended for elimination of the extracellular matrix, thus facilitating the access of the phage to susceptible bacterial cells. In this regard, we have explored the synergistic interaction between phage *K. rodi* and a polysaccharide depolymerase (Dpo7) from another phage (*Rockefellervirus* IPLA7) against biofilms formed by different *S. aureus* strains. Overall, this chapter shows the potential of taking advantage of synergistic interactions between a bacteriophage and proteins with different enzymatic activities derived from other phages that target the two main components of biofilm structure (bacteria and the extracellular matrix) for successful biofilm removal.

All of the results obtain are described in the following sections:

3.2.1. Synergistic action of phage *Kayvirus rodi* and lytic protein CHAPSH3b: a combination strategy to target *Staphylococcus aureus* biofilms

3.2.2. Draft genomes of the Bap-producing strain *Staphylococcus aureus* V329 and its derived phage-resistant mutant BIM-1

3.2.3. Exopolysaccharide depolymerase Dpo7 improves the removal of *Staphylococcus aureus* biofilms by phage *Kayvirus rodi*

3.2.1. Synergistic action of phage *Kayvirus rodi* and lytic protein CHAPSH3b: a combination strategy to target *Staphylococcus aureus* biofilms

ABSTRACT

Staphylococcus aureus is considered a priority pathogen due to its increasing acquisition of antibiotic resistance determinants. Additionally, this microbe has the ability to form recalcitrant biofilms on different biotic and inert surfaces. In this context, bacteriophages and their derived lytic proteins may be a forward-looking strategy to help combat staphylococcal biofilms. However, these antimicrobials exhibit individual limitations that may be overcome by combining them with other compounds.

This work investigates the combination of a phage-derived lytic protein, CHAPSH3b, and the virulent bacteriophage *Kayvirus rodi* (phiIPLA-RODI). The obtained results show the synergy between both antimicrobials for the treatment of 24-h-old *S. aureus* biofilms, with greater reductions in viable cell counts observed when phage and lysin are applied together compared to the individual treatments. Time-kill curves and confocal microscopy revealed that the fast antibacterial action of CHAPSH3b reduces the population up to 7 hours after initial exposure, which is subsequently followed by phage predation, limiting regrowth of the bacterial population. Moreover, at least 90% of bacteriophage insensitive mutants are susceptible to the lytic protein. Therefore, CHAPSH3b might help curtail the development of phage resistance during treatment. The combination of the lysin and *K. rodi* also showed promising results in an *ex vivo* pig skin model of wound infection. Overall, the results of this study demonstrate that the combination of phage-derived lytic proteins and bacteriophages can be a viable strategy to develop improved antibiofilm products.

INTRODUCTION

Staphylococcus aureus is a Gram-positive human opportunistic pathogen responsible for multiple infections (Beenken *et al.*, 2004; Archer *et al.*, 2011), including food poisoning due to the secretion of heat-stable enterotoxins (Schelin *et al.*, 2017; González-Martín *et al.*, 2020). Indeed, this microbe is armed with an arsenal of virulence factors, including numerous toxins, immune evasion factors, and molecules involved in biofilm development (González-Martín *et al.*, 2020).

Biofilm formation is a complex process involving the initial adherence of bacterial cells to a surface, followed by the production of an extracellular matrix (Azeredo and Sutherland, 2008; Lister and Horswill, 2014; Vasudevan, 2014). Importantly, biofilm-embedded cells are known for their increased ability to withstand antibiotics and disinfectants compared to planktonic cells (De la Fuente-Núñez *et al.*, 2013). This makes biofilms the perfect reservoir for pathogenic bacteria on surfaces of clinical and industrial settings. As such, biofilm formation by this pathogen simultaneously favors persistent infection, antibiotic resistance and immune evasion (Moormeier and Bayles, 2017). Moreover, biofilms are considered to be involved in at least 65% of all infections in humans (Costerton *et al.*, 1999; Hall-Stoodley *et al.*, 2004). In *S. aureus*, one of the major matrix components is polysaccharide intercellular adhesin (PIA)/poly-N-acetyl-1,6-b-glucosamine (PNAG), which is synthesized by the proteins encoded by the intercellular adhesion (*ica*) operon (Beloin and Ghigo, 2005) and provides structural integrity to the biofilms. However, some surface proteins, such as protein A (Merino *et al.*, 2009) or the biofilm associated protein (Bap) (Cucarella *et al.*, 2001, 2004), as well as extracellular DNA (eDNA) also contribute to biofilm matrix development and stabilization (Lister and Horswill, 2014).

Antimicrobial resistance has become a major medical threat worldwide and, in this context, *S. aureus* is currently considered a priority pathogen. For example, the World Health Organization (WHO) has estimated that 60% of all reported *S. aureus* infections in Europe are caused by methicillin-resistant strains (MRSA) (WHO, 2014). Also, resistance to vancomycin, the antibiotic of choice to treat MRSA infections, can be a cause of concern (Friães *et al.*, 2015). More recently, the lipopeptide daptomycin was introduced for the treatment of complicated staphylococcal infections, but resistant strains have also been isolated since then (Marty *et al.*, 2006).

In this scenario, bacteriophages (phages) and their derived proteins have been proposed as an alternative or complementary strategy to conventional therapeutics that may help to control the spread of antibiotic resistance in bacterial pathogens. One of the advantages of bacteriophages is their specificity against one bacterial genus or species, being innocuous against non-target bacteria. Moreover, phages are the most abundant biological entities on earth, multiply themselves naturally and are safe for humans (Pires *et al.*, 2017; Fernández *et al.*, 2019). Typically, phages degrade the structural peptidoglycan present in the bacterial cell wall using two classes of lytic proteins: virion-associated peptidoglycan hydrolases (VAPGHs) degrade peptidoglycan in the initial steps of the infection, and endolysins help release the phage progeny during the late phase of the lytic cycle (Schmelcher *et al.*, 2012; Oliveira *et al.*, 2013; Rodríguez-Rubio *et al.*, 2013; Gutiérrez *et al.*, 2018). The modular structure of lytic proteins facilitates the design of new chimeric proteins via domain shuffling, which frequently display improved lytic activity (Diaz *et al.*, 1990; Oliveira *et al.*, 2012; Schmelcher *et al.*, 2012) and overall enhanced traits (De Maesschalck *et al.*, 2020). These enzymes can be used as antibacterial agents targeting bacteria from the outside, accessing the peptidoglycan and destroying the cell walls (Fischetti, 2005; Loessner, 2005; Pires *et al.*, 2016). Furthermore, the rate of selection of bacterial resistance to lysins is very low (Gondil *et al.*, 2020) and, while still being quite specific, their spectrum of action generally exceeds that of bacteriophages. For all these reasons, phage lytic proteins constitute promising antimicrobial candidates.

Nevertheless, there are some disadvantages associated with the therapeutic use of both phages and phage-derived proteins. In the case of phages, it is common to observe the selection of bacteriophage insensitive mutants (BIMs) during therapy (Labrie *et al.*, 2010), together with their narrow host range (Loc-Carrillo and Abedon, 2011), and their potential contribution to horizontal gene transfer (Nobrega *et al.*, 2015). Similarly, there are also concerns associated with the use of phage lytic proteins. For instance, unlike phages, the concentration of these proteins decreases gradually after administration, as is also the case for standard-of-care antibiotics. Furthermore, it is important to ensure protein stability under the desired environmental conditions to avoid protein inactivation by factors like pH, temperature or degradation by proteases amongst others (Gutiérrez *et al.*, 2020).

One way to overcome the individual shortcomings of bacteriophages or lysins is by combining them with other antimicrobial agents. Indeed, several studies have

demonstrated that the combination of phages with antibiotics or antiseptics is promising, exhibiting a synergistic effect in biofilm removal experiments (Rahman *et al.*, 2011; Akturk *et al.*, 2019; Dickey and Perrot, 2019). Another strategy is the combination of multiple phages targeting different receptors in a single phage preparation, known as a phage cocktail (Chan *et al.*, 2013; Gutiérrez *et al.*, 2015). Phage lytic enzymes have also been combined with other antimicrobials like antibiotics (Shavrina *et al.*, 2016; Mirski *et al.*, 2019; Marzanna Łusiak-Szelachowska *et al.*, 2020), or used as part of a multi-enzyme approach by mixing them with depolymerases, which target polysaccharides such as those present in the extracellular matrix of biofilms (Olsen *et al.*, 2018). However, to our knowledge, no study has found synergistic effects between phages and lytic proteins.

In our previous work, we showed that chimeric protein CHAPSH3b, which consists of the CHAP domain from peptidoglycan hydrolase HydH5 and the SH3b cell wall binding domain (CBD) from lysostaphin (Rodríguez-Rubio *et al.*, 2012), displays antistaphylococcal activity in growth medium and milk, as well as biofilm-removal properties (Rodríguez-Rubio *et al.*, 2012; Fernández *et al.*, 2017). Furthermore, CHAPSH3b inhibits *S. aureus* biofilm formation, presumably by the downregulation of autolysin-encoding genes (Fernández *et al.*, 2017). Moreover, we have characterized the virulent phage vB_SauM_phiIPLA-RODI (*Kayvirus rodi*), which is also effective in eliminating staphylococcal biofilms (Gutiérrez *et al.*, 2015). This study aimed to assess the potential interactions between phage *K. rodi* and the phage-derived chimeric lytic protein CHAPSH3b when used together for biofilm removal.

METHODS

Bacterial strains, lytic proteins, bacteriophages and growth conditions

S. aureus strains used in this study included the dairy industry isolate *S. aureus* IPLA1 (Gutiérrez *et al.*, 2012), the clinical strain *S. aureus* 15981 (Valle *et al.*, 2003) and the bovine subclinical mastitis isolate *S. aureus* V329 (Cucarella *et al.*, 2001). These bacterial strains were routinely grown at 37ºC in TSB (tryptic soy broth, Scharlau Microbiology, Barcelona, Spain) by shaking or on plates containing TSB supplemented with 2% (w/v) agar (Roko, S.A., Llanera, Spain) (TSA). TSB top agar composed by TSB supplemented with 0.7% (w/v) agar was used for phage titration. TSB supplemented with 0.25% (v/v) glucose (Merck, Darmstadt, Germany) (TSBg) was used for biofilm formation assays.

Recombinant protein expression was carried out using *Escherichia coli* BL21 carrying the gene coding for CHAPSH3b cloned into plasmid pET21a as described by (Gutiérrez *et al.*, 2020). *E. coli* was routinely grown in LB medium, supplemented with 1 mM IPTG and 100 µg/ml ampicillin when necessary. The chimeric protein CHAPSH3b was subsequently purified as described previously (Gutiérrez *et al.*, 2020). Visual analysis and quantification of the concentration of the purified protein were performed by SDS-PAGE and the quick Start Bradford Protein Assay Kit (Bio-Rad Laboratories, USA), respectively.

Phage *K. rodi* was routinely propagated on *S. aureus* IPLA16 and partially purified by adding 10% polyethylene glycol (PEG) and 0.5 M NaCl for incubation at 4ºC during 16 h. Concentrated phage was obtained by centrifugation (10,000 rpm, 30 min, 4ºC), resuspended in TSB medium and stored at 4ºC until further use.

EOP determination and phage adsorption assays

To determine the EOP of phage *K. rodi* on the different strains, the phage titer on the test strain was divided by the titer on strain *S. aureus* IPLA1.

To estimate the phage adsorption rate, overnight cultures of the different *S. aureus* strains were diluted to an OD_{600} of 1. Next, 900 µl aliquots from these suspensions (~10^8 CFU/ml) were mixed with 100 µl of a *K. rodi* stock leading to final concentration of 10^7 PFU/ml (MOI = 0.1). A negative control was prepared by combining 900 µl of non-inoculated TSB with 100 µl of the phage stock. Phage adsorption was then allowed to occur for 5 min at room temperature. The samples were subsequently centrifuged for 3

min at 10,000 x *g* at 4 ºC. The number of non-adsorbed phages was calculated by titrating the resulting supernatants, and the phage adsorption rate was determined according to the following equation:

(1) phage adsorption rate = [(phage number in supernatant of control – phage number in supernatant sample) / (phage number in supernatant of control)] x 100

Biofilm formation and treatment

Overnight cultures of each *S. aureus* strain were diluted 1:100 (v/v) in fresh TSBg medium. Then, 1 ml of this bacterial suspension was inoculated into each well of a 24-well polystyrene microtiter plate (Thermo Scientific, Nunclon^{TM} Delta Surface) and the plates were incubated for 24 h at 37ºC. Afterwards, the planktonic phase was removed, and the biofilms were washed twice with phosphate-buffered saline (PBS; 137 mM NaCl, 2.7 mM KCl, 10 mM Na_2HPO_4, 2 mM KH_2PO_4 [pH 7.4]). The remaining adhered cells were then treated with 0.5 ml of TSB medium alone or using the same medium with different concentrations of protein CHAPSH3b (4 µM-8 µM) and/or phage *K. rodi* (1×10^9 PFU/ml - 1×10^{10} PFU/ml) at 37ºC. Treatment was allowed to act for 1 h, 3 h, 5 h, 7 h or 24 h. Then, the planktonic phase was removed and the adhered phase was washed twice with PBS. To assess the efficacy of the different treatments, the number of viable attached cells and total biomass were quantified. The number of viable cells present in the biofilms was determined by using the spot test. Briefly, biofilms were scraped and resuspended in PBS. Afterwards, 10 µl droplets from tenfold serial dilutions of this cell suspension were spotted onto TSA plates and allowed to dry. These plates were then incubated at 37ºC for 24 h.

The cell counts obtained in these experiments were first used to determine the number of CFUs per unit area (CFU/cm^2) and, subsequently, the potential interaction between the two antimicrobials (phage and lysin) as indicated using the following equation(Chaudhry *et al.*, 2017):

(2) [$\log_{10}$ CFU/cm^2 (phage+lysin)] - [$\log_{10}$ CFU/cm^2 (phage) + $\log_{10}$ CFU/cm^2 (lysin)]

The values obtained with the aforementioned equation were named interaction indices. The interaction was considered additive when this index was between -0.5 and 0.5, antagonistic when the value was < -0.5 and synergistic when the value was > 0.5.

Total biomass was quantified by performing the crystal violet staining assay as described previously (Gutiérrez *et al.*, 2014). Briefly, after washing the biofilm with PBS, 1 ml of 0.1% (w/v) crystal violet was added to each well. Fifteen minutes later, the excess of crystal violet was removed by washing twice with water. The remaining dye was then solubilized by adding 33% (v/v) acetic acid and the absorbance at 595 nm (A_{595}) was measured using a Benchmark Plus Microplate Spectrophotometer (Bio-Rad Laboratories, Hercules, CA, USA).

To monitor the evolution of the MOI throughout treatment, the number of viable cells and phage particles was determined in both the planktonic phase and the biofilm. Next, the values obtained for both phases were added to calculate the total number of infective phage particles and bacterial cells and the ratio between the two populations was calculated to determine the MOI by dividing the number of PFUs by the number of CFUs.

Determination of minimum inhibitory concentrations (MICs)

The MICs of the protein and the phage were determined using the broth microdilution technique in TSB medium with some modifications (CLSI, 2015). Thus, in the case of the phage, tenfold dilutions of the viral suspension were assayed instead of the usual twofold dilutions. The MIC was defined as the lowest concentration that inhibited visible bacterial growth after 24 h of incubation at 37ºC. The experiment was performed in triplicate and the MIC was expressed as the mode of three independent replicates.

Isolation of bacteriophage insensitive mutants (BIMs)

BIMs of *S. aureus* V329 were isolated as described previously (Gutiérrez *et al.*, 2015). Briefly, 100 µl from an overnight culture were mixed with 100 µl of phage (5×10^9 PFU/ml), spotted onto the centre of a 2% TSA plate and covered with 0.7% TSA. Afterwards, the plates were incubated for 24 h at 37ºC. Some of the surviving colonies were picked with a pipette tip and grown in fresh TSB medium for 16 h at 37ºC. The insensitive phenotype of the selected colonies was then confirmed by using the spot assay.

Quantification of the CHAPSH3b specific lytic activity

Overnight cultures of *S. aureus* V329 and the ten isolated BIM strains were grown at 37ºC with shaking and then the turbidity reduction assay was performed as described previously with some modifications (Obeso *et al.*, 2008). Briefly, after reaching an OD_{600}

of 0.5-0.6, the bacterial cells were washed and then resuspended in NaPi buffer (50 mM, pH 7.4) at a final OD_{600} ~ 1.0. Next, the freshly prepared cell suspensions were treated with two-fold dilutions of purified CHAPSH3b (0.027 – 1.720 mg/ml). The specific lytic activity of the protein was expressed in $OD_{600nm} \times min^{-1} \times mg\ protein^{-1}$ (Donovan *et al.*, 2006).

Analysis by CLSM and time-lapse microscopy

Confocal and time-lapse microscopy were performed as described previously, with some modifications (Fernández *et al.*, 2017). For confocal microscopy analysis, 24-h-old biofilms were formed by inoculating 2 ml of a *S. aureus* V329 cell suspension containing approximately 10^6 CFU/ml in TSBg in two-well µ-slides with a glass bottom (ibidi, Martinsried, Germany), and subsequent incubation under static conditions at 37ºC. After growth, the planktonic phase was removed and the biofilm was washed twice with PBS. Then, TSB medium alone or containing phage *K. rodi* (5×10^9 PFU/ml), protein CHAPSH3b (8 µM) or both together were added to the biofilm and incubated for 24 h at 37ºC. At the end of the treatment, wells were washed twice with PBS and stained with the Live/Dead® BacLight™ kit (Invitrogen AG, Basel, Switzerland). Samples were observed under a confocal scanning laser microscope (DMi8, Leica Microsystems) using a 63 oil objective.

For time-lapse microscopy, 24-h-old biofilms were grown at 37ºC and then washed twice with PBS. Next, different treatments were added to the biofilm: TSB containing protein CHAPSH3b (8 µM) or phage *K. rodi* (5×10^9 PFU/ml) combined with protein CHAPSH3b. Then the plate was placed in an incubation chamber, set at 37ºC, and connected to an inverted microscope (DMi8; Leica Microsystems) equipped with a Leica DFC365FX digital camera. Images were acquired every 15 min using LasX software (Leica Microsystems) for approximately 24 h.

***Ex vivo* pig skin model of wound infection and treatment**

To assess the antibiofilm effect of CHAPSH3b and *K. rodi* on a biotic surface, a previously described pig skin model was used with minor adaptions (Gerstmans *et al.*, 2020). Pig skin was obtained from the Minimally Invasive Surgery Center Jesús Usón (Cáceres, Spain). First, the upper layer was disinfected with 70% ethanol. This

disinfection was repeated after removing residual hair. Next, the skin was cut in 1×1 cm explants. To mimic a wound phenotype, a wound bed of 48 mm diameter and 1 mm depth was made using a hand drill with a cutter bit (Dremel® #192) in specific explants. Next, all the explants, with or without a wound, were submerged in 70% ethanol for 1 h followed by 30 minutes of UV decontamination to ensure complete sterility. Two different experimental setups were carried out in parallel, for explants with and without a wound. For each time point, three explants without a wound and three explants with a wound were placed in 24-well plates containing 1 ml physiological saline agar (0.9% (w/v) NaCl, 0.5% (w/v) agar, pH 5.5) to mimic human skin conditions. The explants were inoculated with *S. aureus* V329 (10^5 CFU/g of skin) and incubated at 37°C (5% CO_2) for 3 h to allow for biofilm formation. Then, the explants were treated with 100 µl CHAPSH3b (8 µM), *K. rodi* (MOI = 588), or 100 µl of a mixture containing CHAPSH3b (8 µM) and *K. rodi* (MOI = 588). Treatment with 100 µl of TSB was used as a negative control. Explants were processed after 0, 1, 5 and 24-h of treatment (37°C, 5% CO_2). After incubation, bacteria were recovered by inserting the explant in a stomacher bag (BagPage, BagSystem, Interscience, St-Nom-la-Breteche, France) containing 5 ml of PBS and homogenized using a stomacher for 2 × 90 seconds (model 80, Seward Medical, London, UK). From this, a tenfold dilution series was made in PBS and colony forming units (CFUs) were determined by plating duplicates on Baird-Parker agar plates that were incubated for 16-h at 37°C.

Statistical analysis. Statistical analysis of the biofilm data was carried out by multiple t-tests, using the Holm-Sidak method or Welch's correction using GraphPad Prism 6 software. p-values lower than 0.05 were considered significant.

RESULTS

Phage *Kayvirus rodi* and chimeric lysin CHAPSH3b act synergistically to remove staphylococcal biofilms

To examine the potential interactions between phage *Kayvirus rodi* and the lytic protein CHAPSH3b for biofilm removal, three *S. aureus* strains were chosen on the basis of their biofilm formation ability and matrix composition. These strains include *S. aureus* V329 and 15981, which have a strong biofilm production phenotype, and *S. aureus* IPLA1, a weak biofilm producer(Cucarella *et al.*, 2001; Gutiérrez *et al.*, 2014). Regarding their

matrix composition, *S. aureus* V329 biofilm is mostly composed of Bap (biofilm associated protein) and eDNA, whereas both *S. aureus* 15981 and IPLA1 biofilms mainly consist of exopolysaccharides (Gutiérrez *et al.*, 2014).

First, the susceptibility of the three strains to *K. rodi* and CHAPSH3b was determined by performing minimum inhibitory concentration (MIC) assays. The MIC values of the chimeric protein were quite similar for all three strains. Indeed, *S. aureus* IPLA1 and V329 strains showed identical susceptibility with an MIC of 60.5 µg/ml (~2 µM), whereas strain *S. aureus* 15981 had a higher MIC of 121.05 µg/ml (~4 µM). For phage *K. rodi*, strain *S. aureus* IPLA1 was the most susceptible, with an MIC of 10^3 PFU/ml, followed by *S. aureus* V329 with an MIC of 10^9 PFU/ml and, finally, *S. aureus* 15981, with an MIC over 10^9 PFU/ml. Additionally, the efficiency of plating (EOP) of *K. rodi* on strains IPLA1, 15981 and V329 were 1.0 ± 0.00, 0.80 ± 0.02 and 0.55 ± 0.19, respectively. In turn, the adsorption rates on strains IPLA1, 15981 and V329 were not significantly different from each other (83.77 ± 2.41 %, 85.34 ± 14.37 % and 79.97 ± 6.53 %, respectively).

Next, to establish the antibiofilm potential of these phage-derived antimicrobials, 24-h biofilms of the three strains were treated with different combinations of the phage at 10^{10} PFU/ml and the chimeric protein at 4 µM or 8 µM. The results indicated potential synergy between *K. rodi* and CHAPSH3b (Figure 3.1). Treatment of biofilms formed by *S. aureus* 15981 with the phage or the protein alone did not significantly affect the number of viable cells compared to an untreated control (Figure 3.7a). Conversely, the combination of both antimicrobials did lead to a significant reduction in viable cells of 1.4 (p=0.0498) and 1.9 log units (p=0.0152) at protein concentrations of 4 µM and 8 µM, respectively (Figure 3.1a). These results suggested a synergistic effect between phage and protein at 8 µM with an interaction index of 0.55. Interestingly, the interaction between the phage and the protein at 4 µM was additive with an interaction index of -0.45. Regarding total biomass, addition of the phage alone or the protein at 4 µM did not have any significant impact, whereas treatment with CHAPSH3b at 8 µM resulted in a significant biomass reduction (p=0.0076) (Figure 3.7b). The combination treatment always led to a decrease in total attached biomass (Figure 3.7b). In *S. aureus* IPLA1 biofilms, there was a significant reduction in viable cells when applying the bacteriophage individually (0.5 log units) (p=0.0284) or in combination with both concentrations of the protein (2.1 (p=0.0239) and 2.2 log units (p=0.0039) corresponding to 4 µM and 8 µM of CHAPSH3b, respectively),

but not with CHAPSH3b alone (Figure 3.7c). Thus, the combination of the phage with the chimeric protein at 4 and 8 μM had a synergistic effect with interaction index values of 1.10 and 1.27, respectively. Moreover, a significant reduction in total biomass was observed when using the phage alone ($p=0.035$) or combined with 8 μM CHAPSH3b ($p=0.011$) (Figure 3.7d). Finally, in the case of strain *S. aureus* V329, a significant reduction in both viable cell counts (Figure 3.7e) and biomass (Figure 3.7f) was observed when combining the phage with the protein at different concentrations. Thus, a reduction of 0.9 log units ($p=0.0059$) was observed when the biofilm was treated with the protein alone (4 μM), whereas a combination of the phage and the protein at 4 μM and 8 μM led to decreases of 2.1 ($p=0.0016$) and 2.2 ($p=0.0013$) log units, respectively. These results indicate that there was a synergistic effect in both cases, with interaction index values of 0.95 and 1.46 for 4 μM and 8 μM CHAPSH3b, respectively. Regarding total biomass, the protein alone or in combination with the phage significantly reduced the biofilm (p-values between <0.0001 and 0.0002). Of note, the reduction in total biomass was higher in V329 than in the other two strains tested.

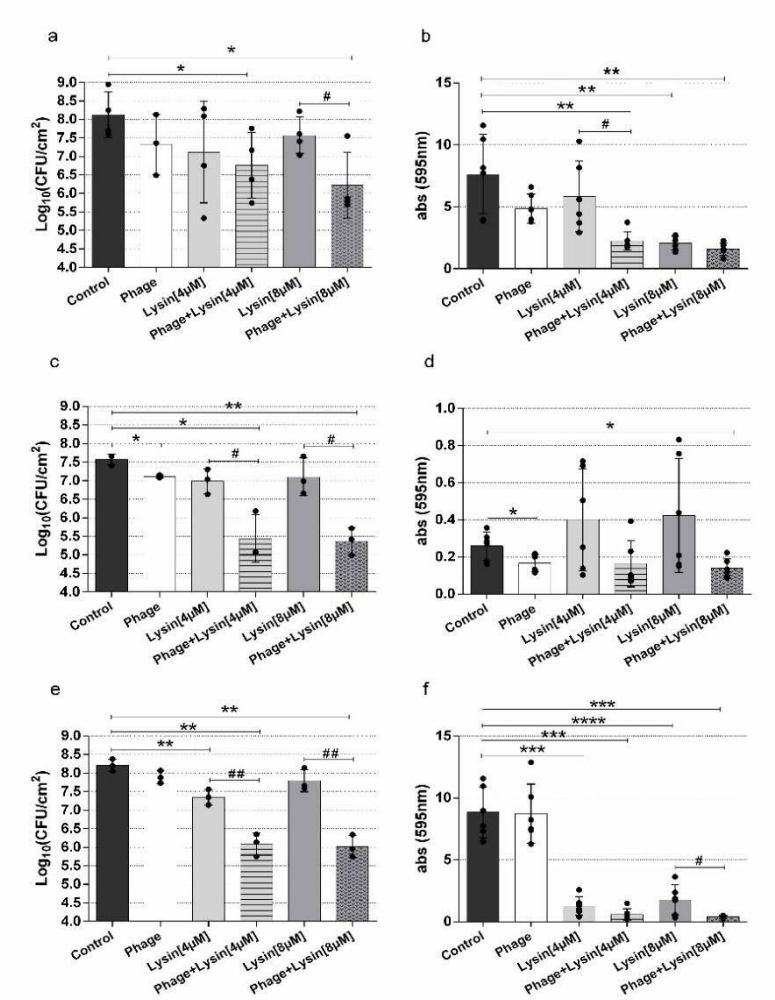

Figure 3.7 - **Treatment of preformed biofilms formed by different *S. aureus* strains.** Biofilms formed by *S. aureus* 15981 (a and b), IPLA1 (c and d) and V329 (e and f) were treated with bacteriophage *K. rodi* (10^{10} PFU/ml) (white bars), chimeric protein CHAPSH3b (4 and 8 μM) (light grey and dark grey bars, respectively) or the combination of both antimicrobials (striped and dotted bars). Biofilms were allowed to develop for 24 h and then treated for another 24 h at 37ºC. TSB medium alone was added to the control wells (black bars). After incubation, the viable cell counts of the three strains was determined (a, c and e) and the adhered biomass was quantified (A_{595}) by crystal violet staining (b, d and f). Data represent the means ± standard deviations of three independent experiments. Bars with an asterisk are statistically different from the untreated control, and bars with a hash sign are statistically different from the treatment with CHAPSH3b alone at the same concentration, according to the unpaired t-test with Welch's correction. */# p-value<0.05, **/## p-value < 0.01, ***/### p-value < 0.001 and ****/#### p-value< 0.0001.

Based on these results, the *S. aureus* strain V329 and a protein concentration of 8 µM were selected for further experiments to examine these synergistic interactions more closely, since these conditions exhibited the highest interaction index. To better understand the effect of the combination treatment on biofilm structure, 24-h-old biofilms were treated with only protein or combined with the phage and compared to an untreated control by visualization with confocal microscopy (CLSM). After 24 h of incubation without treatment, strain *S. aureus* V329 displayed thick, well-structured biofilms (Figure 3.8a and e). However, biofilm thickness was notably reduced after treatment with the protein alone (Figure 3.8b and f). In contrast, treatment with the phage alone did not lead to any major change compared to the untreated control (Figure 3.8c and g). However, the combination treatment had an even larger and more extensive impact than the protein alone (Figure 3.8d and h). Additionally, the latter biofilm contained a higher number of dead or compromised cells, which appeared red due to staining with propidium iodide (Figure 3.8d and h).

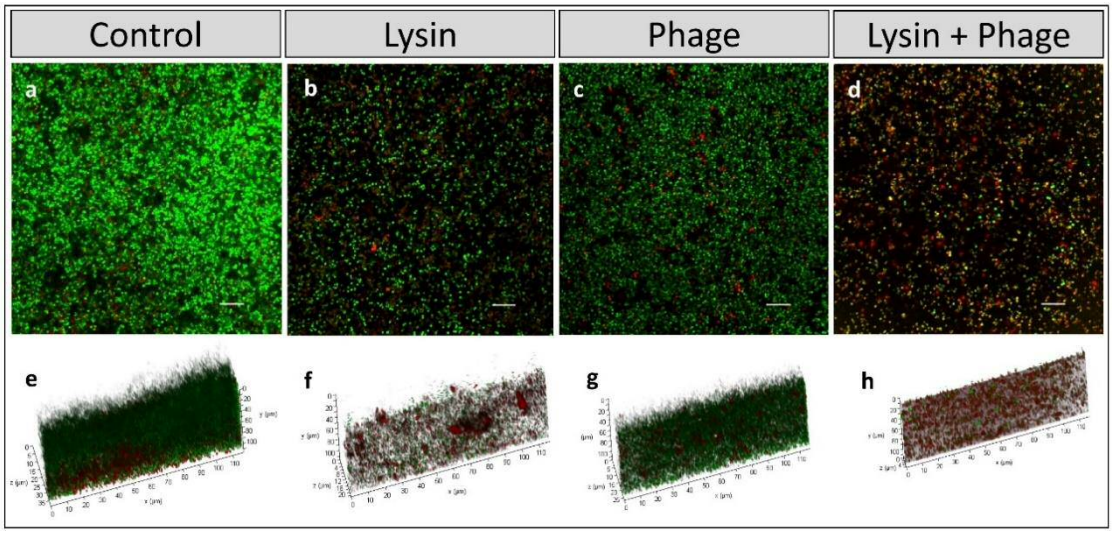

Figure 3.8 - CLSM images of LIVE/DEAD-stained *S. aureus* V329 24-h-old biofilms after different treatments. Preformed *S. aureus* V329 biofilms were treated for 24 h at 37ºC with TSB alone (a and e), 8 µM CHAPSH3b (b and f), 10^9 PFU/ml of phage *K. rodi* (c and g) or a combination of 8 µM CHAPSH3b and 10^9 PFU/ml of phage *K. rodi* (d and h). Green cells were intact cells, whereas eDNA and cells with compromised cell-envelope integrity were stained in red. Scale bars represent 10 µm.

Phage predation curtails regrowth of the microbial population after CHAPSH3b inactivation

To study the killing dynamics of the combination therapy using phage *K. rodi* and the chimeric protein CHAPSH3b, 24-h-old biofilms of strain *S. aureus* V329 were treated with a combination of phage (10^9 PFU/ml) and protein (8 μM) or the two antimicrobials independently. CHAPSH3b exhibited a notable disrupting activity against the biofilm after just 3 h of treatment, judging by the reduction (0.7 log units) in attached bacterial counts (Figure 3.9). Viable cell counts further decreased after 5 h of treatment (1.4 log units), and the maximum reduction (2.5 log units) was achieved after 7 h (Figure 3.9). However, regrowth of the bacterial population was observed after 24 h of incubation at 37ºC, reaching viable cell counts similar to those of the untreated control. In contrast to the lytic protein, phage *K. rodi* was not efficient in killing the bacterial cells attached to the surface at any time point. In spite of this, the phage did have an impact when combined with CHAPSH3b, demonstrating to be even more effective for biofilm removal than the protein alone. Thus, reductions in viable cell counts of 1.4 log units, 2.8 log units and 2.8 log units were respectively observed after 3 h, 5 h and 7 h of treatment. However, the most remarkable difference with the CHAPSH3b treatment was noted at the 24-h time point. In fact, even though the number of cells increased between the 7 h and 24 h time points in samples treated with the phage and protein combination, viable counts remained much lower than those in the untreated control (reduction of 2.2 log units). These results were subsequently confirmed by time-lapse microscopy analysis, although the action of the lysin stopped at an earlier time point under these conditions (Figure 3.10). Thus, when the biofilm was treated with CHAPSH3b alone, there was a gradual reduction in the number of viable cells up to 5 h post-treatment. However, after this time point, there is a gradual increase in bacterial cell coverage during the remaining incubation time. The results observed during the initial 5 h of incubation were fairly similar when treatment was carried out using a combination of the protein and phage. By contrast, cell proliferation after this time point was significantly slowed down by the presence of the phage. Indeed, the number of cells after 24 h of treatment was clearly reduced compared to the individual treatment with CHAPSH3b.

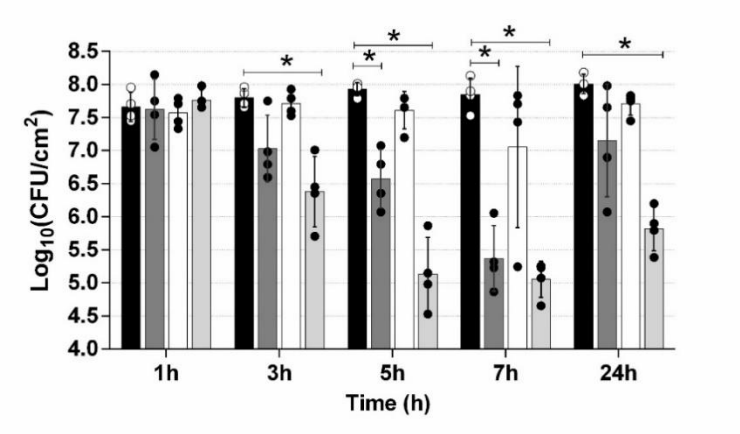

Figure 3.9 - **Time-kill curve of protein CHAPSH3b and/or phage *Kayvirus rodi* against *S. aureus* V329 biofilms.** 24-h-old biofilms were treated with protein at 8 μM (grey bars), phage at 1×10^9 PFU/ml (white bars) or a combination of both (light grey bars) and incubated for 1, 3, 5, 7 or 24 hours at 37ºC. Control wells were treated with TSB medium alone (black bars). Data correspond to the means ± standard deviations of four independent experiments, and represented in logarithmic scale in colony forming units per cm^2 of biofilm. Bars with an asterisk are statistically different ($p<0.05$) from the untreated control according to the Student's t-test using the Holm-Sidak method.

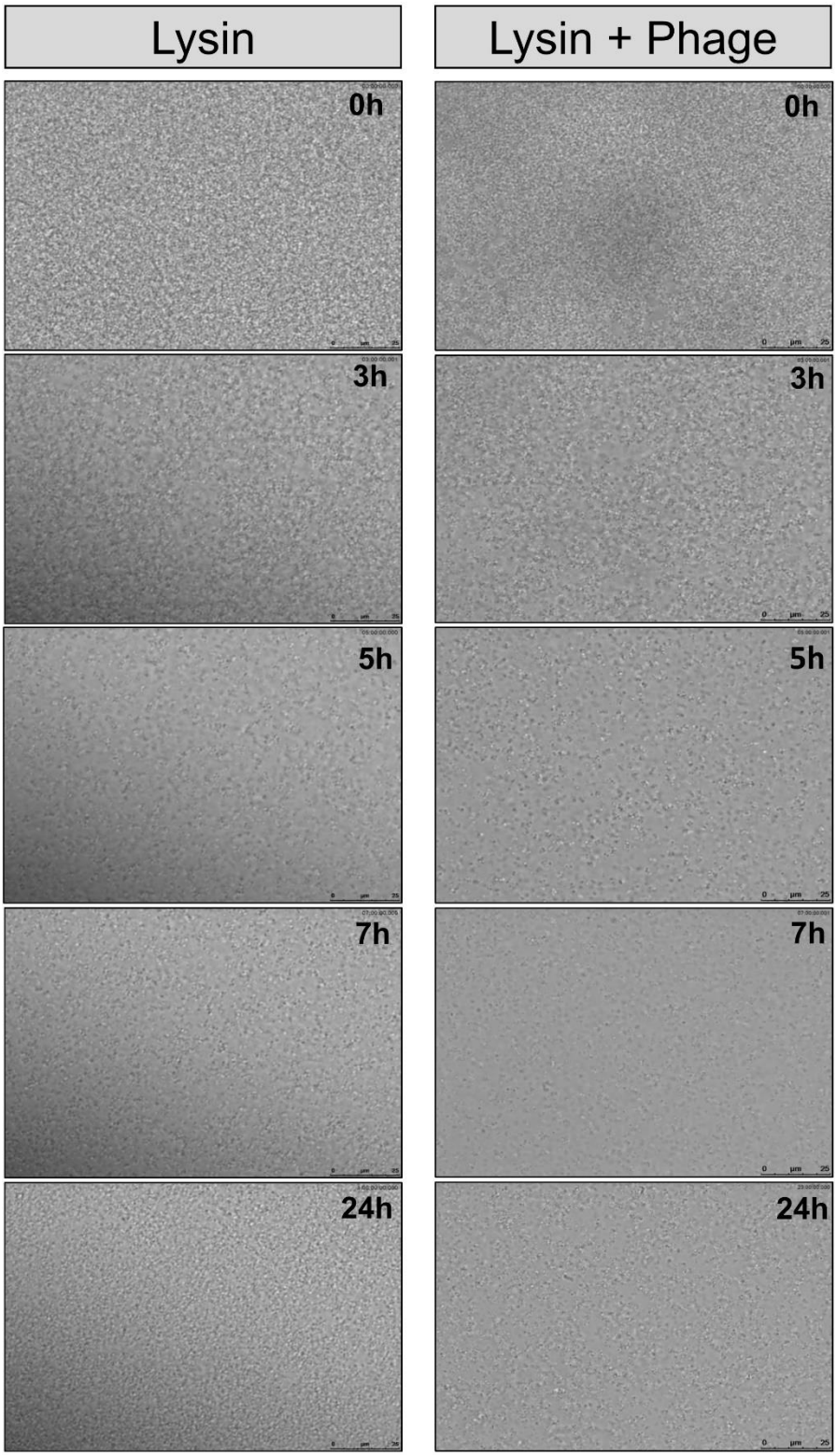

Figure 3.10 - Time-lapse microscopy of 24-h-old *S. aureus* V329 biofilms treated with CHAPSH3b (8 µM) (left) or CHAPSH3b (8 µM) + phage *Kayvirus rodi* (10^9 PFU/ml) (right) during 24 h at 37 ºC. During the treatment is is possible to see changes in bacterial population. There is a decrease in cells until 7 h of treatment in bothe cases.

However, after 7 h the bacterial population regrowth until similar bacterial population of time 0 when used lysin alone. When treatment is added together, lysin and phage, at 24 h the cells are damaged compared with the treatment with lysin alone and with less biomass.

Bacterial killing by CHAPSH3b increases the MOI of *Kayvirus rodi* after three hours of treatment

Next, we sought to explore the mechanism(s) of the synergy between phage *K. rodi* and CHAPSH3b. One potential explanation for this phenomenon is that clearance of the biofilm by the protein might make bacterial cells more accessible to phage particles. Additionally, fast killing by the protein may lead to an increase in the phage-to-bacteria ratio (MOI). This would enhance the ability of the virus to exert a noticeable effect on the bacterial population. To test this possibility, the MOI in V329 biofilms treated with the phage-protein combination was compared to that in biofilms treated with the phage alone (Figure 3.11). After 1 hour of treatment, the starting MOI of 30.67 dropped to 11.89 and 0.70 in the phage and phage-protein treatment, respectively. However, this trend changed at later time points. Indeed, after 3 hours of incubation the MOI was consistently higher in the samples treated with *K. rodi* combined with CHAPSH3b (Figure 3.11). The MOI values after 3, 5, 7 and 24 hours of treatment with phage alone were 1.42, 6.92, 4.78 and 0.46, respectively. In contrast, the values obtained at the same time points in the wells corresponding to the combination treatment were 137.55, 74.65, 510.80 and 43.48, respectively.

A similar trend was observed in *S. aureus* 15981, which forms strong, polysaccharide-based biofilms. In this strain, however, CHAPSH3b exerted a faster effect, with a significant reduction in cell numbers after just one hour of incubation, and regrowth of protein-treated samples was slower than in V329 (supplementary material Figure 7.3a). In this case, the MOI values were consistently higher in the samples treated with the protein-phage combination compared to those exposed only to the phage at all the analysed time points. Indeed, the calculated MOIs after 1, 3, 5, 7 and 24 hours of incubation were 0.001, 0.02, 0.10, 0.12 and 0.06 in samples treated with *K. rodi*, while the values estimated for the combination treatment were 0.30, 16.85, 198.47, 46.70 and 33.94 (supplementary material Figure 7.3b).

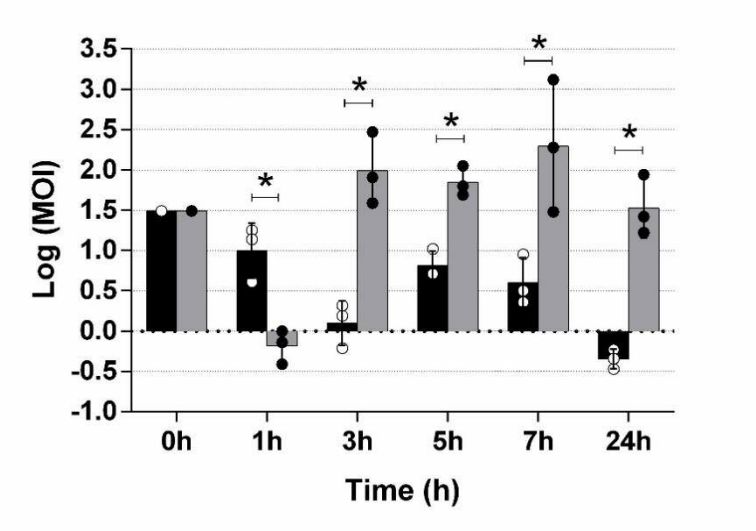

Figure 3.11 - Changes in the MOI during incubation of *S. aureus* V329 biofilms treated with phage *Kayvirus rodi* or a combination of phage and protein CHAP-SH3b. 24-h-old biofilms were treated with phage at 1×10^9 PFU/ml (black bars) or a combination of phage at 1×10^9 PFU/ml and protein at 8 μM (grey bars), and incubated for 1, 3, 5, 7 or 24 hours at 37ºC. Data correspond to the means ± standard deviations of three independent experiments, and represent the logarithm of the MOI for each time point. Bars with an asterisk are statistically different ($p<0.05$) from each other according to the Student's t-test using the Holm-Sidak method.

CHAPSH3b can kill at least 90% of phage-resistant mutants

It is also a possibility that CHAPSH3b may limit phage-resistance development by killing resistant mutants. To better discern if this might be the case, ten BIMs of *S. aureus* V329 with resistance to phage *K. rodi* were isolated to compare their CHAPSH3b susceptibility to that of the wild type. This was achieved by determining the specific lytic activity of CHAPSH3b against the different strains. The specific activity of the chimeric protein against the wild-type strain *S. aureus* V329 was 0.051 $\Delta OD_{600nm} \times min^{-1} \times mg\ protein^{-1}$, with similar results obtained for seven out of ten BIMs (BIM-2, BIM-4, BIM-6, BIM-7, BIM-8, BIM-9 and BIM-10) (Table 3.1). By contrast, the specific activity displayed by CHAPSH3b in mutants BIM-1, BIM-3 and BIM-5 was significantly lower ($p<0.05$) compared to the wild type (Table 3.3). Nonetheless, it must be noted that in BIM-3 and BIM-5 the protein could still effectively eliminate bacterial cells, whereas BIM-1 exhibited resistance to CHAPSH3b. Of note, there was no significant difference in

biofilm formation between the ten BIM strains and the wild-type strain (supplementary material Figure 7.4).

Table 3.3 - Specific lytic activity of the protein CHAPSH3b against *S. aureus* V329 and *S. aureus* V329-derived BIMs. Values represent the means ± standard deviations from three independent replicates. * indicate values that are statistically different ($p<0.05$) from those of wild-type strain using the unpaired t-test with Welch's correction.

Strains	Specific lytic activity $\Delta OD_{600nm} \times min^{-1} \times mg\ protein^{-1}$
V329	0.051 ± 0.004
BIM-1	-0.015 ± 0.010 *
BIM-2	0.060 ± 0.023
BIM-3	0.033 ± 0.001 *
BIM-4	0.039 ± 0.007
BIM-5	0.028 ±0.009 *
BIM-6	0.054 ± 0.013
BIM-7	0.067 ± 0.027
BIM-8	0.063 ± 0.040
BIM-9	0.073 ± 0.020
BIM-10	0.063 ± 0.011

The combination of CHAPSH3b and *Kayvirus rodi* limits bacterial regrowth in an *ex vivo* model of wound infection

To evaluate the antibiofilm potential of our compounds on a biotic surface, we implemented an *ex vivo* pig skin model of wound infection. Premature, 3-h-old biofilms established on both intact and wounded pig skin, were treated with 8 μM CHAPSH3b, phage *K. rodi* (10^9 PFU/ml, MOI=588) or a mixture of both protein and phage (Figure 3.12). Generally speaking, all treatments led to a significant reduction in the bacterial number after 1 h in intact skin. However, in wounded skin, this reduction was only significant for the combination treatment ($p\leq0.05$). Of note, treatments with CHAPSH3b and a combination of protein and *K. rodi* resulted in a bacterial reduction of 1.3 and 1.04 log units, respectively, in the intact skin infection model (Figure 3.12a). These values were almost the same as those observed in the wound infection model (1 and 1.4 log units, respectively, for the same treatments) (Figure 3.12b). 5-h post-treatment, a significant difference in bacterial numbers was observed for the treatment with *K. rodi* (0.8 log units) and the combination of CHAPSH3b/ *K. rodi* (3.3 log units). At the end of the experiment,

all treatments resulted in a reduced number of viable bacteria compared to the untreated control. In both *ex vivo* models, the reduction in bacterial cells after 24 h of treatment was higher when using *K. rodi* or the combination of phage and protein (~2.5 log units of reduction). In contrast, treatment with the protein alone led to final reductions of only ~1 log unit in both models.

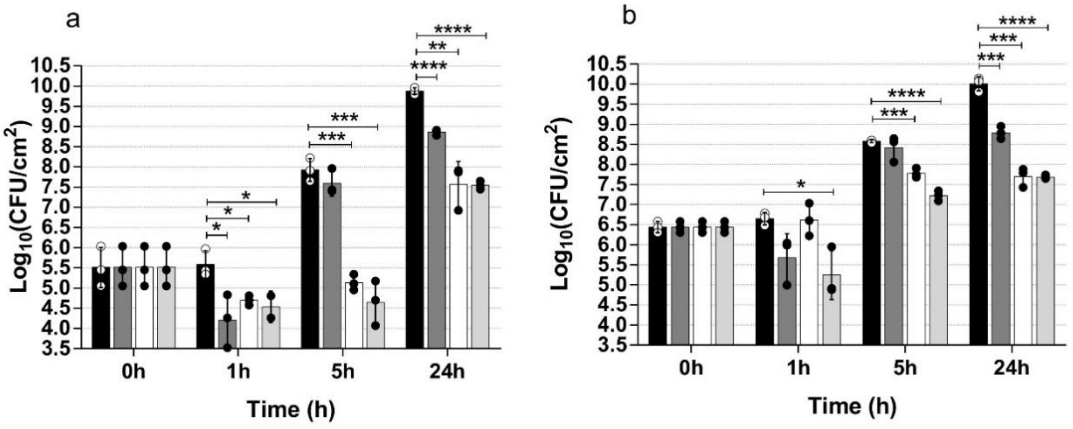

Figura 3.12 - Antibiofilm effect of CHAPSH3b, *Kayvirus rodi* or a combination of both on premature biofilms in an *ex vivo* model of (a) intact and (b) wounded skin. A porcine *ex vivo* model of intact skin and skin wound infection (n=3) infected with 3-h-old biofilms of *S. aureus* V329 (~10^5 CFU/g skin) was treated with either CHAPSH3b (8 µM), *K. rodi* (MOI of 588) or a combination of both (8 µM and MOI of 588, respectively). Bars represent the means and standard deviations of three independent experiments. Bars with an asterisk are statistically different ($p<0.05$) from the untreated control according to the Student's t-test using the Holm-Sidak method.

DISCUSSION

Amidst the current antibiotic resistance crisis, bacterial biofilms pose a particularly dangerous threat. These complex multicellular structures are, by nature, considerably more resistant to antimicrobials than their planktonic counterparts. Moreover, when biofilms are formed by multidrug-resistant bacteria, the chances of successfully eliminating them are even lower. It is, therefore, necessary to find alternative strategies that can replace or complement the currently available antibiofilm agents. In this context, phage-based antimicrobials are promising candidates. Bacterial viruses themselves can

be used for biofilm removal given their ability to specifically infect and kill their host, even when embedded in an extracellular matrix (González *et al.*, 2018). However, bacteriophage treatment is known to select phage-resistant bacteria, even though such resistant variants are often poor biofilm formers and/or display growth defects (Gutiérrez *et al.*, 2015). Phage-derived lytic proteins can also be powerful antibiofilm weapons that rapidly lyse their target cells without the significant selection of resistant variants (Gutiérrez *et al.*, 2018). Like phages, lytic proteins are quite specific and, as a result, harmless for non-target bacteria and, very importantly, eukaryotic cells. Moreover, some lytic proteins have been shown to kill persister cells, a characteristic that is a major asset for an antibiofilm agent (Gutiérrez *et al.*, 2014). Indeed, biofilms usually exhibit a higher proportion of persister cells than planktonic populations, a characteristic that boosts their ability to withstand an antimicrobial challenge (De la Fuente-Núñez *et al.*, 2013). On a critical note, lytic proteins do not increase in number during treatment and, depending on the environmental conditions, can often be unstable and only remain active for a relatively short time, thus allowing bacterial regrowth or requiring repeated dosing. This work explores the potential of harnessing the advantages of both phages and lytic proteins to compensate for each other's weaknesses with the aim of developing a more effective antimicrobial combination.

Previous studies had already shown the ability of phage *Kayvirus rodi* (phiIPLA-RODI) and chimeric protein CHAPSH3b to kill biofilm-embedded *S. aureus* cells belonging to certain strains (Gutiérrez *et al.*, 2015; Fernández *et al.*, 2017). As a result, they seemed a good choice to carry out interaction assays against three *S. aureus* strains. At the end of the 24-hour treatment, neither antimicrobial was effective for controlling the bacterial population. In spite of this, exposure to the protein did decrease the amount of attached biomass in strains 15981 and V329, which might be due to its biofilm inhibiting properties (Fernández *et al.*, 2017). Indeed, Fernández *et al.* (Fernández *et al.*, 2017) already demonstrated that subinhibitory concentrations of this protein had a negative impact on biofilm formation by *S. aureus* that might be linked to downregulation of autolysin-encoding genes. The fact that this effect was not observed in strain IPLA1 might be a consequence of the weak biofilm formation of this strain in TSB without added glucose. In contrast to these results, combination of both antimicrobials had a much more significant impact on the biofilm population for all three strains, independently of their susceptibility to *K. rodi*. In view of these data, it appears that application of phage *K. rodi*

combined with protein CHAPSH3b would constitute a viable antibiofilm strategy. Examples of combining these two phage-based strategies, i.e. phage therapy and lytic proteins, are scarce. In fact, we are only aware of one study in which a phage-endolysin combination was tested in a mouse sepsis model against *Acinetobacter baumannii* (Wu *et al.*, 2018). In this example, the combination gave similar results to the endolysin alone, although it is worth mentioning that the authors only tested one concentration of phage and protein against a single bacterial strain. With that in mind, it cannot be excluded that different conditions might have led to the observation of a synergistic interaction. Nonetheless, it is likely that, as is the case of other antimicrobials, the existence of synergy will depend on the specific phage-protein combination and the bacterial strain. There are several studies reporting the existence of synergy between either phages or phage lytic proteins with antibiotics (Rahman *et al.*, 2011; Shavrina *et al.*, 2016; Akturk *et al.*, 2019; Dickey and Perrot, 2019; Mirski *et al.*, 2019; Marzanna Łusiak-Szelachowska *et al.*, 2020). In some cases, such combinations were able to reduce the biofilm population depending on the antibiotic and its concentration. Nevertheless, there is evidence that antibiotics can also have a negative impact on phage treatment. This is particularly the case for drugs that inhibit nucleic acid or protein synthesis, as they collaterally interfere with phage propagation (Akturk *et al.*, 2019). However, this antagonism depends on the duration of the treatment and the antibiotic concentration used (Torres-Barceló, 2018; Akturk *et al.*, 2019). Moreover, any strategy involving conventional antimicrobials has the potential risk of contributing to the antibiotic resistance problem. These two important shortcomings of phage/antibiotics combination therapy would be avoided when combining phages and lytic proteins.

Once ascertained that combining a virulent phage, *K. rodi*, with CHAPSH3b for biofilm treatment has a positive impact, we sought to better understand the basis for this interaction. The results of this analysis suggest that the presence of the phage, which has no effect by itself, appears to limit the regrowth of the bacterial population that follows inactivation of the lytic protein. On the other hand, the protein, by lysing part of the bacterial population, increases the phage-to-bacteria ratio, thereby allowing the phage to exert a significant impact on biofilm removal. In addition to changing the phage-to-bacteria ratio, CHAPSH3b also might enhance phage efficacy by killing potential phage-resistant variants present in the biofilm. Indeed, our results show that at least 90% of BIMs are susceptible to the lytic protein. Finally, a third potential contribution of the lytic

protein might be by loosening the biofilm, thus making cells more accessible to phage infection.

When comparing the different antibiofilm strategies in *ex vivo* experiments using the pig skin model, we observed that *K. rodi* was more effective than CHAPSH3b in limiting the growth of the bacterial population in the long term. This might be associated with the fact that porcine skin is a nutrient-rich environment that favours bacterial growth and, consequently, facilitates phage propagation. Nonetheless, it must be noted that the combination treatment generally led to a faster decrease in the short term compared to the phage alone.

This study shows how we can take advantage of the synergistic interaction between bacteriophages and lytic proteins to develop a two-speed antibiofilm cocktail. In this model, the lytic proteins initiate rapid killing of the microbial community. Once the lysin activity dwindles, the phage present in the mixture will continue its antimicrobial action. This slower but longer-term effect limits regrowth of the target bacterium, thereby facilitating removal by a subsequent treatment. Overall, this strategy provides an interesting antibiotic-free alternative for biofilm elimination with low potential for resistance selection.

REFERENCES

Akturk, E., Oliveira, H., Santos, S.B., Costa, S., Kuyumcu, S., Melo, L.D.R., and Azeredo, J. (2019) Synergistic action of phage and antibiotics: Parameters to enhance the killing efficacy against mono and dual-species biofilms. *Antibiotics* **8**: 1–19.

Archer, N.K., Mazaitis, M.J., William Costerton, J., Leid, J.G., Powers, M.E., and Shirtliff, M.E. (2011) *Staphylococcus aureus* biofilms: Properties, regulation and roles in human disease. *Virulence* **2**: 445–449.

Azeredo, J. and Sutherland, I. (2008) The Use of Phages for the Removal of Infectious Biofilms. *Curr Pharm Biotechnol* **9**: 261–266.

Beenken, K.E., Dunman, P.M., McAleese, F., Macapagal, D., Murphy, E., Projan, S.J., et al. (2004) Global gene expression in *Staphylococcus aureus* biofilms. *J Bacteriol* **186**: 4665–4684.

Beloin, C. and Ghigo, J.M. (2005) Finding gene-expression patterns in bacterial biofilms. *Trends Microbiol* **13**: 16–19.

Chan, B.K., Abedon, S.T., and Loc-Carrillo, C. (2013) Phage cocktails and the future of phage therapy. *Future Microbiol* **8**: 769–783.

Chaudhry, W.N., Concepcion-Acevedo, J., Park, T., Andleeb, S., Bull, J.J., and Levin, B.R. (2017) Synergy and order effects of antibiotics and phages in killing *Pseudomonas aeruginosa* biofilms. *PLoS One* **12**: e0168615.

CLSI (2015) Performance Standards for Antimicrobial Susceptibility Testing; Twenty-Fifth Informational Supplement An informational supplement for global application developed through the Clinical and Laboratory Standards Institute consensus process. CLSI approved doc, Wayne, PA .

Costerton, J.W., Stewart, P.S., and Greenberg, E.P. (1999) Bacterial Biofilms: A Common Cause of Persistent Infections. *Science* **284**: 1318–1322.

Cucarella, C., Solano, C., Valle, J., Amorena, B., Lasa, Í., and Penadés, J.R. (2001) Bap, a *Staphylococcus aureus* surface protein involved in biofilm formation. *J Bacteriol* **183**: 2888–2896.

Cucarella, C., Tormo, M.Á., Úbeda, C., Trotonda, M.P., Monzón, M., Peris, C., et al. (2004) Role of Biofilm-Associated Protein Bap in the Pathogenesis of Bovine *Staphylococcus aureus*. *Infect Immun* **72**: 2177–2185.

Diaz, E., Lopez, R., and Garcia, J.L. (1990) Chimeric phage-bacterial enzymes: A clue to the modular evolution of genes. *Proc Natl Acad Sci U S A* **87**: 8125–8129.

Dickey, J. and Perrot, V. (2019) Adjunct phage treatment enhances the effectiveness of low antibiotic concentration against *Staphylococcus aureus* biofilms in vitro. *PLoS One* **14**: e0209390.

Donovan, D.M., Lardeo, M., and Foster-Frey, J. (2006) Lysis of Staphylococcal mastitis pathogens by bacteriophage phi11 endolysin. *FEMS Microbiol Lett* **265**: 133–139.

Fernández, L., González, S., Campelo, A.B., Martínez, B., Rodríguez, A., and García, P. (2017) Downregulation of Autolysin-Encoding Genes by Phage-Derived Lytic Proteins Inhibits Biofilm Formation in *Staphylococcus aureus*. *Antimicrob Agents Chemother* **61**: e02724-16.

Fernández, L., Gutiérrez, D., García, P., and Rodríguez, A. (2019) The Perfect Bacteriophage for Therapeutic Applications—A Quick Guide. *Antibiotics* **8**: 126.

Fischetti, V.A. (2005) Bacteriophage lytic enzymes:novel anti-infectives. *Trends Microbiol* **13**: 491–496.

Friães, A., Resina, C., Manuel, V., Lito, L., Ramirez, M., and Melo-Cristino, J. (2015) Epidemiological survey of the first case of vancomycin-resistant *Staphylococcus aureus* infection in Europe. *Epidemiol Infect* **143**: 754–748.

Gerstmans, H., Gerstmans, H., Gerstmans, H., Grimon, D., Gutiérrez, D., Gutiérrez, D., et al. (2020) A VersaTile-driven platform for rapid hit-to-lead development of engineered lysins. *Sci Adv* **6**: eaaz1136.

Gondil, V.S., Harjai, K., and Chhibber, S. (2020) Endolysins as emerging alternative therapeutic agents to counter drug-resistant infections. *Int J Antimicrob Agents* **55**: 105844.

González-Martín, M., Corbera, J.A., Suárez-Bonnet, A., and Tejedor-Junco, M.T. (2020) Virulence factors in coagulase-positive staphylococci of veterinary interest other than *Staphylococcus aureus*. *Vet Q* **40**: 118–131.

González, S., Fernández, L., Gutiérrez, D., Campelo, A.B., Rodríguez, A., and García, P. (2018) Analysis of Different Parameters Affecting Diffusion, Propagation and Survival of Staphylophages in Bacterial Biofilms. *Front Microbiol* **9**: 1–13.

Gutiérrez, D., Delgado, S., Vázquez-Sánchez, D., Martínez, B., Cabo, M.L., Rodríguez, A., et al. (2012) Incidence of *Staphylococcus aureus* and Analysis of Associated Bacterial Communities on Food Industry Surfaces. *Appl Environ Microbiol* **78**: 8547–8554.

Gutiérrez, D., Fernández, L., Rodríguez, A., and García, P. (2018) Are phage lytic proteins the secret weapon to kill *Staphylococcus aureus*? *Am Soc Microbiol* **9**: e01923-17.

Gutiérrez, D., Garrido, V., Fernández, L., Portilla, S., Rodríguez, A., Grilló, M.J., and García, P. (2020) Phage Lytic Protein LysRODI Prevents Staphylococcal Mastitis in Mice. *Front Microbiol* **11**:.

Gutiérrez, D., Ruas-Madiedo, P., Martínez, B., Rodríguez, A., and García, P. (2014) Effective Removal of Staphylococcal Biofilms by the Endolysin LysH5. *PLoS One* **9**: e107307.

Gutiérrez, D., Vandenheuvel, D., Martínez, B., Rodríguez, A., Lavigne, R., and García, P. (2015) Two phages, phiIPLA-RODI and phiIPLA-C1C, lyse mono-and dual-species Staphylococcal biofilms. *Appl Environ Microbiol* **81**: 3336–3348.

Hall-Stoodley, L., Costerton, J.W., and Stoodley, P. (2004) Bacterial biofilms: From the natural environment to infectious diseases. *Nat Rev Microbiol* **2**: 95–108.

De la Fuente-Núñez, C., Reffuveille, F., Fernández, L., and Hancock, R.E.W. (2013) Bacterial biofilm development as a multicellular adaptation: Antibiotic resistance and new therapeutic strategies. *Curr Opin Microbiol* **16**: 580–589.

Labrie, S.J., Samson, J.E., and Moineau, S. (2010) Bacteriophage resistance mechanisms. *Nat Rev Microbiol* **8**: 317–327.

Lister, J.L. and Horswill, A.R. (2014) *Staphylococcus aureus* biofilms: Recent developments in biofilm dispersal. *Front Cell Infect Microbiol* **4**: 1–9.

Loc-Carrillo, C. and Abedon, S.T. (2011) Pros and cons of phage therapy. *Bacteriophage* **1**: 111–114.

Loessner, M.J. (2005) Bacteriophage endolysins — current state of research andapplications. *Curr Opin Microbiol* **8**: 480–487.

De Maesschalck, V., Gutiérrez, D., Paeshuyse, J., Lavigne, R., and Briers, Y. (2020) Advanced engineering of third-generation lysins and formulation strategies for clinical applications. *Crit Rev Microbiol* 1–17.

Marty, F.M., Yeh, W.W., Wennersten, C.B., Venkataraman, L., Albano, E., Alyea, E.P., et al. (2006) Emergence of a clinical daptomycin-resistant *Staphylococcus aureus* isolate during treatment of methicillin-resistant *Staphylococcus aureus* bacteremia and osteomyelitis. *J Clin Microbiol* **44**: 595–597.

Marzanna Łusiak-Szelachowska, M., Weber-Da˛browska, B., and Górski, A. (2020) Bacteriophages and Lysins in Biofilm Control. *Virol Sin* **35**: 125–133.

Merino, N., Toledo-Arana, A., Vergara-Irigaray, M., Valle, J., Solano, C., Calvo, E., et al. (2009) Protein A-mediated multicellular behavior in *Staphylococcus aureus*. *J Bacteriol* **191**: 832–843.

Mirski, T., Lidia, M., Nakonieczna, A., and Gryko, R. (2019) Bacteriophages, phage endolysins and antimicrobial peptides – the possibilities for their common use to combat infections and in the design of new drugs. *Annals Agric Environ Med* **26**: 203–209.

Moormeier, D.E. and Bayles, K.W. (2017) *Staphylococcus aureus* biofilm: a complex developmental organism. *Mol Microbiol* **104**: 365–376.

Nobrega, F.L., Costa, A.R., Kluskens, L.D., and Azeredo, J. (2015) Revisiting phage therapy: New applications for old resources. *Trends Microbiol* **23**: 185–191.

Obeso, J.M., Martínez, B., Rodríguez, A., and García, P. (2008) Lytic activity of the recombinant staphylococcal bacteriophage ΦH5 endolysin active against *Staphylococcus aureus* in milk. *Int J Food Microbiol* **128**: 212–218.

Oliveira, H., Azeredo, J., Lavigne, R., and Kluskens, L.D. (2012) Bacteriophage endolysins as a response to emerging foodborne pathogens. *Trends Food Sci Technol* **28**: 103–115.

Oliveira, H., Melo, L.D.R., Santos, S.B., Nobrega, F.L., Ferreira, E.C., Cerca, N., et al. (2013) Molecular aspects and comparative genomics of bacteriophage endolysins. *J*

Virol **87**: 4558–4570.

Olsen, N.M.C., Thiran, E., Hasler, T., Vanzieleghem, T., Belibasakis, G.N., Mahillon, J., et al. (2018) Synergistic Removal of Static and Dynamic *Staphylococcus aureus* Biofilms by Combined Treatment with a Bacteriophage Endolysin and a Polysaccharide Depolymerase. *Viruses* **10**: 438.

Pires, D.P., Melo, L.D.R., Vilas Boas, D., Sillankorva, S., and Azeredo, J. (2017) Phage therapy as an alternative or complementary strategy to prevent and control biofilm-related infections. *Curr Opin Microbiol* **39**: 48–56.

Pires, D.P., Oliveira, H., Melo, L.D.R., Sillankorva, S., and Azeredo, J. (2016) Bacteriophage-encoded depolymerases: their diversity and biotechnological applications. *Appl Microbiol Biotechnol* **100**: 2141–2151.

Rahman, M., Kim, S., Kim, S.M., Seol, S.Y., and Kim, J. (2011) Characterization of induced *Staphylococcus aureus* bacteriophage SAP-26 and its anti-biofilm activity with rifampicin. *Biofouling* **27**: 1087–1093.

Rodríguez-Rubio, L., Martínez, B., Donovan, D.M., Rodríguez, A., and García, P. (2013) Critical Reviews in Microbiology Bacteriophage virion-associated peptidoglycan hydrolases: potential new enzybiotics. *Crit Rev Microbiol* **39**: 427–434.

Rodríguez-Rubio, L., Martínez, B., Rodríguez, A., Donovan, D.M., and García, P. (2012) Enhanced Staphylolytic Activity of the *Staphylococcus aureus* Bacteriophage vB_SauS-phiIPLA88 HydH5 Virion-Associated Peptidoglycan Hydrolase: Fusions, Deletions, and Synergy with LysH5. *Appl Environ Microbiol* **78**: 2241–2248.

Schelin, J., Susilo, Y.B., and Johler, S. (2017) Expression of Staphylococcal enterotoxins under stress encountered during food production and preservation. *Toxins (Basel)* **9**: 401.

Schmelcher, M., Donovan, D.M., and Loessner, M.J. (2012) Bacteriophage endolysins as novel antimicrobials. *Future Microbiol* **7**: 1147–1171.

Shavrina, M.S., Zimin, A.A., Molochkov, N. V., Chernyshov, S. V., Machulin, A. V., and Mikoulinskaia, G. V. (2016) In vitro study of the antibacterial effect of the bacteriophage T5 thermostable endolysin on *Escherichia coli* cells. *J Appl Microbiol* **121**: 1282–1290.

Torres-Barceló, C. (2018) The disparate effects of bacteriophages on antibiotic-resistant bacteria. *Emerg Microbes Infect* **7**: 1–12.

Valle, J., Toledo-Arana, A., Berasain, C., Ghigo, J.-M., Amorena, B., Penadés, J.R., and Lasa, I. (2003) SarA and not σB is essential for biofilm development by *Staphylococcus aureus*. *Mol Microbiol* **48**: 1075–1087.

Vasudevan, R. (2014) Biofilms: microbial cities of scientific significance. *J Microbiol Exp* **1**: 84–98.

WHO (2014) Antimicrobial Resistance, Global Report on Surveillance, Geneva, Switzerland.

Wu, M., Hu, K., Xie, Y., Liu, Y., Mu, D., Guo, H., et al. (2018) A Novel Phage PD-6A3, and Its Endolysin Ply6A3, With Extended Lytic Activity Against *Acinetobacter baumannii* . *Front Microbiol* **9**: 1–12.

3.2.2. Draft genomes of the Bap-producing strain *Staphylococcus aureus* V329 and its derived phage-resistant mutant BIM-1

ABSTRACT

This study reports the draft genomes of *Staphylococcus aureus* V329, a Bap-producing strain isolated from a case of subclinical bovine mastitis in Spain, and a derived mutant (BIM-1) resistant to phage *Kayvirus rodi* (phiIPLA-RODI). Comparison of the two genomes revealed that the mutant strain has a point mutation in gene *tagO*.

Although *Staphylococcus aureus* is best known for being an opportunistic pathogen in humans, it can also cause infections in a wide range of animal hosts (Haag *et al.*, 2019). For instance, this microbe is one of the etiological agents of mastitis in dairy cows, leading to economic losses in this sector and posing a potential risk to human health due to milk contamination. Such infections often exhibit a persistent nature and cannot be successfully cleared with antibiotic treatment.

It is widely accepted that biofilms play a role in chronic, recalcitrant bacterial infections. For most *S. aureus* strains, the main component of the extracellular matrix is the polysaccharide PIA/PNAG (Cramton *et al.*, 1999). However, some bovine mastitis isolates form strong biofilms rich in the Bap protein (Cucarella *et al.*, 2001), a characteristic that has also been observed in other staphylococcal species (Valle *et al.*, 2020). The first strain identified to produce such biofilms was *S. aureus* V329, isolated in Spain from a mastitic cow (Cucarella *et al.*, 2001). More recently, Duarte *et al.*, (2021) isolated a V329-derived mutant, BIM-1, exhibiting resistance to phage *K. rodi* and decreased susceptibility to the lytic protein CHAPSH3b. This study aimed to sequence the genome of V329, kindly provided by Dr. A. Toledo-Arana (Instituto de Agrobiotecnología, CSIC-Universidad Pública de Navarra, Spain), and compare it to the mutant BIM-1, recently derived in our laboratory, in order to identify the potential mutation(s) responsible for its phenotype.

Both strains were grown on plates containing TSB (tryptic soy broth, Scharlau Microbiology, Barcelona, Spain) supplemented with 2% agar (Roko, S.A., Llanera, Spain) at 37ºC. A single colony was then streaked out on a second plate and incubated overnight under the same conditions. All cells grown on this plate were harvested and stored in Microbank™ cryovials, which contain beads and a cryopreservative (Pro-Lab Diagnostics UK, United Kingdom), until gDNA isolation. Then, beads were washed with extraction buffer containing lysostaphin and RNase A, and incubated for 25 min at 37ºC. Afterwards, Proteinase K and RNase A were added and the samples were further incubated for 5 min at 65ºC. gDNA purification was performed using solid-phase reversible immobilization (SPRI) beads (Beckman Coulter, Brea, USA), and the genomic libraries were prepared using Nextera XT Library Prep Kit (Illumina, San Diego, USA) according to the manufacturer's protocol. The resulting libraries were subsequently sequenced on an Illumina HiSeq platform using a 250 bp paired end protocol. Genome sequencing was provided by MicrobesNG (http://www.microbesng.uk). Default

parameters were used for all software utilized for genome analysis unless otherwise noted. Quality of the reads was assessed using FASTQC v. 0.11.3 (Andrews, 2010). Trimming was carried out with Trimmomatic v. 0.39 using a sliding window quality cutoff of Q15 (Bolger *et al.*, 2014). The genomes were assembled *de novo* using SPAdes v. 3.14.1 (Bankevich *et al.*, 2012), and quality of the assembly was assessed with QUAST v. 5.0.2 (Gurevich *et al.*, 2013). Genome completeness was assessed using BUSCO v. 5 (Simão *et al.*, 2015) and the ortholog set "Bacteria" on the gVolante web server (Nishimura *et al.*, 2017). Contigs were reordered using Mauve v. 20150226 (Rissman *et al.*, 2009). Then, sequences shorter than 500 bp were removed prior to genome annotation with the NCBI Prokaryotic Genome Annotation Pipeline v. 5.1 (Tatusova *et al.*, 2016). Details regarding genome assembly and annotation for both strains are shown in Table 3.4. Comparison of the two genomes using Breseq v. 0.35.5 (Deatherage and Barrick, 2014) subsequently revealed that strain BIM-1 had a point mutation in gene *tagO* (G210E), involved in the biosynthesis of teichoic acids (Soldo *et al.*, 2002). *tagO* deletion is known to result in phage resistance in *S. aureus* (Azam *et al.*, 2018). Further work will be necessary to elucidate if this mutation is responsible for the BIM-1 phenotypes.

Table 3.4 - Genome assembly statistics and annotation features.

Feature	V329	BIM-1
Number of reads	610,303	572,792
Assembly statistics		
Number of contigs	50	53
Number of contigs >500 bp	20	19
Largest contig size (bp)	636,777	636,777
Genome size (bp)	2,719,662	2,718,812
G+C content (%)	32.8	32.8
N50 (bp)	356,410	356,410
Number of Ns per 100 kbp	0	0
Genome completeness (%)	100	100
Annotation features		
Number of genes (coding)	2,539	2,537
Number of tRNAs	53	53
Number of rRNAs	12	11

Data availability. The whole genome shotgun projects corresponding to *S. aureus* V329 and BIM-1 have been deposited at DDBJ/ENA/GenBank under accession numbers JAGTJH000000000 and JAGTJI000000000, respectively. The corresponding files containing the raw reads have been deposited at NCBI under the bioproject number PRJNA723827.

REFERENCES

Andrews, S. (2010) FastQC: a quality control tool for high throughput sequence data. https://www.bioinformatics.babraham.ac.uk/projects/fastqc/

Azam, A.H., Hoshiga, F., Takeuchi, I., Miyanaga, K., and Tanji, Y. (2018) Analysis of phage resistance in *Staphylococcus aureus* SA003 reveals different binding mechanisms for the closely related Twort-like phages ϕSA012 and ϕSA039. *Appl Microbiol Biotechnol* **102**: 8963–8977.

Bankevich, A., Nurk, S., Antipov, D., Gurevich, A.A., Dvorkin, M., Kulikov, A.S., et al. (2012) SPAdes: A new genome assembly algorithm and its applications to single-cell sequencing. *J Comput Biol* **19**: 455–477.

Bolger, A.M., Lohse, M., and Usadel, B. (2014) Trimmomatic: A flexible trimmer for Illumina sequence data. *Bioinformatics* **30**: 2114–2120.

Cramton, S.E., Gerke, C., Schnell, N.F., Nichols, W.W., and Götz, F. (1999) The intercellular adhesion (ica) locus is present in *Staphylococcus aureus* and is required for biofilm formation. *Infect Immun* **67**: 5427–5433.

Cucarella, C., Solano, C., Valle, J., Amorena, B., Lasa, Í., and Penadés, J.R. (2001) Bap, a *Staphylococcus aureus* surface protein involved in biofilm formation. *J Bacteriol* **183**: 2888–2896.

Deatherage, D.E. and Barrick, J.E. (2014) Identification of mutations in laboratory evolved microbes from next-generation sequencing data using breseq. *Methods Mol Biol* **1151**: 165–188.

Duarte, A.C., Fernández, L., De Maesschalck, V., Gutiérrez, D., Campelo, A.B., Briers, Y., et al. (2021) Synergistic action of phage phiIPLA-RODI and lytic protein CHAPSH3b: a combination strategy to target *Staphylococcus aureus* biofilms. *npj Biofilms Microbiomes* **7**: 39.

Gurevich, A., Saveliev, V., Vyahhi, N., and Tesler, G. (2013) QUAST: Quality assessment tool for genome assemblies. *Bioinformatics* **29**: 1072–1075.

Haag, A.F., Ross Fitzgerald, J., and Penadés, J.R. (2019) *Staphylococcus aureus* in animals. *Microbiol Spectr* **7**: GPP3-0060.

Nishimura, O., Hara, Y., and Kuraku, S. (2017) gVolante for standardizing completeness assessment of genome and transcriptome assemblies. *Bioinformatics* **33**: 3635–3637.

Rissman, A.I., Mau, B., Biehl, B.S., Darling, A.E., Glasner, J.D., and Perna, N.T. (2009) Reordering contigs of draft genomes using the Mauve Aligner. *Bioinformatics* **25**: 2071–2073.

Simão, F.A., Waterhouse, R.M., Ioannidis, P., Kriventseva, E. V., and Zdobnov, E.M. (2015) BUSCO: Assessing genome assembly and annotation completeness with single-copy orthologs. *Bioinformatics* **31**: 3210–3212.

Soldo, B., Lazarevic, V., and Karamata, D. (2002) tagO is involved in the synthesis of all anionic cell-wall polymers in *Bacillus subtilis* 168. *Microbiology* **148**: 2079–2087.

Tatusova, T., Dicuccio, M., Badretdin, A., Chetvernin, V., Nawrocki, E.P., Zaslavsky, L., et al. (2016) NCBI prokaryotic genome annotation pipeline. *Nucleic Acids Res* **44**: 6614–6624.

Valle, J., Fang, X., and Lasa, I. (2020) Revisiting Bap Multidomain Protein: More Than Sticking Bacteria Together. *Front Microbiol* **11**: 613581.

3.2.3. Exopolysaccharide depolymerase Dpo7 improves the removal of *Staphylococcus aureus* biofilms by phage *Kayvirus rodi*

ABSTRACT

Bacteriophages have been shown to penetrate biofilms and replicate if they find suitable host cells. Therefore, these viruses appear to be a good option to tackle the biofilm problem and complement or even substitute more conventional antimicrobials. However, in order to successfully remove biofilms, in particular mature biofilms, phages may require help from other compounds. Phage-derived proteins, such as endolysins or depolymerases, offer a safer alternative to other compounds in the era of antibiotic resistance. This study demonstrates a synergistic interaction between phage *Kayvirus rodi* and a polysaccharide depolymerase (Dpo7) from another phage (*Rockefellervirus* IPLA7) against biofilms formed by different *Staphylococcus aureus* strains. This observation was confirmed by microscopy analysis, which also showed that polysaccharide depolymerase treatment reduced but not eliminated extracellular matrix polysaccharides. Activity assays on mutant strains did not identify teichoic acids or PNAG/PIA as the exclusive target of Dpo7, suggesting that may be both are degraded by this enzyme or that there is another unexplored target polysaccharide on the bacterial surface. Phage adsorption to *S. aureus* cells was not significantly altered by incubation with Dpo7, indicating that the mechanism of the observed synergistic interaction is likely through loosening the biofilm structure. This would allow easier access of the phage particles to their host cells and facilitate infection progression within the bacterial population.

INTRODUCTION

The Gram-positive pathogen *Staphylococcus aureus* is currently recognised by the WHO as one of the top 10 global public health threats facing humanity (FAO and WHO, 2019). Armed with an arsenal of virulence factors, this microbe can cause very diverse infections ranging from mild to severe, including skin and soft tissue, osteoarticular, lung or device-related infections, endocarditis and potentially bacteremia (Tong *et al.*, 2015). Indeed, *S. aureus* is a leading cause of hospital-acquired infections. On top of that, some strains of this pathogen secrete heat-stable enterotoxins that can resist thermal inactivation strategies and remain in foods (González-Martín *et al.*, 2020). Because of these toxins, *S. aureus* is responsible for food poisoning outbreaks associated with the consumption of milk, cheese, butter, and ham, among others (Ortega *et al.*, 2010; CDC, 2023). In the food environment, the main sources of contamination include workers and farm animals, with the latter also suffering often from staphylococcal infections (e.g., mastitis). Worryingly, the prevalence of multidrug-resistant isolates of *S. aureus* has been increasing, not only in the clinic but also along the food chain. The most concerning strains are those exhibiting methicillin and vancomycin resistance (MRSA and VRSA, respectively).

This microorganism is also capable of colonising and forming biofilms on both biotic and abiotic surfaces. A biofilm is an agglomeration of bacteria attached to a surface embedded within an extracellular matrix that, in this pathogen, mainly consists of exopolysaccharide (PNAG/PIA), DNA and proteins (Schilcher and Horswill, 2020). This structure provides the bacterial cells with protection from external factors such as antibiotics, disinfectants and host defence mechanisms (Costerton *et al.*, 1999; De la Fuente-Núñez *et al.*, 2013; Lister and Horswill, 2014). As a result, biofilms are much more difficult to eliminate than planktonic cells. In the case of *S. aureus*, the biofilm lifestyle is thought to be involved in most chronic infections, such as those related to indwelling medical devices, and in the persistence of this bacterium on food surfaces (Di Ciccio *et al.*, 2015; Moormeier and Bayles, 2017).

In this scenario, phage therapy appears as a viable alternative to target this pathogen and, consequently, help to control the spread of antimicrobial resistance. Phages are viruses that infect bacteria and offer, as one of their main advantages, high host specificity, being innocuous for non-target microorganisms as well as for humans and animals (Principi *et al.*, 2019). However, bacteria may acquire resistance to these viruses, making it necessary to develop combinations, the so-called phage cocktails, which generally include phages

binding to different receptors on the bacterial surface (Labrie *et al.*, 2010; Fernández *et al.*, 2019). Another strategy is the simultaneous administration of phage therapy together with other types of drugs. For example, several studies have demonstrated that the combination of bacteriophages with antibiotics sometimes increases the chances of a successful treatment (Diallo and Dublanchet, 2022; Roszak *et al.*, 2022). This phenomenon is known as phage-antibiotic synergy (PAS). However, other researchers have found that antagonism between phages and antibiotics also occurs in some cases, making it necessary to study each individual interaction (Nicholls *et al.*, 2023). More recently, a study reported that simultaneous treatment of staphylococcal biofilms with a phage and a phage-derived lytic enzyme displayed better efficacy than either antimicrobial alone (Duarte *et al.*, 2021). This result highlights the possibilities offered by combining phages with proteins derived from other bacterial viruses. For instance, it would be interesting to determine if the combination of phages with phage-encoded exopolysaccharide depolymerases has an enhancing effect on their ability to kill the target pathogen (Cornelissen *et al.*, 2012).

Phage depolymerases are enzymes that help the virus penetrate the carbohydrate barrier posed by the host cell envelope in order to access its receptor and inject the viral genome into the cell (Latka *et al.*, 2017). Exopolysaccharide depolymerases are very diverse proteins whose substrates include lipopolysaccharide (LPS), the capsule (CPS), polysaccharidic extracellular polymeric substance (EPS) or even wall teichoic acid (WTA) (Myers *et al.*, 2015; Latka *et al.*, 2017). These enzymes may be grouped into two classes, hydrolases and lyases, depending on how they degrade their target carbohydrate (22). In a previous work, Gutiérrez *et al.* (2015) identified a pre-neck appendage protein (Dpo7) derived from bacteriophage vB_SepiS-phiIPLA7, containing a pectate lyase domain. Dpo7 exhibits antibiofilm activity, but it does not kill biofilm cells; it just triggers their dispersion to the planktonic phase (Gutiérrez *et al.*, 2015). On the other hand, the virulent staphylophage *Kayvirus rodi* (phiIPLA-RODI) can readily kill biofilm cells, but it does not produce any matrix-degrading enzymes (Gutiérrez *et al.*, 2015b). Within this context, the main goal of this work was to investigate the potential synergy between these two agents against biofilms formed by different *S. aureus* strains in an attempt to improve on the antibiofilm potential of phage *Kayvirus rodi*.

MATERIALS AND METHODS

Bacterial strains, growth conditions, polysaccharide depolymerase and bacteriophages

The staphylococcal strains used in this study are included in Table 3.5. These strains were routinely grown at 37ºC in TSB medium (tryptic soy broth, Scharlau Microbiology, Barcelona, Spain) with shaking, or on plates containing TSB supplemented with 1.5% (w/v) agar (Roko, S.A., Llanera, Asturias, Spain) (TSA).

Recombinant protein expression was carried out using *Escherichia coli* BL21 carrying the gene coding for Dpo7 cloned into plasmid pET21a as described by (Gutiérrez *et al.*, 2020) *E. coli* was routinely grown in LB medium (Luria Bertany broth; Sigma-Aldrich, St. Louis, MO, USA), supplemented with 1 mM IPTG (GoldBio, St. Louis, MO, USA) and 100 µg/ml ampicillin (Sigma-Aldrich, St. Louis, MO, USA) when necessary. The bacteriophage-encoded polysaccharide depolymerase Dpo7 was subsequently purified as described previously (Gutiérrez *et al.*, 2020). Visual analysis and quantification of the concentration of the purified protein were performed by SDS-PAGE and the quick Start Bradford ProteinAssay Kit (Bio-Rad Laboratories, USA), respectively.

Phage *K. rodi* was routinely propagated on *S. aureus* IPLA16 using the double agar overlay technique (Labrie *et al.*, 2010). Briefly, 100 µl of phage suspension were added to TSA plates containing 100 µl of the host and mixed with 5 ml of TSB top agar (TSB supplemented with 0.7% (w/v) agar). The plates were incubated overnight at 37°C after which 3 ml of TSB were added to each Petri dish. The plates were subsequently incubated at room temperature for 3 h, with gentle shaking. Lastly, the TSB and top agar with the eluted phages were collected and centrifuged (10,000 rpm, 4ºC, 30 min). The recovered supernatant was filtered and stored at 4ºC until further use.

Table 3.5 – Staphylococcal strains used in this study.

Strain*	Description	Genome accession number*	Reference
Sa IPLA16	Meat industry surface	CP134617	(Gutiérrez *et al.*, 2012)
Sa 15981	Clinical strain	NA	(Valle *et al.*, 2003)
Sa V329	Cow mastitis	JAGTJH000000000	(Cucarella *et al.*, 2001)
Sa BIM1	Phage resistant mutant	JAGTJI000000000	(Fernández *et al.*, 2021)
Sa Newman	Clinical strain	NC_009641	(Lorenz and Duthie, 1952)
Sa JE2	MRSA, clinical strain	NZ_CP020619	(Fey *et al.*, 2013)
Sa SA113	Derived from NCTC 8325	NZ_JASTSW000000000	(Iordanescu and Surdeanu, 1976)
SA113Δ*ica*	*ica* mutant	NA	(Cramton *et al.*, 1999)
Se F12	Human mastitis	NA	(Delgado *et al.*, 2009)

* Sa, *S. aureus*; Se, *Staphylococcus epidermidis*; NA, not available

Dpo7 activity diffusion assay

For the diffusion test, overnight cultures of different strains were diluted 1:100 in 20 ml of TSB containing 1.2% agar and poured onto a Petri dish. These plates were allowed to dry and subsequently incubated for 24 h at 37°C. The next day, small holes were made with a micropipette tip in which we added 40 µl from a Dpo7 solution (approximately 10 µM). The protein elution buffer was used as a negative control. Results were analysed after further incubation of the plates at 37 ºC for 24 h.

Biofilm formation and treatment

Overnight cultures of each strain were diluted 1:100 (v/v) in fresh TSB supplemented with 0.25% (v/v) glucose (Merck, Darmstadt, Germany) (TSBg), and 1 ml of each bacterial suspension was inoculated into a well of a 24-well polystyrene microplate (Thermo Scientific, NUNC, Madrid, Spain). These plates were incubated for 24 h at 37 ºC. After that, the planktonic phase was removed and the biofilms were washed twice with phosphate-buffered saline (PBS; 137 mM NaCl, 2.7 mM KCl, 10 mM Na_2HPO_4, 2

mM KH_2PO_4 [pH 7.4]). Biofilms were then treated with 0.5 ml of TSB medium alone, as a control, or supplemented with different concentrations of Dpo7 (1 and 2 μM) and/or phage *K. rodi* (1×10^8 PFU/ml and 1×10^9 PFU/ml) and incubated for 24 h at 37 ºC. Again, the planktonic phase was removed, and the adhered cells were washed twice with PBS. To determine the number of viable cells, biofilms were scraped and resuspended in PBS (1 ml). Then, 10-μl droplets from tenfold serial dilutions of each cell suspension were placed onto TSA plates, incubated at 37 ºC for 24 h and the colony forming units per unit area (CFU/cm^2) were determined. Interactions between the phage and Dpo7 were estimated according to the following equation based on Chaudhry *et al.* (2017):

Interaction index = [S(phage+Dpo7) - S(control)] - [[S(phage) - S(control)] + [S(Dpo7) - S(control)]]

In which S = $\log_{10}$ CFU/cm^2 for a specific treatment.

Values of this index between -0.2 and 0.2 indicated an additive interaction, whereas antagonism and synergy were found when the value was < -0.2 or > 0.2, respectively.

The total biomass of biofilms was quantified by crystal violet staining. First, the wells were washed twice with PBS and then 0.1% (v/v) of crystal violet was added to each well and incubated for 15 min at room temperature. The stain was then removed, and the wells washed with water and allowed to dry at room temperature. The remaining dye was solubilized by adding 33% (v/v) acetic acid to each well and the absorbance at 595 nm (A_{595}) was measured with a microplate reader (Benchmark Plus Microplate Spectrophotometer; Bio-Rad Laboratories, Hercules, CA, USA).

Confocal microscopy

Biofilms were formed on 2-well μ-slides with a glass bottom (ibidi, USA) by inoculating 2 ml from a cell suspension prepared as above and allowing growth for 24 hours at 37 ºC. After removing the planktonic phase, wells were washed with PBS and cells were treated with TSB supplemented with phage *K. rodi* at 10^9 PFU/ml, 2 μM Dpo7 or a combination of both. Control wells were treated with TSB alone. Following 24 hours of treatment, the planktonic phase was removed again. The adhered cells were washed with PBS and

subsequently stained with Live/Dead® BacLightTM kit (Invitrogen AG, Basel, Switzerland) and WGA Alexa Fluor® 647 conjugate (Invitrogen, Eugene, Oregon, USA) following the manufacturers' instructions. Samples were observed with a confocal scanning laser microscope (DMi8, Leica Microsystems) using a 63× oil objective.

Extraction and purification of *S. aureus* WTA polymers and monomers

WTA polymers from different *S. aureus* strains were extracted and purified as previously described with some modifications (Shen *et al.*, 2017).

10 ml of overnight cultures of each *S. aureus* strain were inoculated in one litre of TSB with 0.25% (v/v) glucose and incubated at 37 C for 24 h. Then, bacterial cells were harvested by centrifugation at 7,000 × g for 10 min, resuspended in MilliQ water (15 ml per litre of culture), followed by heating at 100 °C for 20 min and centrifuged for 10 min. The pellet was stored overnight at -20 C.

Upon thawing, the cells were resuspended in 10 ml of MilliQ water and then disrupted by two runs through a Pressure Cell Homogenizer (Stansted Fluid Power Ltd., model SPCH-10, UK) at 200 MPa. After disruption, whole cells were centrifuged at 1,400 × g for 5 min and the supernatant was collected for WTA purification.

Since the cell wall material is in the supernatant, the suspension was spun down at 20,000 × g for 30 min. Afterwards the pellet was resuspended in 10 ml of SM buffer supplemented with magnesium (30 mM). Then, 10 µl of 1 U/ml DNase and 1 U/ml RNase were added and samples were incubated for 3 h at 37 C. Next, the same volume of 20 mg/ml proteinase K was added and incubation at 37 °C continued for another 2 h. The cell walls were extracted by boiling the samples in the presence of 4% SDS. The insoluble fraction was recovered by centrifugation (20,000 × g, 30 min, 25 °C). The pellet was washed with MilliQ water and centrifuged again for 20 min at the same speed. This process was repeated five times.

Extraction of WTAs was carried out by resuspending the resulting pellet in 10 ml of 25 mM glycine/HCl buffer and heated in a water bath for 10 min at 100 °C. Afterwards, samples were centrifuged for 30 min at 30,000 × g and the supernatant was transferred to a new tube. WTA extraction was repeated twice and the supernatants were mixed together. To finish, the supernatant was dialyzed against MilliQ water and lyophilized for the next purification step.

Next, the lyophilized product was solved in Milli-Q water and WTAs were purified by anion exchange chromatography by using a HiTrap DEAE FF column. 10 mM Tris-HCl (pH 7.5) was chosen as buffer, with a gradient elution ranging from 0 to 1 M NaCl. The outflow was measured with a UV detector at the following wavelengths: 205 and 212 nm (both indicating carbohydrate signal) as well as 280 nm (for protein signal).
After sugar separation, fractions were collected, lyophilized and resuspended in 1 ml of PBS. Afterwards, the samples were analysed by anion exchange chromatography and and ultra-performance liquid chromatography tandem mass spectrometry (UPLC-MS/MS).

Purified WTA polymers were depolymerized into monomeric repeating units by hydrolysis of the phosphodiester bonds using 48% hydrofluoric acid for 20 h at 0 °C. The WTA monomers were then lyophilized and subjected to UPLC-MS/MS analysis as previously described. All data were collected and processed using MassLynx software, version 4.1 (Waters Corp., USA), and MS spectra were background-corrected by subtracting the signals between 0–1 min of their respective chromatograms.

Phage adsorption assays

Biofilms were grown as described above but inoculating 2 ml into each well of a 12-well polystyrene microplate (Thermo Scientific, NUNC, Madrid, Spain). These plates were incubated for 24 hours at 37 ºC. The following day, the planktonic phase was removed and the biofilms were washed twice with PBS. Then, the adhered cells were harvested in 1 ml of PBS and diluted down to an $OD_{600} = 1$. The resulting suspension was then divided into 1-ml aliquots. Dpo7 was added to one of the tubes at a concentration of 2 µM, while another was the untreated control. Both samples were incubated at 37 ºC for 4 h, after which cells were pelleted by centrifugation and resuspended in 900 µl of PBS. Next, 100 µl of phage suspension were added to each sample (final titer: 10^7 PFU/ml) and PBS containing phage with no cells was used as a control. All samples were then incubated for 5 min at room temperature. After this time, the tubes were centrifuged for 3 minutes at 10,000 × g, and the adsorption rate was calculated according to the following equation:

adsorption rate = [(phage titer in supernatant of control – phage titer in supernatant sample) / (phage titer in supernatant of control)] x 100

RESULTS AND DISCUSSION

Dpo7 exhibits activity against diverse *S. aureus* strains

To establish the potential interactions between the bacteriophage-encoded polysaccharide depolymerase Dpo7 and phage *K. rodi* for biofilm removal, we chose several strains with different biofilm-forming abilities and biofilm matrix composition. Both *S. aureus* V329 and *S. aureus* 15981 form strong biofilms, but the extracellular matrix of V329 is mostly composed of Bap protein and eDNA, while that of strain 15981 is rich in exopolysaccharides (Gutiérrez *et al.*, 2014). On the other hand, strains IPLA16, JE2 and Newman were all poor biofilm formers (Jurado *et al.*, 2024).

Before conducting the interaction assays, we examined the activity of depolymerase Dpo7 on the different *S. aureus* strains and one *S. epidermidis* strain, which was included as a positive control. According to previous data obtained by Gutiérrez *et al.* (2015), strain V329 was expected to be a negative control of depolymerase activity. However, as can be seen in Figure 3.13, all the strains tested displayed a halo indicating Dpo7 enzymatic activity (left hole). No haloes were observed when buffer alone was present (right hole), demonstrating that the turbid zones were due to the protein. Based on these results, all five *S. aureus* strains (15981, V329, Newman, JE2 and IPLA16) were included in the antibiofilm experiments.

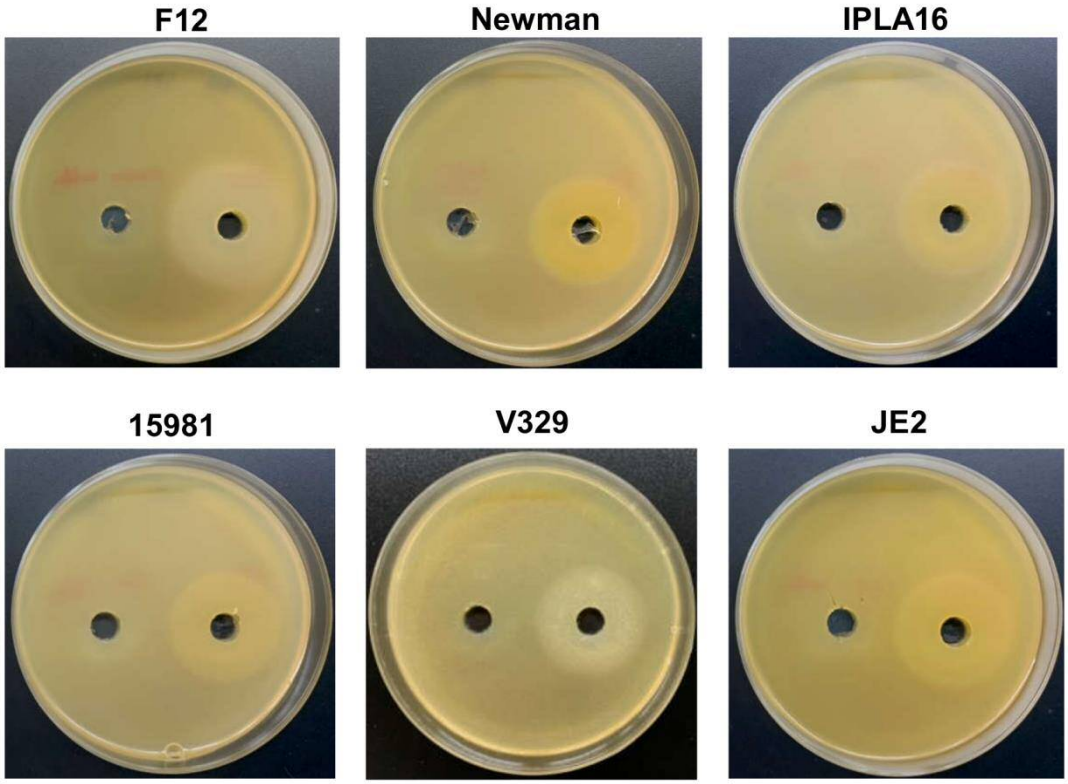

Figure 3.13 - Activity of depolymerase Dpo7 on different staphylococcal strains (indicated on top of each photograph) as determined by the diffusion assay. The protein (40 µl from an 800 µg/ml stock) or buffer alone were respectively added to the right and left well. Activity was observed as a turbid halo around the well.

Dpo7 and phage *Kayvirus rodi* act synergistically to degrade *S. aureus* biofilms

Preformed biofilms of the abovementioned strains were treated with different combinations of phage and enzyme. The obtained results revealed a synergistic interaction between the two antimicrobials in most of the combinations tested (Table 3.6), with greater reductions in viable cell counts observed when phage and Dpo7 were applied together compared to the individual treatments (Figure 3.14). Indeed, treatment with phage or depolymerase alone did not significantly affect the number of viable cells compared to an untreated control, with the exception of strain Newman treated with 10^9 PFU/ml of phage *K. rodi* (Figure 3.14C). In contrast, most of the combinations tested led to significant reductions in viable cell counts.

Table 3.6 - Interaction indices calculated for combinations of *Kayvirus rodi* and Dpo7.

Strain	Treatment	Interaction index*
15981	10^8 PFU/ml phage + 1 μM Dpo7	**0.76**
	10^8 PFU/ml phage + 2 μM Dpo7	**1.77**
	10^9 PFU/ml phage + 1 μM Dpo7	**1.62**
	10^9 PFU/ml phage + 2 μM Dpo7	**2.42**
V329	10^8 PFU/ml phage + 1 μM Dpo7	**0.41**
	10^8 PFU/ml phage + 2 μM Dpo7	**1.80**
	10^9 PFU/ml phage + 1 μM Dpo7	**1.07**
	10^9 PFU/ml phage + 2 μM Dpo7	**2.02**
Newman	10^8 PFU/ml phage + 1 μM Dpo7	**0.42**
	10^8 PFU/ml phage + 2 μM Dpo7	**0.94**
	10^9 PFU/ml phage + 1 μM Dpo7	**0.63**
	10^9 PFU/ml phage + 2 μM Dpo7	**1.27**
JE2	10^8 PFU/ml phage + 1 μM Dpo7	**0.48**
	10^8 PFU/ml phage + 2 μM Dpo7	**0.83**
	10^9 PFU/ml phage + 1 μM Dpo7	**0.45**
	10^9 PFU/ml phage + 2 μM Dpo7	**1.04**
IPLA16	10^8 PFU/ml phage + 1 μM Dpo7	**0.24**
	10^8 PFU/ml phage + 2 μM Dpo7	-0.12
	10^9 PFU/ml phage + 1 μM Dpo7	0.03
	10^9 PFU/ml phage + 2 μM Dpo7	**0.44**

* Values > 0.2 and < -0.2 were considered synergistic (bold) and antagonistic, respectively. Values between -0.2 and 0.2 were considered indicative of an additive interaction.

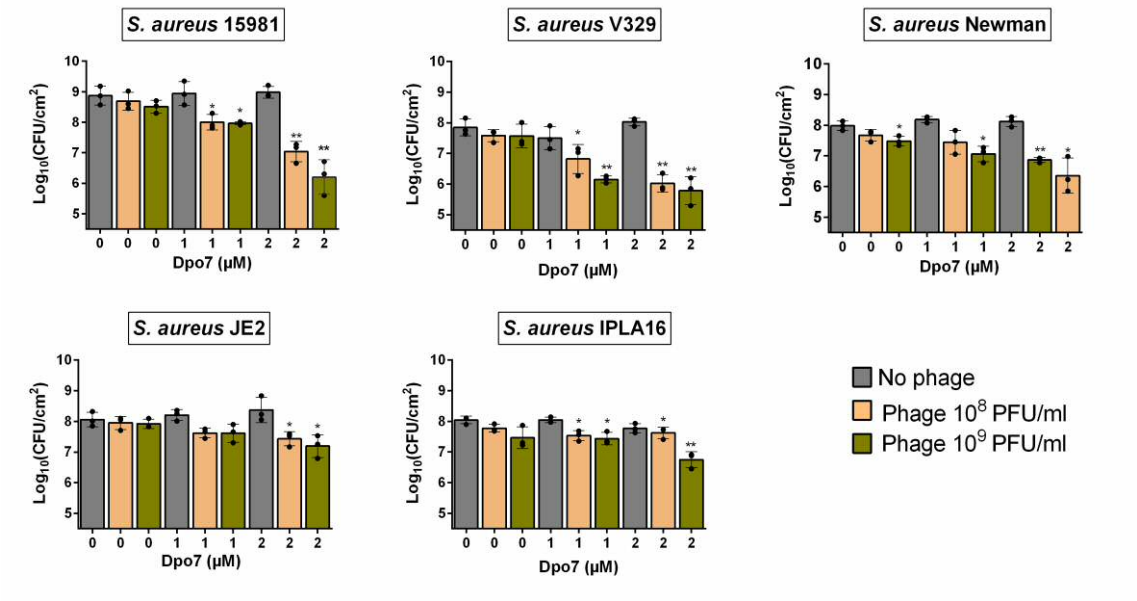

Figure 3.14 - Treatment of *S. aureus* preformed biofilms with different combinations of bacteriophage *Kayvirus rodi* and depolymerase Dpo7. 24-hour biofilms formed by *S. aureus* 15981 (A), V329 (B), Newman (C), JE2 (D) and IPLA16 (E) were treated with 10^8 or 10^9 PFU/ml of phage (orange and green bars, respectively), 1 or 2 μM of depolymerase, or a combination of both antimicrobials. Biofilms were treated for 24 h at 37ºC. TSB medium alone was added to the control wells (grey bars). The graphs show the viable cell counts observed after each treatment. Data represent the means ± standard deviations of three independent experiments. Bars with an asterisk are statistically different from the untreated control. *p-value < 0.05, **p-value < 0.01, ***p-value < 0.001 and ****p-value <0.0001.

In the case of strain 15981, the number of biofilm cells decreased by 0.87 and 1.84 log units for Dpo7 concentrations of 1 μM and 2 μM, respectively, combined with 10^8 PFU/ml of phage, and by 0.91 and 2.67 log units for depolymerase concentrations of 1 μM and 2 μM, respectively, combined with 10^9 PFU/ml of phage (Figure 3.8A). The results were similar for strain V329 (Figure 3.14B). Thus, when combining phage at 10^8 PFU/ml with protein at 1 μM and 2 μM, the reduction in viable cells was 1.02 and 1.82 log units, respectively. Similarly, the combination of Dpo7 with *K. rodi* at 10^9 PFU/ml resulted in a decrease of 1.69 and 2.06 log units for depolymerase concentrations of 1 μM and 2 μM, respectively. For strain Newman, the number of viable cells decreased by 0.54,

1.12, 0.92 and 1.63 log units when biofilms were treated with 10^8 PFU/ml with 1 μM Dpo7, 10^8 PFU/ml with 2 μM Dpo7, 10^9 PFU/ml with 1 μM Dpo7 and 10^9 PFU/ml with 2 μM Dpo7, respectively (Figure 3.14C). The same treatments led to reductions of 0.44, 0.63, 0.44 and 0.87 log units in the number of biofilm cells for *S. aureus* JE2 (Figure 3.14D). The weakest synergy was found for strain IPLA16 according to the interaction index calculation (Table 3.6). Nonetheless, we observed that the combination of *K. rodi* at 10^9 PFU/ml with 2 μM Dpo7 led to a decrease in the number of viable cells of 1.29 log units. This value exceeded the impact of the sum of the individual treatments, since the phage and protein alone at the same concentrations resulted in average reductions of 0.58 and 0.27 log units, respectively, which add up to 0.85 in total. Similarly, treatment with 1 μM Dpo7 or 10^8 PFU/ml of phage *K. rodi* independently led to a reduction of 0 or 0.2 log units, while the combination decreased the number of viable cells by 0.5 log units.

This synergistic interaction with phage *K. rodi* has a broader range than the mechanical antibiofilm activity reported by Gutiérrez *et al.* (2015), which was limited to strains forming biofilms consisting mostly of exopolysaccharide (PNAG/PIA). Most studies assessing potential interactions between a purified phage-derived depolymerase and bacteriophages had found antagonism due to degradation of the phage receptor by the enzyme. This is for instance the case of *Klebsiella* depolymerase Dep_kpv74, which has capsule-degradation activity (Volozhantsev *et al.*, 2022) and the depolymerase of *Acinetobacter* phages K38 (Domingues *et al.*, 2021) and PMK14 (Abdelkader *et al.*, 2022). In contrast, the depolymerase from *Klebsiella* phage KP34 helps phage KP15, probably by exposing its receptor on the bacterial surface (Latka and Drulis-Kawa, 2020). An even greater effect was observed when co-infecting with the two phages. Nevertheless, given the specificity of *Klebsiella* phages and the activity of the depolymerase on the main phage receptor, the capsule, this synergy seems likely to be fairly limited to certain strains.

Impact of the *Kayvirus rodi* combination with Dpo7 on biofilm biomass and integrity

Once established the impact of the phage-depolymerase combination on the number of viable biofilm cells, we studied its effect on total biomass and overall biofilm integrity on two strong biofilm-forming strains, namely 15981 and V329.

Regarding the total biomass, there was a significant decrease for all the different combinations tested compared to the individual antimicrobials (Figure 3.15). In strain 15981, the phage alone significantly reduced the amount of attached biomass at both phage titers (by 29 % and 39 % for 10^8 and 10^9 PFU/ml, respectively) (Figure 3.15A). However, the reduction percentage in the mixed treatments varied between 68 % and 89 %. The difference was even more noticeable for strain V329, given that neither the phage nor the protein had any significant impact on total biomass when used separately. In contrast, the four combinations tested decreased the amount of total biomass between 93% and 97 % (Figure 3.15B).

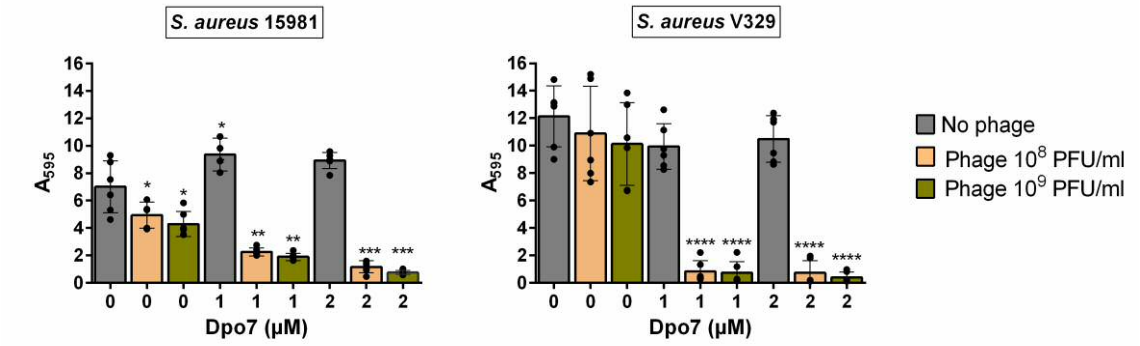

Figure 3.15 - Impact of the treatment with different combinations of bacteriophage *Kayvirus rodi* and depolymerase Dpo7 on *S. aureus* preformed biofilms. 24-hour biofilms formed by *S. aureus* 15981 and V329 were treated with 10^8 or 10^9 PFU/ml of phage (orange and green bars, respectively), 1 or 2 µM of depolymerase Dpo7, or a combination of both antimicrobials for 24 h at 37ºC. TSB medium alone was added to the control wells (grey bars). The graphs show the amount of total biomass as determined by crystal violet staining and subsequent measurement of absorbance at 595 nm. Data represent the means ± standard deviations of three independent experiments. Bars with an asterisk are statistically different from the untreated control. *p-value < 0.05, **p-value < 0.01, ***p-value < 0.001 and ****p-value <0.0001.

Next, we sought to compare more closely the microscopic structure of biofilms of these two strains that had been subjected to four different treatments, namely TSB alone (control), *K. rodi* at 10^9 PFU/ml, 2 µM Dpo7 and a phage-protein combination. In the case of *S. aureus* V329, the effect of the different treatments on the amount of viable cells mirrors the data presented in Figure 3.14B. Indeed, only the combined treatment led to a visible decrease in bacterial cells (Figure 3.16). Additionally, treatment with Dpo7 with or without phage resulted in a noticeable change in the amount of polysaccharide dyed with WGA Alexa Fluor® 647.

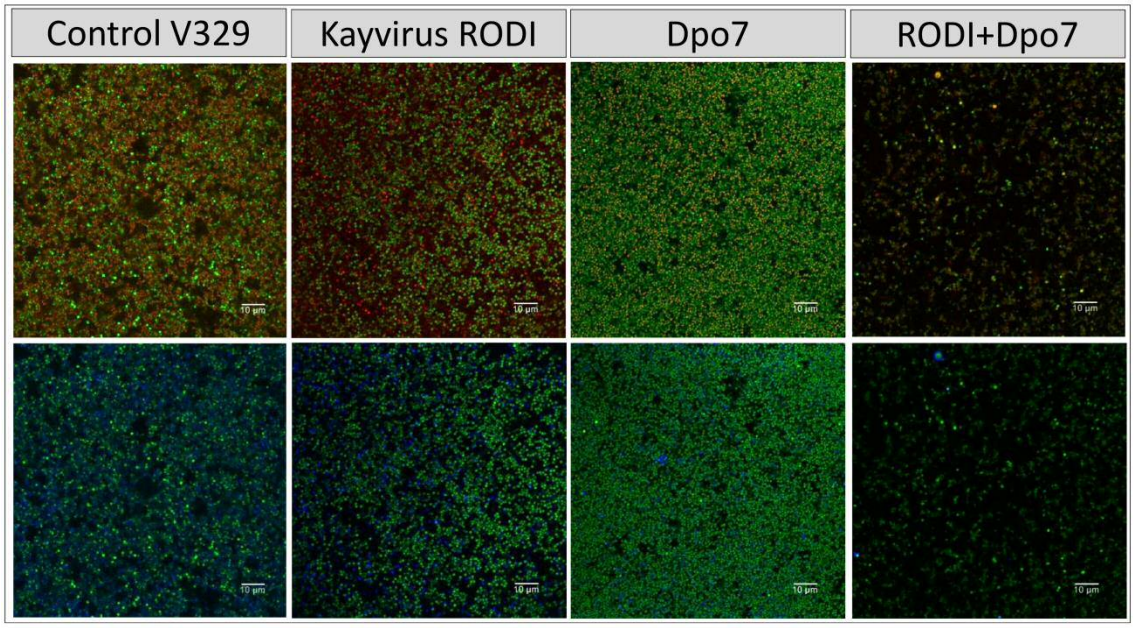

Figure 3.16 - Treatment of biofilms formed by *S. aureus* V329 with *Kayvirus rodi* (10^9 PFU/ml), Dpo7 (2 µM), a combination of both or TSB alone (control). Biofilms were grown for 24 hours at 37 ºC and subsequently treated for the same duration. After removal of the treatment, the attached cells were stained with SYTO® 9, propidium iodide and Wheat Germ Agglutinin (WGA) Alexa Fluor® 647 conjugate. Green represents live cells, red represents dead cells or eDNA and blue indicates the presence of polysaccharides with N-acetylglucosamine residues.

The results observed for strain 15981 were very similar (Figure 3.17). However, the phage alone did have an impact on the number of biofilm cells in this strain, albeit not as dramatic as the combination treatment. Also, Dpo7 only reduced slightly the amount of

stained polysaccharides, probably due to the larger amount of these compounds in this strain compared to V329.

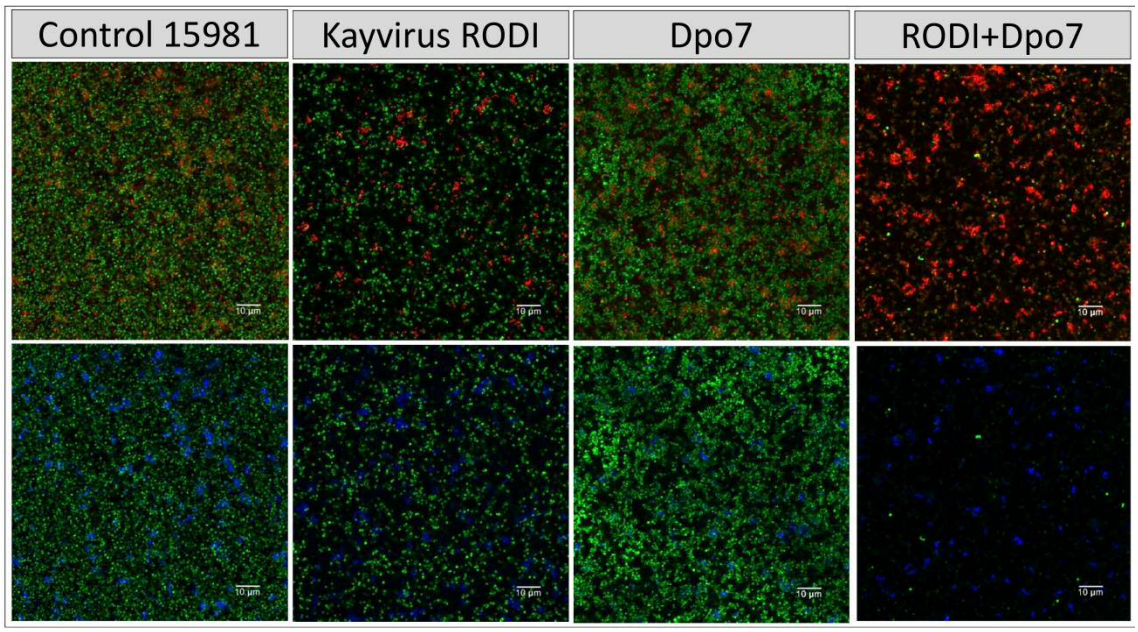

Figure 3.17 - Treatment of biofilms formed by *S. aureus* 15981 with *Kayvirus rodi* (10^9 PFU/ml), Dpo7 (2 µM), a combination of both or TSB alone (control). Biofilms were grown for 24 hours at 37 ºC and subsequently treated for the same duration. After removal of the treatment, the attached cells were stained with SYTO® 9, propidium iodide and Wheat Germ Agglutinin (WGA) Alexa Fluor® 647 conjugate. Green represents live cells, red represents dead cells or eDNA and blue indicates the presence of polysaccharides with N-acetylglucosamine residues.

Assessment of potential targets of depolymerase Dpo7 in *S. aureus* strains

The inherent antibiofilm effect of depolymerase Dpo7 was limited to strains that form biofilms with a high EPS content according to the results obtained by Gutiérrez *et al.* (2015). The only strain tested here that really fits into that description is 15981. However, the synergy between this enzyme and phage *K. rodi* is also observed for poor biofilm-forming strains (Newman, IPLA16 and JE2), as well as for strain V329, whose biofilms consist mainly of Bap protein and eDNA (Gutiérrez *et al.*, 2014). This prompted us to assess the potential of different extracellular or cell-wall polysaccharides to be Dpo7 degradation targets. To do that, we examined the presence of genes involved in polysaccharide production in the genomes of most strains included in this study, with the exception of strain 15981 whose genome is not available.

First, we searched for mutations affecting capsule production because it is considered to somewhat hinder phage infection in this pathogen (Wilkinson and Holmes, 1979). *S. aureus* Newman and *S. aureus* JE2 have been previously described to be capsule positive and negative, respectively. Regarding the other two strains, V329 appears to have an intact *cap* locus, while IPLA16 has a mutation in gene *capD* that would result in a non-functional product. Therefore, it does not seem likely that the capsule is the degradation target of Dpo7 that explains its promoting phage predation, given that some of our strains are capsule negative. Moreover, the microscopy analysis described above show that depolymerase treatment has an effect on a polysaccharide to which wheat germ agglutinin can bind. As far as we know, the *S. aureus* capsule does not have such interactions.

Peptidoglycan does contain N-acetylglucosamine residues, and it has been shown to be agglutinated by WGA. However, it does not seem a probable Dpo7 target either since Gutiérrez *et al.* (2015) already demonstrated that this enzyme does not exhibit lytic activity by carrying out turbidity reduction assays, which are commonly used to detect and quantify peptidoglycan hydrolase activity.

We also examined the genes involved in WTAs production in these four strains and found that the genes responsible for biosynthesis of the WTA backbone as well as *tarS* were seemingly intact in all of them. There were differences, however, regarding gene *tarM*. More specifically, V329 and IPLA16 displayed mutations leading to the synthesis of truncated proteins, resulting in the lack of α-glycosylation in these strains. UPLC-MS analysis confirmed that all four strains produce WTA as well as the two different

glycosylation patterns of V329 and IPLA16 compared to Newman and JE2 (Figure 3.18). WTA would therefore be a candidate target as it is present in at least four of the tested strains. Additionally, glycosylated WTA would bind WGA, so it might be one of the polysaccharides dyed with the Alexa Fluor 647 fluorophore that decreases after Dpo7 treatment (Lotan *et al.*, 1975). To test this hypothesis, we carried out the plate diffusion assay with strain V329-BIM1, a V329-derived strain that has a mutation in *tagO*, the gene coding for the first protein involved in WTA biosynthesis. However, as can be seen in Figure 3.19A, the halo indicating activity of depolymerase Dpo7 was observed as intensely as in the wild-type strain (Figure 3.13). Although these results do not completely discard WTA as a Dpo7 target, they do indicate, at the very least, that it is not the only one.

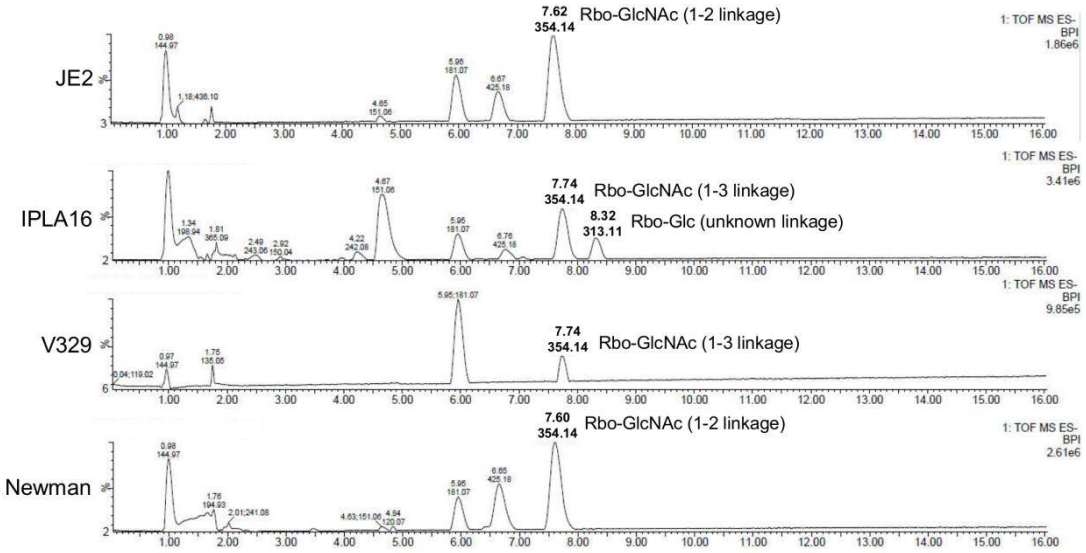

Figure 3.18 - Structural analysis of *S. aureus* WTA repeating units by UPLC-MS. Liquid chromatographic separation and MS-based identification of carbohydrate residues within *S. aureus* WTAs. Peaks are labeled with their respective retention time (*Rt*; [min]) and base peak ion [M-H] (*m*/*z*).

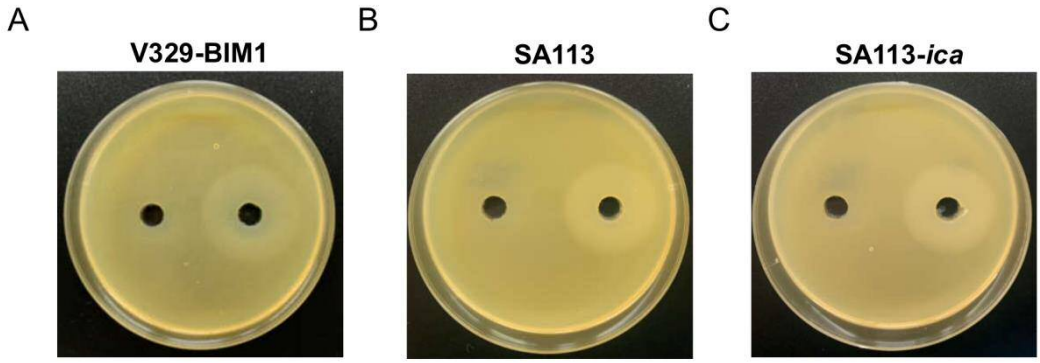

Figure 3.19 - Impact of mutations in teichoic acid biosynthesis gene tagO and the *ica* operon on the activity of Dpo7 as determined by the diffusion assay. The protein (40 µl from an 800 µg/ml stock) or buffer alone were respectively added to the right and left well. Activity was observed as a turbid halo around the well.

Finally, we looked at genes involved in PNAG/PIA biosynthesis, which mostly consists of N-acetylglucosamine residues and would therefore bind WGA. We did not find any mutation that would necessarily abrogate PNAG/PIA production in any of the strains. However, V329 is known to form biofilms whose matrix consists mostly of proteins and eDNA, and strains Newman, JE2 and IPLA16 are poor biofilms formers (Gutiérrez *et al.*, 2014; Jurado *et al.*, 2024). Even though none of these strains would be expected to produce a large amount of exopolysaccharide, they may still have a significant amount, whose degradation facilitates access of the phage to the target cells, explaining the synergy observed in this study. Therefore, exopolysaccharide could still be a target of Dpo7, as predicted by Gutiérrez *et al.* (2015). We put this hypothesis to the test by carrying out the diffusion assay with strain SA113 and its isogenic mutation devoid of the entire *ica* operon. However, Dpo7 exhibited activity on both strains (Fig. 3.19B and 3.19C). This does not necessarily mean that the enzyme cannot degrade PNAG/PIA, but it is clear that it is not the only target. Another potential target would be the newly identified surface polysaccharide Ssc (Lei *et al.*, 2024). This molecule containing N-acetylgalactosamine was shown to affect phage susceptibility. In any case, further enzymatic experiments will be necessary to identify the specific targets of this protein.

Dpo7 treatment does not affect phage adsorption

With the aim of studying the synergy between Dpo7 and *K. rodi* in greater detail, we explored whether the potential effect of the depolymerase on phage adsorption to biofilm cells of strain V329. However, our results indicated no significant difference in the percentage of phage particles that bind to the host cells in samples treated with Dpo7 compared to untreated samples (p-value=0.34). The adsorption rates of untreated and Dpo7-treated samples were 64.79 ± 6.47 % and 59.89 ± 9.35 %, respectively. Therefore, it does not seem that this is the mechanism of the positive impact of enzymatic treatment on the killing ability of the phage. It seems more likely that, as stated above, exogenously added Dpo7 can loosen up the biofilm matrix, making bacterial cells more accessible to *K. rodi*. In that sense, the results observed here are not that dissimilar in terms of mechanism to those reported by Fernández *et al.* (2021) when using a DNAse-phage combination for biofilm treatment. Besides Dpo7, other phage-derived depolymerases have demonstrated antibiofilm activity such as those encoded by phages infecting *Proteus mirabilis*, *K. pneumoniae* and *Pseudomonas aeruginosa* (Mi *et al.*, 2019; Rice *et al.*, 2021; Li *et al.*, 2022). It would be interesting to determine if these enzymes can also promote elimination of biofilms by other phages infecting these same species.

Conclusion

This study highlights the potential of using certain phage-depolymerases as enhancers in phage-based antibiofilm products. Thus far, this is only the second study that identified synergy between phages and this type of enzymes and the first that demonstrates a broad range of action against diverse strains. The main condition to observe this positive interaction seems to be susceptibility to the phage. The data available at the moment does not appear to limit the activity of Dpo7 on one single polysaccharide, being PNAG/PIA and WTAs the most probable targets. Nonetheless, subsequent efforts should examine the enzymatic degradation of these molecules by Dpo7. Understanding the specific activity and the impact of this enzyme on its molecular targets will help use this depolymerase in a more precise manner. In any case, incorporation of Dpo7 in phage-based antibiofilm products seems like a promising strategy to optimize the antimicrobial impact of these viruses.

REFERENCES

Abdelkader, K., Gutiérrez, D., Latka, A., Boeckaerts, D., Drulis-Kawa, Z., Criel, B., et al. (2022) The Specific Capsule Depolymerase of Phage PMK34 Sensitizes *Acinetobacter baumannii* to Serum Killing. *Antibiotics* **11**: 1–20.

CDC, C. for D.C. and P. (2023) Staphylococcal (Staph) Food Poisoning. https://www.cdc.gov/foodsafety/diseases/staphylococcal.html

Di Ciccio, P., Vergara, A., Festino, A.R., Paludi, D., Zanardi, E., Ghidini, S., and Ianieri, A. (2015) Biofilm formation by *Staphylococcus aureus* on food contact surfaces: Relationship with temperature and cell surface hydrophobicity. *Food Control* **50**: 930–936.

Cornelissen, A., Ceyssens, P.J., Krylov, V.N., Noben, J.P., Volckaert, G., and Lavigne, R. (2012) Identification of EPS-degrading activity within the tail spikes of the novel *Pseudomonas putida* phage AF. *Virology* **434**: 251–256.

Costerton, J.W., Stewart, P.S., and Greenberg, E.P. (1999) Bacterial Biofilms: A Common Cause of Persistent Infections. *Science* **284**: 1318–1322.

Cramton, S.E., Gerke, C., Schnell, N.F., Nichols, W.W., and Götz, F. (1999) The intercellular adhesion (ica) locus is present in *Staphylococcus aureus* and is required for biofilm formation. *Infect Immun* **67**: 5427–5433.

Cucarella, C., Solano, C., Valle, J., Amorena, B., Lasa, Í., and Penadés, J.R. (2001) Bap, a *Staphylococcus aureus* surface protein involved in biofilm formation. *J Bacteriol* **183**: 2888–2896.

Delgado, S., Arroyo, R., Jiménez, E., Marín, M.L., Del Campo, R., Fernández, L., and Rodríguez, J.M. (2009) *Staphylococcus epidermidis* strains isolated from breast milk of women suffering infectious mastitis: Potential virulence traits and resistance to antibiotics. *BMC Microbiol* **9**: 82.

Diallo, K. and Dublanchet, A. (2022) Benefits of Combined Phage–Antibiotic Therapy for the Control of Antibiotic-Resistant Bacteria: A Literature Review. *Antibiotics* **11**: 1–11.

Domingues, R., Barbosa, A., Santos, S.B., Pires, D.P., Save, J., Resch, G., et al. (2021)

Unpuzzling friunavirus-host interactions one piece at a time: Phage recognizes *Acinetobacter pittii* via a new k38 capsule depolymerase. *Antibiotics* **10**: 1304.

Duarte, A.C., Fernández, L., De Maesschalck, V., Gutiérrez, D., Campelo, A.B., Briers, Y., et al. (2021) Synergistic action of phage phiIPLA-RODI and lytic protein CHAPSH3b: a combination strategy to target *Staphylococcus aureus* biofilms. *npj Biofilms Microbiomes* **7**: 39.

FAO and WHO (2019) Foody safety, everyone's business: a Guide to World Food Safety.1-8

Fernández, L., Duarte, A.C., Martínez, B., Rodríguez, A., and García, P. (2021) Draft Genome Sequences of the Bap-Producing Strain *Staphylococcus aureus* V329 and Its Derived Phage-Resistant Mutant BIM-1. *Am Soc Microbiol* **10**: 20–22.

Fernández, L., Gutiérrez, D., García, P., and Rodríguez, A. (2019) The Perfect Bacteriophage for Therapeutic Applications—A Quick Guide. *Antibiotics* **8**: 126.

Fey, P.D., Endres, J.L., Yajjala, V.K., Yajjala, K., Widhelm, T.J., Boissy, R.J., et al. (2013) A Genetic Resource for Rapid and Comprehensive Phenotype. *MBio* **4**: e00537-12.

González-Martín, M., Corbera, J.A., Suárez-Bonnet, A., and Tejedor-Junco, M.T. (2020) Virulence factors in coagulase-positive staphylococci of veterinary interest other than *Staphylococcus aureus*. *Vet Q* **40**: 118–131.

Gutiérrez, D., Briers, Y., Rodríguez-Rubio, L., Martínez, B., Rodríguez, A., Lavigne, R., and García, P. (2015) Role of the pre-neck appendage protein (Dpo7) from phage vB_SepiS-phiIPLA7 as an anti-biofilm agent in staphylococcal species. *Front Microbiol* **6**: 1315.

Gutiérrez, D., Delgado, S., Vázquez-Sánchez, D., Martínez, B., Cabo, M.L., Rodríguez, A., et al. (2012) Incidence of *Staphylococcus aureus* and Analysis of Associated Bacterial Communities on Food Industry Surfaces. *Appl Environ Microbiol* **78**: 8547–8554.

Gutiérrez, D., Garrido, V., Fernández, L., Portilla, S., Rodríguez, A., Grilló, M.J., and García, P. (2020) Phage Lytic Protein LysRODI Prevents Staphylococcal Mastitis in Mice. *Front Microbiol* **11**: 7.

Gutiérrez, D., Ruas-Madiedo, P., Martínez, B., Rodríguez, A., and García, P. (2014) Effective Removal of Staphylococcal Biofilms by the Endolysin LysH5. *PLoS One* **9**: e107307.

Gutiérrez, D., Vandenheuvel, D., Martínez, B., Rodríguez, A., Lavigne, R., and García, P. (2015) Two phages, phiIPLA-RODI and phiIPLA-C1C, lyse mono-and dual-species staphylococcal biofilms. *Appl Environ Microbiol* **81**: 3336–3348.

Iordanescu, S. and Surdeanu, M. (1976) Two Restriction and Modification Systems in *Staphylococcus aureus* NCTC8325. *J Gen Microbiol* **96**: 277–281.

Jurado, A., Fernández, L., Rodríguez, A., and García, P. (2024) Prevalence of virulence- and antibiotic resistance-associated genotypes and phenotypes in *Staphylococcus aureus* strains from the food sector compared to clinical and cow mastitis isolates. *Front Cell Infect Microbiol* **14**: 1327131.

De la Fuente-Núñez, C., Reffuveille, F., Fernández, L., and Hancock, R.E.W. (2013) Bacterial biofilm development as a multicellular adaptation: Antibiotic resistance and new therapeutic strategies. *Curr Opin Microbiol* **16**: 580–589.

Labrie, S.J., Samson, J.E., and Moineau, S. (2010) Bacteriophage resistance mechanisms. *Nat Rev Microbiol* **8**: 317–327.

Latka, A. and Drulis-Kawa, Z. (2020) Advantages and limitations of microtiter biofilm assays in the model of antibiofilm activity of *Klebsiella* phage KP34 and its depolymerase. *Sci Rep* **10**: 1–12.

Latka, A., Maciejewska, B., Majkowska-Skrobek, G., Briers, Y., and Drulis-Kawa, Z. (2017) Bacteriophage-encoded virion-associated enzymes to overcome the carbohydrate barriers during the infection process. *Appl Microbiol Biotechnol* **101**: 3103–3119.

Lei MG, Jorgenson MA, Robbs EJ, Black IM, Archer-Hartmann S, Shalygin S, Azadi P, Lee CY. (2024) Characterization of Ssc, an N-acetylgalactosamine-containing *Staphylococcus aureus* surface polysaccharide. J Bacteriol. **7**:e0004824.

Li, P., Ma, W., Shen, J., and Zhou, X. (2022) Characterization of Novel Bacteriophage vB_KpnP_ZX1 and Its Depolymerases with Therapeutic Potential for K57 *Klebsiella pneumoniae* Infection. *Pharmaceutics* **14**: 1916.

Lister, J.L. and Horswill, A.R. (2014) *Staphylococcus aureus* biofilms: Recent developments in biofilm dispersal. *Front Cell Infect Microbiol* **4**: 1–9.

Lorenz, L.L. and Duthie, E.S. (1952) Staphylococcal Coagulase: Mode of Action and Antigenicity. *J Gen Microbiol* **6**: 95–107.

Lotan, R., Sharon, N., and Mirelman, D. (1975) Interaction of Wheat-Germ Agglutinin with Bacterial Cells and Cell-Wall Polymers. *Eur J Biochem* **55**: 257–262.

Mi, L., Liu, Y., Wang, C., He, T., Gao, S., Xing, S., et al. (2019) Identification of a lytic *Pseudomonas aeruginosa* phage depolymerase and its anti-biofilm effect and bactericidal contribution to serum. *Virus Genes* **55**: 394–405.

Moormeier, D.E. and Bayles, K.W. (2017) *Staphylococcus aureus* biofilm: a complex developmental organism. *Mol Microbiol* **104**: 365–376.

Myers, C.L., Ireland, R.G., Garrett, T.A., and Brown, E.D. (2015) Characterization of wall teichoic acid degradation by the bacteriophage φ29 appendage protein GP12 using synthetic substrate analogs. *J Biol Chem* **290**: 19133–19145.

Nicholls, P., Clark, J.R., Liu, C.G., Terwilliger, A., and Maresso, A.W. (2023) Class-Driven Synergy and Antagonism between a *Pseudomonas* Phage and Antibiotics. *Infect Immun* **91**: e00065-23.

Ortega, E., Abriouel, H., Lucas, R., and Gálvez, A. (2010) Multiple Roles of *Staphylococcus aureus* Enterotoxins: Pathogenicity, Superantigenic Activity, and Correlation to Antibiotic Resistance. *Toxins (Basel)* **2**: 2117–2131.

Principi, N., Silvestri, E., and Esposito, S. (2019) Advantages and limitations of bacteriophages for the treatment of bacterial infections. *Front Pharmacol* **10**: 1–9.

Rice, C.J., Kelly, S.A., O'brien, S.C., Melaugh, E.M., Ganacias, J.C.B., Chai, Z.H., et al. (2021) Novel phage-derived depolymerase with activity against *Proteus mirabilis* biofilms. *Microorganisms* **9**: 2172.

Roszak, M., Dołęgowska, B., Cecerska-Heryć, E., Serwin, N., Jabłońska, J., and Grygorcewicz, B. (2022) Bacteriophage-Ciprofloxacin Combination Effectiveness Depends on *Staphylococcus aureus*-Candida albicans Dual-Species Communities' Growth Model. *Microb Drug Resist* **28**: 613–622.

Schilcher, K. and Horswill, A.R. (2020) Staphylococcal Biofilm Development: Structure, Regulation, and Treatment Strategies. *Microbiol Mol Biol Rev* **84**: 1–36.

Shen, Y., Boulos, S., Sumrall, E., Gerber, B., Julian-Rodero, A., Eugster, M.R., et al. (2017) Structural and functional diversity in *Listeria* cell wall teichoic acids. *J Biol Chem* **292**: 17832–17844.

Tong, S.Y.C., Davis, J.S., Eichenberger, E., Holland, T.L., and Fowler, V.G. (2015) *Staphylococcus aureus* infections: Epidemiology, pathophysiology, clinical manifestations, and management. *Clin Microbiol Rev* **28**: 603–661.

Valle, J., Toledo-Arana, A., Berasain, C., Ghigo, J.-M.M., Amorena, B., Penadés, J.R., and Lasa, I. (2003) SarA and not σB is essential for biofilm development by *Staphylococcus aureus*. *Mol Microbiol* **48**: 1075–1087.

Volozhantsev, N. V., Borzilov, A.I., Shpirt, A.M., Krasilnikova, V.M., Verevkin, V. V., Denisenko, E.A., et al. (2022) Comparison of the therapeutic potential of bacteriophage KpV74 and phage-derived depolymerase (β-glucosidase) against *Klebsiella pneumoniae* capsular type K2. *Virus Res* **322**: 198951.

Wilkinson, B.J. and Holmes, K.M. (1979) *Staphylococcus aureus* cell surface: Capsule as a barrier to bacteriophage adsorption. *Infect Immun* **23**: 549–552.

CHAPTER 3

3.3. Isolation of a new *S. epidermidis* phage with potential for biofilm removal

S. epidermidis is the cause of serious skin and prosthetic joint infections despite being a common inhabitant of human body surfaces. Several circumstances suggest that this opportunistic pathogen will be a threat in the near future. These include an increase in the number of antibiotic-resistant strains isolated in hospitals, the identification of more virulence genes associated to this species, and the increasing use of implantable medical devices. Although this microorganism shares multiple characteristics with *S. aureus*, many others are fairly different. For example, *S. epidermidis* biofilms show some peculiarities, whose influence on phage susceptibility have not been studied in depth. In this chapter, we have isolated and characterized a novel virulent phage infecting *S. epidermidis* (*Staphylococcus* phage IPLA-AICAT), belonging to the *Herelleviridae* family. Apart from genomic analysis, we also assessed other properties such as its host range against clinically-relevant *S. epidermidis* strains, which was determined to be quite wide (79%). In terms of antibiofilm activity, phage IPLA-AICAT exhibited good potential, which could be further improved by its combination with the lytic protein CHAPSH3b. Again, as observed in the case of *S. aureus*, there was synergy between the phage and this lytic enzyme. The results presented in this chapter confirm that this type of combination (phage and lytic protein) might be an effective strategy to get better results against biofilms formed by different pathogenic bacteria.
All of the results obtain are described in the following section:

3.3.1. A new bacteriophage infecting *Staphylococcus epidermidis* with potential for removing biofilms by combination with endolysins and antibiotics

3.3.1. A new bacteriophage infecting *Staphylococcus epidermidis* with potential for removing biofilms by combination with endolysins and antibiotics

ABSTRACT

Staphylococcus epidermidis is the cause of serious skin and prosthetic joint infections despite being a common inhabitant of human body surfaces. However, both the rise in antibiotic resistance in this species and its ability to form biofilms are increasingly limiting the available therapeutic options against these illnesses. In this landscape, phage therapy stands out as an interesting alternative to antibiotics. In the present study, we report the isolation and characterization of a novel virulent phage infecting *S. epidermidis* (*Staphylococcus* phage IPLA-AICAT), which belongs to the *Herelleviridae* family. The estimated genome size of this virus is 139,941 bp and sequence analysis demonstrated the absence of antibiotic resistance genes and virulence factors. The phage infects a high proportion (79%) of clinically-relevant *S. epidermidis* strains and exhibits antibiofilm activity. Moreover, combination of this phage with other antimicrobials, i.e. vancomycin and the lytic protein CHAPSH3b, further improved the reduction in surface-attached bacteria. Notably, the combination of *Staphylococcus* phage IPLA-AICAT (10^9 PFU/ml) and CHAPSH3b (8 μM) was able to reduce the number of viable cells by 3.06 log units in 5 h-old biofilms. These results confirm our previous data regarding the potential of phage-lysin mixtures against staphylococcal biofilms.

INTRODUCTION

The gradual increase in antibiotic resistance in bacteria is one of the biggest threats that we are facing today, affecting not only human health, but also the global economy. Some experts estimate that the global economic burden of antimicrobial resistance (AMR) could be in the trillions of dollars by 2050 (Global AMR R&D Hub and WHO, 2023). Increasingly, health care-associated infections (HAIs) represent one of the most common causes of morbidity and mortality worldwide, most frequently affecting immunocompromised or catheterized patients (Vincent, 2003). Furthermore, since bacteria in these facilities are more commonly exposed to antibiotics, nosocomial strains tend to exhibit a higher prevalence of antibiotic resistance than those isolated in the community at large, making these infections more difficult to treat.

Staphylococcus epidermidis is one of the most abundant species in the human skin and mucosal microbiome. Indeed, colonization by this bacterium promotes skin barrier development, maintains homeostasis, actively coordinates the skin response to injury and controls opportunistic pathogens through secretion of AMPs (i.e. phenol soluble modulins, PSMs) (Severn and Horswill, 2023). Even though it may seem harmless for humans, this microorganism can behave as an opportunistic pathogen, mainly affecting hospitalized patients and premature infants (Meskin, 1998). Worryingly, treatment of *S. epidermidis* infections is becoming challenging due to the increasing rates of antibiotic resistance in this species, even in strains isolated from healthy skin (Zhou *et al.*, 2020). Also, there is a high prevalence of virulence genes in this pathogen, such as the extracellular cysteine protease EcpA, which has been related to skin diseases like severe atopic dermatitis (Cau *et al.*, 2021). Apart from that, the biofilm-forming ability of this bacterium allows its colonization of medical devices and human organs (Otto, 2009). A biofilm is a surface-attached bacterial community embedded in an extracellular polymeric substance (EPS) secreted by the cells (Karygianni *et al.*, 2020). This EPS is composed of polysaccharides, proteins, extracellular DNA (eDNA), and other minor components (Yan and Bassler, 2019). EPS promotes cell–cell cohesion (including interspecies recognition) to facilitate microbial aggregation and biofilm formation. Additionally, the physical and chemical properties of the biofilm matrix constituents, together with other properties of these complex communities, protect sessile cells from external challenges, such as antibiotics and host defence mechanisms. This makes the eradication of biofilms rather problematic, being the main reason of chronic recalcitrant infections. Thus, *S. epidermidis*

is a leading cause of prosthetic valve endocarditis and implant-associated infections (Riool *et al.*, 2014). This can be made even worse when these biofilms disseminate into the cardiovascular system and cause potentially fatal bloodstream infections.

Over the last years, the interest in bacteriophages (phages) and their derived proteins as a potential alternative treatment for antibiotic-resistant bacterial infections has been on the rise. Phages are viruses that infect bacteria and have a narrow host range, being able to infect only one or a few species (Loc-Carrillo and Abedon, 2011). More and more studies confirm the effectiveness of phage therapy, based on the successful results of clinical trials and case studies, for example, for untreatable chronic infections (Uyttebroek *et al.*, 2022) or periprosthetic joint infections (Fedorov *et al.*, 2023). Moreover, bacteriophages have been tested as antibiofilm agents *in vitro* (Pires *et al.*, 2022), both alone (individually or in phage cocktails) and in combination with other antimicrobials, such as antibiotics or antiseptics (Jo *et al.*, 2016; Akturk *et al.*, 2019; Joo *et al.*, 2023) or even with phage lytic enzymes (Duarte *et al.*, 2021).

To date, the number of characterized phages that infect *S. epidermidis* is still quite low (Daniel *et al.*, 2007; Aswani *et al.*, 2014; Melo *et al.*, 2014; Freeman *et al.*, 2019). Among them, we have previously studied three siphovirus phages (vB_SepiS-phiIPLA5, vB_SepiSphiIPLA6, and vB_SepiS-phiIPLA7) (Gutiérrez *et al.*, 2010). Phages vB_SepiSphiIPLA5 and vB_SepiS-phiIPLA7 were sequenced, allowing the identification of genes encoding putative depolymerase activities against bacterial biofilms (Gutiérrez *et al.*, 2012). Additionally, we have identified and developed several phage lytic proteins with improved activity against staphylococci, including the chimeric protein CHAPSH3b (CHAP domain from the virion associated protein HydH5 fused to the cell wall binding domain SH3b of lysostaphin) (Rodríguez-Rubio *et al.*, 2012). CHAPSH3b demonstrated not only the ability to eliminate preformed structures, but also inhibited biofilm development (Fernández *et al.*, 2017).

In this study, a new phage, named *Staphylococcus* phage IPLA-AICAT (AICAT), infecting *S. epidermidis* strains from clinical origin was isolated and characterized. Additionally, we tested the combination of this phage with other antimicrobials, the antibiotic vancomycin and the phage lytic protein CHAPSH3b, for biofilm removal.

MATERIALS AND METHODS

Bacterial strains, growth conditions and protein purification

For this study, 24 *S. epidermidis* and 6 *S. aureus* strains were used (Table 3.7). Bacteria were grown at 37 °C in tryptic soy broth (TSB, Scharlau, Barcelona, Spain) or in TSB plates with 1.5% (w/v) agar (Roko, S.A., Llanera, Spain) (TSA). TSB top agar composed of TSB supplemented with 0.7% (w/v) agar was used for phage propagation and titration. For biofilm formation assays, TSB supplemented with 0.25% (v/v) glucose (Merck, Darmstadt, Germany) (TSBg) was used.

The phage-derived protein CHAPSH3b and dispersin B were purified as described previously (García *et al.*, 2010). The proteins were then checked by SDS-PAGE analysis and quantified by using the Quick Start Bradford Protein Assay kit (Bio-Rad).

Phage isolation, purification and titration

Bacteriophage was isolated from samples coming from a sewage treatment plant in Oviedo (Asturias), Spain. For isolation of *S. epidermidis* phages, 2 liters of sewage from a sewage treatment plant in Oviedo (Asturias, Spain) were centrifuged twice during 30 min, at 1000 rpm and 4 °C. The supernatant was filtered by sequentially using cellulose acetate filters with 0.45 µm and 0.22 µm membrane pore size (VWR, Spain). Enrichment cultures were performed by mixing 4 strains of *S. epidermidis* using different combinations (supplementary material Table 7.3). 100 µL of each strain, previously grown to an OD_{600} ~ 0.1, were added to 80 ml of filtered sewage and 20 ml of 5 × TSB medium, and grown overnight at 37 °C with shaking. The next day these cultures were centrifuged and filtered. Three sequential enrichments were carried out to obtain a higher phage titer. To detect the presence of phages in the enrichment cultures, 5 and 10 µl of the supernatant from each mixture were dropped onto TSA plates containing each of the 24 *S. epidermidis* strains using the double layer technique (Gutiérrez *et al.*, 2010). The presence of phages infecting these strains was determined by visualization of an inhibition halo after overnight incubation of these plates at 37 °C. *S. epidermidis* SE11B was selected as host strain for plaquing culture supernatants. Isolated lysis plaques were taken and re-isolated three times. Individual lysis plaques were selected for propagation as described previously (García *et al.*, 2007). Phage enumeration was performed by the double layer technique (Gutiérrez *et al.*, 2010).

One-step growth curve

One-step growth curves were performed to determine the phage growth parameters using the sensitive strain *S. epidermidis* SE11B. First, 10 ml of a mid-exponential phase culture with an OD_{600} of 0.1 were harvested by centrifugation (4000 rpm, 4 °C, 10 min) and resuspended in 1 ml of fresh TSB medium. Phage was added to this suspension at an MOI (multiplicity of infection) of 1 and were allowed to adsorb for 10 min at 37 °C. Next, the mixtures were centrifuged again (4000 rpm, 4°C, 10 min) and the pellet was resuspended in 10 ml of fresh TSB medium. A sample was taken immediately, and the suspension was incubated at 37 °C. Further samples were taken every 10 min over a period of 60 min. Samples were centrifuged (13000 rpm, 1 min) and the supernatant was immediately serially diluted in SM buffer (20 mM Tris-HCl, 10 mM $MgSO_4$, 10 mM $CaCl_2$, 100 mM NaCl, pH 7.5). The pellet was resuspended again and treated with 1% (v/v) chloroform for 1 min (vortex), in order to release the phages inside the cells, and centrifuged again (13000 rpm, 1 min). The supernatant was serial diluted in SM buffer for PFU determination as described above.

Time-killing assay

The time-killing assay was performed to find out the susceptibility of planktonic bacterial cells to phage infection using the microdilution assay. In summary, strain SE11B was grown until OD_{600} ~ 0.1 and diluted 1:10 (v/v). Phage AICAT was added at different MOIs into a 96-well polystyrene microtiter plate and mixed with the bacteria. In order to monitor the evolution of the bacterial population in the presence of increasing phage concentrations, growth was monitored for 24 h at 37 ºC by measuring the OD_{600} every 15 minutes using a multiwell plate reader Tecan Infinite M Nano (Tecan Trading AG).

pH and temperature stability assays

The pH stability of the phage particles was tested by incubation in Britton-Robinson pH universal buffer (150 mM KCl, 10 mM KH_2PO_4, 10 mM sodium citrate, 10 mM H_3BO_3), with adjustment of the pH in the range from 3 to 11. A phage suspension (10^9 PFU/ml) was diluted 1:10 in universal buffer and incubated for 3 h at room temperature. Similarly, the temperature stability of the phage particles was examined by incubation of the phage (10^9 PFU/ml) in SM buffer at different temperatures ranging from 10°C-100°C for 30

min. Afterwards, serial dilutions were performed for PFU determination. Phage stored at 4 °C was used as a control.

Transmission electron microscopy (TEM)

Electron microscopic analysis was performed after negative staining of the phage particles using 2% uranyl acetate. Visualisation was carried out using a JEOL 12.000 EXII transmission electron microscope (JEOL USA Inc., Peabody, MA).

Phage DNA extraction, genome sequencing, and bioinformatics analysis

Phage DNA extraction started with the elimination of the extracellular bacterial DNA of phage suspension (10^9 PFU/ml). Briefly, 250 µl of phage suspension were incubated with benzonase (125 U) (Sigma), RNAse cocktail (5 U) (ThermoFisher scientific), DNAse I (10 U) (Fermentas) and TurboDNAse (5 U) (Invitrogen) during 2 h at 37°C. After digestion, 1 volume of phenol:chloroform (3:1) was added to the phage sample and mixed for 1 min. Then, the samples were centrifuged for 2 min (10,000 rpm) and the upper phase was collected and transferred into a new tube and the same process was repeated. Next, 1 volume of chloroform was added to the sample, mixed for 1 min and centrifuged (10,000 rpm, 5 min). The upper phase was recovered and, after adding 25 µl of sodium acetate 3 M and 625 µl of 100% ethanol, incubated at -80 °C for 30 min. After that, the samples were centrifuged for 15 min at 4°C, the pellet was washed with ethanol 70%, and then washed again with ethanol 100%. The sample was dried, resuspended in milliQ water and stored at -20 °C. The genome sequencing of phage AICAT was carried out at FISABIO Sequencing and Bioinformatics Service (Valencia, Spain) using Illumina technology. Genomic comparisons at the nucleotide level were made with Mauve software, using a progressive alignment with default settings (http://gel. ahabs.wisc.edu/mauve/). Phage genome was autoannotated using tools from Bacterial and Viral Bioinformatics Resource Center (BV-BRC) and Open Reading Frame Finder. BLASTP was used to search for similar proteins. Putative tRNAs, antibiotic resistance genes and virulence genes were predicted using tRNAscan-SE, ResFinder4.1, and VFDB (VFDB: Virulence Factor Database), respectively. Genomic comparison at the nucleotide level was made with BLASTN using the genome sequences available in public databases (NCBI). Before the global alignments could be performed, the genomes were manually

colinearised, placing the arbitrary starting point at a similar position to that of the most similar phage genome in the databases.

Biofilm formation and anti-biofilm efficacy of phages

Overnight cultures of five *S. epidermidis* strains (L05081, B, SE11B, SE2H and F12) were diluted 1:100 (v/v) in fresh TSBg medium. Then, 1 ml from each bacterial suspension was poured into each well of a 24-well polystyrene microtiter plate (Thermo Scientific, NunclonTM Delta Surface) and incubated for 5 h and 24 h, at 37°C, under static conditions. Following incubation, the planktonic phase was removed and the biofilms washed once with phosphate-buffered saline (PBS; 137 mM NaCl, 2.7 mM KCl, 10 mM Na_2HPO_4, 2 mM KH_2PO_4 [pH 7.4]). The remaining adhered cells were treated by addition of: 0.5 ml of TSB alone as a control; or containing a suspension of phage individually (10^9 PFU/ml), phage (10^9 PFU/ml) plus vancomycin (4 µg/ml), or phage plus protein CHAPSH3b (8 µM). All samples were incubated during 24 h at 37 °C. Subsequently, the planktonic phase was removed and the biofilms washed with PBS. The number of viable cells was determined using the spot test. Briefly, the biofilms were scraped and resuspended in 1 ml of PBS. Then, ten-fold serial dilutions were performed and 10 µl from each suspension were placed onto TSA plates and allowed to dry. The results are presented in number of CFUs per unit area (CFU/cm^2). The potential interaction between the antimicrobials (phage and lysin or phage and antibiotic) was calculated (Chaudhry *et al.*, 2017) and the values obtained were named interaction indices. The interaction was considered additive when this index was between −0.5 and 0.5, antagonistic when the value was <−0.5, and synergistic when the value was >0.5.

To determine the composition of the biofilm matrix, the adhered cells from 24-h biofilms were washed once with PBS, and then treated with 0.5 ml of DNAse (100 µg/ml), proteinase K (100 µg/ml) or dispersin B (6 µM) solutions during 1 h at 37 °C. Then, total biomass was quantified by performing the crystal violet staining assay (Gutiérrez *et al.*, 2014). Briefly, 1 ml of 0.1% (w/v) crystal violet was added and incubated for 15 min and next washed once with water to remove the excess of crystal violet and solubilised by adding 33% (v/v) of acetic acid. The amount of dye was quantified by measuring absorbance at 595 nm (A_{595}) using a Benchmark Plus Microplate Spectrophotometer (Bio-Rad Laboratories, Hercules, CA, USA).

Statistical analysis

Statistical analysis of the results was carried out by performing Student's t-test and *P*-values lower than 0.05 were considered significant.

Table 3.7 – Staphylococcal strains used in this work. Sensitivity of the strains to phage AICAT is indicated as: -, no inhibition halo (resistant); +, small halo (low susceptibility); ++, intermediate halo (medium susceptibility); +++, large halo (high susceptibility). MRSE: methicillin-resistant *S. epidermidis*.

Strain	Origin	Reference	AICAT
***S. epidermidis* SE1B**	Blood culture (San Agustín hospital)	This study	-
***S. epidermidis* SE2H**	Blood culture (San Agustín hospital)	This study	+++
***S. epidermidis* SE3H**	Blood culture (San Agustín hospital)	This study	++
***S. epidermidis* SE4B**	Blood culture (San Agustín hospital)	This study	++
***S. epidermidis* SE3C**	Catheter (San Agustín hospital)	This study	++
***S. epidermidis* SE6B**	Blood culture (San Agustín hospital)	This study	+
***S. epidermidis* SE7B**	Blood culture (San Agustín hospital)	This study	++
***S. epidermidis* SE8B**	Blood culture (San Agustín hospital)	This study	-
***S. epidermidis* SE16U**	Urine (San Agustín hospital)	This study	-
***S. epidermidis* SE10B**	Blood culture (San Agustín hospital)	This study	+++
***S. epidermidis* SE11B**	Blood culture (San Agustín hospital)	This study	+++
***S. epidermidis* 47**	Unknown (San Agustín hospital)	This study	+++
***S. epidermidis* 48**	Unknown (San Agustín hospital)	This study	-
***S. epidermidis* F12**	Woman's breast milk	(Delgado *et al.*, 2009)	+++
***S. epidermidis* CECT4183**	Collection strain (Blood of patient with intravascular catheter)	This study	+++
***S. epidermidis* ASLD1**	Woman's breast milk	(Delgado *et al.*, 2009)	++
***S. epidermidis* DG2ñ**	Woman's breast milk	(Delgado *et al.*, 2009)	-
***S. epidermidis* LO5081**	Woman's breast milk	(Delgado *et al.*, 2009)	+++
***S. epidermidis* LX5RB4**	Woman's breast milk	(Delgado *et al.*, 2009)	++
***S. epidermidis* Z2LDC14**	Woman's breast milk	(Delgado *et al.*, 2009)	+++
***S. epidermidis* YLIC13**	Woman's breast milk	(Delgado *et al.*, 2009)	+++
***S. epidermidis* DH3LIK**	Woman's breast milk	(Delgado *et al.*, 2009)	+++
***S. epidermidis* LO5RB1**	Woman's breast milk	(Delgado *et al.*, 2009)	++
***S. epidermidis* B**	Woman's breast milk	(Delgado *et al.*, 2009)	+++
***S. aureus* V329**	Bovine subclinical mastitis	(Cucarella *et al.*, 2001)	-
***S. aureus* BIM1**	V329 derived mutant	(Fernández *et al.*, 2021)	-
***S. aureus* 15981**	Clinical isolate	(Valle *et al.*, 2003)	-
***S. aureus* Newman**	Clinical isolate	(Keinhörster *et al.*, 2019)	-
***S. aureus* USA300 JE2**	Clinical isolate	(Keinhörster *et al.*, 2019)	-
***S. aureus* IPLA16**	Meat industry surface	(Gutiérrez et al. 2012)	-

RESULTS

Isolation and characterization of a new *S. epidermidis* phage

Phage therapy is a promising strategy to fight against *S. epidermidis* infections resilient to current treatments; therefore, our aim was to isolate lytic phages and to investigate their

future potential as therapeutics. For this purpose, twenty-four *S. epidermidis* strains from clinical origin were selected. Nine strains were isolated from bloodstream cultures, ten from breast milk, one from a catheter, and one from a urine culture. Of note, all of the strains were selected considering their lysogenic pattern, using mitomycin C to check the presence/absence of prophages in their genome. After confirming the absence of prophages, these strains were used to design four different mixtures, each of them composed by four strains and chosen arbitrarily. Enrichment cultures were performed using residual water and after three enrichment steps, the supernatants were plaqued on all the strains showing the presence of lysis plaques with a different morphology. Depending on the transparency of the halo, the strains were considered more or less susceptible (Table 3.7). Taking into account the mixtures used for the enrichments (supplementary material Table 7.3) and the susceptibility of the strains to the phages, strain SE11B was selected as a host strain for phage propagation. After three isolation rounds, we isolated one phage, which was named *Staphylococcus* phage IPLA-AICAT (AICAT). The phage showed a wide host range, infecting 19 out of 24 strains tested (79%) (Table 3.7). Only 7 strains (*S. epidermidis* SE1B, *S. epidermidis* SE8B, *S. epidermidis* SE16U, *S. epidermidis* 48, *S. epidermidis* DG2ñ) were resistant, while the rest displayed different degrees of susceptibility. Six *S. aureus* strains were tested and all of them were resistant to the phage. Morphology of the phage particles was observed by TEM. Virions had an icosahedral capsid, with a diameter of 73±0.07 nm, and a long contractile tail, with a length of 97±0.06 nm. The TEM images show that the phage has a hexagonal base plate with possible tail fibres. These characteristics indicate that phage AICAT is a myovirus belonging to the order Caudoviricetes (Figure 3.20).

The infection parameters of phage AICAT were determined by carrying out a one-step growth curve on strain *S. epidermidis* SE11B. As is observed in Figure 3.20, the lytic cycle was around 40 min. Regarding the burst size, the estimated number of particles released per infected cell was 57. Regarding stability, this phage exhibited a high tolerance to pH, being stable in a range between pH 4 and pH 9. No viable infecting phages were recovered after incubation at pH 3 and pH 10 (Figure 3.21A). Also, phage AICAT was very stable at temperatures below 50°C. Incubation at 70 °C reduced the phage titer by 5.99 log units, whereas total inactivation was observed at 80 °C (Figure 3.21B).

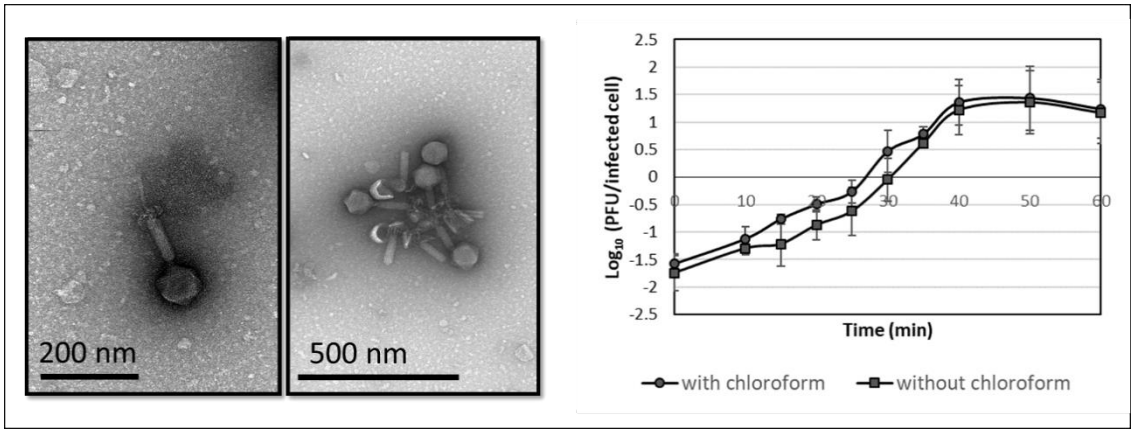

Figure 3.20 - Transmission electron microphotographs and one step growth curve of phage AICAT. Values correspond to the means ± standard deviations of four independent experiments represented in number of PFUs per infected cell. Cells were chloroform treated (circles) or left untreated (squares).

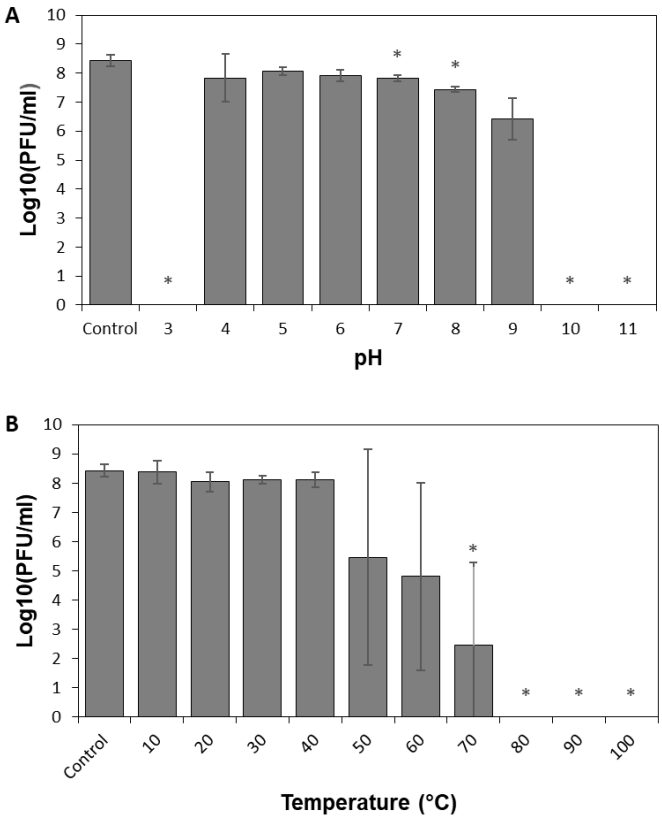

Figure 3.21 - Stability of phage particles to environmental conditions, (A) pH and (B) temperature. Suspensions (10^8 PFU/ml) of Staphylococcus phage AICAT was incubated for 30 min. Data correspond to the means ± standard deviations of three independent experiments and are represented in logarithmic scale in plaque-forming units

per ml. Bars having an asterisk are significantly different ($p < 0.05$) from the control according to Student's t-test.

Planktonic cells have different susceptibility to phage at different concentrations

In order to evaluate susceptibility to phage AICAT, a time killing assay was performed using the host strain SE11B. Phage was incubated at different concentrations with the bacteria during 24 h. The results show that the most efficient startingphage concentration was 5×10^3 PFU/ml (Figure 3.22). Lower starting concentrations did not sufficiently deplete the susceptible bacterial population, and regrowth of the bacterial population potentially due to the selection of bacteriophage resistant mutants was observed at concentrations equal to or greater than 5×10^4 PFU/ml.

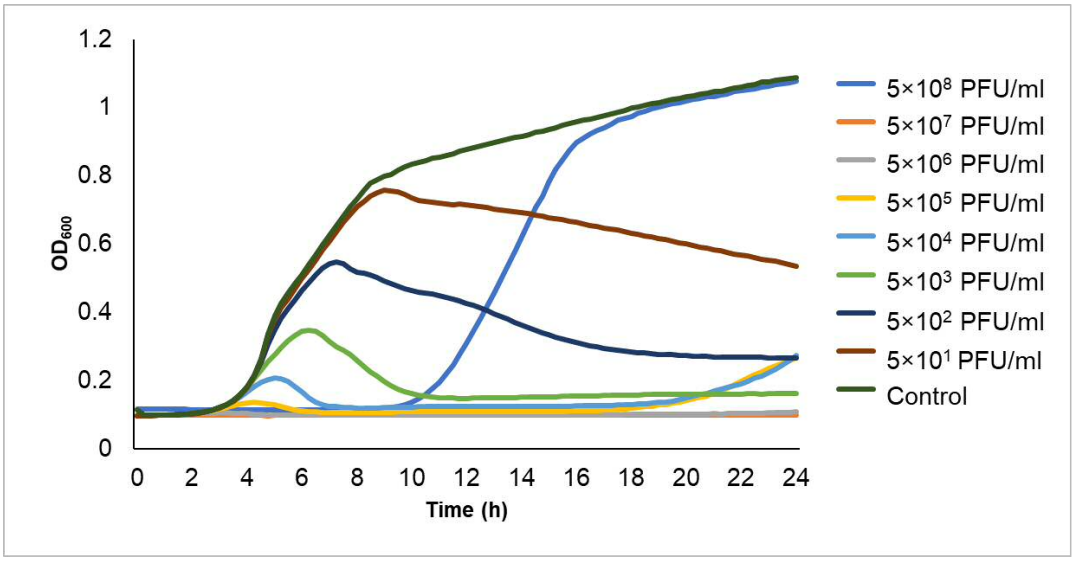

Figure 3.22 - Growth curve of *S. epidermidis* SE11B at 37 ºC in the presence of increasing concentrations of phage AICAT ranging from 0 (control) to 5×10^8 PFU/ml. OD_{600} was monitored for 24 hours. Data represent one representative experiment out of three independent repeats showing the same trend.

Genome characterization of phage AICAT reveals if belongs to the genus *Sepunavirus*

The *staphylococcus* phage IPLA-AICAT has a double-stranded DNA genome consisting of 139,941 bp carrying 209 putative open reading frames (ORFs) (Table 7.4 (supplementary material 7.3)). Comparison of this phage using ORFs were annotated based on similarity to previously characterized phages such as *Staphylococcus* phage vB_SepM_BE04 (accession number MT596501) and *S. epidermidis* phage phiIPLA-C1C (accession number KP027447), respectively. The morphogenesis module was split into two main regions in both genomes, which were separated by the replication/transcription module. Genes encoding the large and small terminase subunits, portal protein, prohead protease, major capsid, major tail sheath, tail fiber, tail baseplate and tape measure protein (TMP) were identified. A group I intron associated with a VRS endonuclease was detected in the middle of the terminase large subunit gene (*orf*65, *orf*66, *orf*67 and *orf*69). A lysis module, containing genes involved in bacterial lysis (holin and endolysin), was located upstream of the morphogenetic module. In addition, a second endolysin and holin genes were identified individually in the replication region. Putative lytic transglycosylase (*orf*97), amidase (*orf*98) and endolysin genes (*orf*96) were identified in the structural module, which may be involved in cell wall hydrolysis necessary for phage infection.

At the nucleotide level, phage AICAT shares a high degree of similarity with *Staphylococcus* virus BESEP4 (99.70%) and 99.27% with the *Staphylococcus* phage 110. Additionally, it was closely related to phage Quidividi, Terranova, 80B, 80A and BESEP5. Mauve software revealed gene synteny between phage AICAT and other *S. epidermidis* phages including the morphogenesis, replication/transcription, long terminal repeat, and lysis modules. (Figure 3.23).

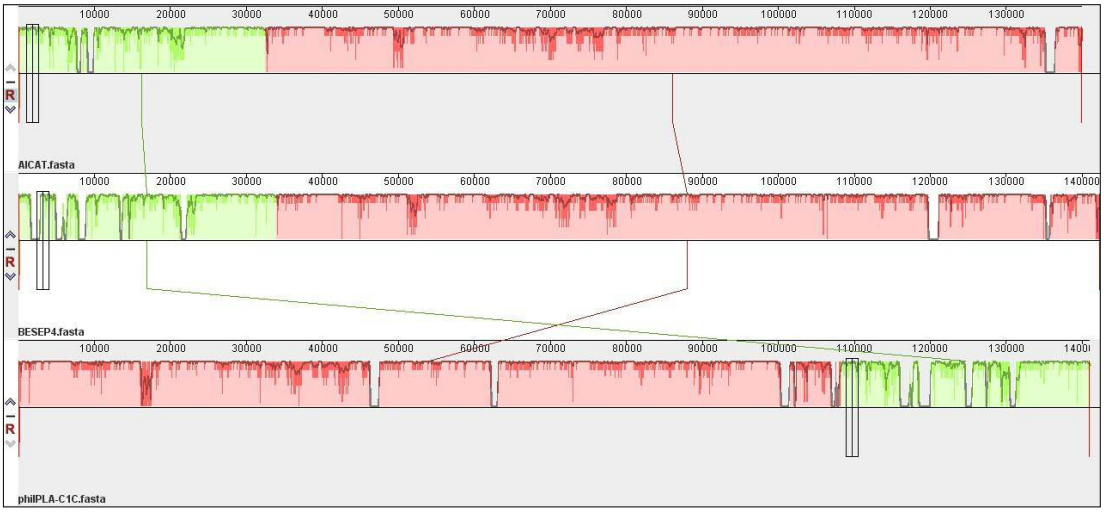

Figure 3.23 - Alignment of the genome of the *S. epidermidis* phage AICAT with other *Staphylococcus* phages using the Mauve software. Each block represents a region of the genome sequence that aligned and is homologous to part of another genome. Lines connecting blocks are indicative of homologous regions.

Phage susceptibility of biofilms might be related to matrix composition

The design of a phage-based antibiofilm strategy against *S. epidermidis* would benefit from knowing the composition and structure of the target biofilms. With this in mind, we selected five *S. epidermidis* strains to determine the composition of their biofilm matrix: *S. epidermidis* SE11B and *S. epidermidis* SE2H because of their high sensitivity to the new phage, and *S. epidermidis* F12, *S. epidermidis* L05081 and *S. epidermidis* B due to our previous knowledge about their phage sensitivity to other phages (Gutiérrez *et al.*, 2015). Treatment of 24 h-old biofilm samples with degrading enzymes (DNAse, proteinase K and dispersin B) indicated that the biofilm matrix of strains *S. epidermidis* L05081, SE11B, SE2H and F12 was mostly composed of eDNA. Interestingly, *S. epidermidis* strain SE11B and SE2H also contained a significant amount of proteins (Figure 3.24).

The use of strains with different biofilm matrix composition provides us with a variety of targets to test antibiofilm efficacy. 24 h-old biofilms formed by these strains were treated individually with the phage (10^9 PFU/ml) for 6 h or 24 h (Figure 3.25 A and B). When 24 h-old biofilms were infected with AICAT for 6 h, significant reductions in CFUs were only observed for *S. epidermidis* strain SE11B (0.69 log units reduction) (Figure 3.25 A).

Apart from that, phage AICAT was not able to reduce viable cell counts in any other strain. The low sensitivity of biofilms to this phage led us to increase the infection time to 24 h. Nonetheless, only strain *S. epidermidis* SE11B was sensitive, with a reduction of 1.28 log units, even though not signifincatly (Figure 3.25 B).

Early biofilms were also treated with AICAT. Interestingly, in 5 h-old biofilms (Figure 3.25 C), there was a significant reduction in viable cells for strains *S. epidermidis* B, *S. epidermidis* SE11B and *S. epidermidis* F12 (0.56, 1.84 and 1.77 log units, respectively) after 24 h of treatment. Overall, *Staphylococcus* phage AICAT seems to be effective, especially against *S. epidermidis* SE11B and *S. epidermidis* F12, which happen to possess a matrix with a high eDNA content. Nonetheless, it is difficult to establish a correlation between matrix composition and phage susceptibility based on such a small number of strains.

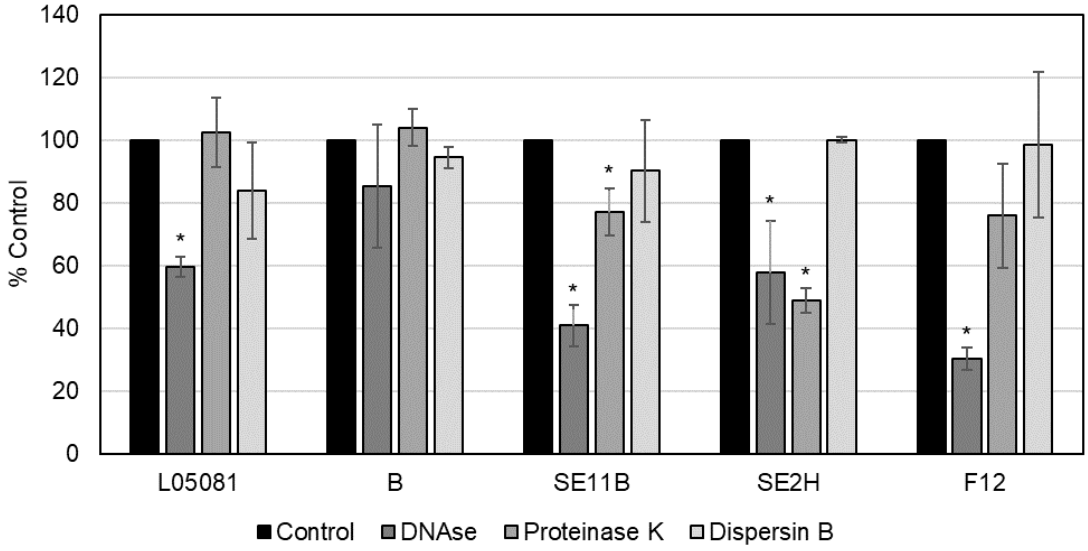

Figure 3.24 - Chemical composition of the extracellular matrix of *S. epidermidis* biofilms. 24 h-old biofilms were treated with DNAse, proteinase K and dispersin B and attached biomass was measured and compared to control samples.

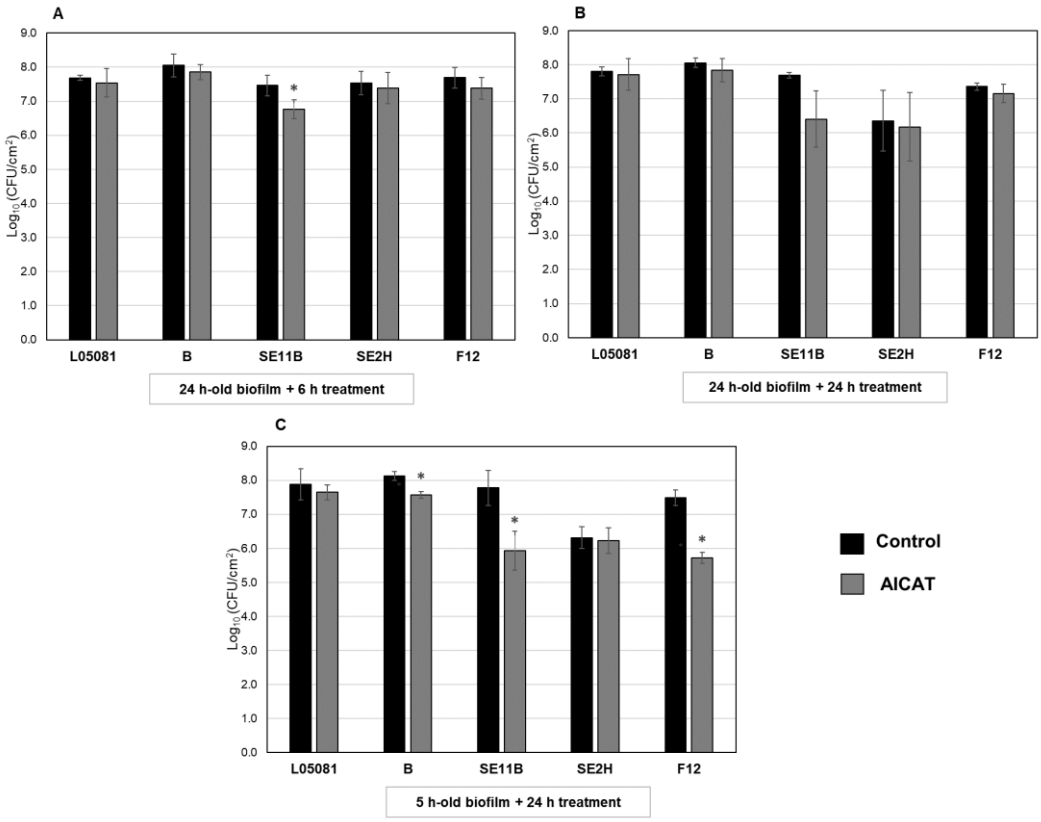

Figure 3.25 - Treatment of biofilms formed by different *S. epidermidis* strains. Biofilms were allowed to develop during 24 h at 37 °C and treated during 6 h (A) and 24 h (B) amd 5 h treated 25 h (c) with phage AICAT (dark grey bars). TSB medium alone was added to the control wells (black bars). After incubation, the viable cell counts of the five strains were determined. Data correspond to the means ± standard deviations of three independent experiments and represented in the logarithmic scale in colony-forming units per cm^2 of biofilm. Bars with an asterisk are statistically different ($p < 0.05$) from the untreated control according to Student t-test.

Combined treatment improves biofilm removal by phages

Given the poor results obtained with the phage alone, we combined phage AICAT (10^9 PFU/ml) with other antimicrobials, namely the lytic protein CHAPSH3b (8 µM) and vancomycin (4 µg/ml). The results demonstrated that the combination of the phage with CHAPSH3b works significantly better (decrease of 2.52 log units) than the phage alone. These results indicated a synergistic effect between phage AICAT and the lytic protein with an interaction index of 0.65. In contrast, there was an additive effect in the combination of the phage with vancomycin, with an interaction index of -0.25. Indeed, the reduction in viable cells using the phage-antibiotic combination was practically the

same as that obtained for the phage alone (1.33 log units). No significant reduction in viable cells was observed when using the lytic protein or the antibiotic alone (Figure 3.26).

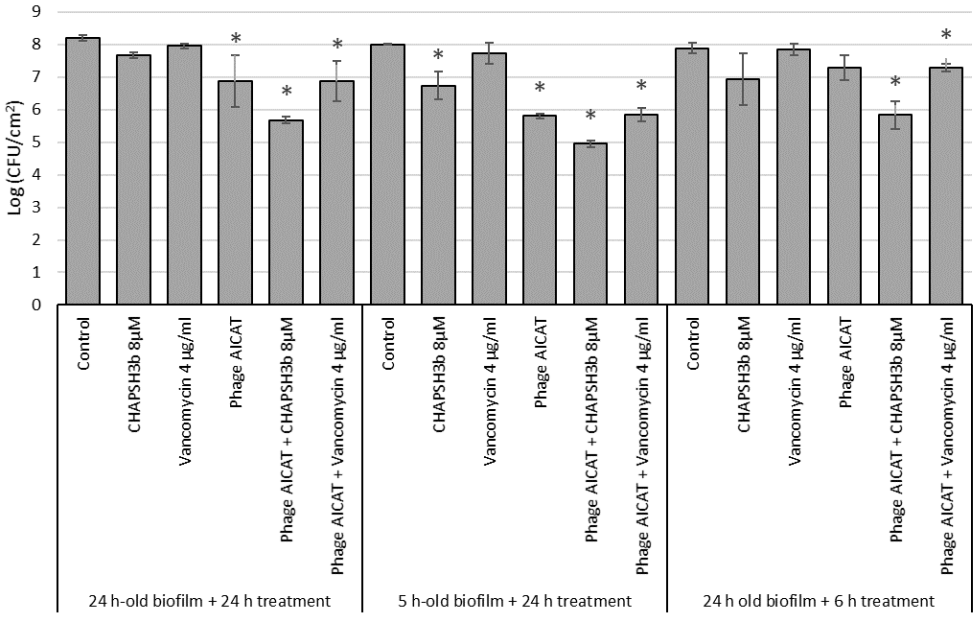

Figure 3.26 - Combined treatment of phage AICAT with different antimicrobials against *S. epidermidis* SE11B biofilms. Biofilms (5 h and 24 h-old) were treated (6 h and 24 h) with phage AICAT (10^9 PFU/ml), chimeric protein CHAPSH3b (8 µM), vancomycin (4 µg/ml) or combinations of the phage with the antimicrobials. Fresh TSB medium was added to the control wells. After incubation, the viable cell counts were determined. Data correspond to the means ± standard deviations of three independent experiments and are represented in the logarithmic scale in colony-forming units per cm^2 of biofilm. Bars with an asterisk are statistically different ($p < 0.05$) from the untreated control according to Student's t-test.

When treatment was implemented only for 6 h in 24 h biofilms, the best combination was the phage with the protein CHAPSH3b with a reduction of 2.06 log units, acting synergistically with an interaction index of 0.50. The combination of the phage with the antibiotic resulted in an additive effect, with an interaction index of -0.03.

This assay was also performed with 5 h-old biofilms (Figure 3.26). Again, the combination of phage and CHAPSH3b gave the best results in terms of biofilm reduction (decrease of 3.06 units log) followed by combination of phage with vancomycin (2.16 log

units). However, these results reflect an additive effect and not synergy, with an interaction index of -0.42 for CHAPSH3b and -0.32 for the antibiotic.

DISCUSSION

Phage therapy is experiencing significant momentum as demonstrated by the fact that several clinical trials are currently underway. Some examples include safety studies of bacteriophages (ClinicalTrials.gov ID NCT04650607), therapy in chronic prosthetic joint infections (ClinicalTrials.gov ID NCT05269121), and therapy in patients with diabetic foot osteomyelitis (ClinicalTrials.gov ID NCT05177107). Phages intended for the treatment of patients must comply with several requirements, such as being strictly virulent, lacking virulence factors and antibiotic resistance genes, and should not be prone to generalized transduction (Pirnay *et al.*, 2015). In this context, we have isolated a new phage infecting a number of *S. epidermidis* strains isolated from clinical samples. The characterization of phage AICAT revealed that it belongs to the *Herelleviridae* family, whose members are obligatorily lytic (https://ictv.global/report/chapter/herelleviridae/herelleviridae), making them suitable for therapy. Also, based on its similarity to other phages in the databases, phage AICAT belongs to the genus *Sepunavirus*.

Regarding the genome sequence, this phage showed a structure very similar to previously identified phages from *Staphylococcus* genus. Actually, the bioinformatic analysis is consistent with the typical characteristics of the *Herelleviridae* family, such as virions with myovirus morphology, dsDNA genomes of 125–170 kbp and obligately lytic (https://ictv.global/report/chapter/herelleviridae/herelleviridae). Moreover, other characteristics found in staphylococcal phages belonging to this family include the presence of homing endonucleases within group I introns, in accordance with previous results reported for other myophages, such as T4, where 11% of the ORFs correspond to homing endonucleases (Edgell *et al.*, 2010).

Besides host range analysis, we evaluated the antibacterial activity, stability and infection parameters of the new phage. Our results showed a high production of phage particles for phage AICAT (57 per infected cell) but a lower stability at high pH. Taking into account that the pH in healthy skin is between 4.7 and 5.75, between 7.15–8.9 in chronic wounds, this phage will be stable enough for therapeutic applications in skin-related infections. In any case, the issue of improving phage stability for their application in the treatment of

wound infections has already been addressed with different solutions that include encapsulation or the design of materials that allow their controlled release and protection (Chhibber *et al.*, 2017; Sun *et al.*, 2022).

Since biofilm formation is critical for the virulence of *S. epidermidis* and it is the principal microbial property leading to the observed outcomes in periprosthetic joint infection management and device-related infections, the effect of phages on mature 24 h-old biofilms formed by different strains was examined. Biofilms formed by five different *S. epidermidis* strains were resistant to phage attack regardless of the strain origin. Similar results were observed by Melo *et al.* (2020), who concluded that the extracellular matrix is a barrier that hampers infection of bacteria rather than inactivate the phages or prevent phage adsorption (Melo *et al.*, 2020). Overall, even though the use of phage did not lead to a higher reduction in the biofilm, we did observe that younger biofilms are more sensitive to the phages individually and in combination with the antimicrobials. Moreover, *S. epidermidis* SE11B and *S. epidermidis* F12 were the most susceptible strains to phage attack. Interestingly, these strains have a high content of eDNA in the extracellular matrix, which is an important component during biofilm maturation. Also DNA release from cells is critical for biofilm attachment during the initial stages of development in *S. aureus* (Mann *et al.*, 2009). Regarding biofilm treatment with phage, it is not clear how eDNA interacts with virions and facilitates infection by *Staphylococcus* phage AICAT. The anionic charge of eDNA would repel phage particles favouring diffusion. On the contrary, polysaccharide intercellular adhesin PIA, which has a net positive charge, may promote phage interactions by binding to the negatively charged virions hindering infection. A previous study described that biofilm matrix composition affects the sensitivity of staphylococci to disinfectants (Fagerlund *et al.*, 2016).

The efficacy of phages as clinical therapeutics depends on several factors, including the development of phage-resistant bacteria, pharmacokinetic complexity and any potential human immune response. Most times, the treatment of patients with phages requires the combination of phage therapy and standard-of-care antibiotic treatment. This combination has several advantages such as avoiding the development of phage resistance (Oechslin, 2018). Taha et al (2023) demonstrated that combining phage Remus and vancomycin led to synergistic interaction against MRSA biofilm-like aggregates *in vitro* and *in vivo* (Taha *et al.*, 2023).

To date, there are no studies reporting total biofilm eradication using only phages; in fact, most studies explore the use of phages combined with other antimicrobials as antibiofilm strategy. The combination of phages with antibiotics has been assessed as a strategy to re-sensitize *S. aureus* antibiotic-resistant strains. Indeed, the treatment of *S. aureus* strains with phage SA11 and subinhibitory concentrations of antibiotics was found to be synergistic in inhibiting bacterial growth (Jo *et al.*, 2016). The use of phages and vancomycin to remove biofilms has also been tested in *S. aureus*. 48-h old biofilms were treated for 72-h with phage K (10^9 PFU); vancomycin (42 μg/mL) and a combination of both showing a synergistic activity (Joo *et al.*, 2023). Taking this into account, we decided to combine phage AICAT with vancomycin, an antibiotic commonly used to treat infections by methicillin-resistant staphylococcal strains. However, we did not observe a synergistic interaction between the phage and the antibiotic in any of the conditions tested. In contrast, we did observe synergy when using a combination of AICAT with a phage-derived lytic protein. This is in good agreement with our previous results using phage *Kayvirus rodi* and the chimeric protein CHAPSH3b for *S. aureus* biofilm elimination (Duarte *et al.*, 2021). The potential of endolysins as adjuvants against biofilms is still poorly explored, although recent studies showed that the application of endolysins and phage exopolysaccharide depolymerase could increase antibiotic susceptibility and decrease cross-resistance to antibiotics (Kim *et al.*, 2023). Also, the combination of endolysins and antimicrobial peptides may be a potential antimicrobial strategy for combating *Enterococcus faecalis* biofilms (Zhang *et al.*, 2023).

The data obtained in this study support the potential of the virulent phage AICAT to be used in phage therapy, having a wide host range against *S. epidermidis* strains. It demonstrates good biofilm removal properties against *S. epidermidis* clinical strains when combined with other antimicrobials, especially with the lytic protein CHAPSH3b . The present results highlight that more studies are still needed to understand the infection dynamics of phage AICAT in biofilms in order to maximize its potential.

REFERENCES

Akturk, E., Oliveira, H., Santos, S.B., Costa, S., Kuyumcu, S., Melo, L.D.R., and Azeredo, J. (2019) Synergistic action of phage and antibiotics: Parameters to enhance the killing efficacy against mono and dual-species biofilms. *Antibiotics* **8**: 1–19.

Aswani, V.H., Tremblay, D.M., Moineau, S., and Shukla, S.K. (2014) Complete genome sequence of a *Staphylococcus epidermidis* bacteriophage isolated from the anterior nares of humans. *Genome Announc* **2**: e00549-14.

Cau, L., Williams, M.R., Butcher, A.M., Nakatsuji, T., Kavanaugh, J.S., Cheng, J.Y., et al. (2021) *Staphylococcus epidermidis* protease EcpA can be a deleterious component of the skin microbiome in atopic dermatitis. *J Allergy Clin Immunol* **147**: 955-966.

Chaudhry, W.N., Concepcion-Acevedo, J., Park, T., Andleeb, S., Bull, J.J., Levin, B.R., et al. (2017) Synergy and order effects of antibiotics and phages in killing *Pseudomonas aeruginosa* biofilms. *PLoS One* **12**: e0168615.

Chhibber, S., Shukla, A., and Kaur, S. (2017) Transfersomal Phage Cocktail Is an Effective Treatment against Methicillin- Resistant *Staphylococcus aureus*- Mediated Skin and Soft Tissue Infections. *Am Soc Microbiol* **61**: 1–9.

Cucarella, C., Solano, C., Valle, J., Amorena, B., Lasa, Í., and Penadés, J.R. (2001) Bap, a *Staphylococcus aureus* surface protein involved in biofilm formation. *J Bacteriol* **183**: 2888–2896.

Daniel, A., Bonnen, P.E., and Fischetti, V.A. (2007) First complete genome sequence of two *Staphylococcus epidermidis* bacteriophages. *J Bacteriol* **189**: 2086–2100.

Delgado, S., Arroyo, R., Jiménez, E., Marín, M.L., Del Campo, R., Fernández, L., and Rodríguez, J.M. (2009) *Staphylococcus epidermidis* strains isolated from breast milk of women suffering infectious mastitis: Potential virulence traits and resistance to antibiotics. *BMC Microbiol* **9**: 82.

Duarte, A.C., Fernández, L., De Maesschalck, V., Gutiérrez, D., Campelo, A.B., Briers, Y., et al. (2021) Synergistic action of phage phiIPLA-RODI and lytic protein CHAPSH3b: a combination strategy to target *Staphylococcus aureus* biofilms. *npj*

Biofilms Microbiomes **7**: 39.

Edgell, D.R., Gibb, E.A., and Belfort, M. (2010) Mobile DNA elements in T4 and related phages. *Virol J* **7**: 1–15.

Fagerlund, A., Langsrud, S., Heir, E., Mikkelsen, M.I., and Møretrø, T. (2016) Biofilm matrix composition affects the susceptibility of food associated Staphylococci to cleaning and disinfection agents. *Front Microbiol* **7**: 1–15.

Fedorov, E., Samokhin, A., Kozlova, Y., Kretien, S., Sheraliev, T., Morozova, V., et al. (2023) Short-Term Outcomes of Phage-Antibiotic Combination Treatment in Adult Patients with Periprosthetic Hip Joint Infection. *Viruses* **15**: 499.

Fernández, L., Duarte, A.C., Martínez, B., Rodríguez, A., and García, P. (2021) Draft Genome Sequences of the Bap-Producing Strain *Staphylococcus aureus* V329 and Its Derived Phage-Resistant Mutant BIM-1. *Am Soc Microbiol* **10**: 20–22.

Fernández, L., González, S., Campelo, A.B., Martínez, B., Rodríguez, A., and García, P. (2017) Downregulation of Autolysin-Encoding Genes by Phage-Derived Lytic Proteins Inhibits Biofilm Formation in *Staphylococcus aureus*. *Antimicrob Agents Chemother* **61**: e02724-16.

Freeman, M.E., Kenny, S.E., Lanier, A., Cater, K., Wilhite, M.C., Gamble, P., et al. (2019) Complete Genome Sequences of *Staphylococcus epidermidis* Myophages Quidividi, Terranova, and Twillingate. *Microbiol Resour Announc* **8**: e00598-19.

García, P., Madera, C., Martínez, B., and Rodríguez, A. (2007) Biocontrol of *Staphylococcus aureus* in curd manufacturing processes using bacteriophages. *Int Dairy J* **17**: 1232–1239.

García, P., Martínez, B., Rodríguez, L., and Rodríguez, A. (2010) Synergy between the phage endolysin LysH5 and nisin to kill *Staphylococcus aureus* in pasteurized milk. *Int J Food Microbiol* **141**: 151–155.

Global AMR R&D Hub and WHO (2023) Incentivising the development of new antibacterial treatments 2023: Progress report by the Global AMR R&D Hub and WHO 1-16.

Gutiérrez, D., Delgado, S., Vázquez-Sánchez, D., Martínez, B., Cabo, M.L., Rodríguez, A., et al. (2012) Incidence of *Staphylococcus aureus* and Analysis of Associated

Bacterial Communities on Food Industry Surfaces. *Appl Environ Microbiol* **78**: 8547–8554.

Gutiérrez, D., Martínez, B., Rodríguez, A., and García, P. (2012) Genomic characterization of two *Staphylococcus epidermidis* bacteriophages with anti-biofilm potential. *BMC Genomics* **13**: 228.

Gutiérrez, D., Martínez, B., Rodríguez, A., and García, P. (2010) Isolation and characterization of bacteriophages infecting *Staphylococcus epidermidis*. *Curr Microbiol* **61**: 601–608.

Gutiérrez, D., Ruas-Madiedo, P., Martínez, B., Rodríguez, A., and García, P. (2014) Effective Removal of Staphylococcal Biofilms by the Endolysin LysH5. *PLoS One* **9**: e107307.

Gutiérrez, D., Vandenheuvel, D., Martínez, B., Rodríguez, A., Lavigne, R., and García, P. (2015) Two phages, phiIPLA-RODI and phiIPLA-C1C, lyse mono-and dual-species Staphylococcal biofilms. *Appl Environ Microbiol* **81**: 3336–3348.

Jo, A., Kim, J., Ding, T., and Ahn, J. (2016) Role of phage-antibiotic combination in reducing antibiotic resistance in *Staphylococcus aureus*. *Food Sci Biotechnol* **25**: 1211–1215.

Joo, H., Wu, S.M., Soni, I., Wang-Crocker, C., Matern, T., Beck, J.P., and Loc-Carrillo, C. (2023) Phage and Antibiotic Combinations Reduce *Staphylococcus aureus* in Static and Dynamic Biofilms Grown on an Implant Material. *Viruses* **15**: 1–14.

Karygianni, L., Ren, Z., Koo, H., and Thurnheer, T. (2020) Biofilm Matrixome: Extracellular Components in Structured Microbial Communities. *Trends Microbiol* **28**: 668–681.

Keinhörster, D., Salzer, A., Duque-Jaramillo, A., George, S.E., Marincola, G., Lee, J.C., et al. (2019) Revisiting the regulation of the capsular polysaccharide biosynthesis gene cluster in *Staphylococcus aureus*. *Mol Microbiol* **112**: 1083–1099.

Kim, J., Wang, J., and Ahn, J. (2023) Combined antimicrobial effect of phage-derived endolysin and depolymerase against biofilm-forming *Salmonella Typhimurium*. *Biofouling* **39**: 763–774.

Loc-Carrillo, C. and Abedon, S.T. (2011) Pros and cons of phage therapy. *Bacteriophage*

1: 111–114.

Mann, E.E., Rice, K.C., Boles, B.R., Endres, J.L., Ranjit, D., Chandramohan, L., et al. (2009) Modulation of eDNA release and degradation affects *Staphylococcus aureus* biofilm maturation. *PLoS One* **4**: e5822.

Melo, L.D.R., Pinto, G., Oliveira, F., Vilas-Boas, D., Almeida, C., Sillankorva, S., et al. (2020) The protective effect of *Staphylococcus epidermidis* biofilm matrix against phage predation. *Viruses* **12**: 1076.

Melo, L.D.R., Sillankorva, S., Ackermann, H.W., Kropinski, A.M., Azeredo, J., and Cerca, N. (2014) Characterization of *Staphylococcus epidermidis* phage vB_SepS_SEP9 - a unique member of the siphoviridae family. *Res Microbiol* **165**: 679–685.

Meskin, I. (1998) *Staphylococcus epidermidis*. *Pediatrics in review / American Academy of Pediatrics, methods and protocols.***19**:105-106.

Oechslin, F. (2018) Resistance development to bacteriophages occurring during bacteriophage therapy. *Viruses* **10**: 1–23.

Otto, M. (2009) *Staphylococcus epidermidis* – the "accidental" pathogen. *Nat Rev Microbiol* **7**: 555–567.

Pires, D.P., Meneses, L., Brandão, A.C., and Azeredo, J. (2022) An overview of the current state of phage therapy for the treatment of biofilm-related infections. *Curr Opin Virol* **53**: 1–7.

Pirnay, J.P., Blasdel, B.G., Bretaudeau, L., Buckling, A., Chanishvili, N., Clark, J.R., et al. (2015) Quality and safety requirements for sustainable phage therapy products. *Pharm Res* **32**: 2173–2179.

Riool, M., De Boer, L., Jaspers, V., Van Der Loos, C.M., Van Wamel, W.J.B., Wu, G., et al. (2014) *Staphylococcus epidermidis* originating from titanium implants infects surrounding tissue and immune cells. *Acta Biomater* **10**: 5202–5212.

Rodríguez-Rubio, L., Martínez, B., Rodríguez, A., Donovan, D.M., and García, P. (2012) Enhanced Staphylolytic Activity of the *Staphylococcus aureus* Bacteriophage vB_SauS-phiIPLA88 HydH5 Virion-Associated Peptidoglycan Hydrolase: Fusions, Deletions, and Synergy with LysH5. *Appl Environ Microbiol* **78**: 2241–2248.

Severn, M.M. and Horswill, A.R. (2023) *Staphylococcus epidermidis* and its dual lifestyle in skin health and infection. *Nat Rev Microbiol* **21**: 97–111.

Sun, W., Xu, J., Liu, B., Zhao, Y. Di, Yu, L., and Chen, W. (2022) Controlled release of metal phenolic network protected phage for treating bacterial infection. *Nanotechnology* **33**: 165102.

Taha, M., Arnaud, T., Lightly, T.J., Peters, D., Wang, L., Chen, W., et al. (2023) Combining bacteriophage and vancomycin is efficacious against MRSA biofilm-like aggregates formed in synovial fluid. *Front Med* **10**: 1134912.

Uyttebroek, S., Chen, B., Onsea, J., Ruythooren, F., Debaveye, Y., Devolder, D., et al. (2022) Safety and efficacy of phage therapy in difficult-to-treat infections: a systematic review. *Lancet Infect Dis* **22**: 208–220.

Valle, J., Toledo-Arana, A., Berasain, C., Ghigo, J.-M.M., Amorena, B., Penadés, J.R., and Lasa, I. (2003) SarA and not σB is essential for biofilm development by *Staphylococcus aureus*. *Mol Microbiol* **48**: 1075–1087.

Vincent, J.L. (2003) Nosocomial infections in adult intensive-care units. *Lancet* **361**: 2068–2077.

Yan, J. and Bassler, B.L. (2019) Surviving as a Community: Antibiotic Tolerance and Persistence in Bacterial Biofilms. *Cell Host Microbe* **26**: 15–21.

Zhang, H., Zhang, X., Liang, S., Wang, J., Zhu, Y., Zhang, W., et al. (2023) Bactericidal synergism between phage endolysin Ply2660 and cathelicidin LL-37 against vancomycin-resistant *Enterococcus faecalis* biofilms. *npj Biofilms Microbiomes* **9**: 16.

Zhou, W., Spoto, M., Hardy, R., Guan, C., Fleming, E., Larson, P.J., et al. (2020) Host-Specific Evolutionary and Transmission Dynamics Shape the Functional Diversification of *Staphylococcus epidermidis* in Human Skin. *Cell* **180**: 454-470.e18.

DISCUSSION

4. DISCUSSION

Maximizing the efficacy of bacteriophages for biofilm eradication

Biofilms formed by multidrug resistant bacteria have become a major problem in the clinic, veterinary medicine, agriculture and different industrial sectors, with an estimated global cost of over 5,000 billion USD (Cámara *et al.*, 2022). In this scenario, bacteriophages have been reconsidered as an alternative for surface decontamination and treatment of biofilm-associated diseases caused by tenacious pathogens. Besides the general advantages of phages compared to antibiotics and general-purpose disinfectants, such as their specificity and ability to kill antibiotic-resistant cells, these viruses offer traits that are particularly valuable in the context of biofilm elimination. For instance, phage particles have been shown to penetrate the complex structure of sessile communities either passively through water channels and/or cell-to-cell propagation (Briandet *et al.*, 2008; Vilas Boas *et al.*, 2016; González *et al.*, 2018). This capability is sometimes enhanced by the production of matrix-degrading enzymes, such as virion-associated polysaccharide depolymerases (Latka *et al.*, 2017). Furthermore, some phages can kill dormant persister cells, which are more common in biofilms than in planktonic cultures (Maffei *et al.*, 2024).

The efficacy of phages in biofilm removal has been established in diverse settings with effective elimination of many bacterial pathogens, including *Streptococcus* sp., *E. coli*, *P. aeruginosa*, *S. aureus*, *K. pneumoniae* and *E. faecalis*. Indeed, phage EFDG1 effectively eradicated two-week-old biofilms of *E. faecalis* V583 (Bolocan *et al.*, 2019). Also, a phage cocktail showed significant *in vitro* anti-biofilm activity against *P. aeruginosa* chronic rhinosinusitis isolates after 48 h of treatment (Fong *et al.*, 2017). *In vivo* experiments have given similar results. A clear example is the successful use of phage therapy in combination with surgical debridement against *S. aureus* biofilm-infected wounds in a rabbit ear model, which decreased the number of viable bacteria by approximately 99% (Seth *et al.*, 2013). The food industry is another potential field of application of phages for biofilm control. Sadekuzzaman *et al.* (2017) investigated the potency of two phages against *Salmonella* spp. in biofilms grown on food (lettuce) and food contact surfaces (stainless steel and rubber). Overall, the treatment was effective for biofilm reduction in all the surfaces tested. *L. monocytogenes* biofilms formed on stainless

steel surfaces and dry-cured ham also appear sensitive to biocontrol with the phage P100-based product PhageGuard Listex (Iacumin *et al.*, 2016).

Despite the abundant evidence of phages as successful antibiofilm agents, complete eradication of attached bacterial communities remains very challenging, especially when using an approach exclusively based on these viral predators. Unlike chemical antimicrobials, bacteriophages establish complex interactions with their target microorganisms that are further modulated by the surrounding environment. For this reason, it is essential to understand the impact of different environmental factors, like temperature, pH, oxygen concentration or nutrient availability, on phage infection dynamics in order to optimize biofilm elimination protocols. For instance, the host metabolic state, which is to a large extent dependent on access to nutrients, is known to affect phage propagation rates (Hadas *et al.*, 1994; Abedon *et al.*, 2001). Additionally, recent studies from our group demonstrated that the environmental pH is a decisive factor controlling the outcome of *S. aureus* biofilm infection by the virulent phage *Kayvirus rodi* (Fernández *et al.*, 2021). Indeed, a mildly acidic environment favoured phage–host coexistence through partial inactivation of the phage population and enhanced biofilm formation.

Another strategy to improve the lytic action of bacteriophages against biofilms involves their combination with other antimicrobials or matrix-removing compounds. Exploring the first alternative, phages have been combined with antibiotics and/or antiseptics, often resulting in a synergistic effect. Indeed, several studies suggest that sublethal concentrations of antibiotics can increase the production and activity of virulent phages. Thus, a combined treatment of phage T4 and cefotaxime significantly enhanced the eradication of *E. coli* ATCC 11303 biofilms compared with antibiotic or phage alone (Ryan *et al.*, 2012). Phage antibiotic synergy was also observed by Akturk *et al.* (2019) against mono and dual-species *S. aureus* and *P. aeruginosa* biofilms. Yet, some results indicate that antagonistic interactions between phages and antibiotics are also possible. This phenomenon is more common when using antimicrobial agents at concentrations above the minimum inhibitory concentration (Abedon ST, 2019). For instance, Chaudhry *et al.*, (2017) reported antagonism between phages and high levels of the aminoglycoside tobramycin when treating *P. aeruginosa* biofilms. More recently, a study found antagonism between the polyvalent phage SaP7, infecting *Salmonella* and *E. coli* strains, and several β-lactam antibiotics in piglet and mouse models (Ma *et al.*, 2022).

This Thesis provides new data concerning the optimization of phage-based strategies to remove staphylococcal biofilms by assessing the impact of temperature on phage infection outcome, and exploiting the synergy between phages infecting *S. aureus* and *S. epidermidis* and phage-derived proteins.

Infection of *S. aureus* biofilms by phage *Kayvirus rodi* is modulated by environmental temperature

As discussed above, the stability of phage *K. rodi* at different pH values has a dramatic impact on its ability to eliminate staphylococcal biofilms. This result prompted us to examine if ambient temperature is also a crucial factor in the utilization of this phage as an antibiofilm agent. More specifically, our primary objective was to contrast phage infectivity at physiological body temperature, reflecting patient treatment conditions, with predation efficacy at room temperature, which would be relevant for surface disinfection in hospitals or the food industry. The results show that this phage has better chances of eliminating contamination with *S. aureus* planktonic or biofilm cells at 25 ºC than at 37 ºC. This effect was more evident in strains that exhibited reduced phage susceptibility at body temperature.

Temperature had already been found to affect infection by another staphylophage, phage K, of strains belonging to the US300 lineage (Lehman *et al.*, 2023). However, in the case of *K. rodi*, this phenomenon was observed in multiple strains isolated from different sources, thus having a wider impact in terms of antibiofilm applications. Another interesting aspect is the fact that, unlike other phages, *K. rodi* is less effective at the optimum growth temperature of its host (37 ºC). At first glance, this seems somewhat surprising given that phages are obligatory parasites that hijack the bacterial replication machinery. Indeed, the viral replication process was slower at room temperature, in agreement with observations made in other phage-host systems (Middelboe, 2000; Zaburlin *et al.*, 2017). However, burst size was comparable or even higher at 25 ºC depending on the specific isolate. This might contribute to the success of phage infection in the context of a slow-growing bacterial population at suboptimal temperatures. Additionally, pH during growth at 25 ºC never reached the phage inactivation threshold, which may also contribute to virion stability throughout incubation at this temperature compared to 37 ºC.

Differential expression of genes involved in synthesis and modification of the phage receptor, in this case WTA, would be expected to modulate adsorption and, as a result, phage multiplication within the bacterial population. A clear link between these parameters could only be demonstrated for strain *S. aureus* IPLA15, in which higher expression of *tarM* might explain the limited adsorption of *K. rodi* at 37 ºC. Glycosylation of WTA by TarM has been recently reported to curtail infection by other *S. aureus* phages in an *agr*-dependent manner (Yang *et al.*, 2023). Susceptibility of *Yersinia enterocolitica* to phage ϕR1-RT at different temperatures is also modulated via transcriptional regulation of *ompF*, which encodes the phage receptor (Leon-Velarde *et al.*, 2016). This pattern was not observed in strain *S. aureus* IPLA16, which did not display differences in adsorption rate between the two temperatures despite exhibiting increased expression of WTA biosynthesis genes at 25 ºC. Based on this result, it appears that the levels of this polymer on the bacterial surface at 37 ºC are sufficient to allow maximum adsorption of the phage particles. Interestingly, strain IPLA16 displays higher transcription of phage defence mechanisms at room temperature, but this does not seem to limit the ability of *K. rodi* under these conditions. By contrast, differences in the transcriptional levels of a restriction-modification system explained changes in the resistance/susceptibility phenotype of *Listeria* at different temperatures (Kim *et al.*, 2012).

Last but not least, our results show that the selection of phage resistant mutants is noticeably higher at 37 ºC and seems to be, to some extent, involved in the reduced susceptibility of some staphylococcal strains to phage infection at this temperature. Differences in the spontaneous mutation rate at different temperatures have been previously reported in preceding studies. For instance, according to Chu *et al.* (2018), *E. coli* exhibits a higher mutation rate at 37 ºC than at temperatures between 25 and 28 ºC, which the authors correlated with the metabolic rate. Interestingly, not all the mutants selected in strain IPLA15 were fully insensitive to phage infection. In fact, a high proportion of the resistant population displays an intermediate phenotype that allows their survival at medium to high phage starting concentrations. In the near future, we intend to better characterize this population to determine the specific mutations behind this phenomenon and their impact on growth, virulence and resistance to other antimicrobials. These results are very promising with regards to the use of this phage for surface decontamination at room temperature but highlight its limitations against some strains in the context of phage therapy. This made it necessary to explore strategies that allow more

efficacious elimination of *S. aureus* biofilms by *K. rodi* at human body temperature. Here, we explored the combination of phages with their derived proteins (lysins and polysaccharide depolymerases).

Combination of phage *Kayvirus rodi* with phage-derived proteins facilitates the elimination of *S. aureus* biofilms

Phage enzymes have emerged as a promising alternative to traditional antibiotics for combating bacterial infections. These enzymes have shown efficacy in targeting and eradicating biofilms by directly killing bacterial cells (lytic proteins) or degrading the biofilm matrix (polysaccharide depolymerases). In this context, treatment of these structures with a mixture of bacteriophages and their derived proteins may be a strategy that remained largely unexplored until this thesis. Indeed, prior to this work there were, to the best of our knowledge, only one example exploring a phage-lysin combination against *Acinetobacter baumannii* and a few articles assessing the interactions between phages (Wu *et al.*, 2018) and polysaccharide depolymerases to treat *Klebsiella pneumoniae* (Latka and Drulis-Kawa, 2020; Volozhantsev *et al.*, 2022) or *A. baumannii* (Abdelkader *et al.*, 2022) (Domingues *et al.*, 2021). In general, these studies did not report very promising results. Nevertheless, we considered that such combinations probably deserved to be examined on a case-by-case basis and assessed their efficacy against *S. aureus* biofilms.

Lytic proteins are safe and fairly specific antimicrobials, with proven antibiofilm potential. However, unlike phages, lysins cannot self-replicate and their concentration dwindles following their application. In this work, we demonstrate that this limitation might be at least partly overcome by combining them with bacteriophages. Indeed, treatment of *S. aureus* biofilms with the virulent phage *K. rodi* and the chimeric lytic protein CHAPSH3b combined was significantly more effective than either individual antimicrobial. This synergistic action occurred independently of the biofilm matrix composition, being observed for strains forming polysaccharide-rich (*S. aureus* 15981 and *S. aureus* IPLA1) and protein-rich (*S. aureus* V329) biofilms alike.

The mechanistic basis for this synergy was complex and involved several factors. On the one hand, CHAPSH3b limits biomass accumulation due to its inherent ability to repress the expression of autolysin-encoding genes (Fernández *et al.*, 2017a). Autolytic activity

is necessary for accumulation of eDNA in the biofilm matrix by partial lysis of the bacterial population. In the presence of phage pressure, a less dense matrix would facilitate viral penetration and infection of susceptible cells. The enzyme would also contribute to phage predation by rapidly depleting the starting bacterial population, thus increasing the MOI, and killing most of the phage-resistant mutants. In this context, it is worth noting that we selected one bacteriophage insensitive strain displaying decreased lysin susceptibility. The mutation conferring resistance to both *K. rodi* and CHAPSH3b was located in gene *tagO*, encoding the first enzyme in the WTA biosynthesis pathway (Soldo *et al.*, 2002). The impact of this mutation on phage resistance had already been established, with WTA being the main receptor of staphylococcal phages (Azam *et al.*, 2018). However, its effect on susceptibility to lytic proteins is more surprising. These proteins are especially known for their low probability of resistance development. Perhaps, this phenomenon is due to the fact that the CBD in CHAPSH3b comes from lysostaphin and not a phage lytic protein (Rodríguez-Rubio *et al.*, 2012). Previous data had shown that resistance selection was more likely when using this staphylococcal bacteriocin compared to the application of phage-derived proteins (Rodríguez-Rubio *et al.*, 2013). The authors showed that chimeric proteins containing the lysostaphin CBD fused to phage-derived lytic domains were also less prone to resistance development than lysostaphin, but the possibility remains that the rate is slightly higher than that of phage endolysins or virion-associated peptidoglycan hydrolases. Nonetheless, this hypothesis would require further experiments to examine whether the *tagO* mutation results in lysostaphin resistance.

The reciprocal nature of this synergistic interaction between phage and lytic protein was demonstrated by the capacity of the phage to keep the bacterial population under control once the lytic protein ceases to be active. This effect would allow delaying the administration of a second round of treatment, thereby reducing the total amount of enzybiotic necessary to eradicate the biofilm. In the context of a biofilm-related infection, this would also make it easier on patients that would not require so many doses of treatment. Moreover, *ex vivo* biofilm models performed on porcine skin show a higher efficacy of the phage, even by itself, compared to the results derived from biofilms formed in culture media. This suggests that perhaps this combination will be even more effective *in vivo* than would be expected from *in vitro* data, a promising prospect for the treatment of staphylococcal infections and/or nasal decontamination in healthy carriers.

A different approach for the improvement of phage-based antibiofilm strategies involves targeting the extracellular matrix with the use of degrading activities that facilitate the access of bacteriophages to biofilm-embedded host cells. Several phage polysaccharide depolymerases had previous displayed matrix-removing properties, including Dpo7, an enzyme encoded by the *S. epidermidis* phage *Rockefellervirus* IPLA7 (Gutiérrez, Briers, *et al.*, 2015), as well as those produced by several phages infecting *Proteus mirabilis*, *K. pneumoniae* and *Pseudomonas aeruginosa* (Mi *et al.*, 2019; Rice *et al.*, 2021; Li *et al.*, 2022). Dpo7 is known to display antibiofilm activity against *S. epidermidis* and *S. aureus* strains, whose matrix consists principally of PNAG/PIA, which would represent the majority of isolates from these two species. Therefore, assessment of the Dpo7 potential to boost phage *K. rodi* antibiofilm activity seemed like a promising research avenue.

This phage-enzyme mixture does exhibit a synergistic activity against *S. aureus* biofilms that, surprisingly, is not limited to isolates with a mainly polysaccharidic matrix. In fact, removal of *S. aureus* V329 biofilms, which are mostly composed of protein and eDNA, with this combination is very effective. Also, the presence of the polysaccharide depolymerase has a high impact in strains that are poor biofilm formers and, as a result produce a low amount of polysaccharides. The phage would not be expected to encounter much difficulty in penetrating these structures to reach target cells. However, its ability to infect the target cells is still facilitated by the depolymerase. Therefore, we can hypothesize that this synergy might involve, not only loosening of the matrix, but also removal of polysaccharides that surround the individual cells and might hinder phage infection. Interestingly, incubation with Dpo7 does not affect phage adsorption in planktonic cells, although there might be differences when cells are within the complex biofilm structure.

Microscopy data showed that Dpo7-treated samples exhibited a lesser amount of an N-acetylglucosamine-containing polysaccharide. However, our efforts to pinpoint the specific substrate of this enzyme as WTA or PNAG/PIA were unsuccessful. Indeed, this enzymatic activity is not affected by mutations in genes required for biosynthesis of either one of these two molecules. It is also possible that Dpo7 can degrade both WTA and PNAG/PIA or that the target is another surface polysaccharide, such as the newly identified Ssc (Lei *et al.*, 2024). Further research will be necessary to fully understand the mechanism behind this synergistic interaction in terms of identifying the Dpo7 enzymatic target and its impact on phage infection.

Lytic protein CHAPSH3b also enhances the antibiofilm activity of phages infecting *S. epidermidis*

The ability of *S. epidermidis* to cause device-associated infections is mainly due to its ability to form stable biofilms attached to human tissues. Besides the inherent antimicrobial tolerance of biofilms, this microorganism is also increasingly becoming resistant to standard-of-care antibiotics. In this scenario, phage therapy is a viable option to complement the available antibiotics in the treatment of recalcitrant infections. However, the number of identified virulent phages infecting this species is relatively small compared to those against *S. aureus*, and data regarding their antibiofilm efficacy remains scarce (Melo *et al.*, 2020; Fanaei Pirlar *et al.*, 2022). In this work, we isolated a novel *S. epidermidis* phages AICAT, belonging to the *Herelleviridae* family, whose members are obligatorily lytic. The phage genome confirmed that it does not carry any genes related to virulence, antibiotic resistance or lysogeny, making this phage suitable for therapeutic purposes (Pirnay *et al.*, 2015). Additionally, AICAT infected an important number of clinical isolates and exhibited good stability at different temperatures and pH values.

Despite its ability against planktonic cells, this phage failed to display promising results when confronted with 24-h-old biofilms. The impact was only slightly better when treating 5-h-old biofilms. A similar difficulty regarding the treatment of biofilm cells had been previously reported for the *S. epidermidis* phage *Sepunavirus* phiIBB-SEP1 (Melo *et al.*, 2020). The authors found that the extracellular matrix was a major hurdle to phage penetration into the biofilm structure. Interestingly, the most susceptible biofilms in our study were those with a high eDNA content in the extracellular matrix. Subsequent work should determine if there is an actual correlation between matrix composition and phage susceptibility in *S. epidermidis*, and study the interactions between biofilm polymers and free viral particles. Differences in matrix composition are known to have an influence on the activity of disinfectants against staphylococcal biofilms (Fagerlund *et al.*, 2016).

As previously observed for *K. rodi*, it was very clear that phage AICAT would require combination with another antimicrobial to achieve better results against sessile cells. On the one hand, we tested vancomycin, a glycopeptide that had synergistic activity with phage Remus for the elimination of MRSA biofilms (Taha *et al.*, 2023). In our case, this antibiotic did not significantly enhance phage predation of *S. epidermidis* biofilms. In

contrast, the chimeric protein CHAPSH3b, which had already proven successful in a combination with *K. rodi*, did exhibit synergistic interactions with phage AICAT. Rodríguez-Rubio *et al.* (2012) had previously demonstrated that CHAPSH3b was not only active against *S. aureus* strains from different origins, but also several *S. epidermidis* isolates. This highlights the versatility of this protein against staphylococci and confirms the potential of treatment strategies involving the combination of phages and phage-derived lysins. Future studies should examine if this approach also works in other types of bacteria, even Gram-negative pathogens, in which lysis-from-without is more challenging due to the presence of an outer membrane.

Final considerations

The development of new methods to combat bacterial biofilms in different environments is currently one of the most significant challenges in the field of clinical microbiology. Nevertheless, the specificity, safety and efficacy of phages and phage-derived proteins are putting them in the spotlight of the biofilm research community as promising antibiofilm agents. As all antimicrobials, they do, however, have some shortcomings that need to be tackled with in order to turn their great potential into resounding success. Even though there is still a long way to go in the field of phage therapy, this thesis aims to contribute to make highly effective phage-based antibiofilm products a reality in the not-so-distant future. Together with the significant progress achieved in the development of diagnostic tools, phages and their derived proteins will bring us much closer to a therapeutic landscape in which we are not so heavily reliant on antibiotics to combat bacterial pathogens.

The first part of this this work builds upon data obtained for other phage-host pairs demonstrating the importance of understanding how phage modulation of bacterial communities is highly dependent on the specific niche conditions. This knowledge will allow optimization of phage-based products and application regimes depending on the specific use. The second part of this work underscores the potential of taking advantage of the synergistic interaction between phages and their derived proteins, both lytic proteins and polysaccharide depolymerases, to develop improved antibiotic- and disinfectant-free antibiofilm cocktails.

Of course, more studies will be required to fully demonstrate the efficacy of these strategies using *in vivo* models and biofilms developed on other inert materials. Moreover, new mixtures should address the elimination of mixed biofilms, which are the most common in real life scenarios. Nonetheless, although more research needs to be conducted, this study paints a promising future regarding the use of phage-related products against biofilm infections and surface contamination.

CONCLUSIONS
CONCLUSIONES

5. CONCLUSIONS

1. *Kayvirus rodi* (phiIPLA-RODI) is a more effective predator at room temperature (25 ºC) compared to body temperature (37 ºC) in both planktonic and sessile bacterial cultures of several *Staphylococcus aureus* strains from different origins and degrees of phage susceptibility. The mechanisms behind this phenomenon vary in a strain-dependent manner and include differences in phage resistance development, phage adsorption, infection parameters, prolonged phage action and metabolic changes leading to a lesser acidification of the surrounding environment.
2. There is a synergistic interaction between phage *Kayvirus rodi* (phiIPLA-RODI) and the lytic protein CHAPSH3b against *S. aureus* biofilms. The fast antibacterial action of the lytic protein is subsequently followed by phage predation, limiting regrowth of the bacterial population. Also, CHAPSH3b helps to curtail the development of phage resistance during treatment. However, mutant BIM-1, derived from *S. aureus* V329 strain, exhibited resistance to both the phage and CHAPSH3b. This strain had a point mutation in gene *tagO* (G210E), involved in the biosynthesis of teichoic acids.
3. The exopolysaccharide depolymerase Dpo7 also exhibits synergy with phage *Kayvirus rodi* (phiIPLA-RODI) against biofilms formed by different *S. aureus* strains, regardless of their biofilm-forming ability and matrix composition. Phage adsorption was not significantly altered by incubation with Dpo7, indicating that the mechanism of the observed synergistic interaction might be through loosening of the biofilm structure. Activity assays on mutant strains did not identify teichoic acids or PNAG/PIA as the exclusive target of Dpo7, suggesting that may be both degraded by this enzyme or that the target is another, yet uncharacterized surface polysaccharide.
4. The bacteriophage IPLA-AICAT (AICAT), belonging to the *Herelleviridae* family and genus *Sepunavirus*, infects a high proportion of clinically-relevant *S. epidermidis* strains and exhibits antibiofilm activity, especially against early-stage (5-h) biofilms. The combination of AICAT with the lytic protein CHAPSH3b further improved its ability to eliminate 24-h biofilms, exhibiting a synergistic interaction.

CONCLUSIONES

1. *Kayvirus rodi* (phiIPLA-RODI) es un predador más eficaz a temperatura ambiente (25 ºC) que a temperatura corporal (37 ºC) frente a cultivos bacterianos tanto planctónicos como sésiles, de varias cepas de *Staphylococcus aureus* con diferentes orígenes y grados de susceptibilidad a fagos. Los mecanismos que explican este fenómeno varían dependiendo de la cepa, e incluyen diferencias en el desarrollo de resistencia al fago, adsorción del fago, parámetros de infección, acción prolongada del fago y cambios metabólicos que conducen a una menor acidificación del entorno circundante.

2. Existe una interacción sinérgica entre el fago *Kayvirus rodi* (phiIPLA-RODI) y la proteína lítica CHAPSH3b frente a biofilms de *S. aureus*. La rápida acción antibacteriana de la proteína lítica es seguida por la acción del fago, lo que limita el recrecimiento de la población de bacterias. Además, CHAPSH3b ayuda a restringir el desarrollo de resistencia al fago durante el tratamiento. Sin embargo, el mutante BIM-1, derivado de la cepa *S. aureus* V329, mostró resistencia tanto al fago como a CHAPSH3b. Esta cepa tiene una mutación puntual en el gen *tagO* (G210E), implicado en la biosíntesis de ácidos teicoicos.

3. La exopolisacárido despolimerasa Dpo7 también exhibe sinergia con el fago *Kayvirus rodi* (phiIPLA-RODI) frente a biofilms formados por diferentes cepas de *S. aureus*, independientemente de su capacidad de formación de biopelículas y composición de la matriz. La incubación con Dpo7 no afecta significativamente a la adsorción del fago, lo que indica que el mecanismo de la interacción sinérgica podría deberse a la pérdida de la estructura del biofilm. Los ensayos de actividad en cepas mutantes no identificaron los ácidos teicoicos o el PNAG/PIA como diana especifica de Dpo7, lo que sugiere que ambos pueden ser degradados por este enzima, o que la diana es otro polisacárido de la superficie aún por caracterizar.

4. El bacteriófago IPLA-AICAT (AICAT), perteneciente a la familia *Herelleviridae* y al género *Sepunavirus*, infecta una alta proporción de cepas de *S. epidermidis* de importancia clínica y exhibe actividad antibiofilm, especialmente frente a biopelículas en etapas tempranas de desarrollo (5 h). La combinación de AICAT con la proteína lítica CHAPSH3b mejoró aún más su capacidad para eliminar biofilms de 24 h, existiendo una interacción sinérgica entre ambos.

BIBLIOGRAPHY

6. BIBLIOGRAPHY

Abdelkader, K., Gutiérrez, D., Latka, A., Boeckaerts, D., Drulis-Kawa, Z., Criel, B., et al. (2022) The Specific Capsule Depolymerase of Phage PMK34 Sensitizes *Acinetobacter baumannii* to Serum Killing. *Antibiotics* **11**: 1–20.

Abedon, S.T. (2019) Phage-antibiotic combination treatments: Antagonistic impacts of antibiotics on the pharmacodynamics of phage therapy? *Antibiotics* **8**: 182.

Abedon, S.T., Herschler, T.D., and Stopar, D. (2001) Bacteriophage Latent-Period Evolution as a Response to Resource Availability. *Appl Environ Microbiol* **67**: 4233–4241.

Adisasmito, W.B., Almuhairi, S., Behravesh, C.B., Bilivogui, P., Bukachi, S.A., Casas, N., et al. (2022) One Health: A new definition for a sustainable and healthy future. *PLoS Pathog* **18**: e1010537.

Akhlaghi, H., Javan, A.J., and Chashmi, S.H.E. (2024) *Helicobacter pullorum* and *Helicobacter canadensis*: Etiology, pathogenicity, epidemiology, identification, and antibiotic resistance implicating food and public health. *Int J Food Microbiol* **413**: 110573.

Aksyuk, A.A. and Rossmann, M.G. (2011) Bacteriophage assembly. *Viruses* **3**: 172–203.

Akturk, E., Oliveira, H., Santos, S.B., Costa, S., Kuyumcu, S., Melo, L.D.R., and Azeredo, J. (2019) Synergistic action of phage and antibiotics: Parameters to enhance the killing efficacy against mono and dual-species biofilms. *Antibiotics* **8**: 1–19.

De Angelis, L.H., Poerio, N., Di Pilato, V., De Santis, F., Antonelli, A., Thaller, M.C., et al. (2021) Phage resistance is associated with decreased virulence in kpc-producing *Klebsiella pneumoniae* of the clonal group 258 clade II lineage. *Microorganisms* **9**:762

Anthony, D.W. and Comps, M. (2005) The Double Stranded DNA Viruses. In *Virus Taxonomy*. pp. 35–55.

Archer, G.L., Niemeyer, D.M., Thanassi, J.A., and Pucci, M.J. (1994) Dissemination among Staphylococci of DNA sequences associated with methicillin resistance. *Antimicrob Agents Chemother* **38**: 447–454.

Argudín, M.Á., Mendoza, M.C., and Rodicio, M.R. (2010) Food Poisoning and *Staphylococcus aureus* Enterotoxins. *Toxins (Basel)* **2**: 1751–1773.

Azam, A.H., Hoshiga, F., Takeuchi, I., Miyanaga, K., and Tanji, Y. (2018) Analysis of phage resistance in *Staphylococcus aureus* SA003 reveals different binding mechanisms for the closely related Twort-like phages ϕSA012 and ϕSA039. *Appl Microbiol Biotechnol* **102**: 8963–8977.

Balamurugan, P., Praveen Krishna, V., Bharath, D., Lavanya, R., Vairaprakash, P., and Adline Princy, S. (2017) *Staphylococcus aureus* quorum regulator SarA targeted compound, 2-[(Methylamino)methyl]phenol inhibits biofilm and down-regulates virulence genes. *Front Microbiol* **8**: 1–10.

Van Bambeke, F., Mingeot-Leclercq, M.P., Glupczynski, Y., and Tulkens, P.M. (2017) Mechanisms of Action. In *Infectious Diseases*. pp. 1162-1180.

Banerji, R., Karkee, A., Kanojiya, P., and Saroj, S.D. (2021) Pore-forming toxins of foodborne pathogens. *Compr Rev Food Sci Food Saf* **20**: 2265–2285.

Bellas, C.M., Schroeder, D.C., Edwards, A., Barker, G., and Anesio, A.M. (2020) Flexible genes establish widespread bacteriophage pan-genomes in cryoconite hole ecosystems. *Nat Commun* **11**: 4403.

Bengtsson-Palme, J. (2017) Antibiotic resistance in the food supply chain: where can sequencing and metagenomics aid risk assessment? *Curr Opin Food Sci* **14**: 66–71.

Benkerroum, N. (2018) Staphylococcal enterotoxins and enterotoxin-like toxins with special reference to dairy products: An overview. *Crit Rev Food Sci Nutr* **58**: 1943–1970.

Bernhardt, T.G., Roof, W.D., and Young, R. (2000) Genetic evidence that the bacteriophage φX174 lysis protein inhibits cell wall synthesis. *Proc Natl Acad Sci U S A* **97**: 4297–4302.

Binda, E., Marinelli, F., and Marcone, G.L. (2014) Old and new glycopeptide antibiotics: Action and resistance. *Antibiotics* **3**: 572–594.

Biswas, R., Voggu, L., Simon, U.K., Hentschel, P., Thumm, G., and Götz, F. (2006) Activity of the major Staphylococcal autolysin Atl. *FEMS Microbiol Lett* **259**: 260–268.

Blanco-Picazo, P., Gómez-Gómez, C., Morales-Cortes, S., Muniesa, M., and Rodríguez-Rubio, L. (2022) Antibiotic resistance in the viral fraction of dairy products and a nut-based milk. *Int J Food Microbiol* **367**: 109590.

Blanco-Picazo, P., Morales-Cortes, S., Ramos-Barbero, M.D., García-Aljaro, C., Rodríguez-Rubio, L., and Muniesa, M. (2023) Dominance of phage particles

carrying antibiotic resistance genes in the viromes of retail food sources. *ISME J* **17**: 195–203.

Bland, M.J., Ducos-Galand, M., Val, M.E., and Mazel, D. (2017) An att site-based recombination reporter system for genome engineering and synthetic DNA assembly. *BMC Biotechnol* **17**: 1–10.

Boles, B.R. and Horswill, A.R. (2008) agr-mediated dispersal of *Staphylococcus aureus* biofilms. *PLoS Pathog* **4**: e1000052.

Bolocan, A.S., Upadrasta, A., De Almeida Bettio, P.H., Clooney, A.G., Draper, L.A., Ross, R.P., and Hill, C. (2019) Evaluation of phage therapy in the context of *Enterococcus faecalis* and its associated diseases. *Viruses* **11**: 1–18.

Brescó, M.S., Harris, L.G., Thompson, K., Stanic, B., Morgenstern, M., O'Mahony, L., et al. (2017) Pathogenic mechanisms and host interactions in *Staphylococcus epidermidis* device-related infection. *Front Microbiol* **8**: 1401.

Briandet, R., Lacroix-Gueu, P., Renault, M., Lecart, S., Meylheuc, T., Bidnenko, E., et al. (2008) Fluorescence correlation spectroscopy to study diffusion and reaction of bacteriophages inside biofilms. *Appl Environ Microbiol* **74**: 2135–2143.

Briers, Y. and Lavigne, R. (2015) Breaking barriers: Expansion of the use of endolysins as novel antibacterials against Gram-negative bacteria. *Future Microbiol* **10**: 377–390.

Brown, S., Santa Maria, J.P., and Walker, S. (2013) Wall teichoic acids of gram-positive bacteria. *Annu Rev Microbiol* **67**: 313–336.

Brown, S., Xia, G., Luhachack, L.G., Campbell, J., Meredith, T.C., Chen, C., et al. (2012) Methicillin resistance in *Staphylococcus aureus* requires glycosylated wall teichoic acids. *Proc Natl Acad Sci U S A* **109**: 18909–18914.

Cámara, M., Green, W., MacPhee, C.E., Rakowska, P.D., Raval, R., Richardson, M.C., et al. (2022) Economic significance of biofilms: a multidisciplinary and cross-sectoral challenge. *npj Biofilms Microbiomes* **8**: 1–8.

Campbell, A. (2003) The future of bacteriophage biology. *Nat Rev* **4**: 471–477.

Centers for Disease Control and Prevention (2024) CDC Current outbreak List. Accessed 11/03/2024. https://www.cdc.gov/outbreaks/index.html

Chambers, H.F. (2001) The Changing Epidemiology of *Staphylococcus aureus*? *Emerg Infect Dis* **7**: 178–182.

Chan, P.F. and Foster, S.J. (1998) Role of SarA in virulence determinant production and

environmental signal transduction in *Staphylococcus aureus*. *J Bacteriol* **180**: 6232–6241.

Chaudhry, W.N., Concepcion-Acevedo, J., Park, T., Andleeb, S., Bull, J.J., Levin, B.R., et al. (2017) Synergy and order effects of antibiotics and phages in killing *Pseudomonas aeruginosa* biofilms. *PLoS One* **12**: e0168615.

Chee, M.S.J., Serrano, E., Chiang, Y.N., Harling-Lee, J., Man, R., Bacigalupe, R., et al. (2023) Dual pathogenicity island transfer by piggybacking lateral transduction. *Cell* **186**: 3414-3426.

Chen, Q., Dharmaraj, T., Cai, P.C., Burgener, E.B., Haddock, N.L., Spakowitz, A.J., and Bollyky, P.L. (2022) Bacteriophage and Bacterial Susceptibility, Resistance, and Tolerance to Antibiotics. *Pharmaceutics* **14**:1425.

Chen, X., Liu, M., Zhang, P., Xu, M., Yuan, W., Bian, L., et al. (2022) Phage-Derived Depolymerase as an Antibiotic Adjuvant Against Multidrug-Resistant *Acinetobacter baumannii* . *Front Microbiol* **13**: 845500.

Cheung, G.Y.C., Bae, J.S., and Otto, M. (2021) Pathogenicity and virulence of *Staphylococcus aureus*. *Virulence* **12**: 547–569.

Chopra, S., Harjai, K., and Chhibber, S. (2016) Potential of combination therapy of endolysin MR-10 and minocycline in treating MRSA induced systemic and localized burn wound infections in mice. *Int J Med Microbiol* **306**: 707–716.

Chu, X.L., Zhang, B.W., Zhang, Q.G., Zhu, B.R., Lin, K., and Zhang, D.Y. (2018) Temperature responses of mutation rate and mutational spectrum in an *Escherichia coli* strain and the correlation with metabolic rate. *BMC Evol Biol* **18**: 1–8.

Collignon, P.J. and McEwen, S.A. (2019) One health-its importance in helping to better control antimicrobial resistance. *Trop Med Infect Dis* **4**: 22.

Costerton, J.W., Geesey, G.G., and Cheng, K.J. (1978) How bacteria stick. *Sci Am* **238**: 86–95.

Crespo-Piazuelo, D. and Lawlor, P.G. (2021) Livestock-associated methicillin-resistant *Staphylococcus aureus* (LA-MRSA) prevalence in humans in close contact with animals and measures to reduce on-farm colonisation. *Ir Vet J* **74**: 1–12.

Cucarella, C., Solano, C., Valle, J., Amorena, B., Lasa, Í., and Penadés, J.R. (2001) Bap, a *Staphylococcus aureus* surface protein involved in biofilm formation. *J Bacteriol* **183**: 2888–2896.

Daniel, A., Euler, C., Collin, M., Chahales, P., Gorelick, K.J., and Fischetti, V.A. (2010)

Synergism between a novel chimeric lysin and oxacillin protects against infection by methicillin-resistant *Staphylococcus aureus*. *Antimicrob Agents Chemother* **54**: 1603–1612.

DeFrancesco, A.S., Masloboeva, N., Syed, A.K., DeLoughery, A., Bradshaw, N., Li, G.W., et al. (2017) Genome-wide screen for genes involved in eDNA release during biofilm formation by *Staphylococcus aureus*. *Proc Natl Acad Sci U S A* **114**: E5969–E5978.

Dengler, V., Foulston, L., DeFrancesco, A.S., and Losick, R. (2015) An electrostatic net model for the role of extracellular DNA in biofilm formation by *Staphylococcus aureus*. *J Bacteriol* **197**: 3779–3787.

Derzelle, S., Dilasser, F., Duquenne, M., and Deperrois, V. (2009) Differential temporal expression of the Staphylococcal enterotoxins genes during cell growth. *Food Microbiol* **26**: 896–904.

Domingues, R., Barbosa, A., Santos, S.B., Pires, D.P., Save, J., Resch, G., et al. (2021) Unpuzzling friunavirus-host interactions one piece at a time: Phage recognizes *Acinetobacter pittii* via a new k38 capsule depolymerase. *Antibiotics* **10**:1304.

Dowah, A.S.A. and Clokie, M.R.J. (2018) Review of the nature, diversity and structure of bacteriophage receptor binding proteins that target Gram-positive bacteria. *Biophys Rev* **10**: 535–542.

Driffield, K., Miller, K., Bostock, J.M., O'neill, A.J., and Chopra, I. (2008) Increased mutability of *Pseudomonas aeruginosa* in biofilms. *J Antimicrob Chemother* **61**: 1053–1056.

ECDC and WHO (2023) Antimicrobial resistance surveillance in Europe 2023 - 2021 data.

EFSA and ECDC (2023a) The European Union One Health 2022 Zoonoses Report. *EFSA J* **21**: e8442.

EFSA and ECDC (2023b) The European Union Summary Report on Antimicrobial Resistance in zoonotic and indicator bacteria from humans, animals and food in 2020/2021.

EMA (2020) Categorisation of antibiotics used in animals promotes responsible use to protect public and animal health.

Erez, Z., Steinberger-Levy, I., Shamir, M., Doron, S., Stokar-Avihail, A., Peleg, Y., et al. (2017) Communication between viruses guides lysis-lysogeny decisions. *Nature*

541: 488–493.

Fagerlund, A., Langsrud, S., Heir, E., Mikkelsen, M.I., and Møretrø, T. (2016) Biofilm matrix composition affects the susceptibility of food associated Staphylococci to cleaning and disinfection agents. *Front Microbiol* **7**: 1–15.

Fanaei Pirlar, R., Wagemans, J., Ponce Benavente, L., Lavigne, R., Trampuz, A., and Gonzalez Moreno, M. (2022) Novel Bacteriophage Specific against *Staphylococcus epidermidis* and with Antibiofilm Activity. *Viruses* **14**: 1–11.

Fedorov, E., Samokhin, A., Kozlova, Y., Kretien, S., Sheraliev, T., Morozova, V., et al. (2023) Short-Term Outcomes of Phage-Antibiotic Combination Treatment in Adult Patients with Periprosthetic Hip Joint Infection. *Viruses* **15**: 499.

Fernández, L., Duarte, A.C., Martínez, B., Rodríguez, A., and García, P. (2021) Draft Genome Sequences of the Bap-Producing Strain *Staphylococcus aureus* V329 and Its Derived Phage-Resistant Mutant BIM-1. *Am Soc Microbiol* **10**: 20–22.

Fernández, L., Cima-Cabal, M.D., Duarte, A.C., Rodriguez, A., García, P., and García-Suárez, M.D.M. (2020) Developing diagnostic and therapeutic approaches to bacterial infections for a new era: Implications of globalization. *Antibiotics* **9**: 1–15.

Fernández, L., González, S., Campelo, A.B., Martínez, B., Rodríguez, A., and García, P. (2017a) Downregulation of autolysin-encoding genes by phage-derived lytic proteins inhibits biofilm formation in *Staphylococcus aureus*. *Antimicrob Agents Chemother* **61**: e02724-16.

Fernández, L., González, S., Campelo, A.B., Martínez, B., Rodríguez, A., and García, P. (2017b) Low-level predation by lytic phage phiIPLA-RODI promotes biofilm formation and triggers the stringent response in *Staphylococcus aureus*. *Sci Rep* **7**: 40965.

Fernández, L., Gutiérrez, D., García, P., and Rodríguez, A. (2021) Environmental pH is a key modulator of *Staphylococcus aureus* biofilm development under predation by the virulent phage phiIPLA-RODI. *ISME J* **15**: 245–259.

Fernández, L., Gutiérrez, D., García, P., and Rodríguez, A. (2019) The Perfect Bacteriophage for Therapeutic Applications—A Quick Guide. *Antibiotics* **8**: 126.

Fernández, L., Rodríguez, A., and García, P. (2018) Phage or foe: An insight into the impact of viral predation on microbial communities. *ISME J* **12**: 1171–1179.

Fillol-Salom, A., Alsaadi, A., de Sousa, J.A.M., Zhong, L., Foster, K.R., Rocha, E.P.C., et al. (2019) Bacteriophages benefit from generalized transduction. *PLoS Pathog* **15**:

1–22.

Flemming, H.C. and Wingender, J. (2010) The biofilm matrix. *Nat Rev Microbiol* **8**: 623–633.

Flórez, A.B., Vázquez, L., Rodríguez, J., and Mayo, B. (2021) Directed recovery and molecular characterization of antibiotic resistance plasmids from cheese bacteria. *Int J Mol Sci* **22**: 7801.

Fong, S.A., Drilling, A., Morales, S., Cornet, M.E., Woodworth, B.A., Fokkens, W.J., et al. (2017) Activity of bacteriophages in removing biofilms of *Pseudomonas aeruginosa* isolates from chronic rhinosinusitis patients. *Front Cell Infect Microbiol* **7**: 418.

Foster, T.J. (2019) The MSCRAMM Family of Cell-Wall-Anchored Surface Proteins of Gram-Positive Cocci. *Trends Microbiol* **27**: 927–941.

Foster, T.J., Geoghegan, J.A., Ganesh, V.K., and Höök, M. (2014) Adhesion, invasion and evasion: The many functions of the surface proteins of *Staphylococcus aureus*. *Nat Rev Microbiol* **12**: 49–62.

Foulston, L., Elsholz, A.K.W., DeFrancesco, A.S., and Losick, R. (2014) The extracellular matrix of *Staphylococcus aureus* biofilms comprises cytoplasmic proteins that associate with the cell surface in response to decreasing pH. *MBio* **5**: e01667-14.

França, A., Gaio, V., Lopes, N., and Melo, D.R. (2021) Virulence Factors in Coagulase-Negative Staphylococci. *Pathogens* **10**: 170.

Fruciano, E. and Bourne, S. (2007) Phage as an antimicrobial agent: d'Herelle's heretical theories and their role in the decline of phage prophylaxis in the West. *Can J Infect Dis Med Microbiol* **18**: 19–26.

García, P., Martínez, B., Obeso, J.M., Lavigne, R., Lurz, R., and Rodríguez, A. (2009) Functional genomic analysis of two *Staphylococcus aureus* phages isolated from the dairy environment. *Appl Environ Microbiol* **75**: 7663–7673.

García, P., Martínez, B., Obeso, J.M., and Rodríguez, A. (2008) Bacteriophages and their application in food safety. *Lett Appl Microbiol* **47**: 479–485.

Gerstmans, H., Criel, B., and Briers, Y. (2018) Synthetic biology of modular endolysins. *Biotechnol Adv* **36**: 624–640.

Ghabbour, R., Awad, A., and Younis, G. (2022) Genetic Characterization and Antimicrobial-Resistant Profiles of *Staphylococcus aureus* isolated from different

food sources. *Biocontrol Sci* **27**: 87–97.

González, S., Fernández, L., Gutiérrez, D., Campelo, A.B., Rodríguez, A., and García, P. (2018) Analysis of Different Parameters Affecting Diffusion, Propagation and Survival of Staphylophages in Bacterial Biofilms. *Front Microbiol* **9**: 1–13.

Gummalla, V.S., Zhang, Y., Liao, Y. Te, and Wu, V.C.H. (2023) The Role of Temperate Phages in Bacterial Pathogenicity. *Microorganisms* **11**: 541.

Guo, Z., Liu, M., and Zhang, D. (2023) Potential of phage depolymerase for the treatment of bacterial biofilms. *Virulence* **14**: 1–19.

Gutiérrez, D., Briers, Y., Rodríguez-Rubio, L., Martínez, B., Rodríguez, A., Lavigne, R., and García, P. (2015) Role of the pre-neck appendage protein (Dpo7) from phage vB_SepiS-phiIPLA7 as an anti-biofilm agent in Staphylococcal species. *Front Microbiol* **6**: 1315.

Gutiérrez, D., Fernández, L., Martínez, B., Ruas-Madiedo, P., García, P., and Rodríguez, A. (2017) Real-time assessment of *Staphylococcus aureus* biofilm disruption by phage-derived proteins. *Front Microbiol* **8**: 1–10.

Gutiérrez, D., Fernández, L., Rodríguez, A., and García, P. (2018) Are phage lytic proteins the secret weapon to kill *Staphylococcus aureus*? *Am Soc Microbiol* **9**: e01923-17.

Gutiérrez, D., Fernández, L., Rodríguez, A., and García, P. (2019) Role of bacteriophages in the implementation of a sustainable dairy chain. *Front Microbiol* **10**: 12.

Gutiérrez, D., Garrido, V., Fernández, L., Portilla, S., Rodríguez, A., Grilló, M.J., and García, P. (2020) Phage Lytic Protein LysRODI Prevents Staphylococcal Mastitis in Mice. *Front Microbiol* **11**: 7.

Gutiérrez, D., Rodríguez-Rubio, L., Martínez, B., Rodríguez, A., and García, P. (2016) Bacteriophages as weapons against bacterial biofilms in the food industry. *Front Microbiol* **7**: 825.

Gutiérrez, D., Vandenheuvel, D., Martínez, B., Rodríguez, A., Lavigne, R., and García, P. (2015) Two phages, phiIPLA-RODI and phiIPLA-C1C, lyse mono-and dual-species Staphylococcal biofilms. *Appl Environ Microbiol* **81**: 3336–3348.

Hadas, H., Einav, M., and Zaritsky, A. (1994) Bacteriophage T4 Development Depends on the Physiology of its host *E. coli*. *Microbiology* **143**: 179–185.

Hanssen, A.M. and Ericson Sollid, J.U. (2006) SCCmec in Staphylococci: Genes on the move. *FEMS Immunol Med Microbiol* **46**: 8–20.

Hawkins, N.C., Kizziah, J.L., Hatoum-Aslan, A., and Dokland, T. (2022) Structure and host specificity of *Staphylococcus epidermidis* bacteriophage Andhra. *Sci Adv* **8**: eade0459.

Heselpoth, R.D., Euler, C.W., Schuch, R., and Fischetti, V.A. (2019) Lysocins: Bioengineered antimicrobials that deliver lysins across the outer membrane of Gram-negative bacteria. *Antimicrob Agents Chemother* **63**: e00342-19.

Hidalgo, G., Burns, A., Herz, E., Hay, A.G., Houston, P.L., Wiesner, U., and Lion, L.W. (2009) Functional tomographic fluorescence imaging of pH microenvironments in microbial biofilms by use of silica nanoparticle sensors. *Appl Environ Microbiol* **75**: 7426–7435.

Holland, L.M., Conlon, B., and O'Gara, J.P. (2011) Mutation of tagO reveals an essential role for wall teichoic acids in *Staphylococcus epidermidis* biofilm development. *Microbiology* **157**: 408–418.

Iacumin, L., Manzano, M., and Comi, G. (2016) Phage inactivation of *listeria monocytogenes* on san daniele dry-cured ham and elimination of biofilms from equipment and working environments. *Microorganisms* **4**: 4.

Ibáñez de Aldecoa, A.L., Zafra, O., and González-Pastor, J.E. (2017) Mechanisms and regulation of extracellular DNA release and its biological roles in microbial communities. *Front Microbiol* **8**: 1–19.

J. C. Linnes, Mikhova, K., and Bryers, J.D. (2012) Adhesion of *Staphylococcus epidermidis* to biomaterials is inhibited by fibronectin and albumin. *Soc Biomater* **100**: 1990–7.

Jamal, M., Ahmad, W., Andleeb, S., Jalil, F., Imran, M., Nawaz, M.A., et al. (2018) Bacterial biofilm and associated infections. *J Chinese Med Assoc* **81**: 7–11.

Jurado, A., Fernández, L., Rodríguez, A., and García, P. (2022) Understanding the Mechanisms That Drive Phage Resistance in Staphylococci to Prevent Phage Therapy Failure. *Viruses* **14**: 1–15.

Kadariya, J., Smith, T.C., and Thapaliya, D. (2014) *Staphylococcus aureus* and Staphylococcal Food-Borne Disease: An Ongoing Challenge in Public Health. *Biomed Res Int* **2014**: 9.

Karygianni, L., Ren, Z., Koo, H., and Thurnheer, T. (2020) Biofilm Matrixome: Extracellular Components in Structured Microbial Communities. *Trends Microbiol* **28**: 668–681.

Kaushik, V., Tiwari, M., and Tiwari, V. (2022) Interaction of RecA mediated SOS response with bacterial persistence, biofilm formation, and host response. *Int J Biol Macromol* **217**: 931–943.

Keinhörster, D., George, S.E., Weidenmaier, C., and Wolz, C. (2019) Function and regulation of *Staphylococcus aureus* wall teichoic acids and capsular polysaccharides. *Int J Med Microbiol* **309**: 151333.

Keller, A.P., Ly, S., Daetwyler, S., Eichenseher, F., Loessner, M.J., and Schmelcher, M. (2022) Chimeric Peptidoglycan Hydrolases Kill Staphylococcal Mastitis Isolates in Raw Milk and within Bovine Mammary Gland Epithelial Cells. *Viruses* **14**: 2801.

Kiedrowski, M.R. and Horswill, A.R. (2011) New approaches for treating Staphylococcal biofilm infections. *Ann N Y Acad Sci* **1241**: 104–121.

Kim, J.W., Dutta, V., Elhanafi, D., Lee, S., Osborne, J.A., and Kathariou, S. (2012) A novel restriction-modification system is responsible for temperature-dependent phage resistance in Listeria monocytogenes ECII. *Appl Environ Microbiol* **78**: 1995–2004.

Kocianova, S., Vuong, C., Yao, Y., Voyich, J.M., Fischer, E.R., DeLeo, F.R., and Otto, M. (2005) Key role of poly-γ-DL-glutamic acid in immune evasion and virulence of *Staphylococcus epidermidis*. *J Clin Invest* **115**: 688–694.

Kropec, A., Maira-Litran, T., Jefferson, K.K., Grout, M., Cramton, S.E., Götz, F., et al. (2005) Poly-N-acetylglucosamine production in *Staphylococcus aureus* is essential for virulence in murine models of systemic infection. *Infect Immun* **73**: 6868–6876.

Kuntová, L., Mašlanová, I., Oborilová, R., Šimecková, H., Finstrlová, A., Bárdy, P., et al. (2023) *Staphylococcus aureus* Prophage-Encoded Protein Causes Abortive Infection and Provides Population Immunity against Kayviruses. *MBio* **14**: e0249022.

De la Fuente-Núñez, C., Reffuveille, F., Fernández, L., and Hancock, R.E.W. (2013) Bacterial biofilm development as a multicellular adaptation: Antibiotic resistance and new therapeutic strategies. *Curr Opin Microbiol* **16**: 580–589.

Lai, W.C.B., Chen, X., Ho, M.K.Y., Xia, J., and Leung, S.S.Y. (2020) Bacteriophage-derived endolysins to target gram-negative bacteria. *Int J Pharm* **589**: 119833.

Lasa, I. and Penadés, J.R. (2006) Bap: A family of surface proteins involved in biofilm formation. *Res Microbiol* **157**: 99–107.

Latka, A. and Drulis-Kawa, Z. (2020) Advantages and limitations of microtiter biofilm

assays in the model of antibiofilm activity of Klebsiella phage KP34 and its depolymerase. *Sci Rep* **10**: 1–12.

Latka, A., Maciejewska, B., Majkowska-Skrobek, G., Briers, Y., and Drulis-Kawa, Z. (2017) Bacteriophage-encoded virion-associated enzymes to overcome the carbohydrate barriers during the infection process. *Appl Microbiol Biotechnol* **101**: 3103–3119.

Lauderdale, K.J., Boles, B.R., Cheung, A.L., and Horswill, A.R. (2009) Interconnections between sigma b, agr, and proteolytic activity in *Staphylococcus aureus* biofilm maturation. *Infect Immun* **77**: 1623–1635.

Le, K.Y., Park, M.D., and Otto, M. (2018) Immune evasion mechanisms of *Staphylococcus epidermidis* biofilm infection. *Front Microbiol* **9**: 359.

Le, K.Y., Villaruz, A.E., Zheng, Y., He, L., Fisher, E.L., Nguyen, T.H., et al. (2019) Role of Phenol-Soluble Modulins in *Staphylococcus epidermidis* Biofilm Formation and Infection of Indwelling Medical Devices. *J Mol Biol* **431**: 3015–3027.

Lee, H. and Yoon, Y. (2021) Etiological agents implicated in foodborne illness world wide. *Food Sci Anim Resour* **41**: 1–7.

Lefkowitz, E.J., Dempsey, D.M., Hendrickson, R.C., Orton, R.J., Siddell, S.G., and Smith, D.B. (2018) Virus taxonomy: The database of the International Committee on Taxonomy of Viruses (ICTV). *Nucleic Acids Res* **46**: D708–D717.

Lehman, S.M., Kongari, R., Glass, A.M., Koert, M., Ray, M.D., Plaut, R.D., and Stibitz, S. (2023) Phage K gp102 Drives Temperature-Sensitive Antibacterial Activity on USA300 MRSA. *Viruses* **15**: 17.

Lei, M.G., Jorgenson, M.A., Robbs, E.J., Black, I.M., Archer-hartmann, S., Shalygin, S., et al. (2024) Characterization of Ssc, an N-acetylgalactosamine-containing *Staphylococcus aureus* surface polysaccharide. *J Bacteriol* **7**: e0004824.

Leon-Velarde, C.G., Happonen, L., Pajunen, M., Leskinen, K., Kropinski, A.M., Mattinen, L., et al. (2016) Yersinia enterocolitica-specific infection by bacteriophages TG1 and φR1-RT is dependent on temperature-regulated expression of the phage host receptor OmpF. *Appl Environ Microbiol* **82**: 5340–5353.

Lewis, K. (2008) Multidrug tolerance of biofilms and persister cells. *Curr Top Microbiol Immunol* **322**: 107–131.

Li, P., Ma, W., Shen, J., and Zhou, X. (2022) Characterization of Novel Bacteriophage vB_KpnP_ZX1 and Its Depolymerases with Therapeutic Potential for K57

Klebsiella pneumoniae Infection. *Pharmaceutics* **14**: 1916.

Li, X., Gerlach, D., Du, X., Larsen, J., Stegger, M., Kuhner, P., et al. (2015) An accessory wall teichoic acid glycosyltransferase protects *Staphylococcus aureus* from the lytic activity of Podoviridae. *Sci Rep* **5**: 17219.

Lindsay, J.A. (2019) Staphylococci: Evolving genomes. *Gram-Positive Pathog* 485–498.

Lister, J.L. and Horswill, A.R. (2014) *Staphylococcus aureus* biofilms: Recent developments in biofilm dispersal. *Front Cell Infect Microbiol* **4**: 1–9.

Liu, J., Chen, D., Peters, B.M., Li, L., Li, B., Xu, Z., and Shirliff, M.E. (2016) Staphylococcal chromosomal cassettes mec (SCCmec): A mobile genetic element in methicillin-resistant *Staphylococcus aureus*. *Microb Pathog* **101**: 56–67.

Fernández, L., Duarte, A.C., Agún, S., Jurado, A.,Rodríguez, A., and García, P. (2023) Los Enimigos de las Bacterias: Los Bacteriófagos. *Virologia* **26**: 52–60.

Lobritz, M.A., Andrews, I.W., Braff, D., Porter, C.B.M., Gutierrez, A., Furuta, Y., et al. (2022) Increased energy demand from anabolic-catabolic processes drives β-lactam antibiotic lethality. *Cell Chem Biol* **29**: 276-286.e4.

Lopatina, A., Tal, N., and Sorek, R. (2020) Abortive Infection: Bacterial Suicide as an Antiviral Immune Strategy. *Annu Rev Virol* **7**: 371–384.

Lu, L., Hu, W., Tian, Z., Yuan, D., Yi, G., Zhou, Y., et al. (2019) Developing natural products as potential anti-biofilm agents. *Chinese Med (United Kingdom)* **14**: 11.

Luo, P., Yun, L., Li, Y., Tian, Y., Liu, Q., Huang, W., and Hu, C. (2018) Complete genomic sequence of the Vibrio alginolyticus bacteriophage Vp670 and characterization of the lysis-related genes, cwlQ and holA. *BMC Genomics* **19**: 1–11.

Ma, D., Li, L., Han, K., Wang, L., Cao, Y., Zhou, Y., et al. (2022) The antagonistic interactions between a polyvalent phage SaP7 and β-lactam antibiotics on combined therapies. *Vet Microbiol* **266**: 109332.

Maffei, E., Woischnig, A.K., Burkolter, M.R., Heyer, Y., Humolli, D., Thürkauf, N., et al. (2024) Phage Paride can kill dormant, antibiotic-tolerant cells of *Pseudomonas aeruginosa* by direct lytic replication. *Nat Commun* **15**: 175.

Maillard, J.Y. and Centeleghe, I. (2023) How biofilm changes our understanding of cleaning and disinfection. *Antimicrob Resist Infect Control* **12**: 1–11.

Marcotte, A.L. and Trzeciak, M.A. (2003) Community-acquired methicillin-resistant *Staphylococcus aureus*: An emerging pathogen in orthopaedics. *J Am Acad Orthop*

Surg **24**: 451–455.

Markoishvili, K., Tsitlanadze, G., Katsarava, R., Morris, J.G., and Sulakvelidze, A. (2002) A novel sustained-release matrix based on biodegradable poly(ester amide)s and impregnated with bacteriophages and an antibiotic shows promise in management of infected venous stasis ulcers and other poorly healing wounds. *Int J Dermatol* **41**: 453–458.

Martínez-Meléndez, A., Morfín-Otero, R., Villarreal-Treviño, L., González-González, G., Llaca-Díaz, J., Rodríguez-Noriega, E., et al. (2015) Staphylococcal Cassette Chromosome mec (SCCmec) in coagulase negative Staphylococci. *Med Univ* **17**: 229–233.

Maxwell, K.L. (2019) Phages Tune in to Host Cell Quorum Sensing. *Cell* **176**: 7–8.

Mazaheri Nezhad Fard, R., Barton, M.D., and Heuzenroeder, M.W. (2011) Bacteriophage-mediated transduction of antibiotic resistance in Enterococci. *Lett Appl Microbiol* **52**: 559–564.

McAdow, M., Missiakas, D.M., and Schneewind, O. (2012) *Staphylococcus aureus* secretes coagulase and von willebrand factor binding protein to modify the coagulation cascade and establish host infections. *J Innate Immun* **4**: 141–148.

McKevitt, A.I., Bjornson, G.L., Mauracher, C.A., and Scheifele, D.W. (1990) Amino acid sequence of a deltalike toxin from *Staphylococcus epidermidis*. *Infect Immun* **58**: 1473–1475.

Melo, L.D.R., Pinto, G., Oliveira, F., Vilas-Boas, D., Almeida, C., Sillankorva, S., et al. (2020) The protective effect of *Staphylococcus epidermidis* biofilm matrix against phage predation. *Viruses* **12**: 1076.

Mendes, R.E., Flamm, R.K., Hogan, P.A., Ross, J.E., and Jones, R.N. (2014) Summary of linezolid activity and resistance mechanisms detected during the 2012 LEADER surveillance program for the United States. *Antimicrob Agents Chemother* **58**: 1243–1247.

Mi, L., Liu, Y., Wang, C., He, T., Gao, S., Xing, S., et al. (2019) Identification of a lytic *Pseudomonas aeruginosa* phage depolymerase and its anti-biofilm effect and bactericidal contribution to serum. *Virus Genes* **55**: 394–405.

Michaelis, C. and Grohmann, E. (2023) Horizontal Gene Transfer of Antibiotic Resistance Genes in Biofilms. *Antibiotics* **12**: 328.

Middelboe, M. (2000) Bacterial growth rate and marine virus-host dynamics. *Microb*

Ecol **40**: 114–124.

Mikkelsen, K., Bowring, J.Z., Ng, Y.K., Svanberg Frisinger, F., Maglegaard, J.K., Li, Q., et al. (2023) An Endogenous *Staphylococcus aureus* CRISPR-Cas System Limits Phage Proliferation and Is Efficiently Excised from the Genome as Part of the SCC mec Cassette. *Microbiol Spectr* **11**: e0127723.

Morris, J.L., Letson, H.L., Elliott, L., Grant, A.L., Wilkinson, M., Hazratwala, K., and McEwen, P. (2019) Evaluation of bacteriophage as an adjunct therapy for treatment of peri-prosthetic joint infection caused by *Staphylococcus aureus*. *PLoS One* **14**: e0226574.

Nguyen, H.T.T., Nguyen, T.H., and Otto, M. (2020) The Staphylococcal exopolysaccharide PIA – Biosynthesis and role in biofilm formation, colonization, and infection. *Comput Struct Biotechnol J* **18**: 3324–3334.

Nocera, F.P., Pizzano, F., Masullo, A., Cortese, L., and De Martino, L. (2023) Antimicrobial Resistant *Staphylococcus* Species Colonization in Dogs, Their Owners, and Veterinary Staff of the Veterinary Teaching Hospital of Naples, Italy. *Pathogens* **12**: 1016.

Nordström, K. and Forsgren, A. (1974) Effect of Protein A on Adsorption of Bacteriophages to *Staphylococcus aureus* . *J Virol* **14**: 198–202.

Novick, R.P. and Bouanchaudt, D. (1971) Extrachromosomal Nature of Drug Resistance in *Staphylococcus aureus*. *Ann New York Acad Sci* **182**: 279–294.

Oleksy, A., Golonka, E., Bańbuła, A., Szmyd, G., Moon, J., Kubica, M., et al. (2004) Growth phase-dependent production of a cell wall-associated elastinolytic cysteine proteinase by *Staphylococcus epidermidis*. *Biol Chem* **385**: 525–535.

Oliveira, H., Drulis-Kawa, Z., and Azeredo, J. (2022) Exploiting phage-derived carbohydrate depolymerases for combating infectious diseases. *Trends Microbiol* **30**: 707–709.

Olson, M.E., Todd, D.A., Schaeffer, C.R., Paharik, A.E., Van Dyke, M.J., Bu¨ttner, H., et al. (2014) *Staphylococcus epidermidis* agr quorum-sensing system: Signal identification, cross talk, and importance in colonization. *J Bacteriol* **196**: 3482–3493.

Ortega, E., Abriouel, H., Lucas, R., and Gálvez, A. (2010) Multiple Roles of *Staphylococcus aureus* Enterotoxins: Pathogenicity, Superantigenic Activity, and Correlation to Antibiotic Resistance. *Toxins (Basel)* **2**: 2117–2131.

Otero, L.H., Rojas-Altuve, A., Llarrull, L.I., Carrasco-López, C., Kumarasiri, M., Lastochkin, E., et al. (2013) How allosteric control of *Staphylococcus aureus* penicillin binding protein 2a enables methicillin resistance and physiological function. *Proc Natl Acad Sci U S A* **110**: 16808–16813.

Otto, M. (2014) *Staphylococcus aureus* toxins. *Curr Opin Microbiol* **17**: 32–37.

Otto, M. (2009) *Staphylococcus epidermidis* – the "accidental" pathogen. *Nat Rev Microbiol* **7**: 555–567.

Palmqvist, N., Foster, T., Tarkowski, A., and Josefsson, E. (2002) Protein A is a virulence factor in *Staphylococcus aureus* arthritis and septic death. *Microb Pathog* **33**: 239–249.

Pamp, S.J., Sternberg, C., and Tolker-Nielsen, T. (2009) Insight into the microbial multicellular lifestyle via flow-cell technology and confocal microscopy. *Cytom Part A* **75A**: 90–103.

Park, J., Friendship, R.M., Poljak, Z., Weese, J.S., and Dewey, C.E. (2013) An investigation of exudative epidermitis (greasy pig disease) and antimicrobial resistance patterns of *Staphylococcus hyicus* and *Staphylococcus aureus* isolated from clinical cases. *Can Vet J* **54**: 139–144.

Paterson, G.K., Larsen, J., Harrison, E.M., Larsen, A.R., Morgan, F.J., Peacock, S.J., et al. (2012) First detection of livestock-associated meticillin-resistant *Staphylococcus aureus* CC398 in bulk tank milk in the United Kingdom, January to July 2012. *Euro Surveill* **17**: 20337.

Peng, Q., Tang, X., Sun, W.D.N., and Yuan, W. (2023) A Review of Biofilm Formation of *Staphylococcus aureus* and its Regulation Mechanism. *Antibiotics* **12**: 12.

Pirnay, J.P., Blasdel, B.G., Bretaudeau, L., Buckling, A., Chanishvili, N., Clark, J.R., et al. (2015) Quality and safety requirements for sustainable phage therapy products. *Pharm Res* **32**: 2173–2179.

Qu, Y., Daley, A.J., Istivan, T.S., Rouch, D.A., and Deighton, M.A. (2010) Densely adherent growth mode, rather than extracellular polymer substance matrix build-up ability, contributes to high resistance of *Staphylococcus epidermidis* biofilms to antibiotics. *J Antimicrob Chemother* **65**: 1405–1411.

Rakhuba, D. V., Kolomiets, E.I., Szwajcer Dey, E., and Novik, G.I. (2010) Bacteriophage receptors, mechanisms of phage adsorption and penetration into host cell. *Polish J Microbiol* **59**: 145–155.

Rhoads, D.D., Wolcott, R.D., Kuskowski, M.A., Wolcott, B.M., Ward, L.S., and Sulakvelidze, A. (2009) Bacteriophage therapy of venous leg ulcers in humans: results of a phase I safety trial. *J. Wound Care* **18**: 237-8–240-3.

Rice, C.J., Kelly, S.A., O'brien, S.C., Melaugh, E.M., Ganacias, J.C.B., Chai, Z.H., et al. (2021) Novel phage-derived depolymerase with activity against *Proteus mirabilis* biofilms. *Microorganisms* **9**: 2172.

Roach, D.R., Leung, C.Y., Henry, M., Morello, E., Singh, D., Di Santo, J.P., et al. (2017) Synergy between the Host Immune System and Bacteriophage Is Essential for Successful Phage Therapy against an Acute Respiratory Pathogen. *Cell Host Microbe* **22**: 38-47.e4.

Rodríguez-Rubio, L., Martínez, B., Donovan, D.M., Rodríguez, A., and García, P. (2013) Critical Reviews in Microbiology Bacteriophage virion-associated peptidoglycan hydrolases: potential new enzybiotics. *Crit Rev Microbiol* **39**: 427–434.

Rodríguez-Rubio, L., Martínez, B., Rodríguez, A., Donovan, D.M., and García, P. (2012) Enhanced Staphylolytic Activity of the *Staphylococcus aureus* Bacteriophage vB_SauS-phiIPLA88 HydH5 Virion-Associated Peptidoglycan Hydrolase: Fusions, Deletions, and Synergy with LysH5. *Appl Environ Microbiol* **78**: 2241–2248.

Rostøl, J.T., Quiles-Puchalt, N., Iturbe-Sanz, P., Lasa, Í., and Penadés, J.R. (2024) Bacteriophages avoid autoimmunity from cognate immune systems as an intrinsic part of their life cycles. *Nat Microbiol* **9***:* 1312–1324.

Roucourt, B. and Lavigne, R. (2009) The role of interactions between phage and bacterial proteins within the infected cell: A diverse and puzzling interactome. *Environ Microbiol* **11**: 2789–2805.

Rumbaugh, K.P. and Sauer, K. (2020) Biofilm dispersion. *Nat Rev Microbiol* **18**: 571–586.

Ryan, E.M., Alkawareek, M.Y., Donnelly, R.F., and Gilmore, B.F. (2012) Synergistic phage-antibiotic combinations for the control of *Escherichia coli* biofilms in vitro. *FEMS Immunol Med Microbiol* **65**: 395–398.

Sadekuzzaman, M., Mizan, M.F.R., Yang, S., Kim, H.S., and Ha, S. Do (2017) Application of bacteriophages for the inactivation of *Salmonella* spp. in biofilms. *Food Sci Technol Int* **24**: 424–433.

Sader, H.S., Farrell, D.J., Flamm, R.K., and Jones, R.N. (2014) Daptomycin activity tested against 164 457 bacterial isolates from hospitalised patients: Summary of 8

years of a Worldwide Surveillance Programme (2005-2012). *Int J Antimicrob Agents* **43**: 465–469.

Salas, M., Wernecki, M., Fernández, L., Iglesias, B., Gutiérrez, D., Álvarez, A., et al. (2020) Characterization of Clinical MRSA Isolates from Northern Spain and Assessment of Their Susceptibility to Phage-Derived Antimicrobials. *Antibiotics* **9**: 447.

Samson, J.E., Magadán, A.H., Sabri, M., and Moineau, S. (2013) Revenge of the phages: Defeating bacterial defences. *Nat Rev Microbiol* **11**: 675–687.

Schmerold, I., van Geijlswijk, I., and Gehring, R. (2023) European regulations on the use of antibiotics in veterinary medicine. *Eur J Pharm Sci* **189**: 106473.

Secor, P.R., Sweere, J.M., Michaels, L.A., Malkovskiy, A. V., Lazzareschi, D., Katznelson, E., et al. (2015) Filamentous bacteriophage promote biofilm assembly and function. *Cell Host Microbe* **18**: 549–559.

Seth, A.K., Geringer, M.R., Nguyen, K.T., Agnew, S.P., Dumanian, Z., Galiano, R.D., et al. (2013) Bacteriophage therapy for *Staphylococcus aureus* biofilm-infected wounds: A new approach to chronic wound care. *Plast Reconstr Surg* **131**: 225–234.

Severn, M.M. and Horswill, A.R. (2023) *Staphylococcus epidermidis* and its dual lifestyle in skin health and infection. *Nat Rev Microbiol* **21**: 97–111.

Shan, J., Korbsrisate, S., Withatanung, P., Adler, N.L., Clokie, M.R.J., and Galyov, E.E. (2014) Temperature dependent bacteriophages of a tropical bacterial pathogen. *Front Microbiol* **5**: 1–7.

Shaw, L.P., Rocha, E.P.C., and Maclean, R.C. (2023) Restriction-modification systems have shaped the evolution and distribution of plasmids across bacteria. *Nucleic Acids Res* **51**: 6806–6818.

Silva, N.C.C., Guimarães, F.F., Manzi, M.D.P., Gómez-Sanz, E., Gómez, P., Araújo, J.P., et al. (2014) Characterization of methicillin-resistant coagulase-negative Staphylococci in milk from cows with mastitis in Brazil. *Antonie van Leeuwenhoek, Int J Gen Mol Microbiol* **106**: 227–233.

Silva, V., Monteiro, A., Pereira, J.E., Maltez, L., Igrejas, G., and Poeta, P. (2022) MRSA in Humans, Pets and Livestock in Portugal: Where We Came from and Where We Are Going. *Pathogens* **11**: 1–15.

Sobhanifar, S., Worrall, L.J., King, D.T., Wasney, G.A., Baumann, L., Gale, R.T., et al. (2016) Structure and Mechanism of *Staphylococcus aureus* TarS, the Wall Teichoic

Acid β-glycosyltransferase Involved in Methicillin Resistance. *PLoS Pathog* **12**: 1–24.

Soldo, B., Lazarevic, V., and Karamata, D. (2002) tagO is involved in the synthesis of all anionic cell-wall polymers in *Bacillus subtilis* 168. *Microbiology* **148**: 2079–2087.

Sugimoto, S., Iwamoto, T., Takada, K., Okuda, K.I., Tajima, A., Iwase, T., and Mizunoe, Y. (2013) *Staphylococcus epidermidis* Esp degrades specific proteins associatedwith *Staphylococcus aureus* biofilm formation and host-pathogen interaction. *J Bacteriol* **195**: 1645–1655.

Sweere, J.M., Van Belleghem, J.D., Ishak, H., Bach, M.S., Popescu, M., Sunkari, V., et al. (2019) Bacteriophage trigger antiviral immunity and prevent clearance of bacterial infection. *Science* **363**: 1416.

Taha, M., Arnaud, T., Lightly, T.J., Peters, D., Wang, L., Chen, W., et al. (2023) Combining bacteriophage and vancomycin is efficacious against MRSA biofilm-like aggregates formed in synovial fluid. *Front Med* **10**: 1134912.

Thomas, V.C. and Hancock, L.E. (2009) Suicide and fratricide in bacterial biofilms. *Int J Artif Organs* **32**: 537–544.

Tormo-Más, M.Á., Mir, I., Shrestha, A., Tallent, S.M., Campoy, S., Lasa, Í., et al. (2010) Moonlighting bacteriophage proteins derepress Staphylococcal pathogenicity islands. *Nature* **465**: 779–782.

Tormo, M.Á., Martí, M., Valle, J., Manna, A.C., Cheung, A.L., Lasa, I., and Penadés, J.R. (2005) SarA is an essential positive regulator of *Staphylococcus epidermidis* biofilm development. *J Bacteriol* **187**: 2348–2356.

Turner, D., Shkoporov, A.N., Lood, C., Millard, A.D., Dutilh, B.E., Alfenas-Zerbini, P., et al. (2023) Abolishment of morphology-based taxa and change to binomial species names: 2022 taxonomy update of the ICTV bacterial viruses subcommittee. *Arch Virol* **168**: 1–9.

Twort, F.W. (1915) An investigation on the nature of ultra-microscopic viruses. *Lancet* **186**: 1241–1243.

Ultee, E., van der Aart, L.T., Zhang, L., van Dissel, D., Diebolder, C.A., van Wezel, G.P., et al. (2020) Teichoic acids anchor distinct cell wall lamellae in an apically growing bacterium. *Commun Biol* **3**: 1–9.

Valle, J., Fang, X., and Lasa, I. (2020) Revisiting Bap Multidomain Protein: More Than Sticking Bacteria Together. *Front Microbiol* **11**: 613581.

Vazquez, V., Liang, X., Horndahl, J.K., Ganesh, V.K., Smeds, E., Foster, T.J., and Hook, M. (2011) Fibrinogen is a ligand for the *Staphylococcus aureus* Microbial Surface Components Recognizing Adhesive Matrix Molecules (MSCRAMM) Bone sialoprotein-binding protein (Bbp). *J Biol Chem* **286**: 29797–29805.

Vilas Boas, D., Almeida, C., Sillankorva, S., Nicolau, A., Azeredo, J., and Azevedo, N.F. (2016) Discrimination of bacteriophage infected cells using locked nucleic acid fluorescent in situ hybridization (LNA-FISH). *Biofouling* **32**: 179–190.

Vlaeminck, J., Lin, Q., Xavier, B.B., De Backer, S., Berkell, M., De Greve, H., et al. (2022) The dynamic transcriptome during maturation of biofilms formed by methicillin-resistant *Staphylococcus aureus*. *Front Microbiol* **13**: 882346.

Vlamakis, H., Aguilar, C., Losick, R., and Kolter, R. (2008) Control of cell fate by the formation of an architecturally complex bacterial community. *Chemtracts* **20**: 427–429.

Volozhantsev, N. V., Borzilov, A.I., Shpirt, A.M., Krasilnikova, V.M., Verevkin, V. V., Denisenko, E.A., et al. (2022) Comparison of the therapeutic potential of bacteriophage KpV74 and phage-derived depolymerase (β-glucosidase) against *Klebsiella pneumoniae* capsular type K2. *Virus Res* **322**: 198951.

Vuong, C. and Otto, M. (2002) *Staphylococcus epidermidis* infections. *Microbes Infect* **4**: 481–489.

Watanabe, R., Matsumoto, T., Sano, G., Ishii, Y., Tateda, K., Sumiyama, Y., et al. (2007) Efficacy of bacteriophage therapy against gut-derived sepsis caused by *Pseudomonas aeruginosa* in mice. *Antimicrob Agents Chemother* **51**: 446–452.

Watts, A., Ke, D., Wang, Q., Pillay, A., Nicholson-Weller, A., and Lee, J.C. (2005) *Staphylococcus aureus* strains that express serotype 5 or serotype 8 capsular polysaccharides differ in virulence. *Infect Immun* **73**: 3502–3511.

WHO (2017) Prioritization of pathogens to guide discovery, research and development of new antibiotics for drug-resistant bacterial infections, including tuberculosis.

Wilkinson, B.J. and Holmes, K.M. (1979) *Staphylococcus aureus* cell surface: Capsule as a barrier to bacteriophage adsorption. *Infect Immun* **23**: 549–552.

Wills, Q.F., Kerrigan, C., and Soothill, J.S. (2005) Experimental bacteriophage protection against *Staphylococcus aureus* abscesses in a rabbit model. *Antimicrob Agents Chemother* **49**: 1220–1221.

World Health Organization (2017) One Health. *acceessed on 07/03/2023* available

online: https://www.who.int/news-room/qu.

Wright, A., Hawkins, C.H., Änggård, E.E., and Harper, D.R. (2009) A controlled clinical trial of a therapeutic bacteriophage preparation in chronic otitis due to antibiotic-resistant *Pseudomonas aeruginosa*; A preliminary report of efficacy. *Clin Otolaryngol* **34**: 349–357.

Wu, B., Wang, R., and Fane, A.G. (2017) The roles of bacteriophages in membrane-based water and wastewater treatment processes: A review. *Water Res* **110**: 120–132.

Wu, M., Hu, K., Xie, Y., Liu, Y., Mu, D., Guo, H., et al. (2018) A Novel Phage PD-6A3, and Its Endolysin Ply6A3, With Extended Lytic Activity Against *Acinetobacter baumannii* . *Front Microbiol* **9**: 1–12.

Xia, G., Corrigan, R.M., Winstel, V., Goerke, C., Gründling, A., and Peschel, A. (2011) Wall teichoic acid-dependent adsorption of Staphylococcal siphovirus and myovirus. *J Bacteriol* **193**: 4006–4009.

Xia, G., Maier, L., Sanchez-Carballo, P., Li, M., Otto, M., Holst, O., and Peschel, A. (2010) Glycosylation of wall teichoic acid in *Staphylococcus aureus* by TarM. *J Biol Chem* **285**: 13405–13415.

Yang, H., Zhang, Y., Yu, J., Huang, Y., Zhang, X.E., and Wei, H. (2014) Novel chimeric lysin with high-Level antimicrobial activity against methicillin-Resistant *Staphylococcus aureus* in vitro and in vivo. *Antimicrob Agents Chemother* **58**: 536–542.

Yang, J., Bowring, J.Z., Krusche, J., Lehmann, E., Bejder, B.S., Silva, S.F., et al. (2023) Cross-species communication via agr controls phage susceptibility in *Staphylococcus aureus*. *Cell Rep* **42**: 113154.

Yarwood, J.M. and Schlievert, P.M. (2003) Quorum sensing in *Staphylococcus* infections. *J Clin Invest* **112**: 1620–1625.

Yilmaz, C., Colak, M., Yilmaz, B.C., Ersoz, G., Kutateladze, M., and Gozlugol, M. (2013) Bacteriophage therapy in implant-related infections: An experimental study. *J Bone Jt Surg* **95**: 117–125.

Yoong, P., Schuch, R., Nelson, D., and Fischetti, V.A. (2004) Identification of a broadly active phage lytic enzyme with lethal activity against antibiotic-resistant *Enterococcus faecalis* and Enterococcus faecium. *J Bacteriol* **186**: 4808–4812.

Yoong, P. and Torres, V.J. (2013) The effects of *Staphylococcus aureus* leukotoxins on the host: Cell lysis and beyond. *Curr Opin Microbiol* **16**: 63–69.

Young, R., Wang, I.N., and Roof, W.D. (2000) Phages will out: Strategies of host cell lysis. *Trends Microbiol* **8**: 120–128.

Zaburlin, D., Quiberoni, A., and Mercanti, D. (2017) Changes in Environmental Conditions Modify Infection Kinetics of Dairy Phages. *Food Environ Virol* **9**: 270–276.

Zampara, A., Sørensen, M.C.H., Grimon, D., Antenucci, F., Vitt, A.R., Bortolaia, V., et al. (2020) Exploiting phage receptor binding proteins to enable endolysins to kill Gram-negative bacteria. *Sci Rep* **10**: 1–12.

Zhang, L., Zhang, C., Gao, R., and Yang, R. (2015) An ensemble method to distinguish bacteriophage virion from non-virion proteins based on protein sequence characteristics. *Int J Mol Sci* **16**: 21734–21758.

Zhang, Y., Agidi, S., and Lejeune, J.T. (2009) Diversity of Staphylococcal cassette chromosome in coagulase-negative Staphylococci from animal sources. *J Appl Microbiol* **107**: 1375–1383.

SUPPLEMENTARY MATERIAL

7.1. Supplementary material Chapter 3.1- Temperature is a key environmental factor modulating phage infection of bacterial biofilms

SUPPLEMENTARY METHODS

Biofilm development numerical simulation model

A numerical simulation model was built in an attempt to understand better the effect of pH changes throughout biofilm development in a 12-well microtiter plate over the bacterial and phage populations. The model considers both the attached and the planktonic populations. For the sake of simplicity, the net exchange of bacterial cells and phage particles between the two phases was considered to be 0. Likewise, selection of phage resistant cells was not taken into account in the model, given its low frequency and the short scale of this experimental set up. Modelling was performed by using the available data to estimate the values of all the required parameters at different developmental stages. The model calculates the numbers of three populations (uninfected bacteria, infected bacteria and free phages) and the pH value every 30 minutes within a 24 hours incubation time.

1. Estimating bacterial growth dynamics

Parameters related to changes in the bacterial attached and planktonic populations, as well as the evolution of pH values, were estimated based on data obtained with strain *S. aureus* IPLA 1 not infected with *K. rodi*. Based on these data, the growth rates of the bacterial population every 30 minutes were as follows:

Table 1

	gr_1	**gr_2**	**gr_3**
Biofilm population	$< 8.5 \times 10^6$ CFU	$< 2.5 \times 10^7$ CFU	$\geq 10^9$ CFU
	1.39	**1.24**	**1.00**
Planktonic population	$< 6 \times 10^6$ CFU	$< 5 \times 10^7$ CFU	$\geq 10^9$ CFU
	1.24	**1.10**	**1.00**

According to these data, doubling time during exponential phase was **63.01 and 74.48 minutes** for biofilm and planktonic cells, respectively, and the predicted initial adherence to the bottom of the well was **0.26**.

These growth rates and the initial fraction of adherence were used to build a basic model simulating bacterial growth without phage predation in the planktonic and biofilm phase throughout a 24 h period with a starting inoculum of 10^6 CFU/well. This model calculates the number of uninfected susceptible bacterial cells (UC) in both phases every 30 minutes according to the following equations:

$UC\_biofilm[0] = 10^6 \times 0.26$

$UC\_planktonic[0] = 10^6 \times (1 - 0.26)$

$UC\_biofilm[i] = UC\_biofilm[i-1] \times growth\_rate*$

$UC\_planktonic[i] = UC\_planktonic[i-1] \times growth\_rate*$

* growth_rate = change in cell number for 30 min intervals (Table 1)

The values obtained with this model resembled the experimental values very closely.

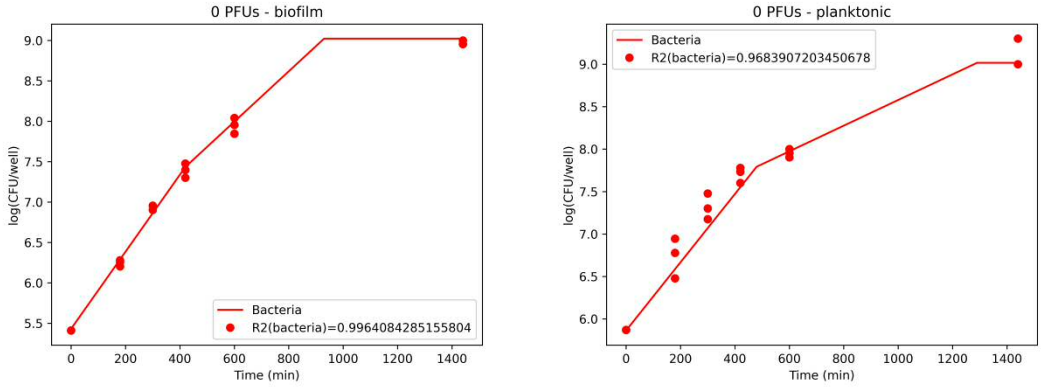

2. Estimating phage propagation rates

Phage propagation rates for 30 min intervals were estimated using the data obtained for biofilms developed in the presence of a starting phage titer of 10 PFU/well.

Table 3

	propr_1	propr_2	propr_3
Biofilm population	$<8.5 \times 10^6$ CFU	$< 2.5 \times 10^7$ CFU	$< 10^9$ CFU
	1.16	**5.79**	**1.98**
Planktonic population	$< 6 \times 10^6$ CFU	$< 5 \times 10^7$ CFU	$< 10^9$ CFU
	1.03	**2.62**	**2.06**

Even though the model estimates phage inactivation, this phenomenon did not play a role in this setting because the minimum pH reached after 24 h of growth at 25 ºC for this strain was 5.72, which is above the inactivation threshold of 5.55 considered in the model.

P_biofilm[0] = Inoculum × 0.26

P_planktonic[0] = Inoculum × (1 - 0.26)

P_biofilm[i] = P_biofilm[i-1] × prop_rate* × inact_rate*

P_planktonic[i] = P_planktonic[i-1] × prop_rate* × inact_rate*

* prop_rate = propagation rate for 30 min intervals (Table 3) and inact_rate = inactivation rate for 30 min intervals (Table 4)

3. Calculating the number of infected bacterial cells

Evidently, if there are no phages in the well, there will be no infected cells (IC). However, in phage-infected wells the number of infected cells will be calculated after each 30 min step based on the number of free phages released in the previous step and the probability of infection rates (infection rates, for short). These values will then be subtracted from the number of uninfected cells.

IC_biofilm[i] = P_biofilm[i-1] * inf_rate

UC_biofilm[i] = UC_biofilm[i] - IC_biofilm[i]

IC_plank[i] = P_plank[i-1] * inf_rate

UC_plank[i] = UC_plank[i] - IC_plank[i]

4. Estimating the infection rates

The infection rate was defined as the number of infected cells per infective viral particle. For example, a rate of 1 would mean that there is 1 infected cell per viral particle, whereas a rate of 0.1 would mean that there is only 1 infected cell for 10 viral particles.

BIOFILM	**UC<8.5 × 10^6**	**8.5 × 10^6 ≥UC<2.5 × 10^7**	**2.5 × 10^7 ≥ UC<10^9**	**UC≥10^9**
Normal growth	a	b	c	d
Delayed growth & i < 31	e	f	-	-
Delayed growth & i ≥ 31	k	l	m	-
PLANKTONIC	**UC<6 × 10^6**	**6 × 10^6≥UC<5×10^7**	**5×10^7 ≥UC<10^9**	**UC≥10^9**
Normal growth	aa	bb	cc	dd
Delayed growth & i < 41	ee	ff	-	-
Delayed growth & i ≥ 41	kk	ll	mm	-

Once the general structure of the model was completed, we estimated the infection rates leading to the best results, that is, the values that most closely resembled the experimental data. This was carried out following several optimization steps, in which different combinations of infection rates for the different growth stages were tested. For each combination, the goodness of fit of the predicted numbers of phage particles and bacteria for all conditions were added up to calculate the overall goodness of fig of the model. In each step, the combination that led to the best overall goodness of fit was selected to continue model optimization. It must be noted that, if several combinations give the best goodness of fit, this algorithm will select the first one it encountered, that is, the lowest infection rate.

BIOFILM	**UC<8.5 × 10^6**	**8.5 × 10^6 ≥UC<2.5 × 10^7**	**2.5 × 10^7 ≥ UC<10^9**	**UC≥10^9**
Normal growth	0.00001	0.9	0.33	0.00001
Delayed growth & i < 31	0.00001	0.00001	-	-
Delayed growth & i >= 31	0.00001	0.49	0.5	-
PLANKTONIC	**UC<6 × 10^6**	**6 × 10^6≥UC<5×10^7**	**5×10^7 ≥UC<10^9**	**UC≥10^9**
Normal growth	0.00001	0.9	0.13	0.00001
Delayed growth & i < 41	0.00001	0.00001	-	-
Delayed growth & i >= 41	0.00001	0.00001	0.00001	-

Grey cells: these infection rates led to weird results when trying to predict the biofilm infection dynamics (unexpected bacterial regrowth prior to complete eradication by the phage)

The infection rate values obtained for d and e led to strange phage-host dynamics in the biofilms when using the model to predict infection at starting phage concentrations of 100, 1000 and 10000, as explained above. For this reason, further refinement of the infection rates was carried out manually to determine the lowest values of d and e that eliminated the aforementioned artifact. The final infection rates were as follows:

BIOFILM	**UC<8.5 × 10^6**	**8.5 × 10^6 ≥UC<2.5 × 10^7**	**2.5 × 10^7 ≥ UC<10^9**	**UC≥10^9**
Normal growth	0.00001	0.9	0.33	0.00001
Delayed growth & i < 31	0.07	0.2	-	-
Delayed growth & i >= 31	0.00001	0.49	0.5	-
PLANKTONIC	**UC<6 × 10^6**	**6 × 10^6≥UC<5×10^7**	**5×10^7 ≥UC<10^9**	**UC≥10^9**
Normal growth	0.00001	0.9	0.13	0.00001
Delayed growth & i < 41	0.00001	0.00001	-	-
Delayed growth & i >= 41	0.00001	0.00001	0.00001	-

5. Estimation of pH change rates

The evolution of pH in the growth medium was also monitored throughout biofilm development and used to estimate the decrease in pH for 30 minute intervals. This decrease was estimated as a function of bacterial number increase, increase in biofilm cells and biofilm cell number. The cut-off values of these parameters were based on the available data and allowed to define how the different rates of pH decrease changed throughout biofilm development. These rates were as follows:

Table 4

	A	**B**	**C**	**D**
pH change rate	1	1	0.99	0.99

A: bacterial number increase $< 10^7$ and increase in biofilm cells $< 10^7$

B: bacterial number increase $\geq 10^7$ and biofilm cell number $< 1.5 \times 10^8$

C: bacterial number increase $\geq 10^7$ and biofilm cell number $\geq 1.5 \times 10^8$

D: bacterial number increase $< 10^7$ and increase in biofilm cells $\geq 10^7$

This parameter was then included in the simulation model. The starting and final pH values were set at 7 and 4.75, respectively.

Table 7.1 – List of genes in biofilms of strain IPLA16 grown at 37 ºC compared to those developed at 25 ºC

Gene	gene_name	function	TIGR protein fam
RL451_06585	mntB	Manganese transport system membrane protein MntB	Transport and bind
RL451_06580	znuC	High-affinity zinc uptake system ATP-binding protein ZnuC	Transport and bind
RL451_11595	-	hypothetical protein	Protein fate
RL451_11630	sarZ	HTH-type transcriptional regulator SarZ	-
RL451_11590	narH	Respiratory nitrate reductase 1 beta chain	Energy metabolism
RL451_03490	-	hypothetical protein	-
RL451_11585	narG	Respiratory nitrate reductase 1 alpha chain	Energy metabolism
RL451_10290	aur	Zinc metalloproteinase aureolysin	-
RL451_11620	narT	putative nitrate transporter NarT	Transport and bind
RL451_06590	mntA	Manganese-binding lipoprotein MntA	Transport and bind
RL451_11070	-	hypothetical protein	-
RL451_06200	-	hypothetical protein	-
RL451_05265	-	hypothetical protein	-
RL451_11565	sirB	Sirohydrochlorin ferrochelatase	-
RL451_10905	yydI	putative peptide export ATP-binding protein YydI	Transport and bind
RL451_00220	-	hypothetical protein	-
RL451_01075	-	hypothetical protein	-
RL451_04835	purC	Phosphoribosylaminoimidazole-succinocarboxamide synthase	"Purines, pyrimidin nucleosides, and nu
RL451_10440	opuD_2	Glycine betaine transporter OpuD	Transport and bind
RL451_11625	-	Acid shock protein	-
RL451_10460	betA	Oxygen-dependent choline dehydrogenase	Cellular processes
RL451_06800	-	hypothetical protein	-
RL451_02410	-	hypothetical protein	-

RL451_09420	-	hypothetical protein	-
RL451_05760	nuc	Thermonuclease	Transport and bind
RL451_10445	opcR	HTH-type transcriptional repressor OpcR	Amino acid biosyn
RL451_04830	purS	Phosphoribosylformylglycinamidine synthase subunit PurS	"Purines, pyrimidir nucleosides, and nu
RL451_12855	-	hypothetical protein	-
RL451_04845	purE	N5-carboxyaminoimidazole ribonucleotide mutase	"Purines, pyrimidir nucleosides, and nu
RL451_12315	-	hypothetical protein	Transport and bind
RL451_03705	-	hypothetical protein	-
RL451_04085	-	hypothetical protein	Protein fate
RL451_01340	-	hypothetical protein	-
RL451_06205	-	hypothetical protein	-
RL451_04930	sspA	Glutamyl endopeptidase	Protein fate
RL451_07865	-	hypothetical protein	-
RL451_06405	sarX	HTH-type transcriptional regulator SarX	Regulatory functio
RL451_06100	dtpT	Di-/tripeptide transporter	Transport and bind
RL451_11065	-	hypothetical protein	-
RL451_04840	purK_2	N5-carboxyaminoimidazole ribonucleotide synthase	"Purines, pyrimidir nucleosides, and nu
RL451_06030	-	hypothetical protein	-
RL451_06920	menE_2	2-succinylbenzoate--CoA ligase	"Biosynthesis of co prosthetic groups, a carriers"
RL451_11600	narX	Nitrate reductase-like protein NarX	Energy metabolism
RL451_05530	-	hypothetical protein	-
RL451_10970	-	hypothetical protein	-
RL451_01440	mrcA	Penicillin-binding protein 1A	Cell envelope

RL451_07405	veg	Protein Veg	-
RL451_00965	-	hypothetical protein	-
RL451_11995	-	hypothetical protein	-
RL451_11060	-	hypothetical protein	-
RL451_11475	gpmA_2	"2,3-bisphosphoglycerate-dependent phosphoglycerate mutase"	-
RL451_08425	esxA	ESAT-6 secretion system extracellular protein A	-
RL451_04360	-	hypothetical protein	-
RL451_05800	-	hypothetical protein	-
RL451_04605	-	UPF0358 protein MW0995	-
RL451_00970	-	hypothetical protein	-
RL451_10680	-	hypothetical protein	Protein synthesis
RL451_01615	cycA_1	D-serine/D-alanine/glycine transporter	Transport and bind
RL451_05930	-	hypothetical protein	-
RL451_00225	-	hypothetical protein	-
RL451_06795	-	hypothetical protein	-
RL451_11990	-	hypothetical protein	-
RL451_08670	-	hypothetical protein	-
RL451_00455	-	hypothetical protein	-
RL451_07720	-	hypothetical protein	-
RL451_06210	saeR	Response regulator SaeR	Regulatory functio transduction
RL451_00845	-	hypothetical protein	-
RL451_11645	-	hypothetical protein	-
RL451_09425	-	hypothetical protein	-
RL451_01195	-	hypothetical protein	-
RL451_05280	-	hypothetical protein	-
RL451_00200	-	hypothetical protein	-

RL451_05190	pepF1_2	"Oligoendopeptidase F, plasmid"	Protein fate
RL451_05550	yutE	UPF0331 protein YutE	-
RL451_07715	lpl2_4	putative lipoprotein SA0397	-
RL451_10455	gbsA	Betaine aldehyde dehydrogenase	Cellular processes
RL451_00620	-	-	-
RL451_04825	purQ	Phosphoribosylformylglycinamidine synthase subunit PurQ	"Purines, pyrimidin nucleosides, and nu
RL451_02405	-	hypothetical protein	Protein fate
RL451_11480	-	hypothetical protein	-
RL451_00215	-	hypothetical protein	Energy metabolism
RL451_13550	polC_2	DNA polymerase III PolC-type	DNA metabolism
RL451_08660	hmp	Flavohemoprotein	Energy metabolism
RL451_08590	tarI'	Ribitol-5-phosphate cytidylyltransferase 2	"Biosynthesis of co prosthetic groups, a carriers"
RL451_08250	ybbH_1	putative HTH-type transcriptional regulator YbbH	-
RL451_01315	-	Putative dipeptidase SACOL1801	-
RL451_05680	mgsR	Regulatory protein MgsR	Regulatory functio
RL451_06365	-	hypothetical protein	-
RL451_06900	-	hypothetical protein	-
RL451_02065	-	hypothetical protein	-
RL451_00855	hit	Protein hit	-
RL451_12005	-	hypothetical protein	Unknown function
RL451_03330	mscL	Large-conductance mechanosensitive channel	-
RL451_05935	yfbR	5'-deoxynucleotidase YfbR	Hypothetical protei
RL451_01450	-	hypothetical protein	Protein fate
RL451_11505	femA_3	Aminoacyltransferase FemA	Unknown function

RL451_00825	cpdA_1	"3',5'-cyclic adenosine monophosphate phosphodiesterase CpdA"	DNA metabolism
RL451_04305	-	hypothetical protein	-
RL451_07610	mccA	O-acetylserine dependent cystathionine beta-synthase	Amino acid biosyn
RL451_08960	-	Formate dehydrogenase	Amino acid biosyn
RL451_09550	-	hypothetical protein	-
RL451_01180	-	hypothetical protein	-
RL451_09220	-	hypothetical protein	-
RL451_01165	-	hypothetical protein	Cellular processes
RL451_08325	-	hypothetical protein	Cell envelope
RL451_09320	-	hypothetical protein	Transport and bind
RL451_00120	-	hypothetical protein	Mobile and extrach element functions
RL451_06215	saeS	Histidine protein kinase SaeS	Signal transduction
RL451_08355	yezG_6	putative antitoxin YezG	-
RL451_11235	-	hypothetical protein	-
RL451_08665	-	hypothetical protein	-
RL451_04370	fib	Fibrinogen-binding protein	-
RL451_00580	bcp	Putative peroxiredoxin bcp	Cellular processes
RL451_11940	glvR	HTH-type transcriptional regulator GlvR	-
RL451_13505	-	hypothetical protein	-
RL451_11605	-	hypothetical protein	Central intermedia metabolism; Regul functions
RL451_00210	-	hypothetical protein	-
RL451_00275	rutB	Peroxyureidoacrylate/ureidoacrylate amidohydrolase RutB	-
RL451_12270	-	hypothetical protein	-

RL451_02570	nudF	ADP-ribose pyrophosphatase	Unknown function
RL451_04355	-	hypothetical protein	-
RL451_06310	mgrA	HTH-type transcriptional regulator MgrA	-
RL451_00300	nos	Nitric oxide synthase oxygenase	-
RL451_12900	deoD1	Purine nucleoside phosphorylase DeoD-type 1	"Purines, pyrimidin nucleosides, and nu
RL451_04980	-	hypothetical protein	-
RL451_04985	-	hypothetical protein	-
RL451_12255	-	hypothetical protein	-
RL451_02830	-	hypothetical protein	Mobile and extrach element functions; functions
RL451_13515	-	putative leukocidin-like protein 2	Cellular processes
RL451_11545	-	hypothetical protein	-
RL451_11790	-	hypothetical protein	-
RL451_10340	-	hypothetical protein	-
RL451_03485	cls_1	Cardiolipin synthase	-
RL451_08435	-	hypothetical protein	-
RL451_06410	rhaR	HTH-type transcriptional activator RhaR	-
RL451_03150	pepF1_1	"Oligoendopeptidase F, plasmid"	Protein fate
RL451_11255	-	hypothetical protein	Cellular processes; extrachromosomal functions
RL451_04390	-	hypothetical protein	-
RL451_01070	-	hypothetical protein	Cellular processes
RL451_00525	recX	Regulatory protein RecX	Central intermedia metabolism
RL451_05990	tagO	putative undecaprenyl-phosphate N-acetylglucosaminyl 1-phosphate transferase	Cell envelope

RL451_10045	-	UPF0312 protein SA2479	-
RL451_11250	-	hypothetical protein	Cellular processes; extrachromosomal functions
RL451_08585	tarJ'	Ribulose-5-phosphate reductase 2	Energy metabolism
RL451_00570	-	hypothetical protein	-
RL451_11975	-	hypothetical protein	Cellular processes
RL451_01150	yvgN	Glyoxal reductase	-
RL451_07560	-	hypothetical protein	-
RL451_12540	-	hypothetical protein	Hypothetical protei
RL451_10490	fda	Fructose-bisphosphate aldolase class 1	"Biosynthesis of co prosthetic groups, a carriers"
RL451_10150	icaR	Biofilm operon icaADBC HTH-type negative transcriptional regulator IcaR	-
RL451_00190	ytrA	HTH-type transcriptional repressor YtrA	Energy metabolism Regulatory functio
RL451_02705	hup	DNA-binding protein HU	DNA metabolism
RL451_05370	ydjZ	TVP38/TMEM64 family inner membrane protein YdjZ	-
RL451_02585	-	hypothetical protein	-
RL451_00625	-	-	-
RL451_03065	-	hypothetical protein	-
RL451_03190	-	hypothetical protein	Unknown function
RL451_13220	-	hypothetical protein	-
RL451_11635	-	hypothetical protein	-
RL451_10560	-	hypothetical protein	-
RL451_06555	tagG	Teichoic acid translocation permease protein TagG	-
RL451_11615	nreC	Oxygen regulatory protein NreC	Cellular processes

RL451_13105	-	hypothetical protein	-	0.22099022
RL451_04935	sspB	Staphopain B	-	0.22107697
RL451_06275	-	hypothetical protein	-	0.22238919
RL451_12250	-	hypothetical protein	-	0.22270283
RL451_09385	-	putative lipoprotein SAOUHSC 00053	-	0.22492541
RL451_00860	ecsA	ABC-type transporter ATP-binding protein EcsA	Transport and binding proteins	0.22497885
RL451_05045	-	hypothetical protein	Protein fate	0.22538911
RL451_11610	nreB	Oxygen sensor histidine kinase NreB	Protein fate; Signal transduction	0.22589106
RL451_11710	paiA	Spermidine/spermine N(1)-acetyltransferase	Protein synthesis	0.22598593
RL451_11925	-	hypothetical protein	-	0.22750042
RL451_11305	opuCA	Carnitine transport ATP-binding protein OpuCA	Transport and binding proteins	0.2286354
RL451_10510	ldh2	L-lactate dehydrogenase 2	Energy metabolism	0.22885669
RL451_12295	-	hypothetical protein	Protein synthesis	0.23205324
RL451_02620	-	hypothetical protein	-	0.23252591
RL451_02375	aroK	Shikimate kinase	-	0.23379543
RL451_05425	mnhA1	Na(+)/H(+) antiporter subunit A1	Transport and binding proteins	0.23384982
RL451_02975	murG	UDP-N-acetylglucosamine--N-acetylmuramyl-(pentapeptide) pyrophosphoryl-undecaprenol N-acetylglucosamine transferase	Cell envelope	0.23437233
RL451_02710	-	hypothetical protein	-	0.23763935
RL451_11550	-	hypothetical protein	-	0.23830769
RL451_00105	entE	Enterotoxin type E	-	0.23875109
RL451_07945	-	hypothetical protein	-	0.23876207
RL451_13540	-	hypothetical protein	-	0.23947054
RL451_00640	-	-	-	0.23953685
RL451_00630	-	-	-	0.23959385
RL451_10075	-	hypothetical protein	Cellular processes	0.23969532

RL451_05420	kapB	Kinase-associated lipoprotein B	-	0.24043342
RL451_07360	pth	Peptidyl-tRNA hydrolase	Protein synthesis	0.24106682
RL451_06925	proP	Proline/betaine transporter	Transport and binding proteins	0.24138773
RL451_05525	dltA_1	D-alanine--D-alanyl carrier protein ligase	Cell envelope	0.24198007
RL451_05515	dltC	D-alanyl carrier protein	Cell envelope	0.24245023
RL451_08580	tarK	Teichoic acid ribitol-phosphate polymerase TarK	-	0.24250102
RL451_01715	-	hypothetical protein	-	0.2425157
RL451_04645	-	hypothetical protein	Cell envelope	0.24303803
RL451_00895	ydeN	Putative hydrolase YdeN	-	0.24318968
RL451_04975	-	hypothetical protein	Protein synthesis	0.2434204
RL451_06300	ydhF	Oxidoreductase YdhF	-	0.24367569
RL451_05560	-	hypothetical protein	-	0.24448692
RL451_04105	gmk	Guanylate kinase	"Purines, pyrimidines, nucleosides, and nucleotides"	0.24501122
RL451_11850	btuD_7	Vitamin B12 import ATP-binding protein BtuD	Transport and binding proteins	0.24539079
RL451_00195	btuD_1	Vitamin B12 import ATP-binding protein BtuD	Transport and binding proteins	0.24576362
RL451_13555	lexA_2	LexA repressor	DNA metabolism; Regulatory functions	0.24626577
RL451_04585	ctaB2	Protoheme IX farnesyltransferase 2	"Biosynthesis of cofactors, prosthetic groups, and carriers"	0.2465401
RL451_06260	-	hypothetical protein	-	0.24683775
RL451_08305	hel	Lipoprotein E	"Biosynthesis of cofactors, prosthetic groups, and carriers; Transport and binding proteins"	0.24707856
RL451_10900	yydJ	putative peptide export permease protein YydJ	-	0.24720735
RL451_02500	-	hypothetical protein	-	0.24879137

RL451_01630	phoP	Alkaline phosphatase synthesis transcriptional regulatory protein PhoP	Regulatory functions; Signal transduction	0.24958126
RL451_05915	hprK	HPr kinase/phosphorylase	Regulatory functions; Signal transduction	0.2496017
RL451_10740	-	hypothetical protein	-	0.25007866
RL451_05520	patA_2	Peptidoglycan O-acetyltransferase	Cell envelope	0.25052856
RL451_07935	-	hypothetical protein	-	0.25086028
RL451_00635	-	-	-	0.25142444
RL451_10835	glcB	PTS system glucoside-specific EIICBA component	Transport and binding proteins	0.25181304
RL451_07015	-	putative epimerase/dehydratase SA0511	Cell envelope	0.25280072
RL451_04855	-	hypothetical protein	-	0.25364444
RL451_09110	-	hypothetical protein	-	0.25372538
RL451_10495	-	hypothetical protein	-	0.25374976
RL451_06295	-	hypothetical protein	-	0.25394737
RL451_03270	mprF	Phosphatidylglycerol lysyltransferase	Unknown function	0.25448309
RL451_03620	bsaA_1	Glutathione peroxidase homolog BsaA	-	0.25454367
RL451_07105	secE	Protein translocase subunit SecE	Protein fate	0.25461668
RL451_04560	-	hypothetical protein	-	0.2558679
RL451_04610	-	hypothetical protein	-	0.25611936
RL451_01945	cymR	HTH-type transcriptional regulator CymR	Unknown function	0.25799259
RL451_00865	-	hypothetical protein	-	0.25837629
RL451_01410	acuA	Acetoin utilization protein AcuA	-	0.25951989
RL451_13545	-	hypothetical protein	-	0.26020443
RL451_03315	-	"1,4-dihydroxy-2-naphthoyl-CoA hydrolase"	Unknown function	0.26045478
RL451_02645	-	hypothetical protein	-	0.26074804
RL451_01560	-	putative peptidase SA1530	Protein fate	0.26084844
RL451_09360	-	putative lipoprotein SAOUHSC 00053	-	0.26160936
RL451_00660	-	-	-	0.26228351

RL451_00530	yfhH	Uncharacterized protein YfhH	-	0.26281333
RL451_06695	nth_2	Endonuclease III	DNA metabolism	0.26386171
RL451_07265	-	-	-	0.26390155
RL451_00440	-	hypothetical protein	-	0.26508615
RL451_01955	-	hypothetical protein	-	0.26512954
RL451_06565	tarA	N-acetylglucosaminyldiphosphoundecaprenol N-acetyl-beta-D-mannosaminyltransferase	Cell envelope	0.26524966
RL451_08860	-	hypothetical protein	-	0.26543915
RL451_05175	yjbK	Putative triphosphatase YjbK	-	0.26561937
RL451_09390	-	putative lipoprotein SAOUHSC 00052	-	0.26616915
RL451_00260	mdlD	NAD(P)-dependent benzaldehyde dehydrogenase	Central intermediary metabolism	0.26661818
RL451_06550	tarB	Teichoic acid glycerol-phosphate primase	Cell envelope	0.26713282
RL451_05910	lgt	Prolipoprotein diacylglyceryl transferase	Protein fate	0.26719511
RL451_09515	-	hypothetical protein	-	0.26854964
RL451_13015	ptpB	Low molecular weight protein-tyrosine-phosphatase PtpB	Cellular processes	0.26875063
RL451_04375	-	hypothetical protein	-	0.26979592
RL451_00700	-	-	-	0.27044794
RL451_07950	-	hypothetical protein	Energy metabolism	0.27059463
RL451_04300	-	hypothetical protein	-	0.27074553
RL451_03285	glcT	GlcA/glcB genes antiterminator	"Biosynthesis of cofactors, prosthetic groups, and carriers"	0.2709182
RL451_08155	-	hypothetical protein	-	0.27098863
RL451_04115	-	hypothetical protein	-	0.27339502
RL451_04820	purL	Phosphoribosylformylglycinamidine synthase subunit PurL	"Purines, pyrimidines, nucleosides, and nucleotides"	0.27343908
RL451_00235	-	hypothetical protein	-	0.27456166

RL451_01455	plsC	1-acyl-sn-glycerol-3-phosphate acyltransferase	Fatty acid and phospholipid metabolism	0.27522934
RL451_05545	yutF	Acid sugar phosphatase	Unknown function	0.2752406
RL451_00325	-	hypothetical protein	-	0.27575373
RL451_03045	-	hypothetical protein	Cellular processes	0.27634856
RL451_09530	-	hypothetical protein	-	0.27639446
RL451_09505	-	hypothetical protein	-	0.27693858
RL451_03530	-	hypothetical protein	-	0.27717798
RL451_11155	-	hypothetical protein	-	0.27728846
RL451_08850	-	hypothetical protein	-	0.277394
RL451_00645	-	-	-	0.27756443
RL451_06785	-	hypothetical protein	-	0.27925227
RL451_01665	nrdR	Transcriptional repressor NrdR	Regulatory functions	0.27935913
RL451_02460	argR_1	Arginine repressor	Amino acid biosynthesis; Regulatory functions	0.2793953
RL451_02760	-	hypothetical protein	-	0.27975553
RL451_00655	-	-	-	0.27981099
RL451_13170	rodA	Peptidoglycan glycosyltransferase RodA	Cell envelope; Cellular processes	0.28045694
RL451_03310	-	Uncharacterized protein SA1186	"Biosynthesis of cofactors, prosthetic groups, and carriers"	0.2810848
RL451_08475	-	hypothetical protein	-	0.28173868
RL451_05135	-	Putative transport protein Rv0205	Cellular processes	0.28201407
RL451_06195	-	hypothetical protein	-	0.28203908
RL451_01320	dat	D-alanine aminotransferase	Energy metabolism	0.28219668
RL451_11150	-	hypothetical protein	-	0.28337364
RL451_07455	-	hypothetical protein	DNA metabolism	0.28401499

RL451_12055	-	hypothetical protein	-	0.28408996
RL451_05260	oppB	Oligopeptide transport system permease protein OppB	Transport and binding proteins	0.28434964
RL451_03685	-	hypothetical protein	Unknown function	0.28441783
RL451_10690	ssaA	Staphylococcal secretory antigen SsaA	-	0.28453379
RL451_06430	-	hypothetical protein	Hypothetical proteins	0.28491073
RL451_00670	-	-	-	0.28531277
RL451_07585	sle1_2	N-acetylmuramoyl-L-alanine amidase sle1	Cellular processes	0.28583522
RL451_12920	luxS	S-ribosylhomocysteine lyase	-	0.28751823
RL451_08650	ldhA	L-lactate dehydrogenase 1	Energy metabolism	0.2881752
RL451_04635	-	UPF0637 protein SA0957	-	0.28846417
RL451_06025	-	hypothetical protein	-	0.28848635
RL451_01200	atl_1	Bifunctional autolysin	-	0.28923623
RL451_09545	recD2_2	ATP-dependent RecD-like DNA helicase	-	0.28946768
RL451_00520	mgt	Monofunctional glycosyltransferase	Cell envelope	0.28970361
RL451_09535	-	hypothetical protein	-	0.289709
RL451_06810	-	hypothetical protein	-	0.29019769
RL451_02840	gpsB	Cell cycle protein GpsB	-	0.29069867
RL451_00665	-	-	-	0.29082064
RL451_07100	nusG	Transcription termination/antitermination protein NusG	Transcription	0.29100224
RL451_11075	pgcA	Phosphoglucomutase	Central intermediary metabolism	0.29132705
RL451_00735	-	-	-	0.29137329
RL451_00650	-	-	-	0.29236949
RL451_11125	-	putative oxidoreductase SA2266	-	0.29246832
RL451_01710	-	hypothetical protein	DNA metabolism	0.2928353
RL451_02690	rpsA	30S ribosomal protein S1	Protein synthesis	0.29363588

RL451_01670	dnaB	Replication initiation and membrane attachment protein	DNA metabolism; Mobile and extrachromosomal element functions	0.29496656
RL451_01065	-	hypothetical protein	Protein fate	0.29515725
RL451_05670	ywqG	Uncharacterized protein YwqG	-	0.29520762
RL451_04770	-	hypothetical protein	-	0.29552509
RL451_07410	rsmA	Ribosomal RNA small subunit methyltransferase A	Protein synthesis	0.29566378
RL451_06875	-	hypothetical protein	Transport and binding proteins	0.29604719
RL451_04575	-	hypothetical protein	-	0.29611162
RL451_05500	-	hypothetical protein	-	0.29633553
RL451_05365	spsB_2	Signal peptidase IB	Protein fate	0.29753425
RL451_00705	-	-	-	0.29817703
RL451_11970	-	hypothetical protein	-	0.29832156
RL451_04295	-	hypothetical protein	Unknown function	0.29867603
RL451_12535	-	putative oxidoreductase MSMEG 2408/MSMEI 2347	-	0.29920766
RL451_07415	rnmV_2	Ribonuclease M5	Transcription	0.2992315
RL451_03050	yccX	Acylphosphatase	Protein fate	0.30022075
RL451_05730	-	hypothetical protein	-	0.30120366
RL451_12960	-	hypothetical protein	-	0.30333327
RL451_10285	isaB	Immunodominant staphylococcal antigen B	-	0.30379122
RL451_05700	-	Organic hydroperoxide resistance protein-like	Cellular processes	0.30609975
RL451_00730	-	-	-	0.30717159
RL451_10280	-	hypothetical protein	Cellular processes	0.30727289
RL451_05180	yjbI	Group 2 truncated hemoglobin YjbI	-	0.30768825
RL451_09790	-	hypothetical protein	-	0.30912074
RL451_10195	-	hypothetical protein	Energy metabolism	0.30997188
RL451_04940	sspC	Staphostatin B	-	0.31025975
RL451_04625	-	hypothetical protein	-	0.31038347

RL451_03890	xerC_1	Tyrosine recombinase XerC	DNA metabolism	0.31083479
RL451_03365	-	UPF0291 protein SA1176	DNA metabolism	0.31124214
RL451_08570	tarI	Ribitol-5-phosphate cytidylyltransferase 1	"Biosynthesis of cofactors, prosthetic groups, and carriers"	0.31162635
RL451_01405	acuC	Acetoin utilization protein AcuC	-	0.31170166
RL451_04595	purK_1	N5-carboxyaminoimidazole ribonucleotide synthase	Energy metabolism	0.31170683
RL451_00945	-	hypothetical protein	-	0.31260049
RL451_02550	proC	Pyrroline-5-carboxylate reductase	Amino acid biosynthesis	0.31265202
RL451_07605	mccB	Cystathionine gamma-lyase	-	0.31278138
RL451_10660	-	hypothetical protein	-	0.31426691
RL451_02965	-	putative CtpA-like serine protease	Protein fate	0.31510108
RL451_00740	-	-	-	0.31554203
RL451_08145	mhqA_2	Putative ring-cleaving dioxygenase MhqA	Energy metabolism	0.31591862
RL451_02240	ccpN	Transcriptional repressor CcpN	Energy metabolism	0.31602059
RL451_12875	gmuF	putative mannose-6-phosphate isomerase GmuF	Energy metabolism	0.31614894
RL451_10575	pyrD	Dihydroorotate dehydrogenase (quinone)	"Purines, pyrimidines, nucleosides, and nucleotides"	0.31628555
RL451_13175	ddl	D-alanine--D-alanine ligase	Cell envelope	0.31738508
RL451_11130	-	hypothetical protein	-	0.317588
RL451_06440	bceA_1	Bacitracin export ATP-binding protein BceA	Protein fate	0.3180113
RL451_06655	sarA	Transcriptional regulator SarA	Regulatory functions	0.3182124
RL451_00335	purB	Adenylosuccinate lyase	"Purines, pyrimidines, nucleosides, and nucleotides"	0.31895581
RL451_02625	-	hypothetical protein	-	0.31960254
RL451_13565	-	hypothetical protein	Regulatory functions	0.31969122
RL451_00725	-	-	-	0.31970254
RL451_13225	-	hypothetical protein	-	0.31974719

RL451_03635	-	Monoacylglycerol lipase	"Biosynthesis of cofactors, prosthetic groups, and carriers"	0.32015222
RL451_03275	-	Putative transport protein Rv0205	Cellular processes	0.32086975
RL451_06685	-	putative ABC transporter permease protein HI 1471	-	0.32154084
RL451_07710	lpl2_3	putative lipoprotein SA0397	-	0.32236479
RL451_13165	-	hypothetical protein	-	0.32404723
RL451_03840	uppS	Isoprenyl transferase	Cell envelope	0.32406145
RL451_02615	-	hypothetical protein	Cellular processes	0.3252231
RL451_05705	-	hypothetical protein	-	0.3253584
RL451_12550	-	hypothetical protein	-	0.32542447
RL451_09620	speG	Spermidine N(1)-acetyltransferase	-	0.32576354
RL451_10930	yjdJ	Uncharacterized protein YjdJ	Protein synthesis	0.32581765
RL451_06460	-	hypothetical protein	Protein synthesis	0.32681866
RL451_09490	-	hypothetical protein	-	0.32821963
RL451_10720	bacF	Transaminase BacF	-	0.32823112
RL451_02105	rsfS	Ribosomal silencing factor RsfS	Protein synthesis	0.32882168
RL451_09920	dnaA	Chromosomal replication initiator protein DnaA	DNA metabolism	0.32883201
RL451_00230	-	hypothetical protein	-	0.32934944
RL451_08350	yezG_5	putative antitoxin YezG	-	0.3312408
RL451_05075	-	hypothetical protein	"Purines, pyrimidines, nucleosides, and nucleotides"	0.33146554
RL451_02190	-	hypothetical protein	-	0.33162146
RL451_01030	-	hypothetical protein	-	0.33184372
RL451_08405	essB	ESAT-6 secretion machinery protein EssB	Protein fate	0.33224203
RL451_04890	lytR_1	Transcriptional regulator LytR	Regulatory functions	0.33250529
RL451_02980	-	hypothetical protein	Protein fate	0.3328474
RL451_01185	-	hypothetical protein	-	0.33292842

RL451_00695	-	-	-	0.3330104
RL451_13060	atpH	ATP synthase subunit delta	Energy metabolism	0.33317404
RL451_05995	-	hypothetical protein	Regulatory functions; Signal transduction	0.33320469
RL451_11490	-	putative amino-acid ABC transporter-binding protein HI 1080	Transport and binding proteins	0.3342116
RL451_01215	-	hypothetical protein	Protein synthesis	0.3344068
RL451_06230	-	UPF0053 protein Rv1842c	-	0.3355106
RL451_01880	yajC	Sec translocon accessory complex subunit YajC	Protein fate	0.33566445
RL451_06690	btuF	Vitamin B12-binding protein	-	0.33575381
RL451_09095	cap8A_1	Capsular polysaccharide type 8 biosynthesis protein cap8A	Transport and binding proteins	0.3363636
RL451_11985	ybbH_3	putative HTH-type transcriptional regulator YbbH	-	0.33673589
RL451_12530	adhR	HTH-type transcriptional regulator AdhR	Regulatory functions	0.33677684
RL451_12710	sepA	Multidrug resistance efflux pump SepA	-	0.33719147
RL451_11570	nasD	Nitrite reductase [NAD(P)H]	Central intermediary metabolism	0.33756639
RL451_06330	-	hypothetical protein	-	0.33864676
RL451_05255	oppC	Oligopeptide transport system permease protein OppC	Transport and binding proteins	0.33908975
RL451_02590	scpA	Segregation and condensation protein A	-	0.33918644
RL451_02835	ypsA	UPF0398 protein YpsA	-	0.33964442
RL451_02300	pbpH	Penicillin-binding protein H	Cell envelope	0.34035575
RL451_10520	-	Putative 2-dehydropantoate 2-reductase	"Biosynthesis of cofactors, prosthetic groups, and carriers"	0.34052336
RL451_09860	-	hypothetical protein	-	0.34130912
RL451_00720	-	-	-	0.34151552
RL451_09570	-	hypothetical protein	-	0.34231733
RL451_07025	hchA	Protein/nucleic acid deglycase HchA	Protein fate	0.34294405

RL451_00710	-	-	-	0.34372623
RL451_11950	-	hypothetical protein	-	0.34446984
RL451_13020	ywlG	UPF0340 protein YwlG	Hypothetical proteins	0.34510493
RL451_08440	-	hypothetical protein	-	0.34525854
RL451_09785	-	hypothetical protein	-	0.34596683
RL451_00790	rluD_1	Ribosomal large subunit pseudouridine synthase D	Protein synthesis	0.34612224
RL451_11510	-	hypothetical protein	-	0.3465347
RL451_10335	-	S-formylglutathione hydrolase	Cellular processes	0.34684814
RL451_05250	oppD_3	Oligopeptide transport ATP-binding protein OppD	Transport and binding proteins	0.34691968
RL451_01535	-	hypothetical protein	DNA metabolism	0.34694024
RL451_10855	yicL	putative inner membrane transporter YicL	Transport and binding proteins	0.34785907
RL451_02715	menG_1	Demethylmenaquinone methyltransferase	"Biosynthesis of cofactors, prosthetic groups, and carriers"	0.34914589
RL451_10415	citN	Citrate transporter	Transport and binding proteins	0.34919627
RL451_05600	-	hypothetical protein	-	0.34958869
RL451_09630	-	hypothetical protein	-	0.34973467
RL451_12275	-	hypothetical protein	-	0.35234078
RL451_02110	tam	Trans-aconitate 2-methyltransferase	"Biosynthesis of cofactors, prosthetic groups, and carriers"	0.35237925
RL451_09780	-	hypothetical protein	-	0.35245274
RL451_12145	fhuD	Iron(3+)-hydroxamate-binding protein FhuD	-	0.35342521
RL451_03055	-	hypothetical protein	-	0.3537562
RL451_05830	-	hypothetical protein	-	0.35444072
RL451_08245	nanE	Putative N-acetylmannosamine-6-phosphate 2-epimerase	-	0.35457697
RL451_12880	-	hypothetical protein	Cellular processes	0.35546484

RL451_02565	-	hypothetical protein	-	0.35592324
RL451_05185	-	UPF0413 protein SA0860	-	0.3573152
RL451_04600	ftsW	putative peptidoglycan glycosyltransferase FtsW	Cell envelope; Cellular processes	0.35796762
RL451_08855	-	hypothetical protein	-	0.35808161
RL451_07845	-	hypothetical protein	-	0.35845631
RL451_02425	accB_2	Biotin carboxyl carrier protein of acetyl-CoA carboxylase	Fatty acid and phospholipid metabolism	0.35894212
RL451_07840	-	hypothetical protein	-	0.35976921
RL451_03200	femA_1	Aminoacyltransferase FemA	Protein synthesis	0.36029798
RL451_11805	-	hypothetical protein	-	0.36047525
RL451_07030	-	Putative pyridoxal phosphate-dependent acyltransferase	-	0.36061098
RL451_05430	mnhB1	Na(+)/H(+) antiporter subunit B1	Transport and binding proteins	0.36132554
RL451_08165	slyA_2	Transcriptional regulator SlyA	-	0.36169301
RL451_11965	-	hypothetical protein	-	0.36201874
RL451_00240	-	hypothetical protein	Energy metabolism; Protein fate	0.36208438
RL451_10695	-	hypothetical protein	-	0.36411846
RL451_08525	yydK	putative HTH-type transcriptional regulator YydK	Regulatory functions	0.3646309
RL451_12885	-	hypothetical protein	-	0.36489942
RL451_02435	-	Uncharacterized protein Spy1535	-	0.36517292
RL451_12130	ureA	Urease subunit gamma	Central intermediary metabolism	0.36607473
RL451_05330	yitU	5-amino-6-(5-phospho-D-ribitylamino)uracil phosphatase YitU	Unknown function	0.36632868
RL451_00715	-	-	-	0.36659623
RL451_00205	btuD_2	Vitamin B12 import ATP-binding protein BtuD	-	0.36661312
RL451_04100	rpoZ	DNA-directed RNA polymerase subunit omega	Transcription	0.36663248

RL451_06790	-	hypothetical protein	-	0.3676147
RL451_02440	nusB	Transcription antitermination protein NusB	Transcription	0.36769484
RL451_00690	-	-	-	0.36771404
RL451_06420	sle1_1	N-acetylmuramoyl-L-alanine amidase sle1	Cellular processes	0.36780072
RL451_07890	xpt	Xanthine phosphoribosyltransferase	"Purines, pyrimidines, nucleosides, and nucleotides"	0.36818872
RL451_08330	yezG_1	putative antitoxin YezG	-	0.36855355
RL451_01910	-	hypothetical protein	Cell envelope; Cellular processes	0.36859017
RL451_12620	opuD_3	Glycine betaine transporter OpuD	Transport and binding proteins	0.36910783
RL451_07555	hdfR_1	HTH-type transcriptional regulator HdfR	-	0.37037891
RL451_05345	-	Uncharacterized protein SA0829	-	0.37103341
RL451_11640	gltT	Proton/sodium-glutamate symport protein	-	0.37107701
RL451_06885	-	hypothetical protein	-	0.37167737
RL451_11705	yhfP	Putative quinone oxidoreductase YhfP	Unknown function	0.37392684
RL451_05510	dltD	Protein DltD	-	0.37411265
RL451_04580	-	hypothetical protein	-	0.37427812
RL451_04225	ftsA	Cell division protein FtsA	Cellular processes	0.37695916
RL451_09760	-	hypothetical protein	-	0.37953053
RL451_00535	tagH_1	Teichoic acids export ATP-binding protein TagH	Transport and binding proteins	0.38049393
RL451_05410	yugI	General stress protein 13	Transcription	0.3805953
RL451_09525	-	hypothetical protein	-	0.38096037
RL451_00815	-	UPF0342 protein SA1663	Transport and binding proteins	0.38299047
RL451_06305	yciC_1	Putative metal chaperone YciC	"Biosynthesis of cofactors, prosthetic groups, and carriers"	0.38305825
RL451_00830	-	hypothetical protein	Cellular processes; DNA metabolism	0.38309627

RL451_05360	spsB_1	Signal peptidase IB	Protein fate	0.38457036
RL451_10710	crtM	Dehydrosqualene synthase	-	0.3859672
RL451_05170	-	hypothetical protein	-	0.38613578
RL451_07580	-	hypothetical protein	-	0.38644959
RL451_05245	oppF_2	Oligopeptide transport ATP-binding protein OppF	Transport and binding proteins	0.38707364
RL451_10895	-	hypothetical protein	Cell envelope; Protein fate	0.38723613
RL451_10675	isaA	putative transglycosylase IsaA	-	0.38740335
RL451_06455	-	hypothetical protein	Hypothetical proteins	0.38746558
RL451_04455	-	hypothetical protein	-	0.38780913
RL451_11840	-	Putative 3-methyladenine DNA glycosylase	DNA metabolism	0.3884328
RL451_06130	btuD_5	Vitamin B12 import ATP-binding protein BtuD	Transport and binding proteins	0.38855864
RL451_05720	-	hypothetical protein	-	0.38902766
RL451_06235	nagA	N-acetylglucosamine-6-phosphate deacetylase	Central intermediary metabolism	0.38962485
RL451_11820	-	hypothetical protein	Unknown function	0.38965453
RL451_08985	cmpD	Bicarbonate transport ATP-binding protein CmpD	Transport and binding proteins	0.38975355
RL451_04765	rlmI	Ribosomal RNA large subunit methyltransferase I	Protein synthesis	0.39032697
RL451_06415	-	hypothetical protein	-	0.39034982
RL451_13025	glyA	Serine hydroxymethyltransferase	Cellular processes	0.3913345
RL451_02695	der_1	GTPase Der	Protein synthesis	0.39230028
RL451_03585	-	hypothetical protein	-	0.39339401
RL451_00510	-	hypothetical protein	Regulatory functions	0.3938101
RL451_05040	-	hypothetical protein	Cell envelope	0.39417594
RL451_09380	-	putative lipoprotein SAOUHSC 00053	-	0.39453508
RL451_00980	-	hypothetical protein	-	0.3949686
RL451_08340	yezG_3	putative antitoxin YezG	-	0.3950195
RL451_08565	tarJ	Ribulose-5-phosphate reductase 1	Energy metabolism	0.3955382
RL451_12170	modA	Molybdate-binding protein ModA	Transport and binding proteins	0.39640544

RL451_05735	-	hypothetical protein	-	0.3968286
RL451_02855	-	hypothetical protein	-	0.39700213
RL451_03305	plsY	Glycerol-3-phosphate acyltransferase	Fatty acid and phospholipid metabolism	0.39705236
RL451_07690	-	hypothetical protein	Cellular processes; DNA metabolism	0.39725148
RL451_07900	-	hypothetical protein	-	0.39726515
RL451_02555	-	putative oxidoreductase SA2266	-	0.39744166
RL451_13055	atpF	ATP synthase subunit b	Energy metabolism	0.39747849
RL451_01905	dtd	D-aminoacyl-tRNA deacylase	Protein synthesis	0.39849276
RL451_11960	-	Phosphorylated carbohydrates phosphatase TM 1254	-	0.39853039
RL451_06890	ung	Uracil-DNA glycosylase	DNA metabolism	0.40219967
RL451_01335	ytnP	putative quorum-quenching lactonase YtnP	Transcription	0.40300164
RL451_00540	-	hypothetical protein	-	0.4031377
RL451_08300	-	putative ABC transporter permease Rv0072	Transport and binding proteins	0.40396263
RL451_13250	mazF	Endoribonuclease MazF	Unknown function	0.40415866
RL451_06575	mntR	Transcriptional regulator MntR	-	0.40498375
RL451_09410	-	hypothetical protein	-	0.40549048
RL451_01870	queA	S-adenosylmethionine:tRNA ribosyltransferase-isomerase	Protein synthesis	0.4055717
RL451_08495	rbsD	D-ribose pyranase	-	0.40684573
RL451_02415	ypdF	Aminopeptidase YpdF	Protein fate	0.40703022
RL451_05675	gcvH	Glycine cleavage system H protein	Energy metabolism	0.40728597
RL451_04775	-	hypothetical protein	-	0.40787186
RL451_00370	gatC_1	Aspartyl/glutamyl-tRNA(Asn/Gln) amidotransferase subunit C	Protein synthesis	0.40809932
RL451_05050	-	Lipoate--protein ligase 1	Protein fate	0.41025789
RL451_06465	-	hypothetical protein	-	0.41109186

RL451_10555	-	hypothetical protein	-	0.41118516
RL451_07835	-	hypothetical protein	-	0.41181354
RL451_10570	-	hypothetical protein	-	0.41245247
RL451_08125	ydaF	Putative ribosomal N-acetyltransferase YdaF	-	0.41306583
RL451_01190	sigS	RNA polymerase sigma factor SigS	-	0.41343844
RL451_02310	yqgN	Uncharacterized protein YqgN	Central intermediary metabolism	0.41350904
RL451_08105	tatC2	Sec-independent protein translocase protein TatCy	Protein fate	0.41417406
RL451_04705	-	hypothetical protein	Cellular processes; DNA metabolism	0.41452841
RL451_08445	-	hypothetical protein	-	0.41466888
RL451_13455	-	hypothetical protein	-	0.41501465
RL451_02560	-	hypothetical protein	-	0.41541995
RL451_07470	speA	Arginine decarboxylase	-	0.41548434
RL451_03260	msrR	Regulatory protein MsrR	Regulatory functions	0.41554168
RL451_11700	-	hypothetical protein	Protein synthesis	0.41582376
RL451_10790	ogt	Methylated-DNA--protein-cysteine methyltransferase	DNA metabolism	0.41655305
RL451_04995	catD	Putative oxidoreductase CatD	-	0.41755863
RL451_06385	-	hypothetical protein	-	0.41792311
RL451_11845	-	hypothetical protein	-	0.41851729
RL451_06705	ywiB	putative beta-barrel protein YwiB	-	0.41943893
RL451_00295	pheA	Prephenate dehydratase	-	0.41949756
RL451_02865	der_2	GTPase Der	Protein synthesis	0.41995341
RL451_12290	glcU_2	putative glucose uptake protein GlcU	Transport and binding proteins	0.42053842
RL451_01485	-	hypothetical protein	-	0.42099649
RL451_13400	yheS	putative ABC transporter ATP-binding protein YheS	-	0.42132362
RL451_03460	-	hypothetical protein	Transport and binding proteins	0.42185694
RL451_02970	-	hypothetical protein	Protein synthesis	0.42204413

RL451_01675	dnaI	Primosomal protein DnaI	DNA metabolism	0.42298168
RL451_01490	glpQ_1	Glycerophosphodiester phosphodiesterase	-	0.42300644
RL451_09915	dnaN	Beta sliding clamp	DNA metabolism	0.42330608
RL451_06350	-	hypothetical protein	-	0.42340302
RL451_06355	-	hypothetical protein	Cellular processes; Regulatory functions	0.42409007
RL451_04570	-	hypothetical protein	Cellular processes; Transport and binding proteins	0.42452972
RL451_04745	-	hypothetical protein	-	0.42483334
RL451_01035	-	hypothetical protein	-	0.4263242
RL451_02430	cfiB	2-oxoglutarate carboxylase small subunit	Fatty acid and phospholipid metabolism	0.4266127
RL451_06280	-	hypothetical protein	-	0.42674604
RL451_07320	hpt	Hypoxanthine-guanine phosphoribosyltransferase	"Purines, pyrimidines, nucleosides, and nucleotides"	0.4275483
RL451_01300	murJ	Lipid II flippase MurJ	Cellular processes	0.42843794
RL451_02465	recN	DNA repair protein RecN	DNA metabolism	0.42892147
RL451_03785	truB	tRNA pseudouridine synthase B	Protein synthesis	0.42970402
RL451_05295	-	hypothetical protein	-	0.43000685
RL451_04025	-	Uncharacterized protein Spy1614	-	0.430573
RL451_13575	-	hypothetical protein	-	0.43221857
RL451_06155	kipI_2	Kinase A inhibitor	Hypothetical proteins	0.43301584
RL451_03535	-	hypothetical protein	-	0.43333495
RL451_08575	tarF	Teichoic acid glycerol-phosphate transferase	-	0.43334585
RL451_03415	-	hypothetical protein	-	0.43370847
RL451_12760	-	-	-	0.43378717
RL451_01940	-	putative AAA domain-containing protein Rv2559c	DNA metabolism	0.43471765
RL451_09355	-	hypothetical protein	-	0.43543715

RL451_08420	esaA	ESAT-6 secretion accessory factor EsaA	-	0.43715495
RL451_11080	nudG	CTP pyrophosphohydrolase	DNA metabolism	0.43740613
RL451_03565	-	hypothetical protein	-	0.43813787
RL451_11785	bcr_2	Bicyclomycin resistance protein	-	0.43847526
RL451_07965	-	hypothetical protein	Protein fate	0.44006668
RL451_08990	-	hypothetical protein	-	0.44022262
RL451_00460	-	hypothetical protein	-	0.44167357
RL451_10860	-	hypothetical protein	-	0.44315581
RL451_05540	ghrB_2	Glyoxylate/hydroxypyruvate reductase B	Amino acid biosynthesis	0.44378622
RL451_00575	hemL2	"Glutamate-1-semialdehyde 2,1-aminomutase 2"	"Biosynthesis of cofactors, prosthetic groups, and carriers"	0.44392451
RL451_04895	-	hypothetical protein	-	0.4459313
RL451_02720	hepT	Heptaprenyl diphosphate synthase component 2	"Biosynthesis of cofactors, prosthetic groups, and carriers"	0.44594292
RL451_09105	-	hypothetical protein	-	0.44613782
RL451_06435	bceB_1	Bacitracin export permease protein BceB	-	0.44652643
RL451_00805	-	hypothetical protein	Regulatory functions	0.44737511
RL451_11855	yhaP	Uncharacterized protein YhaP	"Purines, pyrimidines, nucleosides, and nucleotides"	0.44892703
RL451_10590	-	hypothetical protein	-	0.4515233
RL451_04640	mntH_2	Divalent metal cation transporter MntH	Transport and binding proteins	0.45219395
RL451_11340	flp	Protein flp	-	0.45219997
RL451_08395	-	hypothetical protein	-	0.45221266
RL451_03080	yxeP_1	putative hydrolase YxeP	Protein fate	0.45259964
RL451_09740	-	hypothetical protein	-	0.45356342
RL451_11375	bcr_1	Bicyclomycin resistance protein	-	0.45533027

RL451_10995	ywaC	GTP pyrophosphokinase YwaC	Cellular processes	0.45577588
RL451_13520	-	putative leukocidin-like protein 1	Cellular processes	0.4558112
RL451_01975	yrrB	TPR repeat-containing protein YrrB	-	0.45604951
RL451_03985	rnc	Ribonuclease 3	Transcription	0.45728494
RL451_06540	tarD	Glycerol-3-phosphate cytidylyltransferase	Cell envelope	0.45762199
RL451_07005	ppaX	Pyrophosphatase PpaX	-	0.45884994
RL451_05580	-	hypothetical protein	-	0.45969635
RL451_11815	-	hypothetical protein	-	0.46001806
RL451_05860	cggR	Central glycolytic genes regulator	DNA metabolism	0.46035578
RL451_08345	yezG_4	putative antitoxin YezG	-	0.46106115
RL451_11485	emrB	Multidrug export protein EmrB	Cellular processes; Transport and binding proteins	0.46118123
RL451_05495	yjlD	NADH dehydrogenase-like protein YjlD	-	0.46134811
RL451_11495	tcyB	L-cystine transport system permease protein TcyB	-	0.46308622
RL451_09575	-	hypothetical protein	-	0.46317173
RL451_02545	rnz	Ribonuclease Z	Transcription	0.46344695
RL451_09500	-	hypothetical protein	-	0.46384661
RL451_06805	-	hypothetical protein	-	0.46499672
RL451_01040	-	hypothetical protein	-	0.46517176
RL451_10250	-	N-carbamoylsarcosine amidase	-	0.46619551
RL451_05435	mnhC1	Na(+)/H(+) antiporter subunit C1	Transport and binding proteins	0.46647149
RL451_05445	mnhE1	Na(+)/H(+) antiporter subunit E1	Transport and binding proteins	0.46654076
RL451_04230	divIB	Cell division protein DivIB	Cell envelope; Transport and binding proteins	0.46723607
RL451_02100	-	hypothetical protein	Unknown function	0.46747046
RL451_07905	-	Uncharacterized protein SA0370	DNA metabolism	0.46762542
RL451_08335	yezG_2	putative antitoxin YezG	-	0.46814315

RL451_02675	cmk	Cytidylate kinase	"Purines, pyrimidines, nucleosides, and nucleotides"	0.46887441
RL451_04120	-	hypothetical protein	-	0.46957757
RL451_03380	-	hypothetical protein	-	0.46985477
RL451_02445	xseA	Exodeoxyribonuclease 7 large subunit	DNA metabolism	0.47030659
RL451_05285	map_3	Protein map	-	0.4707653
RL451_11720	-	hypothetical protein	Mobile and extrachromosomal element functions	0.47171573
RL451_00305	pncB2	Nicotinate phosphoribosyltransferase pncB2	"Biosynthesis of cofactors, prosthetic groups, and carriers"	0.47353277
RL451_02540	zwf	Glucose-6-phosphate 1-dehydrogenase	Energy metabolism	0.47538058
RL451_11285	yveA	Aspartate-proton symporter	Transport and binding proteins	0.47587102
RL451_04365	scn_2	Staphylococcal complement inhibitor	-	0.47622873
RL451_12865	czrA	HTH-type transcriptional repressor CzrA	Regulatory functions	0.47704787
RL451_01950	-	UPF0337 protein SA1452	-	0.47759972
RL451_13485	-	hypothetical protein	-	0.47760618
RL451_01900	relA	GTP pyrophosphokinase	Cellular processes	0.47813755
RL451_05555	-	hypothetical protein	-	0.47881557
RL451_04970	menA	"1,4-dihydroxy-2-naphthoate octaprenyltransferase"	"Biosynthesis of cofactors, prosthetic groups, and carriers"	0.47889577
RL451_13290	-	-	-	0.47957801
RL451_05655	metN2	Methionine import ATP-binding protein MetN 2	-	0.48087888
RL451_04045	rsgA	Small ribosomal subunit biogenesis GTPase RsgA	Protein synthesis	0.48132839
RL451_10465	-	hypothetical protein	-	0.48174581
RL451_07685	-	hypothetical protein	-	0.48271623
RL451_08975	ssuC	Putative aliphatic sulfonates transport permease protein SsuC	Transport and binding proteins	0.48325556

RL451_05355	addB	ATP-dependent helicase/deoxyribonuclease subunit B	DNA metabolism	0.48340836
RL451_05905	dapH_2	"2,3,4,5-tetrahydropyridine-2,6-dicarboxylate N-acetyltransferase"	-	0.48382709
RL451_12185	-	hypothetical protein	"Biosynthesis of cofactors, prosthetic groups, and carriers"	0.48415778
RL451_06545	tagX	Putative glycosyltransferase TagX	-	0.48422496
RL451_10355	-	hypothetical protein	Cellular processes	0.48648304
RL451_08555	-	hypothetical protein	-	0.48746475
RL451_05465	-	Putative esterase PA1618	-	0.48760937
RL451_05085	-	Serine protease HtrA-like	Protein fate	0.48766388
RL451_05890	-	Nucleotide-binding protein SA0720	Transport and binding proteins	0.48799588
RL451_04720	-	hypothetical protein	-	0.48822095
RL451_13150	cls_2	Cardiolipin synthase	-	0.49051025
RL451_04170	lspA	Lipoprotein signal peptidase	Protein fate	0.49151827
RL451_06270	-	hypothetical protein	-	0.49158438
RL451_13590	-	hypothetical protein	-	0.4935763
RL451_03100	asd	Aspartate-semialdehyde dehydrogenase	Amino acid biosynthesis	0.49550796
RL451_08545	ypdA	Sensor histidine kinase YpdA	Signal transduction	0.49593782
RL451_13480	-	hypothetical protein	-	0.49594729
RL451_06880	ywdK	UPF0382 membrane protein YwdK	-	0.49619532
RL451_02450	xseB	Exodeoxyribonuclease 7 small subunit	DNA metabolism	0.49624871
RL451_06870	-	hypothetical protein	-	0.49663908
RL451_04250	ftsL	Cell division protein FtsL	Cellular processes	0.49776933
RL451_04480	-	Putative TrmH family tRNA/rRNA methyltransferase	Protein synthesis	0.4978609
RL451_00780	-	hypothetical protein	-	0.4980631
RL451_05210	trpS	Tryptophan--tRNA ligase	Protein synthesis	0.49924372
RL451_12690	ydjM	Inner membrane protein YdjM	Energy metabolism	0.49926695

RL451_05100	-	hypothetical protein	-	2.00435181
RL451_05395	gluD	NAD-specific glutamate dehydrogenase	Cellular processes	2.0046877
RL451_13080	atpC	ATP synthase epsilon chain	Energy metabolism	2.00539957
RL451_11915	yxeP_4	putative hydrolase YxeP	Protein fate	2.00741794
RL451_11200	-	hypothetical protein	-	2.01263587
RL451_10165	ywqE_2	Tyrosine-protein phosphatase YwqE	-	2.01327799
RL451_02385	gcvPA	putative glycine dehydrogenase (decarboxylating) subunit 1	Energy metabolism	2.02313608
RL451_01730	clpX	ATP-dependent Clp protease ATP-binding subunit ClpX	Protein fate	2.0264924
RL451_08010	rpsF	30S ribosomal protein S6	Protein synthesis	2.03399142
RL451_12135	-	Urea transporter DVU1160	Transport and binding proteins	2.03514285
RL451_13075	atpD	ATP synthase subunit beta	Energy metabolism	2.03767917
RL451_10295	argR_2	Arginine repressor	Amino acid biosynthesis; Regulatory functions	2.04680904
RL451_08090	-	hypothetical protein	Regulatory functions	2.04802894
RL451_03740	phaB	Acetoacetyl-CoA reductase	-	2.04809199
RL451_13680	-	hypothetical protein	-	2.04949513
RL451_06610	mrpE	Na(+)/H(+) antiporter subunit E	Transport and binding proteins	2.05237382
RL451_08905	ipdC	Indole-3-pyruvate decarboxylase	Central intermediary metabolism	2.05306532
RL451_03610	-	hypothetical protein	Energy metabolism	2.05411603
RL451_07875	guaA	GMP synthase [glutamine-hydrolyzing]	"Purines, pyrimidines, nucleosides, and nucleotides"	2.05459751
RL451_10870	-	hypothetical protein	Energy metabolism	2.06323597
RL451_09985	bceA_2	Bacitracin export ATP-binding protein BceA	Cellular processes; Transport and binding proteins	2.06353554
RL451_04290	-	-	-	2.06356376
RL451_06660	pip	Proline iminopeptidase	Energy metabolism	2.06526491

RL451_11725	lctP_2	L-lactate permease	Transport and binding proteins	2.06612012
RL451_07600	metN	Methionine import ATP-binding protein MetN	-	2.06994
RL451_00315	-	UPF0316 protein SA1727	-	2.07191302
RL451_09285	sarU	HTH-type transcriptional regulator SarU	Regulatory functions	2.07700336
RL451_06945	nagB_2	Glucosamine-6-phosphate deaminase	Central intermediary metabolism	2.07989159
RL451_00250	-	hypothetical protein	-	2.08039788
RL451_10940	mhqA_3	Putative ring-cleaving dioxygenase MhqA	-	2.08513166
RL451_11540	-	hypothetical protein	Transport and binding proteins	2.08521366
RL451_09010	ybaN	Inner membrane protein YbaN	-	2.08549003
RL451_03395	rpmG1	50S ribosomal protein L33 1	Protein synthesis	2.09147802
RL451_01345	pepA_1	Glutamyl aminopeptidase	Protein fate	2.09484341
RL451_00045	-	hypothetical protein	-	2.09511415
RL451_03970	-	UPF0122 protein SAV1236	-	2.09635418
RL451_05205	spxA	Regulatory protein Spx	Regulatory functions	2.09894865
RL451_04655	potD	Spermidine/putrescine-binding periplasmic protein	Transport and binding proteins	2.10083099
RL451_03910	femA_2	Aminoacyltransferase FemA	Unknown function	2.10177715
RL451_05200	mecA	Adapter protein MecA 1	-	2.10242508
RL451_06915	yhfS	Putative acetyl-CoA C-acetyltransferase YhfS	Fatty acid and phospholipid metabolism	2.11454864
RL451_03020	-	hypothetical protein	-	2.11637542
RL451_07345	-	hypothetical protein	Unknown function	2.11858559
RL451_12490	rpsI	30S ribosomal protein S9	Protein synthesis	2.12255426
RL451_05960	secA1_1	Protein translocase subunit SecA 1	Protein fate	2.12344313
RL451_02955	crr	PTS system glucose-specific EIIA component	-	2.12356207
RL451_05770	ssp	Extracellular matrix protein-binding protein emp	-	2.12467766
RL451_09750	-	hypothetical protein	-	2.13841496

RL451_04955	menD	2-succinyl-5-enolpyruvyl-6-hydroxy-3- cyclohexene-1-carboxylate synthase	"Biosynthesis of cofactors, prosthetic groups, and carriers"	2.14068499
RL451_04005	plsX	Phosphate acyltransferase	Fatty acid and phospholipid metabolism	2.14361326
RL451_09970	cspLA	Cold shock-like protein CspLA	Cellular processes; DNA metabolism	2.1444146
RL451_11745	hssS	Heme sensor protein HssS	Signal transduction	2.1468147
RL451_00015	-	hypothetical protein	-	2.14884087
RL451_08620	gatA_2	PTS system galactitol-specific EIIA component	Signal transduction; Transport and binding proteins	2.1572093
RL451_06490	dhaL	"PTS-dependent dihydroxyacetone kinase, ADP-binding subunit DhaL"	-	2.16041787
RL451_12120	ureC	Urease subunit alpha	Central intermediary metabolism	2.16087915
RL451_12370	rpsQ	30S ribosomal protein S17	Protein synthesis	2.16400974
RL451_04710	def	Peptide deformylase	Protein fate	2.16762859
RL451_03335	sbcC	Nuclease SbcCD subunit C	-	2.17401475
RL451_02960	-	UPF0346 protein MW1311	-	2.17694111
RL451_12615	-	Zinc-type alcohol dehydrogenase-like protein SA1988	Energy metabolism	2.17891795
RL451_08840	-	hypothetical protein	Transport and binding proteins	2.17916551
RL451_07940	-	hypothetical protein	-	2.17931449
RL451_09225	-	hypothetical protein	-	2.18362926
RL451_09885	hutH	Histidine ammonia-lyase	Energy metabolism	2.1940134
RL451_05920	uvrA	UvrABC system protein A	DNA metabolism	2.19690247
RL451_00990	splB	Serine protease SplB	Protein fate; Regulatory functions	2.1996795
RL451_02250	dnaG	DNA primase	DNA metabolism	2.20454792
RL451_03205	trpA	Tryptophan synthase alpha chain	Amino acid biosynthesis	2.2050485

RL451_02640	-	Ferredoxin	Central intermediary metabolism	2.20641144
RL451_06060	fatD	Ferric-anguibactin transport system permease protein FatD	-	2.2067142
RL451_12355	rpsC	30S ribosomal protein S3	Protein synthesis	2.20879981
RL451_04165	rluD_2	Ribosomal large subunit pseudouridine synthase D	Protein synthesis	2.21256578
RL451_01895	apt	Adenine phosphoribosyltransferase	"Purines, pyrimidines, nucleosides, and nucleotides"	2.21397612
RL451_08885	murQ	N-acetylmuramic acid 6-phosphate etherase	Cell envelope	2.22016629
RL451_10270	manP	PTS system mannose-specific EIIBCA component	-	2.22175276
RL451_00470	vraR	Response regulator protein VraR	Cellular processes	2.22384127
RL451_11290	-	hypothetical protein	-	2.2262857
RL451_12375	rplN	50S ribosomal protein L14	Protein synthesis	2.22632177
RL451_02040	accB_1	Biotin carboxyl carrier protein of acetyl-CoA carboxylase	Fatty acid and phospholipid metabolism	2.23043795
RL451_04350	hly	Alpha-hemolysin	Cellular processes	2.23481728
RL451_10240	gtf2	Glycosyltransferase-stabilizing protein Gtf2	Protein fate	2.23709317
RL451_09825	walR	Transcriptional regulatory protein WalR	Regulatory functions; Signal transduction	2.23830601
RL451_09130	glnQ	Glutamine transport ATP-binding protein GlnQ	Transport and binding proteins	2.23918614
RL451_13185	cshA	DEAD-box ATP-dependent RNA helicase CshA	DNA metabolism	2.24144288
RL451_01520	thiI	putative tRNA sulfurtransferase	"Biosynthesis of cofactors, prosthetic groups, and carriers; Protein synthesis"	2.24546455
RL451_11215	gsiD	Glutathione transport system permease protein GsiD	Transport and binding proteins	2.24556312
RL451_00130	sak	Staphylokinase	-	2.2458081
RL451_00885	hemH	Ferrochelatase	"Biosynthesis of cofactors, prosthetic groups, and carriers"	2.24690347

RL451_10600	-	Baeyer-Villiger flavin-containing monooxygenase	Unknown function	2.24717047
RL451_03110	ybiT	putative ABC transporter ATP-binding protein YbiT	-	2.25191588
RL451_02035	kipA_1	KipI antagonist	Unknown function	2.25472733
RL451_07770	-	hypothetical protein	-	2.25684889
RL451_01285	-	Sulfurtransferase Alvin 2599	Protein synthesis	2.25776921
RL451_03025	nirQ	Denitrification regulatory protein NirQ	Cellular processes	2.25868601
RL451_10020	cna	Collagen adhesin	-	2.27200716
RL451_11795	aaeA	p-hydroxybenzoic acid efflux pump subunit AaeA	Transport and binding proteins	2.2769168
RL451_12510	aldC_2	Alpha-acetolactate decarboxylase	Energy metabolism	2.28159087
RL451_11330	panE	2-dehydropantoate 2-reductase	"Biosynthesis of cofactors, prosthetic groups, and carriers"	2.28344065
RL451_12505	alsS	Acetolactate synthase	Energy metabolism	2.28557062
RL451_08050	yitJ	"Bifunctional homocysteine S-methyltransferase/5,10-methylenetetrahydrofolate reductase"	Amino acid biosynthesis	2.28731647
RL451_05165	yjbM	GTP pyrophosphokinase YjbM	Cellular processes	2.29331165
RL451_04410	murI	Glutamate racemase	Cell envelope	2.29977927
RL451_12140	ydbM	Putative acyl-CoA dehydrogenase YdbM	-	2.30117206
RL451_00360	-	hypothetical protein	Cellular processes	2.30475205
RL451_11165	-	hypothetical protein	Transport and binding proteins	2.30525987
RL451_12575	lacB	Galactose-6-phosphate isomerase subunit LacB	Energy metabolism	2.3060949
RL451_12975	yodB	HTH-type transcriptional regulator YodB	-	2.3064619
RL451_07290	folK	2-amino-4-hydroxy-6- hydroxymethyldihydropteridine pyrophosphokinase	"Biosynthesis of cofactors, prosthetic groups, and carriers"	2.30899281
RL451_06955	bshB2	putative N-acetyl-alpha-D-glucosaminyl L-malate deacetylase 2	"Biosynthesis of cofactors, prosthetic groups, and carriers"	2.31198145

RL451_04245	pbpB	Penicillin-binding protein 2B	Cell envelope; Cellular processes	2.31586455
RL451_13530	xerC_2	Tyrosine recombinase XerC	DNA metabolism	2.31924176
RL451_10920	-	Putative NAD(P)H nitroreductase SA2311	"Biosynthesis of cofactors, prosthetic groups, and carriers"	2.3192509
RL451_00955	lukEv	Leucotoxin LukEv	Cellular processes	2.31986156
RL451_06935	hxlB	3-hexulose-6-phosphate isomerase	-	2.32257979
RL451_11100	-	Uncharacterized protein SA2269	-	2.33759262
RL451_11425	bioB	Biotin synthase	"Biosynthesis of cofactors, prosthetic groups, and carriers"	2.34205179
RL451_02350	comGC	ComG operon protein 3	Cellular processes; Protein fate	2.3462745
RL451_00410	-	Putative bifunctional exonuclease/endonuclease protein Rv2191	DNA metabolism	2.34735791
RL451_12790	glmM	Phosphoglucosamine mutase	Cell envelope; Central intermediary metabolism	2.3531239
RL451_05460	-	hypothetical protein	Protein synthesis	2.35676412
RL451_02140	lepA	Elongation factor 4	Unknown function	2.35733693
RL451_06640	-	hypothetical protein	-	2.36262604
RL451_10525	panB	3-methyl-2-oxobutanoate hydroxymethyltransferase	"Biosynthesis of cofactors, prosthetic groups, and carriers"	2.36950115
RL451_01840	-	hypothetical protein	-	2.36988132
RL451_10620	-	hypothetical protein	-	2.37994169
RL451_05970	-	hypothetical protein	Cellular processes	2.3870566
RL451_05780	-	hypothetical protein	-	2.40176987
RL451_05840	gpmI	"2,3-bisphosphoglycerate-independent phosphoglycerate mutase"	Energy metabolism	2.40278962

RL451_09275	yfiZ_1	putative siderophore transport system permease protein YfiZ	-	2.42118451
RL451_03800	rplGA	putative ribosomal protein YlxQ	-	2.42451839
RL451_06315	-	Putative multidrug export ATP-binding/permease protein SA1683	-	2.42899697
RL451_10260	-	hypothetical protein	-	2.43295343
RL451_08965	-	hypothetical protein	-	2.43601133
RL451_10235	gtf1_3	Glycosyltransferase Gtf1	Protein fate	2.43884826
RL451_12670	yfiZ_2	putative siderophore transport system permease protein YfiZ	-	2.44309565
RL451_05775	-	hypothetical protein	-	2.44983778
RL451_11435	bioW	6-carboxyhexanoate--CoA ligase	"Biosynthesis of cofactors, prosthetic groups, and carriers"	2.45229474
RL451_08765	uhpT	Hexose-6-phosphate:phosphate antiporter	Transport and binding proteins	2.45312661
RL451_09585	-	hypothetical protein	-	2.4574211
RL451_07040	tuf	Elongation factor Tu	Protein synthesis	2.47080747
RL451_06445	graS_1	Sensor histidine kinase GraS	Signal transduction	2.47464298
RL451_02820	recU	Holliday junction resolvase RecU	DNA metabolism	2.476229
RL451_11770	tcaR	HTH-type transcriptional regulator TcaR	-	2.47990653
RL451_10765	ydfJ	Membrane protein YdfJ	Transport and binding proteins	2.48109023
RL451_01965	iscS_2	Cysteine desulfurase IscS	-	2.4850682
RL451_10265	yvyI	Putative mannose-6-phosphate isomerase YvyI	Energy metabolism	2.48523997
RL451_12970	murA2	UDP-N-acetylglucosamine 1-carboxyvinyltransferase 2	Cell envelope	2.4882012
RL451_01915	hisS	Histidine--tRNA ligase	Protein synthesis	2.49714022
RL451_12385	rplE	50S ribosomal protein L5	Energy metabolism	2.49974753
RL451_03145	phoU	Phosphate-specific transport system accessory protein PhoU	Regulatory functions; Transport and binding proteins	2.500988

RL451_01785	valS	Valine--tRNA ligase	Protein synthesis	2.50812186
RL451_12985	rho	Transcription termination factor Rho	Transcription	2.51654547
RL451_05595	yfjD	UPF0053 inner membrane protein YfjD	-	2.53251034
RL451_03390	rpsN2	Alternate 30S ribosomal protein S14	-	2.53611061
RL451_08080	btuD_6	Vitamin B12 import ATP-binding protein BtuD	-	2.53688303
RL451_09695	-	IS6 family transposase IS431R	-	2.53766283
RL451_05630	sufC	Vegetative protein 296	"Biosynthesis of cofactors, prosthetic groups, and carriers"	2.54157697
RL451_04990	yfmC_1	Fe(3+)-citrate-binding protein YfmC	-	2.553701
RL451_02225	era	GTPase Era	Protein synthesis	2.55608021
RL451_04490	isdG_1	Heme oxygenase (staphylobilin-producing) 1	Amino acid biosynthesis	2.56012808
RL451_13685	-	hypothetical protein	-	2.56211304
RL451_10785	clpL	ATP-dependent Clp protease ATP-binding subunit ClpL	Protein fate	2.56442745
RL451_01525	yfcA	putative membrane transporter protein YfcA	-	2.56989536
RL451_09995	nhoA	N-hydroxyarylamine O-acetyltransferase	-	2.57195435
RL451_04285	-	Antibacterial protein 3	-	2.57600066
RL451_03440	yclM	Aspartokinase 3	Amino acid biosynthesis	2.58822634
RL451_10910	ybiV	Sugar phosphatase YbiV	Unknown function	2.58887885
RL451_06845	galK	Galactokinase	Central intermediary metabolism	2.61094073
RL451_09040	-	hypothetical protein	-	2.61103827
RL451_07310	hslO	33 kDa chaperonin	-	2.61434804
RL451_13410	yeeE	UPF0394 inner membrane protein YeeE	-	2.62080715
RL451_06080	nrdI	Protein NrdI	"Purines, pyrimidines, nucleosides, and nucleotides"	2.62323603

RL451_07785	-	hypothetical protein	"Biosynthesis of cofactors, prosthetic groups, and carriers"	2.62407256
RL451_12390	rpsZ	30S ribosomal protein S14 type Z	Hypothetical proteins	2.62418175
RL451_03130	-	hypothetical protein	Transport and binding proteins	2.6363674
RL451_03945	rplS	50S ribosomal protein L19	Protein synthesis	2.63732579
RL451_04525	isdB	Iron-regulated surface determinant protein B	-	2.65017079
RL451_08685	carA_2	Caffeate CoA-transferase	-	2.65242732
RL451_11245	yehR	putative lipoprotein YehR	Transport and binding proteins	2.65385039
RL451_10580	-	hypothetical protein	-	2.65681961
RL451_03170	-	hypothetical protein	Transport and binding proteins	2.66132582
RL451_04425	sdhC	Succinate dehydrogenase cytochrome b558 subunit	Energy metabolism	2.66229111
RL451_13445	agrA	Accessory gene regulator A	Central intermediary metabolism; Regulatory functions; Signal transduction	2.66520612
RL451_03760	ftsK	DNA translocase FtsK	Protein fate	2.67507648
RL451_00270	ppaC	putative manganese-dependent inorganic pyrophosphatase	-	2.67586066
RL451_03600	glnA	Glutamine synthetase	Amino acid biosynthesis	2.68087368
RL451_12580	lacC_2	Tagatose-6-phosphate kinase	Energy metabolism	2.68405395
RL451_03210	trpB	Tryptophan synthase beta chain	Amino acid biosynthesis	2.68781525
RL451_10775	feoB	Fe(2+) transporter FeoB	Transport and binding proteins	2.6880869
RL451_08895	ptsG_3	PTS system glucose-specific EIICBA component	Transport and binding proteins	2.69249035
RL451_12675	fecD	Fe(3+) dicitrate transport system permease protein FecD	-	2.69437906
RL451_09035	epsL	putative sugar transferase EpsL	-	2.69625813
RL451_04550	rsmD	Ribosomal RNA small subunit methyltransferase D	Protein synthesis	2.69662395
RL451_06615	mnhD1_2	Na(+)/H(+) antiporter subunit D1	Transport and binding proteins	2.69958669

RL451_12395	rpsH	30S ribosomal protein S8	-	2.70653437
RL451_03805	-	hypothetical protein	-	2.70868007
RL451_11680	-	hypothetical protein	-	2.70998159
RL451_04125	pyrE	Orotate phosphoribosyltransferase	"Purines, pyrimidines, nucleosides, and nucleotides"	2.72075534
RL451_06255	ybaK	Cys-tRNA(Pro)/Cys-tRNA(Cys) deacylase YbaK	Protein synthesis	2.72217871
RL451_08170	-	hypothetical protein	Signal transduction; Transport and binding proteins	2.73593522
RL451_03925	sucC	Succinate--CoA ligase [ADP-forming] subunit beta	Energy metabolism	2.73949377
RL451_01890	-	hypothetical protein	DNA metabolism	2.7409218
RL451_01130	-	hypothetical protein	Energy metabolism	2.74537591
RL451_08060	-	hypothetical protein	Energy metabolism	2.75913631
RL451_10160	ywqD_2	Tyrosine-protein kinase YwqD	Transport and binding proteins	2.76213781
RL451_06825	rclA	putative pyridine nucleotide-disulfide oxidoreductase RclA	-	2.76564333
RL451_12115	ureE	Urease accessory protein UreE	Central intermediary metabolism	2.7673561
RL451_08880	-	PTS system EIIBC component SA0186	-	2.77639638
RL451_13275	yhgF	Protein YhgF	Protein synthesis	2.77973723
RL451_03185	-	hypothetical protein	Energy metabolism	2.78101415
RL451_04545	coaD	Phosphopantetheine adenylyltransferase	"Biosynthesis of cofactors, prosthetic groups, and carriers"	2.78110857
RL451_09280	yfhA	putative siderophore transport system permease protein YfhA	-	2.78592758
RL451_10420	nrdD	Anaerobic ribonucleoside-triphosphate reductase	"Purines, pyrimidines, nucleosides, and nucleotides"	2.79144908
RL451_04800	purH	Bifunctional purine biosynthesis protein PurH	"Purines, pyrimidines, nucleosides, and nucleotides"	2.800211

RL451_07050	rpsG	30S ribosomal protein S7	Protein synthesis	2.80499268
RL451_11045	sarT	HTH-type transcriptional regulator SarT	Regulatory functions	2.80892666
RL451_11740	-	putative HTH-type transcriptional regulator SACOL2360	-	2.81252153
RL451_09580	-	hypothetical protein	-	2.81260962
RL451_08150	glpT	Glycerol-3-phosphate transporter	Transport and binding proteins	2.81482946
RL451_12570	lacA	Galactose-6-phosphate isomerase subunit LacA	Energy metabolism	2.81702002
RL451_04735	ythB	Putative cytochrome bd menaquinol oxidase subunit II	-	2.81751828
RL451_11030	fnbA_2	Fibronectin-binding protein A	Cell envelope	2.81814681
RL451_13285	-	-	-	2.81956031
RL451_05975	comFA	ComF operon protein 1	-	2.82403761
RL451_11220	oppD_4	Oligopeptide transport ATP-binding protein OppD	Transport and binding proteins	2.8262956
RL451_06835	-	Phosphomevalonate kinase	Central intermediary metabolism	2.83204324
RL451_10955	fbp	"Fructose-1,6-bisphosphatase class 3"	-	2.83964387
RL451_13315	ilvA	L-threonine dehydratase biosynthetic IlvA	Amino acid biosynthesis	2.84074076
RL451_07550	gltA	Glutamate synthase [NADPH] large chain	-	2.85932869
RL451_13700	-	hypothetical protein	-	2.87341121
RL451_02390	gcvPB	putative glycine dehydrogenase (decarboxylating) subunit 2	Energy metabolism	2.88136271
RL451_04785	ykoD_1	Putative HMP/thiamine import ATP-binding protein YkoD	Transport and binding proteins	2.88407043
RL451_11320	opuCD	Carnitine transport permease protein OpuCD	-	2.89395185
RL451_03810	nusA	Transcription termination/antitermination protein NusA	Transcription	2.89987779
RL451_07615	-	hypothetical protein	-	2.90012212
RL451_04400	-	hypothetical protein	Unknown function	2.90344487
RL451_03820	polC_1	DNA polymerase III PolC-type	DNA metabolism	2.90765335

RL451_04310	-	hypothetical protein	Transport and binding proteins	2.9083364
RL451_12330	rplD	50S ribosomal protein L4	Protein synthesis	2.9086678
RL451_11890	hutG	Formimidoylglutamase	Energy metabolism	2.90909258
RL451_09735	-	hypothetical protein	-	2.90915583
RL451_10310	arcB_2	"Ornithine carbamoyltransferase, catabolic"	Amino acid biosynthesis	2.92122571
RL451_10545	cocE	Cocaine esterase	Unknown function	2.92492928
RL451_12025	-	hypothetical protein	-	2.93313447
RL451_07925	ahpC	Alkyl hydroperoxide reductase C	Cellular processes	2.9462596
RL451_09950	noc	Nucleoid occlusion protein	-	2.94789346
RL451_02475	bfmBAA	2-oxoisovalerate dehydrogenase subunit alpha	Energy metabolism	2.94938613
RL451_06625	mrpB	Na(+)/H(+) antiporter subunit B	Transport and binding proteins	2.95147548
RL451_10540	-	hypothetical protein	-	2.95266735
RL451_09605	-	hypothetical protein	-	2.95453606
RL451_09940	mnmG	tRNA uridine 5-carboxymethylaminomethyl modification enzyme MnmG	Protein synthesis	2.95472765
RL451_10915	ldhD_2	D-lactate dehydrogenase	Amino acid biosynthesis	2.95559688
RL451_04665	potB	Spermidine/putrescine transport system permease protein PotB	Transport and binding proteins	2.95856464
RL451_04405	-	dITP/XTP pyrophosphatase	DNA metabolism	2.96693907
RL451_11800	mdtD	Putative multidrug resistance protein MdtD	Cellular processes; Transport and binding proteins	2.96833405
RL451_06485	dhaM	"PTS-dependent dihydroxyacetone kinase, phosphotransferase subunit DhaM"	-	2.97600532
RL451_10615	-	putative hydrolase SA2367	Energy metabolism	2.97834836
RL451_01655	coaE	Dephospho-CoA kinase	"Biosynthesis of cofactors, prosthetic groups, and carriers"	2.98154543
RL451_12400	rplF	50S ribosomal protein L6	Protein synthesis	2.98316037
RL451_04185	ileS	Isoleucine--tRNA ligase	Protein synthesis	2.98946836

RL451_13350	ilvB_1	Acetolactate synthase large subunit	-	2.99911643
RL451_03005	odhA	2-oxoglutarate dehydrogenase E1 component	Energy metabolism	3.00412203
RL451_05225	oppF_1	Oligopeptide transport ATP-binding protein OppF	Transport and binding proteins	3.00930243
RL451_08830	-	hypothetical protein	-	3.02222077
RL451_01565	-	UPF0173 metal-dependent hydrolase SA1529	Cellular processes	3.03252073
RL451_13525	hlb_2	Phospholipase C	Cellular processes	3.03531255
RL451_07350	-	hypothetical protein	Cellular processes	3.04133895
RL451_11945	malP	PTS system maltose-specific EIICB component	Transport and binding proteins	3.0446136
RL451_12335	rplW	50S ribosomal protein L23	Protein synthesis	3.05023743
RL451_13280	-	Protein SprT-like	Regulatory functions	3.05802948
RL451_09980	bceB_2	Bacitracin export permease protein BceB	-	3.06058733
RL451_03230	trpG_1	Anthranilate synthase component 2	-	3.06875733
RL451_06515	-	hypothetical protein	-	3.0750188
RL451_07805	-	hypothetical protein	-	3.07517222
RL451_10875	sdhA	"L-serine dehydratase, alpha chain"	Energy metabolism	3.08055567
RL451_07595	metP_2	Methionine import system permease protein MetP	Transport and binding proteins	3.0894105
RL451_12915	-	hypothetical protein	-	3.10864781
RL451_10865	-	hypothetical protein	-	3.11460086
RL451_00320	-	hypothetical protein	-	3.1156678
RL451_09685	merR1	Mercuric resistance operon regulatory protein	Regulatory functions	3.11591941
RL451_09820	walK	Sensor protein kinase WalK	Signal transduction	3.11931992
RL451_06525	nupG	Purine nucleoside transport protein NupG	Transport and binding proteins	3.14125172
RL451_09230	btrK	L-glutamyl-[BtrI acyl-carrier protein] decarboxylase	-	3.15248148
RL451_09600	-	hypothetical protein	-	3.16691353
RL451_12590	lacF	PTS system lactose-specific EIIA component	Transport and binding proteins	3.16694177
RL451_08615	gatB_2	PTS system galactitol-specific EIIB component	Signal transduction; Transport and binding proteins	3.18445963
RL451_09030	fcl	GDP-L-fucose synthase	Cell envelope	3.19046992

RL451_03915	lytN	putative cell wall hydrolase LytN	-	3.19997812
RL451_00020	clpP_1	ATP-dependent Clp protease proteolytic subunit	Protein fate	3.21859383
RL451_13320	leuD	3-isopropylmalate dehydratase small subunit	Amino acid biosynthesis	3.22247057
RL451_07980	-	hypothetical protein	Hypothetical proteins	3.2231019
RL451_08745	pflB	Formate acetyltransferase	Energy metabolism	3.22810112
RL451_08485	degA	HTH-type transcriptional regulator DegA	Regulatory functions	3.26171878
RL451_12600	lacG	6-phospho-beta-galactosidase	Energy metabolism	3.26524618
RL451_13600	-	hypothetical protein	-	3.26996679
RL451_09195	wbnH	O-antigen biosynthesis glycosyltransferase WbnH	-	3.27503936
RL451_09025	wecC	UDP-N-acetyl-D-mannosamine dehydrogenase	-	3.28006661
RL451_01495	rpsD	30S ribosomal protein S4	Protein synthesis	3.28198681
RL451_09305	norG	HTH-type transcriptional regulator NorG	-	3.29515504
RL451_04680	-	UPF0223 protein BH2638	-	3.30227652
RL451_05965	hpf	Ribosome hibernation promotion factor	Protein synthesis	3.31923294
RL451_09020	mnaA_1	UDP-N-acetylglucosamine 2-epimerase	Cell envelope	3.32783782
RL451_06930	gph	Phosphoglycolate phosphatase	Energy metabolism	3.33004623
RL451_08950	dltA_2	D-alanine--poly(phosphoribitol) ligase subunit 1	-	3.33906019
RL451_04870	qoxB	putative quinol oxidase subunit 1	Energy metabolism	3.34089832
RL451_05825	secG	putative protein-export membrane protein SecG	Protein fate	3.35049384
RL451_04740	ythA	Putative cytochrome bd menaquinol oxidase subunit I	-	3.35086497
RL451_03930	rnhB	Ribonuclease HII	DNA metabolism	3.35258151
RL451_06840	-	hypothetical protein	Central intermediary metabolism	3.35263486
RL451_09190	-	hypothetical protein	-	3.35543672
RL451_03495	ltaE	Low specificity L-threonine aldolase	-	3.35952081
RL451_12035	atl_3	Bifunctional autolysin	DNA metabolism	3.36312259
RL451_12895	dps	General stress protein 20U	Transport and binding proteins	3.37441984
RL451_04155	pyrP	Uracil permease	Transport and binding proteins	3.39928036

RL451_08075	-	hypothetical protein	-	3.41120756
RL451_11920	yghA	putative oxidoreductase YghA	Fatty acid and phospholipid metabolism	3.41468784
RL451_06505	feuB	Iron-uptake system permease protein FeuB	-	3.42085412
RL451_13130	thiM	Hydroxyethylthiazole kinase	"Biosynthesis of cofactors, prosthetic groups, and carriers"	3.42559933
RL451_06600	-	hypothetical protein	Transport and binding proteins	3.42673044
RL451_12340	rplB	50S ribosomal protein L2	Protein synthesis	3.42847215
RL451_13690	-	hypothetical protein	-	3.43305507
RL451_10515	aldC_1	Alpha-acetolactate decarboxylase	Energy metabolism	3.43414901
RL451_13510	dapE	putative succinyl-diaminopimelate desuccinylase	Protein fate	3.44104332
RL451_02295	sodA	Superoxide dismutase [Mn] 1	-	3.45257926
RL451_11390	-	hypothetical protein	-	3.45829042
RL451_09480	entC3	Enterotoxin type C-3	-	3.46147836
RL451_10105	hisH	Imidazole glycerol phosphate synthase subunit HisH	Amino acid biosynthesis	3.46453824
RL451_13345	-	hypothetical protein	Amino acid biosynthesis	3.46623656
RL451_09770	-	Putative monooxygenase Rv1533	-	3.47396383
RL451_03370	-	hypothetical protein	-	3.48399444
RL451_08005	ssbA_1	Single-stranded DNA-binding protein A	DNA metabolism	3.49024047
RL451_03320	acnA	Aconitate hydratase A	Energy metabolism	3.49203917
RL451_02610	srrB	Sensor protein SrrB	Signal transduction	3.51690517
RL451_03140	pstB3	Phosphate import ATP-binding protein PstB 3	Transport and binding proteins	3.51691987
RL451_10825	cidB	Holin-like protein CidB	Hypothetical proteins	3.51788222
RL451_08460	yxeI	Uncharacterized protein YxeI	-	3.52573365
RL451_04135	carB	Carbamoyl-phosphate synthase large chain	"Purines, pyrimidines, nucleosides, and nucleotides"	3.5314618
RL451_01080	-	hypothetical protein	-	3.54094135

RL451_08870	-	hypothetical protein	-	3.5433998
RL451_02025	greA	Transcription elongation factor GreA	Transcription	3.54829746
RL451_12595	lacE_1	PTS system lactose-specific EIICB component	-	3.5490709
RL451_09245	iucA	N(2)-citryl-N(6)-acetyl-N(6)-hydroxylysine synthase	-	3.55714177
RL451_01845	rpmA	50S ribosomal protein L27	Protein synthesis	3.56366238
RL451_12405	rplR	50S ribosomal protein L18	Protein synthesis	3.56511199
RL451_01350	ytpP	Thioredoxin-like protein YtpP	Energy metabolism	3.57171885
RL451_08690	lcfB	Long-chain-fatty-acid--CoA ligase	"Biosynthesis of cofactors, prosthetic groups, and carriers"	3.57406518
RL451_11730	mqo1	putative malate:quinone oxidoreductase 1	Energy metabolism	3.57494426
RL451_00100	-	hypothetical protein	-	3.57724409
RL451_13610	-	hypothetical protein	-	3.61423092
RL451_08180	-	hypothetical protein	-	3.63081524
RL451_01100	-	hypothetical protein	Cellular processes	3.63742275
RL451_04320	argF	Ornithine carbamoyltransferase	Amino acid biosynthesis	3.64987773
RL451_08015	-	hypothetical protein	-	3.66329721
RL451_04430	uvrC	UvrABC system protein C	DNA metabolism	3.66618027
RL451_11225	sapF	Putrescine export system ATP-binding protein SapF	Transport and binding proteins	3.68131187
RL451_10975	sauU	putative sulfoacetate transporter SauU	Transport and binding proteins	3.6843763
RL451_13215	kdpC	Potassium-transporting ATPase KdpC subunit	Transport and binding proteins	3.70777155
RL451_02815	ponA	Penicillin-binding protein 1A/1B	Cell envelope	3.70786219
RL451_05055	-	hypothetical protein	-	3.71137409
RL451_06500	feuC	Iron-uptake system permease protein FeuC	-	3.71902061
RL451_12415	rpmD	50S ribosomal protein L30	Protein synthesis	3.72315776
RL451_08175	cmtB	Mannitol-specific cryptic phosphotransferase enzyme IIA component	Signal transduction; Transport and binding proteins	3.72381554

RL451_04130	pyrF	Orotidine 5'-phosphate decarboxylase	"Purines, pyrimidines, nucleosides, and nucleotides"	3.73320204
RL451_04140	carA_1	Carbamoyl-phosphate synthase small chain	"Purines, pyrimidines, nucleosides, and nucleotides"	3.74395224
RL451_03555	-	hypothetical protein	-	3.75101107
RL451_07045	fusA	Elongation factor G	Protein synthesis	3.76127754
RL451_02480	bfmBAB	2-oxoisovalerate dehydrogenase subunit beta	"Biosynthesis of cofactors, prosthetic groups, and carriers"	3.76344164
RL451_01085	-	hypothetical protein	-	3.76460539
RL451_10770	-	hypothetical protein	-	3.77042814
RL451_05880	whiA	Putative sporulation transcription regulator WhiA	Cellular processes	3.77051195
RL451_04280	-	Antibacterial protein 3	-	3.77375844
RL451_07675	yciC_2	Putative metal chaperone YciC	"Biosynthesis of cofactors, prosthetic groups, and carriers"	3.80172235
RL451_02275	nfo	putative endonuclease 4	DNA metabolism	3.80576284
RL451_04000	fabD	Malonyl CoA-acyl carrier protein transacylase	Fatty acid and phospholipid metabolism	3.81597491
RL451_03175	oppD_1	Oligopeptide transport ATP-binding protein OppD	Transport and binding proteins	3.83029075
RL451_01620	citZ	Citrate synthase 2	-	3.83913373
RL451_06290	-	hypothetical protein	Transport and binding proteins	3.85206738
RL451_01570	-	hypothetical protein	Unknown function	3.8599036
RL451_12520	-	Hyaluronate lyase	Hypothetical proteins	3.85990611
RL451_13620	-	hypothetical protein	-	3.86033852
RL451_08845	gsiA	Glutathione import ATP-binding protein GsiA	Transport and binding proteins	3.86154854
RL451_12045	-	Putative 2-hydroxyacid dehydrogenase SA2098	Amino acid biosynthesis	3.87424524

RL451_10610	-	hypothetical protein	"Biosynthesis of cofactors, prosthetic groups, and carriers"	3.8875737
RL451_03690	-	hypothetical protein	-	3.89872093
RL451_01595	accD	Acetyl-coenzyme A carboxylase carboxyl transferase subunit beta	Fatty acid and phospholipid metabolism	3.91580457
RL451_09015	isdI	Heme oxygenase (staphylobilin-producing) 2	-	3.92599013
RL451_12410	rpsE	30S ribosomal protein S5	Protein synthesis	3.92826285
RL451_09155	tet(38)	tetracycline efflux MFS transporter Tet(38)	Cellular processes; Transport and binding proteins	3.92878888
RL451_09180	sodM	Superoxide dismutase [Mn/Fe] 2	-	3.93198476
RL451_12110	ureF	Urease accessory protein UreF	-	3.93387959
RL451_07795	-	hypothetical protein	-	3.93689672
RL451_12595	lacE_2	PTS system lactose-specific EIICB component	Signal transduction; Transport and binding proteins	3.96307561
RL451_13380	tsaD	tRNA N6-adenosine threonylcarbamoyltransferase	Protein synthesis	3.969601
RL451_01330	trmB	tRNA (guanine-N(7)-)-methyltransferase	Protein synthesis	4.00000512
RL451_04145	pyrC	Dihydroorotase	"Purines, pyrimidines, nucleosides, and nucleotides"	4.0022717
RL451_06850	lipL	Octanoyl-[GcvH]:protein N-octanoyltransferase	Protein fate	4.01387982
RL451_08465	norB_2	Quinolone resistance protein NorB	Cellular processes; Transport and binding proteins	4.01991966
RL451_11025	fnbA_1	Fibronectin-binding protein A	Cell envelope	4.02348497
RL451_11765	-	hypothetical protein	-	4.03619038
RL451_09140	phnE_2	Phosphate-import permease protein PhnE	Transport and binding proteins	4.04129402
RL451_05765	-	hypothetical protein	-	4.04459434
RL451_09945	rsmG	Ribosomal RNA small subunit methyltransferase G	Protein synthesis	4.05979441
RL451_13695	-	hypothetical protein	-	4.10136109
RL451_13625	-	hypothetical protein	-	4.1071753

RL451_04950	menH	"2-succinyl-6-hydroxy-2, 4-cyclohexadiene-1-carboxylate synthase"	"Biosynthesis of cofactors, prosthetic groups, and carriers"	4.10902418
RL451_12685	-	UPF0457 protein SA1975.1	-	4.13736568
RL451_11270	fetB	putative iron export permease protein FetB	Hypothetical proteins	4.16001892
RL451_05160	nadK	NAD kinase	-	4.16229871
RL451_10735	copA	Copper-exporting P-type ATPase	-	4.18589491
RL451_09240	iucC	Aerobactin synthase	-	4.19499107
RL451_01325	-	hypothetical protein	"Biosynthesis of cofactors, prosthetic groups, and carriers"	4.19638695
RL451_06630	mrpA	Na(+)/H(+) antiporter subunit A	Transport and binding proteins	4.20154666
RL451_00095	-	hypothetical protein	-	4.22473441
RL451_08875	ybbH_2	putative HTH-type transcriptional regulator YbbH	-	4.24031179
RL451_00085	-	hypothetical protein	Mobile and extrachromosomal element functions	4.24089068
RL451_05015	-	hypothetical protein	Hypothetical proteins	4.25417837
RL451_09590	-	hypothetical protein	-	4.25631267
RL451_12085	-	hypothetical protein	Regulatory functions	4.2677394
RL451_00405	dinB	DNA polymerase IV	-	4.26885405
RL451_11420	bioK	L-Lysine--8-amino-7-oxononanoate transaminase	"Biosynthesis of cofactors, prosthetic groups, and carriers"	4.27880576
RL451_10400	cysJ	Sulfite reductase [NADPH] flavoprotein alpha-component	-	4.27976934
RL451_02255	sigA	RNA polymerase sigma factor SigA	Transcription	4.28389557
RL451_02485	pdhC_1	Dihydrolipoyllysine-residue acetyltransferase component of pyruvate dehydrogenase complex	-	4.28680508
RL451_07855	-	hypothetical protein	-	4.28823517

RL451_03920	sucD	Succinate--CoA ligase [ADP-forming] subunit alpha	Energy metabolism	4.29567519
RL451_12080	rhaS_2	HTH-type transcriptional activator RhaS	-	4.30432448
RL451_00055	-	hypothetical protein	-	4.32474857
RL451_12040	auaG	Aurachin C monooxygenase/isomerase	-	4.33038596
RL451_10820	cidA	Holin-like protein CidA	-	4.3426165
RL451_06960	folE2	GTP cyclohydrolase FolE2	"Biosynthesis of cofactors, prosthetic groups, and carriers"	4.34862235
RL451_13605	-	hypothetical protein	-	4.3530416
RL451_13670	-	hypothetical protein	Energy metabolism	4.36476876
RL451_10780	-	hypothetical protein	DNA metabolism	4.36901083
RL451_07375	glmU	Bifunctional protein GlmU	Cell envelope; Central intermediary metabolism	4.38403609
RL451_01755	-	hypothetical protein	-	4.38629976
RL451_10140	icaD	"Poly-beta-1,6-N-acetyl-D-glucosamine synthesis protein IcaD"	Cell envelope	4.38936893
RL451_04945	menB	"1,4-dihydroxy-2-naphthoyl-CoA synthase"	"Biosynthesis of cofactors, prosthetic groups, and carriers"	4.42000742
RL451_09720	-	hypothetical protein	-	4.45169557
RL451_04150	pyrB	Aspartate carbamoyltransferase	"Purines, pyrimidines, nucleosides, and nucleotides"	4.45303139
RL451_07680	-	hypothetical protein	-	4.45763754
RL451_05010	-	putative ABC transporter ATP-binding protein Rv0986	Cellular processes; Transport and binding proteins	4.46597311
RL451_01415	acsA_1	Acetyl-coenzyme A synthetase	-	4.46692514
RL451_07860	-	hypothetical protein	-	4.48374574
RL451_08925	argC	N-acetyl-gamma-glutamyl-phosphate reductase	Amino acid biosynthesis	4.48717039
RL451_02010	ydcP	putative protease YdcP	-	4.48809996

RL451_05095	prfC	Peptide chain release factor 3	Protein synthesis	4.49518654
RL451_11015	gntT	High-affinity gluconate transporter	Transport and binding proteins	4.52520271
RL451_01600	accA	Acetyl-coenzyme A carboxylase carboxyl transferase subunit alpha	Fatty acid and phospholipid metabolism	4.53222278
RL451_04660	ydcV	Inner membrane ABC transporter permease protein YdcV	Transport and binding proteins	4.5390898
RL451_09250	mdtG_1	Multidrug resistance protein MdtG	-	4.54136689
RL451_03695	korA	2-oxoglutarate oxidoreductase subunit KorA	-	4.56996438
RL451_10750	rocA	1-pyrroline-5-carboxylate dehydrogenase	Energy metabolism	4.58355861
RL451_03995	fabG	3-oxoacyl-[acyl-carrier-protein] reductase FabG	Fatty acid and phospholipid metabolism	4.60216713
RL451_08930	argJ	Arginine biosynthesis bifunctional protein ArgJ	Amino acid biosynthesis	4.60854021
RL451_11415	bioD	ATP-dependent dethiobiotin synthetase BioD	"Biosynthesis of cofactors, prosthetic groups, and carriers"	4.63549334
RL451_10945	mhqD	Putative hydrolase MhqD	"Biosynthesis of cofactors, prosthetic groups, and carriers"	4.64949169
RL451_12665	yfmC_2	Fe(3+)-citrate-binding protein YfmC	-	4.6712037
RL451_13645	-	hypothetical protein	-	4.68728149
RL451_09165	-	hypothetical protein	Regulatory functions	4.7064996
RL451_12860	czcD_2	"Cadmium, cobalt and zinc/H(+)-K(+) antiporter"	Transport and binding proteins	4.72262636
RL451_13330	leuB	3-isopropylmalate dehydrogenase	Amino acid biosynthesis	4.74219962
RL451_00355	ligA	DNA ligase	DNA metabolism	4.74516422
RL451_09160	deoD	Purine nucleoside phosphorylase DeoD-type	"Purines, pyrimidines, nucleosides, and nucleotides"	4.7660259
RL451_04795	purD	Phosphoribosylamine--glycine ligase	"Purines, pyrimidines, nucleosides, and nucleotides"	4.78510048

RL451_10535	panD	Aspartate 1-decarboxylase	"Biosynthesis of cofactors, prosthetic groups, and carriers"	4.78811652
RL451_02885	steT	Serine/threonine exchanger SteT	Transport and binding proteins	4.81350163
RL451_04265	bshC	Putative cysteine ligase BshC	-	4.865349
RL451_03250	umuC	Protein UmuC	-	4.87771749
RL451_10530	panC	Pantothenate synthetase	"Biosynthesis of cofactors, prosthetic groups, and carriers"	4.89363949
RL451_03425	thrB	Homoserine kinase	Amino acid biosynthesis	4.91056731
RL451_08000	rpsR	30S ribosomal protein S18	Protein synthesis	4.91718443
RL451_03010	odhB	Dihydrolipoyllysine-residue succinyltransferase component of 2-oxoglutarate dehydrogenase complex	Energy metabolism	4.92327157
RL451_12910	pdp	Pyrimidine-nucleoside phosphorylase	"Purines, pyrimidines, nucleosides, and nucleotides"	4.93954768
RL451_13490	groS	10 kDa chaperonin	-	4.94210936
RL451_08110	-	hypothetical protein	Unknown function	4.94915404
RL451_03135	pstA	Phosphate transport system permease protein PstA	Transport and binding proteins	4.9711032
RL451_09290	spa	Immunoglobulin G-binding protein A	-	4.99301097
RL451_09835	-	-	-	5.00629794
RL451_09145	deoB	Phosphopentomutase	"Purines, pyrimidines, nucleosides, and nucleotides"	5.01840073
RL451_04445	mutS2	Endonuclease MutS2	DNA metabolism	5.05047401
RL451_06650	-	hypothetical protein	-	5.08099748
RL451_01290	-	hypothetical protein	-	5.08520937
RL451_13325	leuC	3-isopropylmalate dehydratase large subunit	Amino acid biosynthesis	5.09630952
RL451_08740	pflA	Pyruvate formate-lyase-activating enzyme	Energy metabolism; Protein fate	5.09642021
RL451_07775	-	hypothetical protein	-	5.11271982

RL451_03590	-	hypothetical protein	-	5.11708244
RL451_13630	-	hypothetical protein	-	5.12159897
RL451_05590	-	Putative monooxygenase Rv1533	-	5.14073411
RL451_07540	-	-	-	5.15022974
RL451_01790	fpgS	Folylpolyglutamate synthase	"Biosynthesis of cofactors, prosthetic groups, and carriers"	5.16891952
RL451_12820	glmS	Glutamine--fructose-6-phosphate aminotransferase [isomerizing]	Cell envelope; Central intermediary metabolism	5.19763133
RL451_08115	efeN	putative deferrochelatase/peroxidase EfeN	-	5.2150526
RL451_00420	ftnA	Bacterial non-heme ferritin	Transport and binding proteins	5.23027901
RL451_01115	menC	o-succinylbenzoate synthase	"Biosynthesis of cofactors, prosthetic groups, and carriers"	5.23317349
RL451_04790	ecfT_1	Energy-coupling factor transporter transmembrane protein EcfT	Transport and binding proteins	5.2802842
RL451_08700	fadN	putative 3-hydroxyacyl-CoA dehydrogenase	-	5.29095953
RL451_04700	pdhA	Pyruvate dehydrogenase E1 component subunit alpha	Energy metabolism	5.30024212
RL451_05625	-	UPF0051 protein SA0778	"Biosynthesis of cofactors, prosthetic groups, and carriers"	5.30470785
RL451_07070	rpoB	DNA-directed RNA polymerase subunit beta	Transcription	5.34413039
RL451_06250	ydjF	putative HTH-type transcriptional regulator YdjF	Regulatory functions	5.34885403
RL451_03965	ffh	Signal recognition particle protein	Protein fate	5.35875256
RL451_08595	gatD	Galactitol 1-phosphate 5-dehydrogenase	Energy metabolism	5.37248045
RL451_11835	gltS	Sodium/glutamate symporter	Transport and binding proteins	5.37640544
RL451_07280	lysS	Lysine--tRNA ligase	Protein synthesis	5.37923918
RL451_10730	copZ	Copper chaperone CopZ	Transport and binding proteins	5.38686294
RL451_09725	-	hypothetical protein	-	5.40966866

RL451_10205	sraP	Serine-rich adhesin for platelets	-	5.41261559
RL451_05940	-	hypothetical protein	Cellular processes	5.42661072
RL451_10425	-	hypothetical protein	"Protein fate; Purines, pyrimidines, nucleosides, and nucleotides"	5.42850257
RL451_09235	garL	5-keto-4-deoxy-D-glucarate aldolase	-	5.44728243
RL451_07640	-	hypothetical protein	-	5.44742307
RL451_08455	lytM	Glycyl-glycine endopeptidase LytM	Transcription	5.48341889
RL451_05610	-	UPF0051 protein SA0778	"Biosynthesis of cofactors, prosthetic groups, and carriers"	5.49474239
RL451_10145	icaA_1	"Poly-beta-1,6-N-acetyl-D-glucosamine synthase"	-	5.50196625
RL451_01240	putB	Proline dehydrogenase 2	-	5.52513494
RL451_06645	-	hypothetical protein	-	5.54421514
RL451_08825	ggt	Glutathione hydrolase proenzyme	"Biosynthesis of cofactors, prosthetic groups, and carriers"	5.60709551
RL451_09730	-	hypothetical protein	-	5.61001175
RL451_13335	leuA_2	2-isopropylmalate synthase	Amino acid biosynthesis	5.61019971
RL451_03180	nikE	Nickel import ATP-binding protein NikE	Transport and binding proteins	5.63805063
RL451_01970	mnmA	tRNA-specific 2-thiouridylase MnmA	-	5.66551039
RL451_12610	yfmJ	Putative NADP-dependent oxidoreductase YfmJ	-	5.68350765
RL451_08610	gatC_2	PTS system galactitol-specific EIIC component	Signal transduction; Transport and binding proteins	5.70344903
RL451_10830	ydaP	Putative thiamine pyrophosphate-containing protein YdaP	Energy metabolism	5.7137238
RL451_08735	-	hypothetical protein	-	5.71512516
RL451_01430	isdH	Iron-regulated surface determinant protein H	-	5.73476284
RL451_09610	-	hypothetical protein	-	5.73705397

RL451_09215	butA	Diacetyl reductase [(S)-acetoin forming]	Energy metabolism	5.74050637
RL451_06050	yusV	putative siderophore transport system ATP-binding protein YusV	-	5.76116287
RL451_02805	nth_1	Endonuclease III	DNA metabolism	5.77211242
RL451_11830	fni	Isopentenyl-diphosphate delta-isomerase	"Biosynthesis of cofactors, prosthetic groups, and carriers"	5.77712789
RL451_08945	-	hypothetical protein	Protein fate	5.78929455
RL451_04030	rpmB	50S ribosomal protein L28	Protein synthesis	5.7992979
RL451_01095	-	hypothetical protein	-	5.79989428
RL451_12105	ureG	Urease accessory protein UreG	Central intermediary metabolism	5.81047553
RL451_07930	ahpF	Alkyl hydroperoxide reductase subunit F	Cellular processes	5.90939707
RL451_03435	-	hypothetical protein	Regulatory functions	5.91823103
RL451_13655	-	hypothetical protein	-	5.9799453
RL451_07625	est_2	Carboxylesterase	"Biosynthesis of cofactors, prosthetic groups, and carriers"	5.9805748
RL451_05235	appA	Oligopeptide-binding protein AppA	Transport and binding proteins	5.98966208
RL451_01920	aspS	Aspartate--tRNA ligase	Protein synthesis	6.01526211
RL451_07370	prs	Ribose-phosphate pyrophosphokinase	"Purines, pyrimidines, nucleosides, and nucleotides"	6.01643237
RL451_07730	-	hypothetical protein	-	6.03307912
RL451_00065	-	hypothetical protein	-	6.05688888
RL451_09335	yxeP_3	putative hydrolase YxeP	Protein fate	6.06954829
RL451_02230	recO	DNA repair protein RecO	DNA metabolism	6.09539329
RL451_13650	-	hypothetical protein	-	6.12245789
RL451_03950	trmD	tRNA (guanine-N(1)-)-methyltransferase	Protein synthesis	6.13669495
RL451_07170	mcsA	Protein-arginine kinase activator protein	DNA metabolism	6.13801268

RL451_07545	gltB	Glutamate synthase [NADPH] small chain	-	6.22652422
RL451_03975	ftsY	Signal recognition particle receptor FtsY	Protein fate	6.22931394
RL451_07590	-	hypothetical protein	Cell envelope	6.24566821
RL451_05635	-	hypothetical protein	-	6.25581551
RL451_03030	-	hypothetical protein	"Biosynthesis of cofactors, prosthetic groups, and carriers"	6.30164386
RL451_01690	lysP_1	Lysine-specific permease	Transport and binding proteins	6.30569303
RL451_10330	clfB	Clumping factor B	-	6.31205396
RL451_08605	-	D-arabitol-phosphate dehydrogenase	Energy metabolism	6.31784347
RL451_00070	-	hypothetical protein	-	6.32012519
RL451_12680	-	hypothetical protein	Cellular processes	6.32163233
RL451_08045	metC	Cystathionine beta-lyase MetC	-	6.32991573
RL451_00010	-	hypothetical protein	-	6.33170311
RL451_09260	arcB_1	Delta(1)-pyrroline-2-carboxylate reductase	Cellular processes	6.33464387
RL451_06135	recQ_2	ATP-dependent DNA helicase RecQ	DNA metabolism	6.36881236
RL451_08600	-	hypothetical protein	-	6.38139685
RL451_10830	ilvB_2	Acetolactate synthase large subunit	Amino acid biosynthesis	6.41146162
RL451_12585	lacD	"Tagatose 1,6-diphosphate aldolase"	Energy metabolism	6.42096174
RL451_09815	-	hypothetical protein	-	6.47032865
RL451_08805	ugpC	sn-glycerol-3-phosphate import ATP-binding protein UgpC	Transport and binding proteins	6.51764683
RL451_03640	glpD	Aerobic glycerol-3-phosphate dehydrogenase	Energy metabolism	6.52468186
RL451_00890	hemY	Protoporphyrinogen oxidase	"Biosynthesis of cofactors, prosthetic groups, and carriers"	6.52534151
RL451_09330	norB_3	Quinolone resistance protein NorB	Cellular processes; Transport and binding proteins	6.52986245

RL451_12075	ssaA2	Staphylococcal secretory antigen ssaA2	-	6.53411445
RL451_08235	lip2	Lipase 2	-	6.5516182
RL451_07365	rplY	50S ribosomal protein L25	Protein synthesis	6.57025343
RL451_06075	nrdE1	Ribonucleoside-diphosphate reductase subunit alpha 1	-	6.58074161
RL451_09680	-	hypothetical protein	-	6.59397354
RL451_07175	ctsR	Transcriptional regulator CtsR	-	6.6019967
RL451_00090	-	hypothetical protein	-	6.60815701
RL451_11665	treP_2	PTS system trehalose-specific EIIBC component	-	6.73094819
RL451_05305	leuA_1	2-isopropylmalate synthase	-	6.7400144
RL451_02045	accC	Biotin carboxylase	Fatty acid and phospholipid metabolism	6.74344644
RL451_03375	lexA_1	LexA repressor	DNA metabolism; Regulatory functions	6.75040928
RL451_09255	-	hypothetical protein	-	6.77999845
RL451_11530	yoeB	Toxin YoeB	Cellular processes; Mobile and extrachromosomal element functions	6.79604336
RL451_01090	-	hypothetical protein	Cellular processes	6.8085365
RL451_13205	kdpA	Potassium-transporting ATPase potassium-binding subunit	Transport and binding proteins	6.87281425
RL451_11055	-	hypothetical protein	-	6.89849067
RL451_10035	-	UPF0176 protein SP 0095	Protein synthesis	6.91669155
RL451_10210	secY_1	Protein translocase subunit SecY	Protein fate	6.91931317
RL451_04475	pheS	Phenylalanine--tRNA ligase alpha subunit	Protein synthesis	6.96317982
RL451_05820	est_1	Carboxylesterase	-	7.05401987
RL451_04315	arcC1	Carbamate kinase 1	Energy metabolism	7.06924013
RL451_07190	pdxS	Pyridoxal 5'-phosphate synthase subunit PdxS	"Biosynthesis of cofactors, prosthetic groups, and carriers"	7.26018159

RL451_13635	ssbA_3	Single-stranded DNA-binding protein A	-	7.27195337
RL451_04695	pdhB	Pyruvate dehydrogenase E1 component subunit beta	"Biosynthesis of cofactors, prosthetic groups, and carriers"	7.3195973
RL451_10315	arcD	Arginine/ornithine antiporter	Transport and binding proteins	7.34217836
RL451_08280	hldE	Bifunctional protein HldE	Energy metabolism	7.35589682
RL451_02810	-	hypothetical protein	-	7.37230445
RL451_03795	infB	Translation initiation factor IF-2	Protein synthesis	7.37383382
RL451_09830	-	-	-	7.42299328
RL451_11525	yefM	Antitoxin YefM	Cellular processes; Mobile and extrachromosomal element functions	7.46279619
RL451_01985	alaS	Alanine--tRNA ligase	Protein synthesis	7.47709193
RL451_12100	ureD1	Urease accessory protein UreD	-	7.49084192
RL451_09265	sbnA	putative siderophore biosynthesis protein SbnA	Cellular processes	7.65604817
RL451_13665	-	hypothetical protein	-	7.6584968
RL451_04875	qoxC	Quinol oxidase subunit 3	Energy metabolism	7.68602873
RL451_08705	fadA	3-ketoacyl-CoA thiolase	Fatty acid and phospholipid metabolism	7.84741361
RL451_06830	-	hypothetical protein	Protein synthesis	7.85756624
RL451_02880	tdcB	L-threonine dehydratase catabolic TdcB	Amino acid biosynthesis	7.85874656
RL451_10405	sirC	Precorrin-2 dehydrogenase	"Biosynthesis of cofactors, prosthetic groups, and carriers"	7.86056705
RL451_01010	splF	Serine protease SplF	Protein fate	7.87792945
RL451_13335	leuA_3	2-isopropylmalate synthase	Amino acid biosynthesis	7.95639687
RL451_09645	-	hypothetical protein	-	7.99526826
RL451_13340	ilvC	Ketol-acid reductoisomerase (NADP(+))	Amino acid biosynthesis	8.12017261
RL451_04420	frdA	Fumarate reductase flavoprotein subunit	Energy metabolism	8.29274565

RL451_05805	-	-	-	8.31364042
RL451_13210	kdpB	Potassium-transporting ATPase ATP-binding subunit	Transport and binding proteins	8.37536306
RL451_08695	caiA	Crotonobetainyl-CoA dehydrogenase	-	8.40278601
RL451_03430	thrC	Threonine synthase	Amino acid biosynthesis	8.81709174
RL451_05620	csd	putative cysteine desulfurase	"Biosynthesis of cofactors, prosthetic groups, and carriers"	8.96985098
RL451_00755	tcyC_1	L-cystine import ATP-binding protein TcyC	-	9.14069242
RL451_01760	hemB	Delta-aminolevulinic acid dehydratase	-	9.15365972
RL451_09650	-	hypothetical protein	-	9.15473396
RL451_04880	qoxD	Quinol oxidase subunit 4	Energy metabolism	9.24820538
RL451_02050	-	UPF0271 protein TTHB195	-	9.35638208
RL451_08040	metI	Cystathionine gamma-synthase/O-acetylhomoserine (thiol)-lyase	Amino acid biosynthesis	9.40667447
RL451_07650	ndhB	"NAD(P)H-quinone oxidoreductase subunit 2, chloroplastic"	Energy metabolism	9.48118325
RL451_00560	-	Putative multidrug export ATP-binding/permease protein SA1683	Cell envelope; Transport and binding proteins	9.52441552
RL451_09170	-	Uncharacterized protein SAOUHSC 00094	-	9.58015669
RL451_05615	sufU	Zinc-dependent sulfurtransferase SufU	"Biosynthesis of cofactors, prosthetic groups, and carriers"	9.7674979
RL451_08270	nupC_2	Nucleoside permease NupC	Transport and binding proteins	9.82140013
RL451_01625	icd	Isocitrate dehydrogenase [NADP]	Energy metabolism	9.86943962
RL451_02890	norB_1	Quinolone resistance protein NorB	Cellular processes; Transport and binding proteins	10.0637508
RL451_10110	hisA	1-(5-phosphoribosyl)-5-[(5-phosphoribosylamino)methylideneamino] imidazole-4-carboxamide isomerase	Amino acid biosynthesis	10.1957371

RL451_07185	pdxT	Pyridoxal 5'-phosphate synthase subunit PdxT	"Biosynthesis of cofactors, prosthetic groups, and carriers"	10.2062405
RL451_09810	-	hypothetical protein	-	10.4215417
RL451_13660	-	hypothetical protein	-	10.4436471
RL451_00750	mltF	Membrane-bound lytic murein transglycosylase F	-	10.540125
RL451_02015	-	hypothetical protein	-	10.6620638
RL451_08800	cycB	Cyclodextrin-binding protein	-	10.7044942
RL451_09655	-	hypothetical protein	-	10.7906855
RL451_02020	udk	Uridine kinase	"Purines, pyrimidines, nucleosides, and nucleotides"	11.1170676
RL451_07165	mcsB	Protein-arginine kinase	-	11.1741997
RL451_00075	-	hypothetical protein	Mobile and extrachromosomal element functions	11.216511
RL451_00125	-	hypothetical protein	-	11.3826669
RL451_09675	-	hypothetical protein	-	11.5814594
RL451_08275	psuG	Pseudouridine-5'-phosphate glycosidase	-	11.614791
RL451_07060	rplGB	Ribosome-associated protein L7Ae-like	-	11.758504
RL451_10225	-	hypothetical protein	Cellular processes; Protein fate	11.9163617
RL451_11905	hutU	Urocanate hydratase	Energy metabolism	12.0969981
RL451_05385	argH	Argininosuccinate lyase	Amino acid biosynthesis	12.2746085
RL451_08795	-	hypothetical protein	Transport and binding proteins	12.2907902
RL451_11910	hutI	Imidazolonepropionase	Energy metabolism	12.3265191
RL451_02055	mntH_1	Divalent metal cation transporter MntH	-	12.3947559
RL451_13355	ilvD	Dihydroxy-acid dehydratase	Amino acid biosynthesis	12.4090994
RL451_13705	-	hypothetical protein	-	12.4454076
RL451_03645	glpK	Glycerol kinase	Energy metabolism	12.4741468
RL451_05380	argG	Argininosuccinate synthase	Amino acid biosynthesis	12.6552402

RL451_12795	-	hypothetical protein	-	12.79042
RL451_02525	malR	HTH-type transcriptional regulator MalR	Regulatory functions	12.7907913
RL451_10215	-	hypothetical protein	Cellular processes; Protein fate	12.9798325
RL451_04415	frdB	Fumarate reductase iron-sulfur subunit	Energy metabolism	13.0148125
RL451_06285	phrB	Deoxyribodipyrimidine photo-lyase	DNA metabolism	13.1220057
RL451_01660	gapA2	Glyceraldehyde-3-phosphate dehydrogenase 2	Energy metabolism	13.3094699
RL451_04690	pdhC_2	Dihydrolipoyllysine-residue acetyltransferase component of pyruvate dehydrogenase complex	Energy metabolism	13.5335632
RL451_00080	-	hypothetical protein	-	13.6091396
RL451_10220	asp2	Accessory Sec system protein Asp2	Cellular processes; Protein fate	13.9448405
RL451_06245	lacC_1	Tagatose-6-phosphate kinase	-	14.1172471
RL451_07065	rpoC	DNA-directed RNA polymerase subunit beta'	Transcription	14.3159863
RL451_10320	arcC2	Carbamate kinase 2	Energy metabolism	14.3854897
RL451_02150	hrcA	Heat-inducible transcription repressor HrcA	Regulatory functions	14.4656416
RL451_01135	pckA	Phosphoenolpyruvate carboxykinase (ATP)	Energy metabolism	14.5283506
RL451_05815	rnr	Ribonuclease R	Transcription	14.5347764
RL451_10115	hisF	Imidazole glycerol phosphate synthase subunit HisF	Amino acid biosynthesis	14.6875069
RL451_08780	iolG	Inositol 2-dehydrogenase/D-chiro-inositol 3-dehydrogenase	Energy metabolism	14.9397227
RL451_01765	hemL1	"Glutamate-1-semialdehyde 2,1-aminomutase 1"	"Biosynthesis of cofactors, prosthetic groups, and carriers"	15.024351
RL451_02155	grpE	Protein GrpE	-	15.0304543
RL451_10125	lipA_2	Lipase 1	-	15.2784405
RL451_10325	arcR	HTH-type transcriptional regulator ArcR	Regulatory functions	16.5719188
RL451_09660	merB	Alkylmercury lyase	-	16.9929649
RL451_05810	smpB	SsrA-binding protein	Protein synthesis	17.2750302
RL451_01545	-	Putative universal stress protein SA1532	DNA metabolism	17.5442066

RL451_02895	ebh	Extracellular matrix-binding protein ebh	-	17.6369052
RL451_06240	fruA	PTS system fructose-specific EIIABC component	-	19.2588488
RL451_09670	-	hypothetical protein	-	19.3050801
RL451_09665	merA	Mercuric reductase	-	19.3442072
RL451_07160	clpC	ATP-dependent Clp protease ATP-binding subunit ClpC	Protein fate	20.153135
RL451_08770	-	hypothetical protein	-	20.2180786
RL451_04685	pdhD	Dihydrolipoyl dehydrogenase	-	20.539887
RL451_08790	malG	Maltose transport system permease protein MalG	-	22.4124242
RL451_08775	-	hypothetical protein	Energy metabolism	25.9603592
RL451_04470	pheT_2	Phenylalanine--tRNA ligase beta subunit	Protein synthesis	26.4474566
RL451_08785	gfo	Glucose--fructose oxidoreductase	Energy metabolism	27.3854433
RL451_02530	malL	"Oligo-1,6-glucosidase"	-	29.347855
RL451_09005	aldA	Putative aldehyde dehydrogenase AldA	Cellular processes	29.8438367
RL451_02165	dnaJ	Chaperone protein DnaJ	-	31.0353538
RL451_13495	groL	60 kDa chaperonin	Protein fate	32.8846161
RL451_09615	-	hypothetical protein	-	39.0404334
RL451_07645	-	hypothetical protein	Amino acid biosynthesis	39.8820691
RL451_02170	prmA	Ribosomal protein L11 methyltransferase	Protein synthesis	41.7723502
RL451_06975	sdrC	Serine-aspartate repeat-containing protein C	-	45.4969026
RL451_05090	ygdQ	UPF0053 inner membrane protein YgdQ	-	49.0134773
RL451_02160	dnaK	Chaperone protein DnaK	Protein fate	61.1453892
RL451_01685	thrS	Threonine--tRNA ligase	Protein synthesis	67.1354414
RL451_07525	treR_1	HTH-type transcriptional regulator TreR	Regulatory functions	75.4208532
RL451_11755	-	hypothetical protein	-	140.495301
RL451_07530	treA	Trehalose-6-phosphate hydrolase	-	186.070781
RL451_05315	clpB	Chaperone protein ClpB	Protein fate	293.884237
RL451_07535	treP_1	PTS system trehalose-specific EIIBC component	-	343.131834

RL451_11760	hrtA_2	Putative hemin import ATP-binding protein HrtA	-	398.863522

RL453_06940	*capA*	Capsular polysaccharide biosynthesis protein	1.40 ± 0.39

* p-value < 0.05

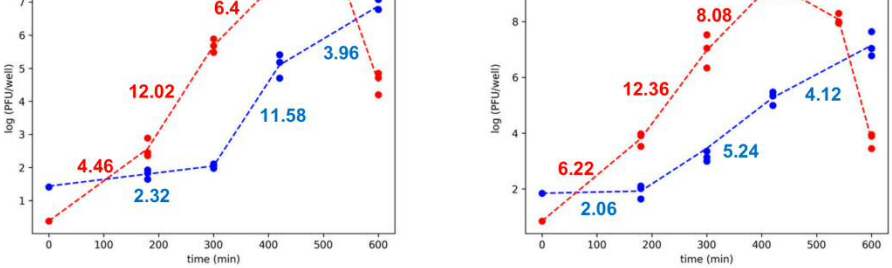

Figure 7.1 - Comparison between the bacterial growth rates (A and B) and phage propagation rates (C and D) obtained during biofilm development at 25 ºC (blue) and 37 ºC (red).

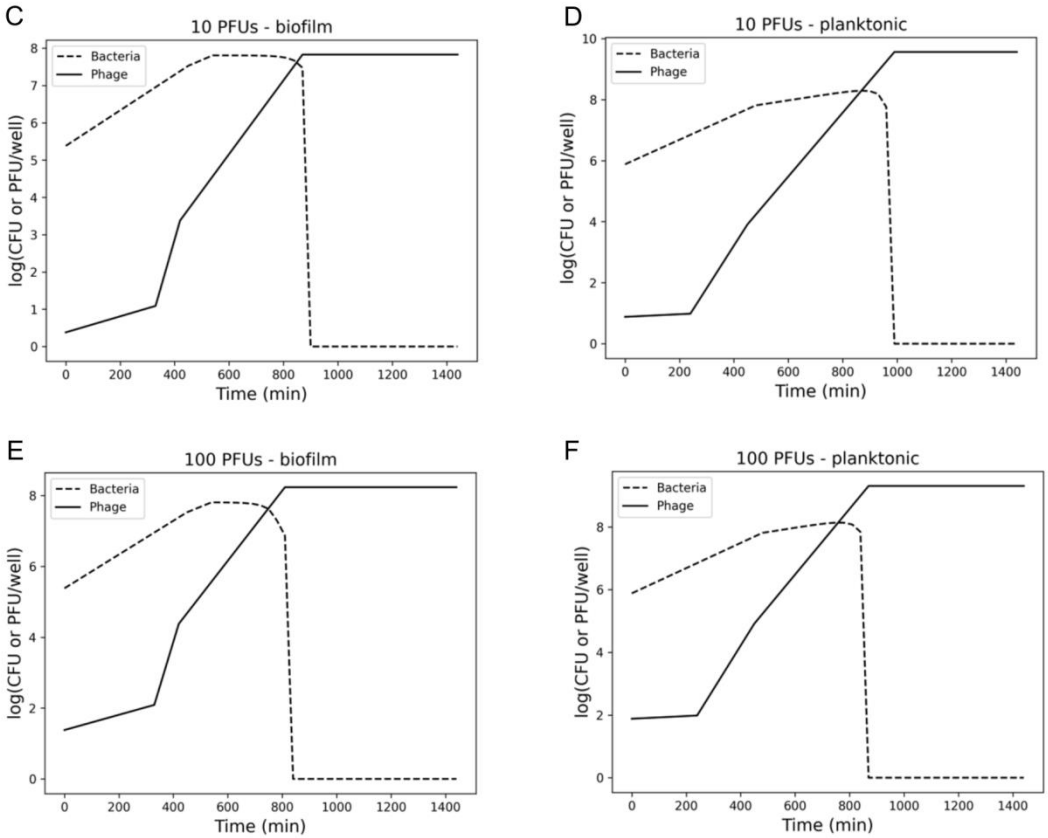

Figure 7.2 - Output of the *Kayvirus rodi* infection model for biofilms developed at 25 ºC for different starting phage concentrations: 0 PFU/well (A and B), 10 PFU/well (C and D) and 100 PFU/well (E and F) in the biofilm and the planktonic phase. The lowest possible pH value was set at 4.75, the initial pH was set at 7 and the starting number of cells was always set at 10^6 CFU/well. The predictions corresponding to the bacterial and phage populations are represented by a discontinuous line and a continuous line, respectively.

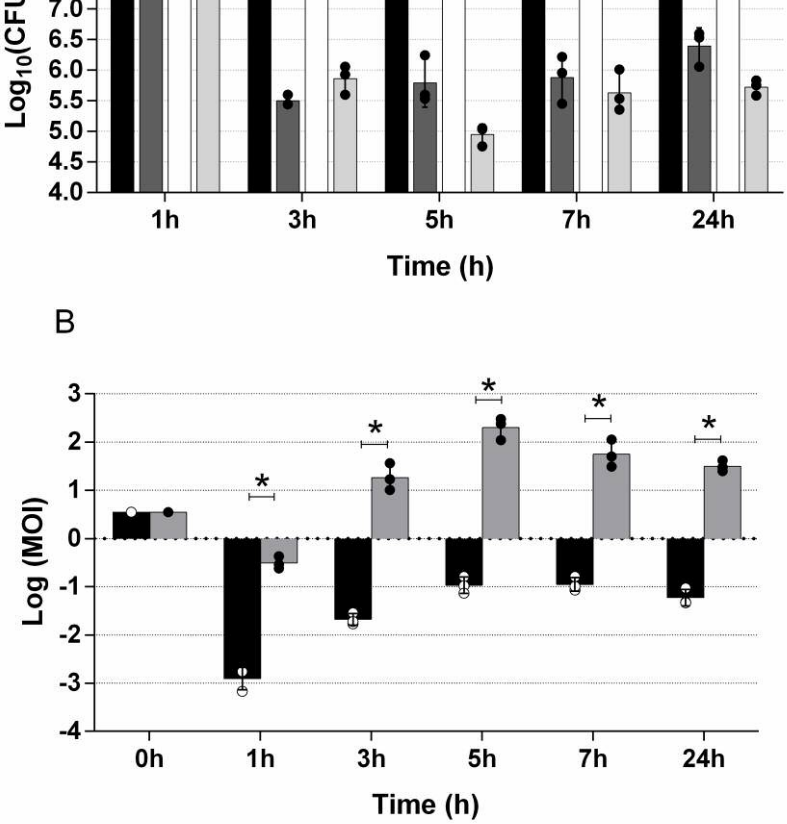

Figure 7.3 - Time-kill curve of *S. aureus* 15981 biofilms treated with protein CHAPSH3b and/or phage *Kayvirus rodi*. a) 24-h-old biofilms were treated with protein at 8 μM (grey bars), phage at 1×10^9 PFU/ml (white bars) or a combination of both (light grey bars) and incubated for 1, 3, 5, 7 or 24 hours at 37ºC. Control wells were treated with TSB medium alone (black bars). Data correspond to the means ± standard deviations of three independent experiments, and represented in logarithmic scale in colony forming units per cm^2 of biofilm. Bars with an asterisk are statistically different ($p<0.05$) from the untreated control according to the Student's t-test using the Holm-Sidak method. b) 24-h-old biofilms were treated with phage at 1×10^9 PFU/ml (black bars) or a combination of

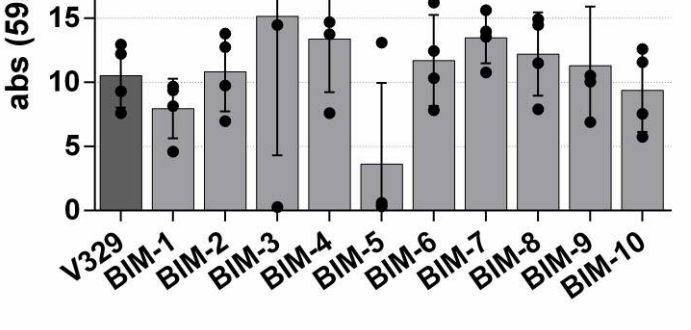

Figure 7.4 - Biofilm formation of BIMs derived from strain V329 after 24 hours of incubation at 37 ºC. The depicted values correspond to the average and standard deviation of three independent repeats. After growth, biofilms were stained with crystal violet and A_{595} was then measured to quantify attached biomass. * P-values < 0.05 were considered significant according to the Student's t-test using the Holm-Sidak method

MIX 2	*S. epidermidis* SE11B
	S. epidermidis 48
MIX 3	*S. epidermidis* SE2H
	S. epidermidis SE3H
	S. epidermidis SE11B
	S. epidermidis 48
MIX 4	*S. epidermidis* SE4B
	S. epidermidis SE3C
	S. epidermidis SE6B
	S. epidermidis SE16U

Table 7.4 - Features of bacteriophage IPLA-AICAT *orfs*, gene products (gp) and functional assignment

orf	start	stop	predicted function	aa	Closes hit
1	415	149	hypothetical protein	88	hypothetical protein AVU40_gp140 [*Staphylococcus* phage phiIPLA-C1C]
2	693	433	hypothetical protein	86	hypothetical protein AVU40_gp141 [*Staphylococcus* phage phiIPLA-C1C]
3	1071	766	hypothetical protein	101	hypothetical protein BE25_0229 [*Staphylococcus* phage vB_SepM_BE25]
4	1485	1147	hypothetical protein	112	hypothetical protein Terranova_003 [*Staphylococcus* phage Terranova]
5	1627	2301	pentapeptide repeat-containing protein	224	pentapeptide repeat protein [*Staphylococcus* phage phiIPLA-C1C]
6	2388	2735	hypothetical protein	115	hypothetical protein Terranova_008 [*Staphylococcus* phage Terranova]
7	2737	3078	hypothetical protein	113	hypothetical protein BESEP4_00009 [*Staphylococcus* phage vB_SepM_BE04]
8	3220	3555	hypothetical protein	111	hypothetical protein BESEP4_00010 [*Staphylococcus* phage vB_SepM_BE04]
9	3580	3780	hypothetical protein	66	hypothetical protein AVU40_gp146 [*Staphylococcus* phage phiIPLA-C1C]
10	4126	3908	putative membrane protein	72	putative membrane protein [*Staphylococcus* phage Twillingate]
11	4221	4030	hypothetical protein	63	hypothetical protein BE24_0206 [*Staphylococcus* phage vB_SepM_BE24]
12	4831	4631	hypothetical protein	66	hypothetical protein AVU40_gp147 [*Staphylococcus* phage phiIPLA-C1C]

13	5085	4864	hypothetical protein	73	hypothetical protein BE25_0002 [*Staphylococcus* phage vB_SepM_BE25]
14	5662	5979	hypothetical protein	105	hypothetical protein 110_00150 [*Staphylococcus* phage 110]
15	6179	6460	treK	90	TreK [*Staphylococcus* phage 110]
16	6506	6769	hypothetical protein	87	hypothetical protein Biyabedamokiny1_00058 [*Staphylococcus* phage Biyabeda-mokiny_1]
17	7621	7887	hypothetical protein	88	hypothetical protein 110_00154 [*Staphylococcus* phage 110]
18	8478	8735	hypothetical protein	85	hypothetical protein 110_00156 [*Staphylococcus* phage 110]
19	9043	9381	hypothetical protein	112	hypothetical protein AVU40_gp156 [*Staphylococcus* phage phiIPLA-C1C]
20	9489	9818	hypothetical protein	109	
21	9890	10057	-	55	DNA repair family protein [*Staphylococcus* phage Twillingate]
22	10256	10603	hypothetical protein	115	hypothetical protein Twillingate_025 [*Staphylococcus* phage Twillingate]
23	10870	11148	hypothetical protein	92	hypothetical protein Twillingate_027 [*Staphylococcus* phage Twillingate]
24	11969	11541	hypothetical protein	142	hypothetical protein Terranova_027 [*Staphylococcus* phage Terranova]
25	12527	12042	hypothetical protein	161	hypothetical protein FDH45_gp156 [*Staphylococcus* phage phiIBB-SEP1]
26	13386	12802	hypothetical protein	194	hypothetical protein 80A_00159 [*Staphylococcus* phage 80A]
27	13794	13426	hypothetical protein	122	hypothetical protein Quidividi_030 [*Staphylococcus* phage Quidividi]
28	14219	13929	tail protein	96	major tail protein [*Staphylococcus* phage phiIPLA-C1C]

29	15246	14668	hypothetical protein	192	hypothetical protein AVU40_gp170 [*Staphylococcus* phage phiIPLA-C1C]
30	15613	15266	major tail protein	115	major tail protein [*Staphylococcus* phage phiIPLA-C1C]
31	16448	15699	transglicosidase	249	transglycosylase [*Staphylococcus* phage vB_SepM_BE24]
32	16642	16490	RinB-like transcriptional activator	50	RinB-like transcriptional activator [*Staphylococcus* phage phiIBB-SEP1]
33	16963	16646	hypothetical protein	105	hypothetical protein FDH45_gp167 [*Staphylococcus* phage phiIBB-SEP1]
34	17372	16956	nucleotide kinase	138	nucleotide kinase [*Staphylococcus* phage phiIBB-SEP1]
35	18112	17495	hypothetical protein	205	HNH endonuclease [*Staphylococcus* phage phiIBB-SEP1]
36	18407	18093	MazG-like family protein	104	NTP pyrophosphohydrolase [*Staphylococcus* phage vB_SepM_BE04]
37	18620	18453	hypothetical protein	55	hypothetical protein FDH45_gp171 [*Staphylococcus* phage phiIBB-SEP1]
38	18895	18701	virion structural protein	64	virion structural protein [*Staphylococcus* phage vB_SepM_BE25]
39	19583	18948	hypothetical protein	211	membrane protein [*Staphylococcus* phage Terranova]
40	19955	19653	membrane protein	100	membrane protein [*Staphylococcus* phage vB_SepM_BE25]
41	20550	19957	nuclease 2-deoxyribosyltransferase	197	nucleoside-2-deoxyribosyltransferase [*Staphylococcus* phage 110]
42	20824	20564	hypothetical protein	86	hypothetical protein BESEP5_00022 [*Staphylococcus* phage vB_SepM_BE05]
43	21146	20901	hypothetical protein	81	hypothetical protein 80A_00177 [*Staphylococcus* phage 80A]
44	21952	21215	PhoH- related protein	245	PhoH-related protein [*Staphylococcus* phage 80A]
45	22491	21979	hypothetical protein	170	hypothetical protein BESEP4_00050 [*Staphylococcus* phage vB_SepM_BE04]

46	22958	22506	ribonuclease H	150	Rnase H [*Staphylococcus* phage phiIPLA-C1C]
47	23109	22912	hypothetical protein	65	hypothetical protein AVU40_gp190 [*Staphylococcus* phage phiIPLA-C1C]
48	23719	23123	hypothetical protein	198	hypothetical protein AVU40_gp191 [*Staphylococcus* phage phiIPLA-C1C]
49	23939	23712	transcriptional regulator	75	transcriptional regulator [*Staphylococcus* phage phiIPLA-C1C]
50	24164	23943	hypothetical protein	73	hypothetical protein Quidividi_057 [*Staphylococcus* phage Quidividi]
51	25069	24335	endolysin	244	endolysin [*Staphylococcus* phage vB_SepM_BE04]
52	26150	25413	chap domain-contaning protein	245	endolysin [*Staphylococcus* phage 80A]
53	26713	26153	holin	186	holin [*Staphylococcus* phage phiIBB-SEP1]
54	26812	27048	hypothetical protein	78	hypothetical protein 7AX1_17 [uncultured Caudovirales phage]
55	27391	27026	hypothetical protein	121	hypothetical protein AVU40_gp196 [*Staphylococcus* phage phiIPLA-C1C]
56	27866	28093	hypothetical protein	75	hypothetical protein BE24_0039
57	28601	28380	ribosome associated inhibitor A; zinc finger domain	73	ribosome associated inhibitor A; zinc finger domain [*Staphylococcus* phage phiIPLA-C1C]
58	29562	28681	BRO N-terminal domain-containing protein	293	BRO N-terminal domain-containing protein [*Staphylococcus* phage Quidividi]
59	30224	30015	hypothetical protein	69	hypothetical protein BESEP5_00037 [*Staphylococcus* phage vB_SepM_BE05]
60	30567	30235	hypothetical protein	110	hypothetical protein [*Staphylococcus* phage Stab23]
61	30578	30901	hypothetical protein	107	hypothetical protein FDH45_gp196 [*Staphylococcus* phage phiIBB-SEP1]
62	31193	31930	membrane protein	87	membrane protein [*Staphylococcus* phage Quidividi]

63	31312	30671	membrane protein	119	membrane protein [*Staphylococcus* phage phiIPLA-C1C]
64	31652	31915	membrane protein	87	membrane protein [*Staphylococcus* phage vB_SepM_ phiIPLA-C1C]
65	31920	32339	terminase small subunit	139	terminase small subunit [*Staphylococcus* phage phiIBB-SEP1]
66	32350	32565	terminase large subunit	71	terminase large subunit [*Staphylococcus* phage phiIPLA-C1C]
67	33283	33990	terminase large subunit	235	terminase large subunit [*Staphylococcus* phage vB_SepM_BE04]
68	34228	35190	endonuclease	320	group I intron-associated VSR homing endonuclease [*Staphylococcus* phage Terranova]
69	35284	36057	terminase large subunit	257	terminase large subunit [*Staphylococcus* phage phiIBB-SEP1]
70	36071	36874	virion structural protein	267	virion structural protein [*Staphylococcus* phage phiIPLA-C1C]
71	36858	37022	membrane protein	54	membrane protein [*Staphylococcus* phage phiIPLA-C1C]
72	37036	37527	hypothetical protein	163	hypothetical protein Terranova_082 [*Staphylococcus* phage Terranova]
73	37604	37990	membrane protein	128	membrane protein [*Staphylococcus* phage phiIPLA-C1C]
74	38031	38342	portal protein	103	portal protein [*Staphylococcus* phage 80A]
75	38305	40035	portal protein	576	portal protein [*Staphylococcus* phage vB_SepM_BE25]
76	40177	40947	head phage protease	256	head maturation protease [*Staphylococcus* phage phiIPLA-C1C]
77	40950	41963	hypothetical protein	337	hypothetical protein FDH45_gp010 [*Staphylococcus* phage phiIBB-SEP1]
78	42090	43481	major capsid protein	463	major head protein [*Staphylococcus* phage phiIBB-SEP1]
79	43582	43848	hypothetical protein	88	hypothetical protein Twillingate_088 [*Staphylococcus* phage Twillingate]
80	43858	44766	tail fiber protein	302	tail fiber protein [*Staphylococcus* phage phiIBB-SEP1]

81	44780	45655	capsid protein	291	capsid protein [*Staphylococcus* phage Twillingate]
82	45655	46290	hypothetical protein	211	hypothetical protein AVU40_gp015 [*Staphylococcus* phage phiIPLA-C1C]
83	43306	47163	hypothetical protein	285	hypothetical protein BESEP6_00060 [*Staphylococcus* phage vB_SepM_BE06]
84	47138	47359	hypothetical protein	73	hypothetical protein AVU40_gp017 [*Staphylococcus* phage phiIPLA-C1C]
85	47379	49163	tail sheath	594	tail sheath [*Staphylococcus* phage phiIPLA-C1C]
86	49223	49588	virion structural protein	121	virion structural protein [*Staphylococcus* phage phiIPLA-C1C]
87	49831	50004	-	57	-
88	50336	51325	hypothetical protein	329	hypothetical protein BESEP4_00090 [*Staphylococcus* phage vB_SepM_BE04]
89	51373	51531	hypothetical protein	52	hypothetical protein Terranova_098 [*Staphylococcus* phage Terranova]
90	51655	52116	hypothetical protein	153	hypothetical protein BESEP4_00093 [*Staphylococcus* phage vB_SepM_BE04]
91	52121	52315	hypothetical protein	64	hypothetical protein BESEP4_00094 [*Staphylococcus* phage vB_SepM_BE04]
92	52381	52674	virion structural protein	97	hypothetical protein Quidividi_098 [*Staphylococcus* phage Quidividi]
93	52800	53210	tail assembly chaperone	136	tail tape measure protein [*Staphylococcus* phage vB_SepM_BE06]
94	53242	53751	RNA polymerase beta subunit/ tape measure chaperone	169	RNA polymerase beta subunit [*Staphylococcus* phage phiIPLA-C1C]
95	53806	57123	tail lisin	1105	tail lysin [*Staphylococcus* phage vB_SepM_BE05]
96	57867	58448	endolysin	193	endolysin [*Staphylococcus* phage phiIPLA-C1C]

97	58511	59308	lytic transglycosylase	265	lytic transglycosylase [*Staphylococcus* phage phiIPLA-C1C]
98	59365	61971	amidase	868	amidase [*Staphylococcus* phage vB_SepM_BE04]
99	61986	62894	endopeptidase	302	endopeptidase [*Staphylococcus* phage 110]
100	63629	65050	chromosome segregation protein	473	chromosome segregation protein [*Staphylococcus* phage vB_SepM_BE04]
101	63311	65050	Tail fiber protein	579	tail fiber protein [*Staphylococcus* phage Twillingate]
102	65071	65739	poly-gamma-glutamate hydrolase ?	222	poly-gamma-glutamate hydrolase [*Staphylococcus* phage phiIPLA-C1C]
103	65850	66647	hypothetical protein	265	hypothetical protein BESEP4_00105 [*Staphylococcus* phage vB_SepM_BE04]
104	66647	67171	hypothetical protein	174	hypothetical protein Twillingate_112 [*Staphylococcus* phage Twillingate]
105	67171	67875	baseplate wedge protein	234	baseplate wedge protein [*Staphylococcus* phage Twillingate]
106	67888	68934	baseplate J-like protein	348	baseplate J-like protein [*Staphylococcus* phage phiIBB-SEP1]
107	68951	71605	hypothetical protein	884	hypothetical protein BESEP5_00084 [*Staphylococcus* phage vB_SepM_BE05]
108	71729	72250	virion structural protein	173	hypothetical protein Twillingate_116 [*Staphylococcus* phage Twillingate]
109	72271	75726	tail protein	1151	tail protein [*Staphylococcus* phage vB_SepM_BE04]
110	75779	75940	hypothetical protein	53	hypothetical protein BE24_0098 [*Staphylococcus* phage vB_SepM_BE24]
111	75946	77874	hypothetical protein	642	hypothetical protein BESEP4_00113 [*Staphylococcus* phage vB_SepM_BE04]
112	77887	78279	DUF2977 domain-containing protein	130	tail fiber protein [*Staphylococcus* phage phiIPLA-C1C]

113	78286	79656	tail fiber protein	456	hypothetical protein BESEP4_00115 [*Staphylococcus* phage vB_SepM_BE04]	0.0	99%	QLF86849.1
114	79748	81490	DNA helicase	580	DNA helicase [*Staphylococcus* phage vB_SepM_BE04]	0.0	100%	QLF86850.1
115	81506	83119	winged HTH transcriptional regulator	537	winged HTH transcriptional regulator [*Staphylococcus* phage Terranova]	0.0	99%	AXY84003.1
116	83116	84555	helicase DnaB-like protein	479	DnaB-like helicase [*Staphylococcus* phage vB_SepM_BE06]	0.0	99%	QLF87246.1
117	84627	84932	hypothetical protein	101	hypothetical protein BESEP4_00120 [*Staphylococcus* phage vB_SepM_BE04]	3.00E-63	100%	QLF86854.1
118	84932	85495	hypothetical protein	187	hypothetical protein AVU40_gp050 [*Staphylococcus* phage phiIPLA-C1C]	6.00E-128	100%	YP_009214505.1
119	85495	86529	recombination exonuclease	344	recombination exonuclease [*Staphylococcus* phage vB_SepM_BE04]	0.0	100%	QLF86856.1
120	86607	86996	hypothetical protein	129	hypothetical protein BESEP4_00123 [*Staphylococcus* phage vB_SepM_BE04]	4.00E-87	100%	QLF86857.1
121	86989	88902	recpombination endonuclease	637	recombination endonuclease [*Staphylococcus* phage vB_SepM_BE04]	0.0	99%	QLF86858.1
122	88909	89508	anti-sigma factor	199	anti-sigma factor [*Staphylococcus* phage phiIPLA-C1C]	2.00E-140	99%	YP_009214509.1
123	89520	90575	DNA primase	351	DNA primase [*Staphylococcus* phage vB_SepM_BE04]	0.0	100%	QLF86860.1
124	90637	90948	hypothetical protein	103	hypothetical protein AVU40_gp056 [*Staphylococcus* phage phiIPLA-C1C]	1.00E-64	100%	YP_009214511.1
125	90948	91382	hypothetical protein	144	hypothetical protein AVU40_gp057 [*Staphylococcus* phage phiIPLA-C1C]	5.00E-95	100%	YP_009214512.1
126	91375	91986	RusA-like Holliday junction resolvase	203	RusA-like Holliday junction resolvase [*Staphylococcus* phage phiIBB-SEP1]	3.00E-148	100%	YP_009600983.1
127	92004	92402	flavodoxin	132	flavodoxin [*Staphylococcus* phage phiIPLA-C1C]	5.00E-91	100%	YP_009214514.1

128	92407	94524	ribonucleoside-diphosphate reductase 2 subunit alpha	705	ribonucleoside-diphosphate reductase 2 subunit alpha [*Staphylococcus* phage vB_SepM_BE04]	0.0	100%	QLF86865.1
129	94512	95585	ribonucleoside diphosphate reductase small subunit	357	ribonucleoside diphosphate reductase small subunit [*Staphylococcus* phage vB_SepM_BE24]	0.0	99%	WEU70370.1
130	95625	95936	hypothetical protein	103	hypothetical protein Terranova_138 [*Staphylococcus* phage Terranova]	1.00E-67	100%	AXY84018.1
131	95939	96262	thioredoxin-like protein	107	thioredoxin-like protein [*Staphylococcus* phage phiIPLA-C1C]	4.00E-68	100%	YP_009214520.1
132	96328	97053	hypothetical protein	241	hypothetical protein BESEP4_00135 [*Staphylococcus* phage vB_SepM_BE04]	3.00E-173	100%	QLF86869.1
133	97062	97361	DNA binding protein	99	DNA binding protein [*Staphylococcus* phage phiIPLA-C1C]	3.00E-63	100%	YP_009214522.1
134	97442	99673	DNA polymerase	743	DNA polymerase [*Staphylococcus* phage phiIBB-SEP1]	0.0	99%	YP_009600992.1
135	99821	100648	HNH homing endonuclease	275	HNH homing endonuclease [*Staphylococcus* phage Twillingate]	0.0	99%	AXF38579.1
136	100912	101757	DNA polymerase	281	DNA polymerase [*Staphylococcus* phage phiIBB-SEP1]	0.0	99%	YP_009600992.1
137	101811	102293	hypothetical protein	160	hypothetical protein AVU40_gp071 [*Staphylococcus* phage phiIPLA-C1C]	1.00E-113	100%	YP_009214526.1
138	102384	103619	hypothetical protein	411	hypothetical protein BESEP5_00116 [*Staphylococcus* phage vB_SepM_BE05]	0.0	99%	QLF87058.1
139	103647	103901	RecA	84	RecA [*Staphylococcus* phage Quidividi]	4.00E-42	100%	AXF38373.1
140	104281	104114	hypothetical protein	55	MAG: hypothetical protein [*Staphylococcus* phage RP2]	2.00E-28	100%	UKH47762.1
141	104246	105214	endonuclease	322	endonuclease [*Staphylococcus* phage phiIPLA-C1C]	0.0	100%	YP_009214529.1
142	105263	106282	UvsX-like recombinase	339	RecA [*Staphylococcus* phage Quidividi]	0.0	100%	AXF38373.1
143	106279	106647	hypothetical protein	122	hypothetical protein AVU40_gp076 [*Staphylococcus* phage phiIPLA-C1C]	1.00E-83	100%	YP_009214531.1
144	106610	107284	RNA polymerase signal factor	224	RNA polymerase sigma factor [*Staphylococcus* phage phiIBB-SEP1]	8.00E-154	100%	YP_009600998.1

145	107360	107707	holin	115	holin [*Staphylococcus* phage phiIBB-SEP1]	3.00E-72	100%	YP_009600999.1
146	107720	108379	hypothetical protein	219	Ig domain containing protein [*Staphylococcus* phage phiIPLA-C1C]	2.00E-157	99%	YP_009214534.1
147	108483	108746	hypothetical protein	87	hypothetical protein Quidividi_149 [*Staphylococcus* phage Quidividi]	5.00E-56	99%	AXF38379.1
148	109022	109489	hypothetical protein	155	hypothetical protein BESEP4_00148 [*Staphylococcus* phage vB_SepM_BE04]	5.00E-105	99%	QLF86882.1
149	109492	110757	exonuclease	421	exonuclease [*Staphylococcus* phage phiIBB-SEP1]	0.0	100%	YP_009601003.1
150	110770	111108	hypothetical protein	112	membrane protein [*Staphylococcus* phage Terranova]	8.00E-72	99%	AXY84033.1
151	111173	111712	hypothetical protein	179	hypothetical protein AVU40_gp084 [*Staphylococcus* phage phiIPLA-C1C]	2.00E-125	100%	YP_009214539.1
152	111702	112451	hypothetical protein	249	hypothetical protein FDH45_gp081 [*Staphylococcus* phage phiIBB-SEP1]	0.0	100%	YP_009601006.1
153	112426	112857	hypothetical protein	143	hypothetical protein BE24_0143 [*Staphylococcus* phage vB_SepM_BE24]	8.00E-99	99%	WEU70396.1
154	112857	113702	hypothetical protein	281	hypothetical protein AVU40_gp087 [*Staphylococcus* phage phiIPLA-C1C]	0.0	99%	YP_009214542.1
155	113786	114286	hypothetical protein	166	membrane protein [*Staphylococcus* phage Quidividi]	8.00E-112	99%	AXF38388.1
156	114624	115349	hypothetical protein	241	hypothetical protein AVU40_gp089 [*Staphylococcus* phage phiIPLA-C1C]	2.00E-171	100%	YP_009214544.1
157	115374	115862	virion structural protein	162	virion structural protein [*Staphylococcus* phage phiIPLA-C1C]	2e-111	99%	YP_009214545.1
158	115905	116366	transposase domain-containing protein	153	transposase domain-containing protein [*Staphylococcus* phage Quidividi]	5e-102	99%	AXF38391.1
159	116378	117079	hypothetical protein	233	hypothetical protein Quidividi_162 [*Staphylococcus* phage Quidividi]	5.00E-166	99%	AXF38392.1

160	117144	117527	membrane protein	127	membrane protein [*Staphylococcus* phage Quidividi]	1.00E-84	99%	
161	117664	117846	hypothetical protein	60	hypothetical protein AVU40_gp094 [*Staphylococcus* phage phiIPLA-C1C]	3.00E-34	98%	YP_009214549.1
162	117839	118036	hypothetical protein	65	hypothetical protein Terranova_166 [*Staphylococcus* phage Terranova]	3.00E-32	95%	AXY84046.1
163	118116	118469	hypothetical protein	117	hypothetical protein AVU40_gp096 [*Staphylococcus* phage phiIPLA-C1C]	3.00E-75	100%	YP_009214551.1
164	118469	118969	hypothetical protein	166	hypothetical protein Quidividi_168 [*Staphylococcus* phage Quidividi]	7e-114	100%	AXF38398.1
165	118973	119296	hypothetical protein	107	hypothetical protein AVU40_gp098 [*Staphylococcus* phage phiIPLA-C1C]	1.00E-66	99%	YP_009214553.1
166	119380	119949	hypothetical protein	189	hypothetical protein BE25_0188 [*Staphylococcus* phage vB_SepM_BE25]	5e-128	99%	WEU70674.1
167	120003	120350	hypothetical protein	115	hypothetical protein BESEP4_00168 [*Staphylococcus* phage vB_SepM_BE04]	1.00E-73	100%	QLF86902.1
168	120364	120564	hypothetical protein	66	hypothetical protein AVU40_gp133 [*Staphylococcus* phage phiIPLA-C1C]	2.00E-37	98%	YP_009214588.1
169	120595	120822	hypothetical protein	75	hypothetical protein AVU40_gp101 [*Staphylococcus* phage phiIPLA-C1C]	6.00E-46	100%	YP_009214556.1
170	120840	123176	RNA ligase	778	RNA ligase [*Staphylococcus* phage vB_SepM_BE04]	0.0	99%	QLF86905.1
171	123245	123517	hypothetical protein	90	hypothetical protein BESEP5_00145 [*Staphylococcus* phage vB_SepM_BE05]	1.00E-51	99%	QLF87087.1
172	123520	124326	lipoprotein	268	lipoprotein [*Staphylococcus* phage phiIPLA-C1C]	0.0	99%	YP_009214559.1
173	124444	124632	membrane protein	62	membrane protein [*Staphylococcus* phage phiIPLA-C1C]	5.00E-30	100%	YP_009214560.1
174	124647	124823	hypothetical protein	58	hypothetical protein AVU40_gp106 [*Staphylococcus* phage phiIPLA-C1C]	3.00E-31	100%	YP_009214561.1

175	124839	125348	endolysin	169	endolysin [*Staphylococcus* phage phiIPLA-C1C]	1.00E-118	100%	YP_009214562.1
176	125402	126511	hypothetical protein	369	hypothetical protein AVU40_gp108 [*Staphylococcus* phage phiIPLA-C1C]	0.0	99%	YP_009214563.1
177	126587	126781	hypothetical protein	64	hypothetical protein AVU40_gp109 [*Staphylococcus* phage phiIPLA-C1C]	2.00E-36	100%	YP_009214564.1
178	126814	127323	hypothetical protein	169	hypothetical protein PHAGE6E_73 [*Staphylococcus* phage 6ec]	7.00E-115	99%	YP_009042578.1
179	127353	127520	hypothetical protein	55	hypothetical protein AVU40_gp111 [*Staphylococcus* phage phiIPLA-C1C]	4.00E-29	100%	YP_009214566.1
180	127655	127963	hypothetical protein	102	hypothetical protein AVU40_gp112 [*Staphylococcus* phage phiIPLA-C1C]	3.00E-65	100%	YP_009214567.1
181	127990	128151	hypothetical protein	53	hypothetical protein AVU40_gp113 [*Staphylococcus* phage phiIPLA-C1C]	8.00E-29	100%	YP_009214568.1
182	128167	128673	hypothetical protein	168	hypothetical protein AVU40_gp114 [*Staphylococcus* phage phiIPLA-C1C]	2.00E-117	100%	YP_009214569.1
183	128700	128936	hypothetical protein	78	hypothetical protein AVU40_gp115 [*Staphylococcus* phage phiIPLA-C1C]	4.00E-50	100%	YP_009214570.1
184	128960	129370	membrane protein	136	membrane protein [*Staphylococcus* phage phiIPLA-C1C]	2.00E-85	100%	YP_009214571.1
185	129376	129912	hypothetical protein	178	hypothetical protein AVU40_gp117 [*Staphylococcus* phage phiIPLA-C1C]	1.00E-125	100%	YP_009214572.1
186	129928	130128	hypothetical protein	66	hypothetical protein AVU40_gp118 [*Staphylococcus* phage phiIPLA-C1C]	9.00E-40	100%	YP_009214573.1
187	130154	130414	hypothetical protein	86	hypothetical protein AVU40_gp119 [*Staphylococcus* phage phiIPLA-C1C]	6.00E-52	99%	YP_009214574.1
188	130416	130916	membrane protein	166	membrane protein [*Staphylococcus* phage phiIBB-SEP1]	5.00E-110	100%	YP_009601034.1
189	131005	131298	hypothetical protein	97	hypothetical protein Terranova_189 [*Staphylococcus* phage Terranova]	6.00E-63	99%	AXY84069.1

190	131319	131537	hypothetical protein	72	hypothetical protein FDH45_gp111 [*Staphylococcus* phage phiIBB-SEP1]	2.00E-41	99%	YP_009601036.1
191	131541	131894	hypothetical protein	117	hypothetical protein BESEP6_00161 [*Staphylococcus* phage vB_SepM_BE06]	1.00E-80	100%	QLF87315.1
192	131923	132321	hypothetical protein	132	hypothetical protein AVU40_gp128 [*Staphylococcus* phage phiIPLA-C1C]	4.00E-92	100%	YP_009214583.1
193	132375	132578	hypothetical protein	67	hypothetical protein AVU40_gp129 [*Staphylococcus* phage phiIPLA-C1C]	7.00E-40	99%	YP_009214584.1
194	132590	132859	hypothetical protein	89	hypothetical protein AVU40_gp130 [*Staphylococcus* phage phiIPLA-C1C]	5.00E-54	97%	YP_009214585.1
195	132871	133284	hypothetical protein	137	hypothetical protein AVU40_gp131 [*Staphylococcus* phage phiIPLA-C1C]	1.00E-92	100%	YP_009214586.1
196	133516	133917	hypothetical protein	133	hypothetical protein AVU40_gp132 [*Staphylococcus* phage phiIPLA-C1C]	7.00E-91	98%	YP_009214587.1
197	133930	134130	hypothetical protein	66	hypothetical protein AVU40_gp133 [*Staphylococcus* phage phiIPLA-C1C]	9.00E-37	98%	YP_009214588.1
198	134162	134578	hypothetical protein	138	hypothetical protein BESEP5_00173 [*Staphylococcus* phage vB_SepM_BE05]	2.00E-94	100%	QLF87115.1
199	134581	134817	hypothetical protein	78	hypothetical protein BESEP5_00174 [*Staphylococcus* phage vB_SepM_BE05]	3.00E-46	99%	QLF87116.1
200	134833	135276	hypothetical protein	147	hypothetical protein Quidividi_199 [*Staphylococcus* phage Quidividi]	8.00E-100	99%	AXF38429.1
201	135295	135651	hypothetical protein	118	hypothetical protein AVU40_gp137 [*Staphylococcus* phage phiIPLA-C1C]	1.00E-56	82%	YP_009214592.1
202	135660	135980	hypothetical protein	106	hypothetical protein BESEP5_00177 [*Staphylococcus* phage vB_SepM_BE05]	8.00E-67	94%	QLF87119.1

203	136043	136432	hypothetical protein	129	hypothetical protein BESEP5_00178 [*Staphylococcus* phage vB_SepM_BE05]	1.00E-80	99%	QLF87120.1
204	136434	136937	YopX-like protein	167	YopX-like protein [*Staphylococcus* phage Terranova]	7.00E-76	75%	AXY84082.1
205	136937	137380	hypothetical protein	147	hypothetical protein Terranova_203 [*Staphylococcus* phage Terranova]	7.00E-98	98%	AXY84083.1
206	137394	137858	hypothetical protein	154	hypothetical protein FDH45_gp125 [*Staphylococcus* phage phiIBB-SEP1]	4.00E-98	99%	YP_009601050.1
207	137936	138421	hypothetical protein	161	hypothetical protein FDH45_gp126 [*Staphylococcus* phage phiIBB-SEP1]	2.00E-109	100%	YP_009601051.1
208	138437	138838	membrane protein	133	membrane protein [*Staphylococcus* phage phiIBB-SEP1]	3.00E-82	98%	YP_009601052.1
209	138968	139981	hypothetical protein	337	hypothetical protein BESEP4_00208 [*Staphylococcus* phage vB_SepM_BE04]	0	99%	QLF86942.1